Dottorato in Biotecnologie
Università di Napoli Federico II

Sondos Hejazi

XXXVI ciclo

Dottorato in Biotecnologie- **XXXVI ciclo**
Università di Napoli Federico II

POLY-γ-GLUTAMIC ACID BASED BIOPLASTIC

BY
SONDOS HEJAZI

Dottorando	Sondos Hejazi
Relatore	Prof. Raffaele Porta
Co-Tutor	Prof. C. Valeria L. Giosafatto
Coordinatore	Prof. Marco Moracci
Settore Scientifico Disciplinare	BIO/10

(November 1st, 2020 -January 31st, 2024)

To my dearest sister, ***Aya****, the soul, whose curiosity ignited my own, who gifted me this painting "****Whisper of the Universe****" during my visit to Palestine on December 22, 2022. Which holds a special place in my heart, its vibrant hues and inky depths mirroring her boundless curiosity.*

To My loving parents ***Mohammed and Hanan*** *my guiding lights, my supportive siblings****, Bara'ah, Amenah, Fadi, and Abdul Rahman,*** *your support and love have been the driving force behind my academic journey.*

*To my homeland****, Palestine,*** *a land of resilience, beauty, and rich history.*

I dedicate this work from the depths of my heart with testament to our pursuit of knowledge, progress, and a brighter future for all...

Acknowledgments

In the crucible of adversity, I found the spark of innovation!

Guided by the divine principles of Allah, the Most Gracious, the Most Merciful, the Giver of Peace, and the Giver of Life, and inspired by **the first word in the Qur'an "Iqra"-Seek knowledge!**", I embraced the boundless potential of learning. As a Palestinian woman pursuing a Ph.D., I faced countless obstacles, yet I discovered a power within me – the ability to transform grief, sadness, anger, and all negative emotions into creativity; with each setback, I found solace in my research, channeling my frustration and disappointment into fuel for innovation.

However, my PhD journey to academic success would not have been possible without the support of **my mentors, colleagues, friends, and family**.

Professor Marco Moracci, the coordinator of the PhD School of Biotechnology, for his support throughout my doctoral journey.

Professor Raffaele Porta, my steadfast supervisor, has been my compass and guiding light to pursue my goals. With his deep visionary insights, he has not only expanded my knowledge but also opened my mind to the boundless possibilities that science holds.

Professor Valeria Giosafatto has treated me like her own daughter, offering guidance, encouragement, and openness to new ideas throughout my academic journey welcoming my ideas, and fostering a collaborative and supportive learning environment.

Professor Loredana Mariniello provided me with love, kindness, and her dedication to fostering a collaborative and supportive environment within the BBE group.

Dr. Odile Restaino, her willingness to share her knowledge and expertise has been a true blessing.

My heartfelt thanks go to **Michela Famiglietti**, who has always been there for me, like a true sister.

To **Professor Di Pierro Prospero**, to my **BBE colleagues**, my second family, all of you individually whom I met during my PhD, our shared passion for science, and our willingness to help each other was a source of strength throughout my journey.

I would also like to express my gratitude to **Professor Chiara Schiraldi** from **Università degli Studi di Napoli 'Luigi Vanvitelli'** for her invaluable collaboration on this project.
Special thanks to **Dr. Gabriella Santagata** who has always encouraged me to pursue further with curiosity.
I would like to express my sincere gratitude to **Dr. Cinzia Calvio** for organizing valuable research at **Pavia University** for introducing me to γ-PGA production by bacterial engineering strains.

I am deeply appreciative of **Professor Marcin Lukaszewicz's** guidance and support during my research stay at the **University of Wroclaw**.

My deepest gratitude to **Zainab Qazanfazadeh**, a dear friend, for engaging in stimulating discussions, and her ability to think critically has enriched my scientific journey.
Last but not least, I am deeply thankful to **Dr. Mohammed Sabbah** for his support during my Ph.D.
I am truly grateful to **Edoardo Vegliante**, my hidden supporter, who was always a blessing, and to **Lucia Gallo** for hosting me during my research visit to Pavia.
My beloved uncles **Ahmed and Khaled**, my sage advisors, have been a source of wisdom and guidance.
My dearest cousin **Anna Nasrallah** and my dearest friend Haneen Hamed, along with her family, ultimately supported me throughout my Ph.D. journey.
I am truly grateful for the support and encouragement I have received from all of you.

Table of Content

SUMMARY

Inspired by the microorganism *Bacillus* species bacteria, this project explores the extraordinary world of poly-γ-glutamic acid (γ-PGA), a polypeptide with remarkable properties for diverse applications. An eco-friendly purification method of γ-PGA, based on an ultrafiltration process, was developed, and extensive characterization of low molecular weight purified fractions of γ-PGA (R1 and R2), revealing their remarkable properties and potential applications, was carried out. The use of purified R1 and R2 for biodegradable film preparation, using both casting and thermal pressing, was investigated, leading to the development of novel biomaterials. Building upon this success, an innovative blending approach between the anionic γ-PGA fractions and cationic chitosan (CH) was performed, employing a simple complexation method based on the physical electrostatic interaction between the two biopolymers. The resulting biomaterials were obtained as hydrogel in a hydrated form and a glass-like state in a dehydrated form. The novel biomaterials produced through this approach were characterized for their physicochemical features and their potential as bio-glue was explored. In this project fermentation techniques to produce high molecular weight γ-PGA, using two genetically modified *Bacillus subtilis* strains able to hyper-produce γ-PGA, were also investigated, and the resulting biopolymer was characterized. Subsequently, taking advantage of the crosslinking method previously exploited for the R1 and R2 fractions, the γ-PGA produced by the modified bacteria was used for the preparation of hydrogels thanks, once again, to its blending with CH, a biocompatible polymer derived from chitin, the second most abundant polysaccharide occurring in Nature. Also, in this case, new materials were manufactured and shown to be endowed with interesting characteristics for the potential development of biodegradable agents to be used in the biomedical field. During three months three-month stay at Wroclaw University, it was also explored the production of γ-PGA from bacterial strains isolated from local honey. Furthermore, a new spectrophotometric ninhydrin-based method, developed in foreign laboratories, enabled the reliable quantification of γ-PGA. In conclusion, it is possible to assume from the research carried out over the last three years that γ-PGA is an anionic polymer with great potential for sustainable and eco-compatible applications. **Therefore, the general objective of the present Ph.D. project such as the optimization of the γ-PGA-based bioplastic production to obtain new materials was achieved**, since before this study very little was known about the ability of polypeptides made up of the same amino acid unit to give rise to materials with plastic-like properties.

RIASSUNTO

Questo progetto ha esplorato lo straordinario mondo dell'acido γ-poliglutammico (γ-PGA), un omopolipeptide naturale derivante da unità ripetitive di acido glutammico dotato di proprietà molto interessanti per diverse applicazioni industriali. La prima parte del presente studio ha riguardato lo sviluppo di metodi di purificazione del γ-PGA a basso peso molecolare partendo da un prodotto disponibile commercialmente. In particolare, due distinti metodi di purificazione sono stati adottati: 1) purificazione mediante precipitazione grazie all'uso di un solvente organico, quale il metanolo; 2) purificazione basata su un metodo di ultra- e nano-filtrazione che ha consentito di ottenere frazioni aventi peso molecolare specifico ed uniforme (R1= 55-59 kDa; R2= 20 kDa, R3= 6.6 kDa). Più nel dettaglio, dopo la caratterizzazione chimica delle frazioni ottenute, la ricerca ha esplorato la bioattività e la capacità di formare materiali biodegradabili delle frazioni ottenute. Infatti sono stati ottenuti nuovi film idrocolloidali utilizzando sia il metodo del casting che della compressione a caldo. La compressione a caldo delle frazioni ottenute mediante ultrafiltrazione, nonché del precipitato ottenuto mediante trattamento con metanolo, ha portato alla formazione di film meno resistenti ma più estensibili rispetto ai materiali ottenuti mediante il metodo del casting, mentre l'analisi termica ha rivelato una maggiore stabilità termica dei campioni prodotti con la frazione a più alto peso molecolare (R1). Questi biomateriali potrebbero potenzialmente essere utilizzati in campo cosmetico e come veicolo di molecole attive in campo farmaceutico, dal momento che studi *in vitro* effettuati grazie alla collaborazione con la prof. Chiara Schiraldi (Dipartimento di Medicina Sperimentale dell'Università della Campania Luigi Vanvitelli) è stato scoperto che il γ-PGA purificato mediante ultrafiltrazione è in grado di proteggere i cheratinociti dall'essiccamento e dallo stress ossidativo. Il progetto inoltre ha portato alla produzione di biocompositi reticolati in modo non covalente miscelando le frazioni R1 e R2 del γ-PGA con il polisaccaride CH, sfruttando il principio della complessazione di polielettroliti. I biomateriali ottenuti previa precipitazione del complesso formatosi tra i due biopolimeri, presentavano una consistenza morbida e gommosa (hydrogel), facilmente modellabili, che, dopo la loro disidratazione, si trasformavano in materiali estremamente duri, rigidi, completamente insolubili in acqua e solventi organici, tali da assumere caratteristiche di tipo vetroso. Analisi strutturali, fisico-chimiche e termiche hanno confermato forti interazioni fisiche tra le catene del CH e quelle del γ-PGA, dovute essenzialmente all'attrazione elettrostatica e a legami idrogeno. Studi di caratterizzazione chimico-fisica hanno dimostrato che tali biomateriali avevano strutture sia cristalline che amorfe, e che erano dotati di buona stabilità termica oltre che di un buon grado di biodegradabilità nel suolo. Questi biocompositi termoplastici rappresentano pertanto un immenso potenziale nella medicina rigenerativa, come dispositivi biomedici, per l'imballaggio alimentare e la stampa 3D. Inoltre, le loro proprietà rispettose dell'ambiente li rendono candidati interessanti per lo sviluppo di materiali

sostenibili in altri vari settori industriali. In particolare, il progetto ha esplorato l'uso degli idrogel prodotti come bio-adesivi per diversi tipi di materiali quali legno e alluminio. Le analisi reologiche hanno mostrato una significativa forza adesiva/coesiva delle miscele ottenute sui substrati analizzati, forza paragonale a quella delle colle viniliche esistenti in commercio. Infatti, esperimenti di microscopia elettronica a scansione hanno rivelato la formazione di forti legami tra la "biocolla" prodotta e i substrati di legno e alluminio utilizzati come substrato, indicando la formazione di robuste giunzioni adesive. Al di là del loro potenziale come colle innovative biodegradabili, le proprietà di questi materiali li rendono adatti per ulteriori applicazioni in vernici, rivestimenti e adesivi da utilizzare per diversi fini, non ultimo quello della conservazione e restauro del patrimonio artistico-culturale. Inoltre, durante la permanenza presso i laboratori della dott.ssa Cinzia Calvio (Dipartimento di Biologia e Biotecnologie dell'Università di Pavia), sono state utilizzate nuove tecniche fermentative per la produzione di γ-PGA ad alto peso molecolare, utilizzando due ceppi di *Bacillus subtilis* modificati geneticamente, il PB5390 e PB5523. Il primo, che possiede una mutazione del gene degS, presente sull'operone *pgs*, che porta ad una maggiore produzione di γ-PGA , il secondo che, oltre alla mutazione sopradescritta, è un ceppo in cui è stato eseguita una delezione (knockout) dei geni *pgdS* e ggt, geni che svolgono un ruolo nella sintesi dell'idrolasi responsabile della degradazione del γ-PGA. Il γ-PGA ottenuto da questi ceppi geneticamente modificati è stato caratterizzato in base al peso molecolare e sono stati applicati metodi di quantificazione utilizzando tecniche di NMR. Successivamente, sulla base dei metodi di complessazione utilizzati per le frazioni R1 ed R2, il polimero ad alto peso molecolare prodotto dai batteri modificati è stato utilizzato per la preparazione di nuovi idrogel grazie, ancora una volta, all'utilizzo del polimero biocompatibile CH. Anche in questo caso sono stati prodotti nuovi materiali con caratteristiche interessanti per una potenziale produzione di formulati da utilizzare in campo biomedico..

L'esecuzione del presente progetto di ricerca è continuato nel corso di un soggiorno di 3 mesi (da giugno 2023 a settembre 2023) in Polonia, presso il Dipartimento di Biotrasformazione della Facoltà di Biotecnologie dell'Università di Wroclaw, sotto la guida del Prof. Łukaszewicz. In questo periodo è stato dimostrato che alcuni ceppi batterici (da analisi morfologiche preliminari mediante microscopio presumibilmente appartenenti al genere *Bacillus*) isolati dal miele, hanno la capacità di produrre γ-PGA. In particolare, questo studio ha portato alla produzione di γ-PGA da parte di otto ceppi isolati dal miele polacco, esplorando l'influenza della composizione dei terreni, degli additivi metallici e delle condizioni saline sui modelli di crescita adottati e sulle capacità di produzione di γ-PGA. I risultati hanno rivelato che tali ceppi rispondono diversamente a questi vari fattori, dimostrando caratteristiche di crescita e profili di produzione di γ-PGA distinti. Di particolare interesse si sono rivelati i ceppi MMS4 e MMS6, isolati dal miele di Gąski (prodotto dalla pianta *Urtica dioica*). Questi ceppi hanno mostrato una produzione di γ-PGA nel mezzo di coltura, confermata da analisi di spettroscopia NMR, con un

ulteriore miglioramento della produzione osservato grazie all'aggiunta di rame e/o zinco. Inoltre, un nuovo approccio spettrofotometrico basato sulla ninidrina, ulteriormente ottimizzato presso i laboratori del Prof. Łukaszewicz, ha permesso anche una quantificazione affidabile e attendibile di γ-PGA. Questi risultati hanno dimostrato il potenziale di questi ceppi per la produzione di γ-PGA e suggeriscono ulteriori studi per l'ottimizzazione delle loro capacità di produzione.
In conclusione è possibile dedurre dalla ricerca effettuata durante questi 3 anni che il γ-PGA è un omopolipeptide con potenzialità enormi per diverse applicazioni ecosostenibili e, più in generale, gli studi effettuati indicano che polipeptidi costituiti dalla stessa unità amminoacidica sono in grado di dare origine, in condizioni sperimentali selettive, a biomateriali con proprietà simili a quelle delle plastiche di sintesi.

INTRODUCTION

1.1. Micro- and nano-plastics, silent invaders

Human exposure to plastics, microplastics (MPs) and nanoplastics (NPs) has raised concerns about their potential health risks (Koelmans et al., 2019). Annual exposure to MPs can range from 74,000 to 121,000 particles (Cox et al., 2019; Sana et al., 2020) and humans can be exposed to MPs and derived NPs through ingestion, inhalation, and skin contact (Shi et al., 2022) (**Fig. 1, Shi et al., 2021**).

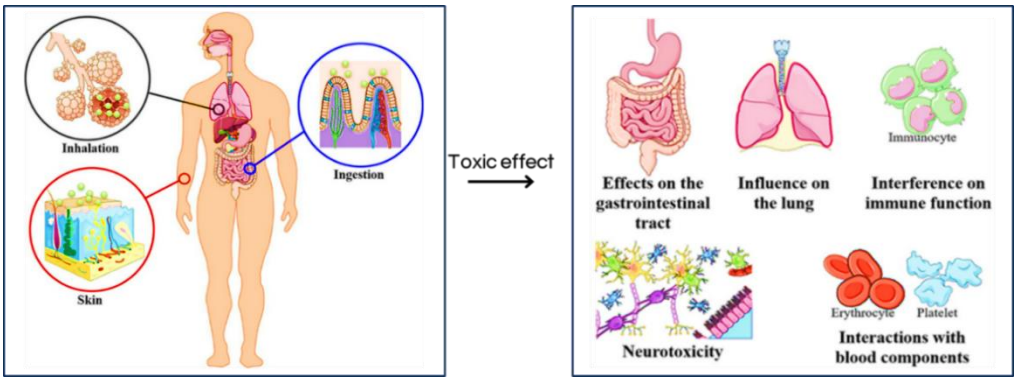

Fig. 1. Schematic diagram of the exposure route and toxic effects of MPs and NPs potentially harmful for humans (adapted from Shi et al., 2021).

MPs are used in various products, including exfoliates in personal care products (Kosuth et al., 2018), while NPs are found in a variety of consumer products, including electronics, paints, drug delivery systems, adhesives, and 3D printing (Stephens et al., 2013; Browne, et al., 2011). MPs can also be released into public wastewater from textile washing machines (Shi et al., 2022). Besides humans can absorb toxins from the environment, such as polycyclic aromatic hydrocarbons, organochlorine pesticides, and polychlorinated biphenols (Horvatits et al., 2022; Chen et al., 2022; Yan et al., 2021). MPs can also lead to oxidative stress, abrasion, satiation, ulcers, decreased growth rate, and decreased fitness for reproduction (Sana et al., 2020). NPs have different physical and chemical properties than macroscopic objects based on the same material (Llorca & Farré, 2021), as they have small size, high specific surface area, and strong biological penetration (Anderson et al., 2015).

These features allow them to reach and penetrate organs, including the placenta and brain, having a marked impact on biological functions (Kutralam-Muniasamy et al., 2023). Studies have found MPs in 15 human biological tissues and fluids, including blood, breast milk, liver, spleen, placenta and meconium, lung, and Bronchoalveolar Lavage (Kutralam-Muniasamy et al., 2023) with different levels among different tissues and individuals. For instance, as shown in **Fig. 2, Kutralam-Muniasamy et al., 2023**, MP levels were found higher in the liver tissue samples of patients with cirrhosis compared to those without liver disease (Shi et al., 2022). NPs account for 58.46% of the total MPs detected in tumor tissues compared to 41.54% present in normal tissues (Chen et al., 2022; Yan et al., 2021). In addition, as reported by Yan et al. (2021), fecal MP concentration in inflammatory bowel disease patients was found to be significantly higher than that in healthy people. Further studies have also shown that MPs (i) can induce genotoxicity in human peripheral blood lymphocytes (Çobanoglu et al., 2021), (ii) significantly increased micronucleation, nucleoplasmic bridge formation, and nuclear bud formation frequencies (Hwang et al., 2019), and (iii) stimulate the immune system enhancing potential hypersensitivity in certain cell types (peripheral blood mononuclear cells PBMCs, raw 264.7 and human mast cell line−1 HMC-1 cells) (Hwang et al., 2019). Therefore, all the available studies suggest that MPs pose a potential health risk that exposure should be minimized. Addressing the global plastic impact on the universe matrix and human health, one potential approach is to replace conventional plastics with alternative materials derived from non-oil polymers that undergo degradation in a much shorter timeframe, breaking down in months rather than years or centuries. It is crucial to acknowledge that the traditional plastic era is nearing its end, and the dawn of bioplastics is upon us (Porta et al., 2019). This transition signifies a shift towards a more sustainable and environmentally friendly future.

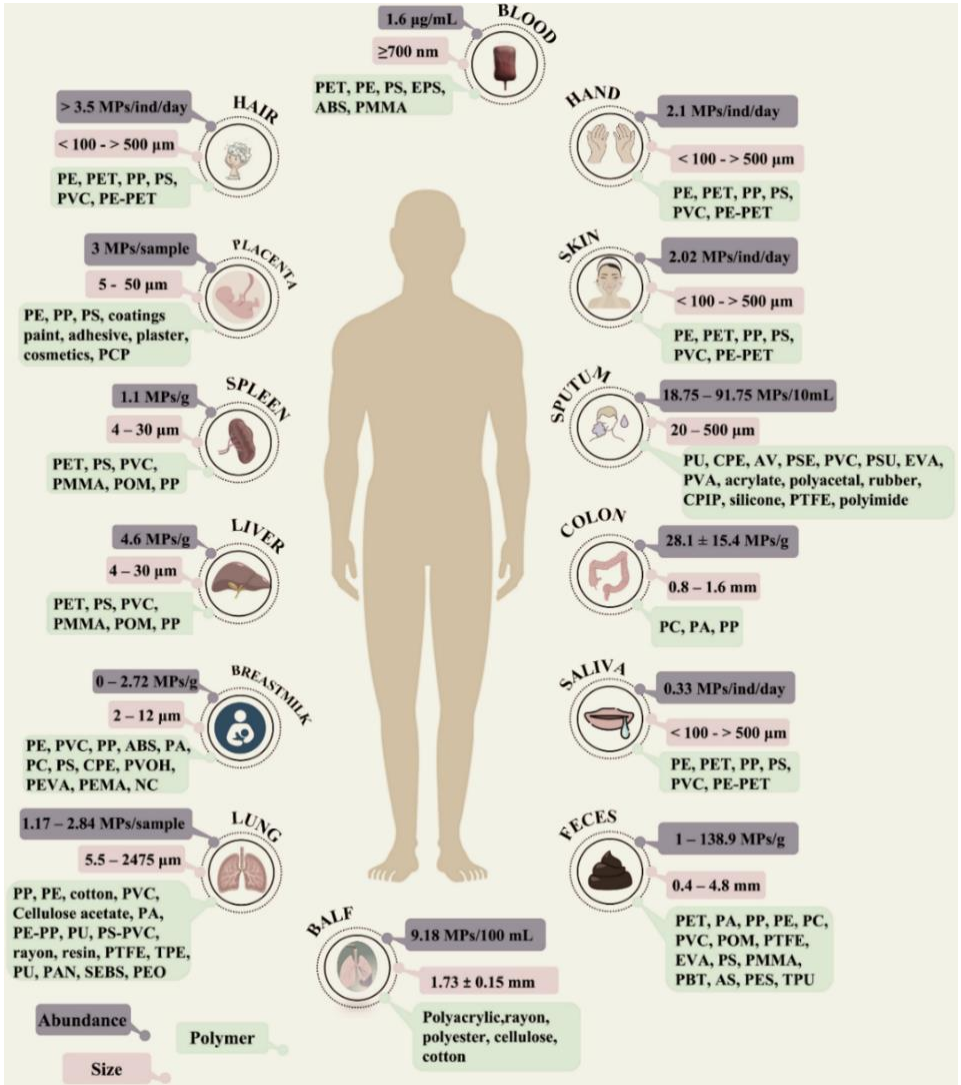

Fig. 2. An overview of microplastic (MPs) occurrence and abundance in a diverse range of human biological samples (adapted from Kutralam-Muniasamy et al., 2023)**.** Detailed abbreviations: Bronchoalveolar lavage fluid (BALF); polyethylene terephthalate (PET); polyamide(PA); p polypropylene (PP), polyethylene (PE), polycarbonate (PC), polyvinyl chloride (PVC), polyoxymethylene (POM), polytetrafluoroethylene (PTFE), ethylene vinyl alcohol (EVA), polystyrene (PS), polymethyl methacrylate (PMMA), polybutylene terephthalate (PBT), acrylonitrile butadiene styrene (ABS), polyethersulfone (PES), thermoplastic polyurethane (TPU), chlorinated polyethylene (CPE), alkyd varnish (AV), polyester (PSE), polysulfone (PSU), polyvinyl alcohol (PVOH), chlorinated polyisoprene (CPIP), polyethyl methacrylate (PEMA), nitrocellulose (NC), polyethylene-co-vinyl acetate (PEVA), personal care products (PCP), thermoplastic elastomer (TPE), styrene-ethylene-butylene copolymer (SEBS), polyacrylonitrile (PAN), and polyethylene oxide (PEO).

1.2. Bioplastics sunrise

Bioplastics, innovative materials that challenge the dominance of conventional plastics, may derive from renewable resources and may offer a sustainable alternative to petroleum-based plastics with their potential to decompose naturally. They, hence, may have a determinant impact on the plastics reduction in the environment, so the European Sustainable Development Agenda set a goal of expanding the utilization of bioplastics by 2030 (commission.europa.eu/strategy-and-policy_it). Many scientific articles have been published in the last 20 years on the application of bioplastics in edible packaging and coatings. However, it is appropriate to make clarification on the different types of bioplastics between biodegradable polymers and bio-based polymers. In fact, they are two distinct categories with some overlapping characteristics and some differences. Biodegradable polymers, like polycaprolactone, undergo decomposition by microorganisms or other aerobic and anaerobic processes. Bio-based polymers, on the other hand, can have either biodegradable or non-biodegradable properties, depending on their composition. Biopolymers, primarily derived from natural sources like corn and other feedstocks, have advancements in research and technology, being used as food thickeners and bioplastic manufacture, and more recently, in high-end regenerative medicine (Babu et al., 2013). However, food packaging and coating application currently remain the most prevalent sector for bioplastics, accounting for approximately 50% of the market (transport and construction sectors contribute 14% and 13%, respectively, while other consumer goods account for 23%) (Porta et al., 2019). It is worthy to note that the biopolymers so far demonstrated to have the best plastic-like performance, such as polylactic acid, starch, and cellulose, as well as the conventional petroleum-derived plastics, are composed of polymers with specific repeating units. This observation strongly suggests that this feature might be essential for determining the plastic performance of the derived materials (Nakajima et al.,2017). Consequently, despite the extensive research efforts focused in the last years on protein-based bioplastics, it remains a lack of understanding regarding the ability of homo-polypeptides to give rise to materials with higher plastic-like properties. Among these, poly-γ-glutamic acid (γ-PGA) stands out due to its exceptional properties, including biodegradability, biocompatibility, and shape memory.

1.3. γ-PGA, a sleeping giant among biopolymers

γ-PGA is a polyamino acid whose anionic polymeric structure is made of D-glutamic acid and/or L-glutamic acid monomers linked to each other via peptide bonds through their gamma carboxylic groups (Buescher and Margaritis, 2007) (**Fig. 3**).

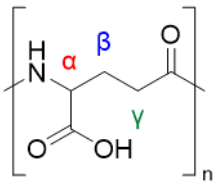

Fig. 3. Structure of γ-PGA

γ-PGA is produced naturally by different microbes such as *Natrialba aegyptiaca, Natronococcus occultus and Fusobacterium nucleatum (*Sirisansaneeyakul et al., 2017). Although there are different γ-PGA producer strains known, gram-positive bacteria of the *Bacillus* genus (*e.g. Bacillus subtilis, B. subtilis subsp. natto, Bacillus licheniformis)* are still considered the most potent producers (Luo et al., 2016). Conversely, naturally occurring microbes are not known to synthesize α-PGA, unless genetically engineered (Buescher and Margaritis, 2007). However, α-PGA could be chemically synthesized by nucleophilic polymerization of L-glutamic acid in the presence of aprotic solvents like toluene and a metal catalyst. *Bacillus* species produce γ-PGA in response to various environmental stresses, such as starvation, pollution, and drought. γ-PGA biosynthesis helps these organisms to adapt to these harsh environments (Luo et al., 2016). For example, in pathogens like *B. anthracis and Staphylococcus epidermidis*, the secretion of γ-PGA plays a role in virulence and creates a protective barrier around the pathogen, helping it resist phagocytosis by immune cells. This barrier also enhances the pathogen's ability to invade host tissues (Bajaj and Singhal, 2011). Depending on these factors, γ-PGA can either be cell-bound to elicit virulence or may be secreted to withstand an extreme environment. Nowadays, γ-PGA is considered a polypeptide of high commercial interest, since it is widely used in agriculture, environmental bioremediation, food industry, and drug and cosmetic manufacturing, thanks to its biodegradable, edible, non-toxic, non-immunogenic and superabsorbent properties (Bajaj and Singhal, 2011). However, the different industrial applications of γ-PGA depend on its molecular

weight (Mw) which ranges from 2 to 2000 kDa, conformation, purity, solubility, and pH value at which it is dissolved (Ashiuchi et al., 2003, Ho et al., 2006). Despite its promising properties, γ-PGA is currently quite expensive, with a pure powder costing approximately € 234 per 100 mg according to Sigma Aldrich (sigmaaldrich.com/IT/it/product/sigma/p4886). This high cost is due to the limited commercial production of γ-PGA as well as the purification process of the polymer. γ-PGA production can be L-glutamic acid-dependent or independent (Buescher and Margaritis, 2007; Sung et al., 2005). In the first case, supplementing the growth medium with L-glutamic acid leads to higher biopolymer yields. However, the use of L-glutamic acid as a precursor makes γ-PGA more expensive. On the other hand, L-glutamic acid independent production involves microorganisms that can synthesize their L-glutamic acid from other sources, such as glucose or other carbon sources. This method is less expensive, but it typically leads to lower γ-PGA yields than L-glutamic acid-dependent production (Buescher and Margaritis, 2007; Sung et al., 2005). In a study published by Ito et al., (1996) it was investigated a glutamate-independent strain of *B. subtilis* TAM-4 that exhibited *de novo* synthesis of γ-PGA in the growth medium. When eight different carbon and nitrogen sources were evaluated, glucose and ammonium chloride proved to be the most effective, achieving a maximum production of 13.4 g/L within four days. Microbial γ-PGA production has primarily focused on two approaches: identifying superior producer strains and optimizing fermentation conditions. Researchers have identified and characterized γ-PGA-producing *Bacillus* strains, such as *B. subtilis*, and optimized their growth conditions to enhance γ-PGA production (Bajaj and Singhal, 2011). However, a less common strategy involves the genetic engineering of γ-PGA producer strains to introduce modifications that improve production efficiency, by inactivation of specific γ-PGA degrading enzymes so that prolonging the polymer's lifespan (Scoffone et al., 2013). While microbial production has made significant progress, further advancements in strain development, fermentation processes, and cost optimization are crucial for unlocking the full potential of γ-PGA in industrial applications.

1.3.1. Biosynthetic pathway of γ-PGA

The current bottleneck hindering the widespread use of γ-PGA is the high production cost. Understanding the gene involved in γ-PGA synthesis leads to improved production methods. The mechanism of γ-PGA synthesis varies among different strains, with diverse metabolic pathways and associated enzymes involved. **(Fig. 4., Park et al., 2021)** shows the metabolic pathway of γ-PGA biosynthesis and its gene cluster which is involved in three main stages: racemization, polymerization and transfer, and catabolism (Buescher and Margaritis, 2007; Park et al. 2021).

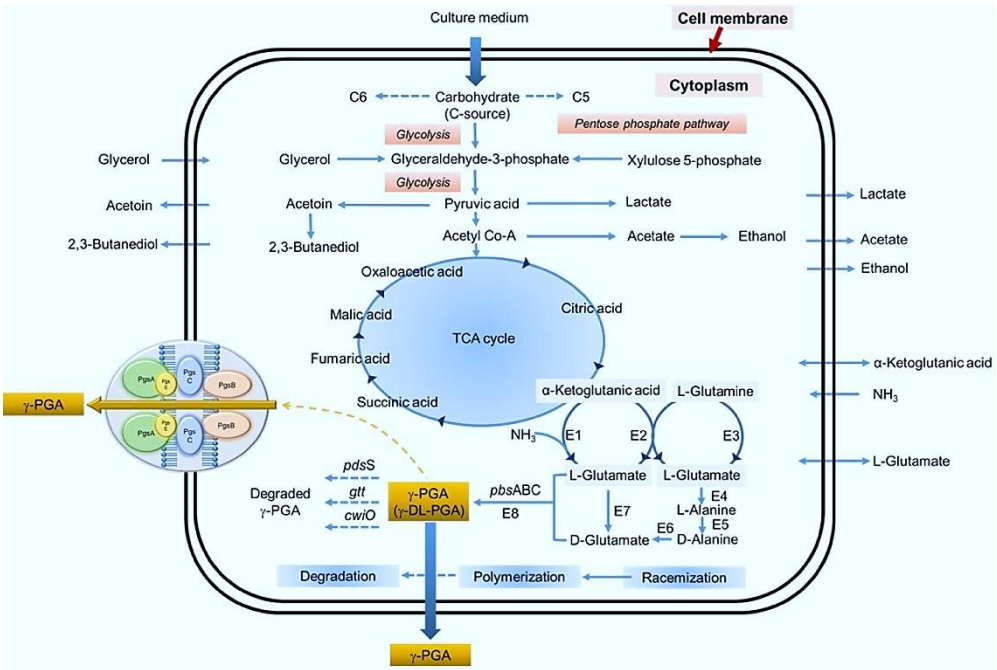

Fig. 4. γ-PGA biosynthetic pathway adapted from Park et al., 2021.

L-Glutamic acid, the crucial component for γ-PGA production, can be either obtained from external sources or synthesized endogenously (Wang et al., 2017). When sourced externally, L-glutamic acid directly enters the γ-PGA biosynthesis pathway in which 2-oxoglutarate aminotransferase catalyzes the conversion of α-ketoglutaric acid and glutamine to L-glutamic acid. However, in the endogenous pathway, carbon sources are converted to acetyl CoA via glycolysis then glutamate dehydrogenase is converted to α-ketoglutaric acid and

ammonium chloride through the Krebs cycle, which gives rise to L-glutamic acid (Wang et al.,2017). The γ-PGA biosynthesis pathway involves a series of enzymes such as racemase, synthase, and peptidase, that are involved in γ-PGA biosynthesis (Ogunleye et al., 2015; Wang et al., 2017; Ashiuchi et al., 2010). The first step in γ-PGA biosynthesis is racemization, which involves the conversion of L-glutamate to D-glutamate by glutamate racemase (RacE) coding gene (Luo et al., 2016). This process can be carried out using either exogenous or endogenous L-glutamate. The resulting D-glutamate monomers then polymerize into the growing L-chain (Ashiuchi et al., 2004). In *B. subtilis*, two genes, *racE/glr* and *yrpC,* encode proteins that are homologous to RacE (Ashiuchi et al.,1999; Ashiuchi et al., 2002). An indirect conversion pathway, involving pyruvate as a precursor and three enzymes (L-glutamic acid/pyruvic acid aminotransferase, D-glutamic acid/pyruvic acid aminotransferase, and alanine racemase), is devoted to the transformation to D-glutamic acid (Shih et al., 2001; Wu et al., 2006). The second stage is polymerization and transfer (Buescher and Margaritis, 2007; Luo et al.,2016). L-Glutamate and D-glutamate monomers are transported from the cytoplasm to the cell membrane by γ-PGA synthetase (Pgs), which is encoded by an active membrane enzyme complex (four gene subunits operons: *pgsB, C, A,* and *E*) and the γ-PGA-release gene (*PgsS*) (Ashiuchi, et al., 2002; Urushibata et al., 2002). The PgsBCA complex is responsible for assembling these monomers into γ-PGA and is essential for polymerizing and transporting γ-PGA to the cell membrane (Cao et al., 2018; Ogunleye et al., 2015). *PgsE* is also involved in γ-PGA biosynthesis, particularly when zinc is present (Yamashiro et al., 2011). γ-PGA can be either attached to the cell wall through the homologs of PgsBCA called CapD catalysis or secreted into the surrounding environment through *PgsS* catalysis (Yamashiro et al., 2011). γ-PGA biosynthesis is regulated by intracellular signal transduction mechanisms: ComP-ComA regulator, *DegS-DegU* regulator, whereas SwrA is another regulator of PgsBCA. These mechanisms inhibit γ-PGA production and downregulate the expression level of degradation enzymes. Both *ComP-ComA* and *DegS-DegU* systems regulate the front-end transcription, while SwrA assists in regulation at the post-transcription stage (Osera et al., 2009; Do et al., 2011). Lastly, since γ-PGA is considered a secondary metabolite for *Bacillus* species it can be degraded and utilized as substrate. The catabolism pathway of γ-PGA is tightly regulated by intracellular regulatory mechanisms (Birrer, 1994; Cao et al., 2018).

Three types of hydrolases can degrade γ-PGA:

- **Native γ-PGA hydrolase (PgdS),** encoded by a gene located downstream of the PgsBCA operon, cleaves the γ-glutamyl bonds within the γ-PGA molecule and its expression is tightly regulated (Sha et al., 2019).
- **Cell wall lyases (D- or L-endopeptidase),** such as CwlO, CwlS, LytE, and LytF, break the peptide bonds between glutamic acid residues in γ-PGA (Ashiuchi et al., 2003).
- **γ-Glutamyl transferase (GGT)** hydrolyzes γ-PGA from the N-terminal and releases shorter D- or L-glutamic acid residues, forming di- and tripeptides of γ-glutamic acid (Mitsui et al., 2011).

Gene knockout of *Bacillus* strains can be one effective strategy to regulate and increase γ-PGA production (Scoffone et al., 2013).

1.3.2. γ-PGA production by bacterial fermentation

The biosynthesis of γ-PGA is critically influenced by fermentation conditions, which are crucial determinants of polymer yield. Various factors play pivotal roles in γ-PGA production, including carbon source, nitrogen source, metal ions, temperature, pH, dissolved oxygen, stirring methods, and other aspects of the fermentation system. These factors can all significantly impact the final yield of γ-PGA (Rehm et al., 2022). The main downstream process for γ-PGA production by bacterial fermentation involves the following steps: substrate selection, bacterial inoculation, fermentation, extraction, and purification. The choice of media components and cultivation conditions significantly impacts the yield and properties of γ-PGA. A variety of substrates have been explored for γ-PGA production using either synthetic medium or waste, each with its own set of fermentation conditions for improving γ-PGA yields. Wu et al. (2008) employed ^{13}C isotope tracer methods to investigate the pathway of γ-PGA glutamate-dependent synthesis in a γ-PGA-producing strain of *B. subtilis NX-2*. Their findings revealed that glucose (via glycolysis, the pentose phosphate pathway, the tricarboxylic acid cycle, and other pathways) was metabolized to generate glutamic acid precursors. These precursors were then polymerized to form γ-PGA. Notably, when the glucose concentration in the medium was 40 g/L, only about 9% of the carbon skeleton of γ-PGA derived from glucose. This suggests that glucose served primarily as a growth-limiting substrate for growth and energy metabolism, while

L-glutamic acid was the main source of the carbon skeleton for γ-PGA molecules (Wu et al., 2008). Chen et al. (2005) reported a γ-PGA yield of 45 g/L using soybean cake and swine manure as substrates with *B. subtilis* CCTCC202048, supplemented with glutamic acid and citric acid, following a 48-hour fermentation at 37°C. Zhang et al. (2012) employed cane molasses supplemented with glutamic acid and ammonium sulfate, using *B. subtilis* NX-2, to produce 51.1 g/L of γ-PGA after 96 hours of fermentation at 32°C. Tang et al. (2015) further enhanced the yield by using rice straw hydrolysate, also with glutamic acid and ammonium sulfate, to achieve 73 g/L of γ-PGA using *B. subtilis* NX-2 after 90 hours of fermentation at 32°C. Finally, Kim et al. (2019) examined the potential of macroalgae, sucrose, and L-glutamate, combined with *B. subtilis*. SJ-10, obtaining a γ-PGA yield of 6 g/L after 48 hours of fermentation at 37°C. The addition of metal ions in the medium (including K^{2+}, Ca^{2+}, Na^{2+}, Fe^{2+}, Mg^{2+}, Zn^{2+}, and Mn^{2+}) can promote bacterial cell growth and increase the production of γ-PGA. PgsA contains membrane-anchoring regions that are responsible for positioning the PgsBCA complex on the membrane (Ashiuchi et al., 2002). Homologous sequences of this protein are found in a variety of biological genes, belonging to the family of cytosolute protein serine/threonine phosphatases with divalent cation binding sites, including Zn^{2+}, Mn^{2+}, Fe^{2+}, and Ca^{2+}. PgsA may be responsible for the extracellular transport of γ-PGA (Nordlund et al., 1995; Rusnak and Mertz, 2000). The fermentation process can be conducted using either batch, continuous, or shake flask and different bioreactors can be employed, including submerged fermentation, solid-state fermentation, and moving bed bioreactor. Shake flasks are commonly used for laboratory scale γ-production (Parati et al., 2022).

Following fermentation, centrifugation is typically employed to remove bacterial cells, and the subsequent purification process can significantly impact the efficiency of γ-PGA extraction, which is challenging particularly due to the high viscosity of γ-PGA of high molecular weight (Parati et al., 2022). Upon completion of the purification procedure, γ-PGA can be suspended in water and then subjected to freeze-drying.

1.3.3. γ-PGA purification strategies

The purification process and the hindered recovery due to the high viscosity of the fermentation broth are a major bottleneck for the γ-PGA production and contribute to its high costs (Zhang et al.,2021; Do et al., 2001). The process generally includes centrifugation or sedimentation of the bacterial cells and γ-PGA is recovered from the broth supernatant by alcohol precipitation (75–80% methanol or ethanol *v/v*), or by the addition of divalent copper salts. The ethanol precipitation does not assure the removal of proteins that precipitate along with γ-PGA. Thus, further purification steps are required as concentration by ultra-filtration membranes, dialysis/diafiltration or chromatography to remove small molecules such as salts, exhaust nutrients, and even glutamate monomers. Then, the purified product is further dried by freeze-drying or spray-drying (Do et al., 2001; Kreyenschulte et al., 2014; Kumar et al., 2015; Zhang et al., 2021). New strategies for the recovery and the purification of γ-PGA from the broth supernatant were reported. They include four-unit operations, like acidification, plate and frame filtration, cyclic ultrafiltration, and freeze-drying, to avoid any inefficient precipitation steps and to reduce the purification costs (Zhang et al., 2021). In another case, a hybrid reactor system, that integrated cross-flow microfiltration modules in a fermentation vessel, was employed to continuously produce γ-PGA and directly purify it by using two-stage membrane treatments (Kumar et al., 2015). This approach assured continuous, high-yield production and productivity of γ-PGA by recycling the bacterial cells and an efficient downstream process up to high product purity by removing any inhibiting fermentation products (Kumar et al., 2015). As the fermentative conditions influence the titer of the produced γ-PGA, as well as its Mw and polydispersity index, and because the downstream purification process is a complex and not efficient procedure in which the different chain length populations of γ-PGA are not separated, the commercial samples often contain not pure, highly dispersed γ-PGA multiple forms with different Mw. As the Mw is critical for the γ-PGA applications, new downstream purification approaches are needed, as the classical precipitation procedures are not efficient in obtaining specific, highly homogenous Mw fractions, but only a mixture of different size populations of the homopolypeptide. Previous research has employed ultra-filtration (UF) with plate and frame cassettes of 10 and 100 kDa, combined with nano-filtration, to purify small quantities of γ-PGA (25 g) on a laboratory scale (Sabbah et al., 2020). However, Restaino et al.

(2022) developed a tangentially driven UF process to enhance the recovery of certain fractions by slightly modifying the UF membrane size in the second step. They used this process to purify a larger amount of commercial γ-PGA (COM-PGA) (300 g), which contained a mixture of three different low molecular weight γ-PGA populations. This resulted in increased representation of the other two macromolecular species and high γ-PGA recovery percentages, without requiring extensive purification of the commercial sample or selecting a specific size population of the homopolypeptide. The membrane-based process, on the other hand, enabled the isolation of fractions with relatively homogeneous sizes (54.7 and 17.9 kDa) and a higher purity grade (Restaino et al., 2022).

1.3.4. γ-PGA production challenges

Despite the significant progress in γ-PGA production through microbial fermentation, the process remains encumbered by several challenges. One of the primary hurdles is the intricate quantification of γ-PGA. Factors such as its water-holding capacity, viscosity, structural complexity, and variations in solubility and stability depending on purity, all contribute to the challenges faced during sample preparation. The presence of byproducts further exacerbates this issue, as they compete for substrate and energy, thereby diminishing γ-PGA yield and interfering with its downstream separation and purification (Li et al., 2022). Moreover, while rigorous optimization of variables through methods like *response surface methodology* and *central composite design* have been employed, attaining optimal γ-PGA production remains an objective to pursuit (Mohanraj et al., 2019; Dexin et al., 2020). Genetic and metabolic engineering strategies, while promising, pose their own set of challenges, in fact, even with these modifications, the yield often falls short of expectations (Zhang et al., 2021). Additionally, the selection of suitable microorganisms for γ-PGA production is difficult, particularly when employing high-throughput methods. The lack of precision and repeatability in existing γ-PGA quantification methods further complicates the application of numerical methods such as the design of experiments for optimizing production processes. These complexities underscore the need for more refined methodologies and innovative approaches to overcome these hurdles in γ-PGA production. Microbial fermentation is the most cost-effective method for γ-PGA production compared to alternatives like chemical synthesis and biotransformation, but it still falls short of the desired

economic viability. The need for genetic engineering, the synergistic effect between L-glutamic acid-dependent and independent strain, the growth medium optimization, the process control, and the downstream processing significantly drive-up costs. In summary, despite significant efforts and technological advancements, γ-PGA production through microbial fermentation remains a challenging endeavor marked by complex quantification processes and unsatisfactory yields.

1.3.5. γ-PGA quantification methods

There are several methods for quantifying γ-PGA, each with its advantages and limitations. These methods range from simple and rapid UV-spectrophotometric and colorimetric techniques to more sophisticated but reliable ones, such as ultra-high-performance liquid chromatography and nuclear magnetic resonance analysis. The most used method, developed by Zeng et al. (2012), utilizes the UV absorption spectrum of γ-PGA in aqueous solution, with a maximum absorption wavelength occurring at 216 nm. However, this method requires the sample to be pure, as other polysaccharides may interfere with the measurement. Mohanraj et al. (2019) utilized the dry weight of purified and lyophilized γ-PGA to estimate γ-PGA yield. In 2015, Kongklom et al. employed the surfactant cetyltrimethylammonium bromide (CTAB) method to quantify γ-PGA. This method relies on the formation of a highly specific complex between CTAB and γ-PGA. CTAB binds to γ-PGA chains, forming water-insoluble, highly dispersed micelle-like structures. This complexation leads to an increase in the turbidity of the solution. The γ-PGA concentration is determined by measuring the turbidity of the mixture using a spectrophotometer at 400 nm and comparing it to a standard curve prepared with a pure γ-PGA sample. However, CTAB may also interact with other polysaccharides present in the sample. Kubo et al., 2021 have also developed a High-Performance Liquid Chromatography (HPLC) method specifically for quantifying γ-PGA content in natto, a fermented soybean product rich in γ-PGA. The process involves lyophilizing and powdering natto, optimizing protein and peptide removal, ethanol precipitation, hydrochloric acid degradation, and quantifying glutamic acid using HPLC. Restaino et al. (2022) have developed a new method based on Ultra High-Performance Liquid Chromatography (UHPLC) to determine γ-PGA concentration on the base of the L-glutamic acid monomer determination after acidic hydrolysis of the homopolypeptide.

NMR and FTIR are additional methods that have been used for γ-PGA quantification (Rafalskiy et al., 2022).

1.3.6. γ-PGA applications

γ-PGA has astonishing applications across diverse fields, including agriculture, food, cosmeceuticals, tissue engineering, regenerative medicine, drug delivery, environmental protection, and wastewater treatment. In agriculture, γ-PGA has been employed as a fertilizer, as demonstrated by Wang et al. (2008). Additionally, Pang et al. (2018) reported that γ-PGA effectively alleviated the growth inhibition of cucumber seedlings induced by Pb and Cd stresses. As γ-PGA concentration increased, chlorophyll a and b levels in cucumber seedings also augmented, as the concentration of Pb and Cd in cucumber seedings declined by 74.13% and 38.65%, respectively. In the food industry, γ-PGA holds remarkable applications as a flavoring agent, shelf-life extender, stability enhancer and oil reduction tool for fried foods (Lim et al., 2012; Guan et al., 2023). Moreover, γ-PGA functions as a dietary supplement by reducing the sensitivity of gastrointestinal enzymes, increasing calcium absorption and solubility, and contributing to the treatment of osteoporosis. Notably, γ-PGA inhibits the formation of calcium phosphate in our body by enhancing the passive transport in the small intestine (Tanimoto et al., 2001; Tanimoto et al., 2007). Sakamoto and Kawase (2016) employed both water-insoluble γ-PGA and water-soluble sodium salt forms of γ-PGA (γ-PGA-Na) as a low-cost, safe, and environmentally friendly biological adsorbent to recover cesium from radioactive wastewater. The adsorption of cesium (Cs) by γ-PGA and γ-PGA-Na in radioactive wastewater occurs through electrostatic interaction between carboxylic acid anions ($-COO^-$) and cesium cations (Cs^+) via a chemical reaction. Furthermore, Sun et al. (2020) modified the double bond of γ-PGA and incorporated antibacterial polylysine through photopolymerization using visible light to create an antibacterial and biocompatible hydrogel that effectively repaired and regenerated skin infections. In addition, γ-PGA with high molecular weight demonstrates exceptional moisture retention and water absorption, forming a protective barrier on the skin. It effectively inhibits skin moisture loss and can penetrate deep into the skin, effectively restoring the skin's natural moisture balance (Li et al., 2022). More recently, Restaino et al., 2022 investigated the low Mw of ultrafiltrate γ-PGA fractions for their potential bioactivity. Purified γ-PGA fractions were found to counteract desiccation and oxidative stress in

keratinocyte monolayers, suggesting a potential therapeutic option for oxidative stress-related diseases and modulating antioxidant defense pathways. Considering environmental concerns, novel crosslinked materials derived from γ-PGA, showcasing thermoplastic and saloplastic properties with promising applications across various fields including bio-packaging, were developed (Hejazi et al., 2023).

1.4. Chitosan

CH is a biopolymer composed of β-1,4-linked glucosamine (**Fig.5**), partially acetylated (≤ 25%), obtained through alkaline deacetylation (Pakizeh et al., 2021) from chitin, the second most abundant polysaccharide in nature (an estimated 1 billion tons of chitin are produced each year in the biosphere). Commercially, chitin is extracted from the shells of crabs, shrimps, shellfish and lobsters, which are major by-products of the seafood industry. CH dissolves in acidic aqueous solutions where its amino groups are protonated (Motiei et al., 2021), enabling the formation of polyelectrolyte complexes with highly negatively charged polymers like γ-PGA (Paini et al., 2015). CH exhibits excellent biocompatibility, non-toxicity, non-immunogenicity, and biodegradability (Baharlouei et al., 2022). Moreover, its sustainable production from renewable resources makes it an appealing material for bio-ink, 3D printing, and scaffolding in various applications, including regenerative tissue engineering, drug delivery, and food packaging (Lazaridou et al., 2022; Moeini et al., 2018; Motiei et al., 2021).

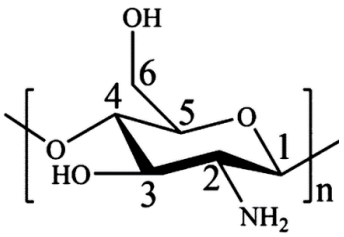

Fig.5. Chitosan (CH) structure

1.5. Polyelectrolyte complexations and hydrogels formation

Polyelectrolyte complexes (PECs) are formed when two or more oppositely charged polymers interact with each other. While this is typically the case, PECs can also form among polymers with similar charges (both positive or both negative) under certain conditions

(Kizilay et al., 2011). 3D PECs have been investigated since the early 20th century when coacervation phenomena were first described (Bungenberg de Jong, & Kruyt, 1929; Overbeek & Voorn, 1957). However, their sensitivity to environmental factors like salt and humidity limited their use in large-scale applications (Visakh, 2014). In the 1960s, Michaeles (1965) proposed casting PECs into films, and much later, the group led by Shclenoff (2012) introduced a novel extrusion method based on saloplastics. Saloplastics, or hydrated compact PECs, are highly promising materials from a polymer science perspective due to their interpenetrated networks (Porcel and Schlenoff, 2009). Mundo et al. (2020) successfully prepared insoluble PECs using anionic γ-PGA and cationic ε-poly-L-lysine (PLL) under acidic conditions where the electrostatic attraction is strong. However, soluble complexes formed when the electrostatic attraction was weaker. Hydrogels are materials that offer significant promising applications thanks to their 3D polymer network structure capable of retaining substantial amounts of water in a swollen state. The swelling behavior of hydrogels is finely tuned by a balance between hydration forces and counteracting forces exerted by crosslinked polymer chains that resist expansion (Chiesa et al., 2019). Polymer crosslinking can be achieved through chemical covalent bonds, non-covalent interactions between the chains, or by a combination of both. Synthetic polymers such as polyacrylamides, poly (ethylene glycol)-polyester block copolymers, and naturally occurring polymers (such as CH, alginate, hyaluronic acid, and gelatin) have been extensively explored as the basis for thermosetting hydrogels (Zhang et al., 2012; Ju et al., 2014; Piao et al., 2015; Ghobril et al., 2015, Zhuang et al., 2015). Recently, Hejazi et al. (2023) developed a new class of crosslinked materials that exhibit both saloplastic and thermoplastic properties (data contained in the present PhD thesis). As at acidic pH value, CH and γ-PGA are positively and negatively charged, respectively, they could be employed for the preparation of new hydrogel materials based on non-covalent, electrostatic interactions. They were prepared by physical blending of CH and γ-PGA using three different ratios of ultrafiltrate low molecular weight γ-PGA. These materials can exist as rubbery hydrogels or glass-like thermoplastics depending on their hydration levels. The obtained supramolecular complexes exhibited advantageous physical characteristics, thermal stability, and amorphous and crystalline structures, opening new possibilities for applications of the obtained biomaterials in diverse fields.

In the pursuit of sustainable development for the new materials, a promising possibility involves the potential use of biodegradable hydrogels in heritage restorations and renovations as well as bio-adhesive materials. In its various forms and uses, adhesive products have become indispensable in modern life, playing a vital role in assembling, and repairing numerous items and structures (Ferdosian et al., 2017). Finding a bio-based glue to replace petroleum-based glues is essential, as commercial glues such as formaldehyde, phenolic resin, and synthetic polyvinyl-based ones are a major concern due to their toxicity, carcinogenicity, and immigrant airborne pollutants (Gajra et al., 2012). Thus, in recent times, hydrophilic adhesives have garnered attention from both researchers and consumers owing to their compatibility, environmentally friendly nature, and user-friendly applications. Santoni et al. (2013) investigated various protein sources for their potential as wood adhesives suitable for indoor applications. These protein sources included zein, a component of maize (*Zea mays L*.), pea (*Pisum sativum L*.) protein, and two different soy (*Glycine max L*.) protein-based products, one treated with alkali and the other untreated (Santoni et al., 2013). Recently, Hejazi et al. (unpublished data object of the present PhD thesis, *a*) explored the potential of using the 3D hydrogel developed as a bio-adhesive on various substrates, including aluminum and wood. This research focuses on investigating the structural, rheological, morphological, and thermal properties of the innovative CH/γ-PGA hydrogel and its potential applications on different surfaces. Six hydrogels were prepared by physically blending CH (285 kDa) with two different γ-PGA fractions with distinct molecular weights obtained via ultrafiltration of a microbial product, and the polypeptide was crosslinked with CH at three different ratios following the method described previously by Hejazi et al. (2023).

This research represents a significant breakthrough in biotechnology, particularly in the utilization of γ-PGA for the development of bioplastics. For the first time, we successfully created these novel materials using commercially available γ-PGA, subjecting it to ultrafiltration purification and employing cost-effective methods such as traditional casting and thermal compression. The resulting bioplastics exhibit edible properties, making them suitable for different industrial applications. Additionally, novel materials were produced through the physical blending of polyelectrolytes, leading to the formation of 3D smart material. These materials demonstrate dual characteristics, opening up diverse possibilities for applications. In a pioneering move,

we applied these materials as a bio-glue on wood and aluminum, exploring their potential for cultural heritage and restoration purposes. Furthermore, our study delves into the production of γ-PGA using bacterial engineering strains. Through mutations and double knockout on *Bacillus subtilus* JH642, we achieved higher molecular weight γ-PGA. This variant of γ-PGA was employed in the preparation of hydrogel materials, yielding intriguing results and expanding its potential for medical applications. In contrast to previous studies focusing on high molecular weight γ-PGA (>200 kDa), our approach considers the broader scope of applications. Notably, we diverge from the traditional methods, as exemplified by Yang et al. (2021) using 700 kDa γ-PGA with thiol-methacrylate Michael chemistry-mediated post-stabilization. Meanwhile, Bajestani et al. (2020) utilized 800 kDa γ-PGA for creating γ-PGA-keratin based hydrogel, targeting wound healing. Pisani et al. (2019) employed MW 800 kDa γ-PGA from Natto Bioscience, utilizing polyelectrolyte complex formation for 3D bioink applications. Importantly, our study uniquely explores the dual characteristics of the crosslinked material, providing innovative solutions for challenges in the plastic industry, medical field, 3D printing, cosmeceuticals, and cultural heritage, setting it apart from traditional approaches.

1.5. Aim of PhD project

Like an astronaut venturing into the depths of space, this project delved into the exploration of the microbial poly-γ-glutamic acid (γ-PGA), a polypeptide possessing immense potential for sustainable and eco-friendly applications. Hence, the general objective of the present PhD project was the **optimization and reinforcement of homopolypeptide-based bioplastics** to obtain novel materials with improved technological properties. In fact, little is known about the ability of polypeptides constituted by the same amino acid to give rise, under selective experimental conditions, to materials with plastic-like properties. Hence this project aimed to address the critical challenges concerning γ-PGA, including its low yield, purity, and cost which hinder its widespread adoption. An eco-friendly and industrial scale-up purification process was adopted to purify the commercially available inexpensive γ-PGA, and its physicochemical characterization was explored. The possibility of using purified and low molecular weight homopolypeptide was also investigated and innovative materials were obtained by hot compression. Furthermore, an innovative material by

blending γ-PGA with the polysaccharide CH was prepared, aiming to enhance both polymers properties and expand their applicability synergistically. The materials were obtained using a pioneering approach based on physical blending. Their physicochemical characterization was performed, shedding light on their structure, properties, and potential applications. In addition, the feasibility of employing an engineered bacterial strain for synthesizing pure γ-PGA was also investigated. The resulting material was blended with CH, leading to the development of a promising biomaterial with potential biomedical applications (Hejazi et al., unpublished *chapter 5*). The final part of the thesis, completed during a study abroad in Wroclaw University, involved developing a novel spectrophotometric approach based on the ninhydrin reaction for γ-PGA quantification. Additionally, a screening of various bacterial strains isolated from different polish kinds of honey was conducted to assess their potential for producing γ-PGA. This project was aimed at significantly understanding the properties, production and applications of γ-PGA, while also contributing to the development of sustainable and environmentally friendly materials with a wide range of potential applications. In the next paragraphs, the results obtained during the first 2 years of the PhD course are reported as published articles (**Chapter 2** and **Chapter 3)**. **Chapter 2** (Restaino et al., 2022) is related to the purification methods of γ-PGA contained in the commercial source (COM-PGA) by means of organic solvent precipitation and ultrafiltration. **Chapter 3** (Hejazi et al., 2023) instead focuses on the manufacture and the physicochemical characterization of novel glass-like crosslinked materials by employing a polyelectrolyte complexation approach between the purified anionic γ-PGA and the cationic polysaccharide CH. Since these crosslinked materials appeared in hydrated forms as manipulable and mouldable hydrogels, this aspect is the topic of **Chapter 4,** where the characterization and application as bio-glue of the obtained hydrogels are reported (Hejazi et al. unpublished). The data from **Chapter 2 and Chapter 3** were obtained also thanks to the collaboration with Prof. Chiara Schiraldi (University of Campania Luigi Vanvitelli, Department of Experimental Medicine). During the 3rd year of PhD, 10 days were spent at the University of Pavia (Department of Biology and Biotechnology) where, under the supervision of Dr. Cinzia Calvio, two different bacterial engineering *Bacillus* strains were used for high molecular weight γ-PGA production through a fermentation process in shake flasks. The produced γ-PGA was further characterized according to its molecular weight through gel chromatography

technique and quantified through NMR. All these data are presented in **Chapter 5** where the formation of a crosslinked material between the produced γ-PGA and CH for potential application in biomedical sector is also detailed. Finally, thanks to the collaboration at the University of Wroclaw with Prof. Marcin Łukaszewicz, 3 months were spent (from June 2023 to September 2023) at the Department of Biotransformation, Biotechnology Faculty. A comprehensive study to screen different *Bacillus* strains for possible γ-PGA were carried out. The multiple techniques employed to evaluate the γ-PGA production, including mucoidal assessment and NMR analysis, and its quantification through a novel developed method based on ninhydrin assay, are extensively illustrated in **Chapter 6**.

References:

1. Anderson, A., Andrady, A., Arthur, C., Baker, J., Bouwman, H., Gall, S., ... & Wyles, K. (2015). Sources, fate and effects of microplastics in the marine environment: a global assessment. GESAMP Rep Stud (90).
2. Ashiuchi, M. (2010). Occurrence and biosynthetic mechanism of poly-gamma-glutamic acid. Amino-acid homopolymers occurring in nature, 77-93.
3. Ashiuchi, M., & Misono, H. (2002). Biochemistry and molecular genetics of poly-γ-glutamate synthesis. Applied microbiology and biotechnology, 59, 9-14.
4. Ashiuchi, M., Kamei, T., & Misono, H. (2003). Poly-γ-glutamate synthetase of Bacillus subtilis. Journal of Molecular Catalysis B: Enzymatic, 23(2-6), 101-106.
5. Ashiuchi, M., Nakamura, H., Yamamoto, T., Kamei, T., Soda, K., Park, C., ... & Misono, H. (2003). Poly-γ-glutamate depolymerase of Bacillus subtilis: production, simple purification and substrate selectivity. Journal of Molecular Catalysis B: Enzymatic, 23(2-6), 249-255.
6. Ashiuchi, M., Shimanouchi, K., Nakamura, H., Kamei, T., Soda, K., Park, C., ... & Misono, H. (2004). Enzymatic synthesis of high-molecular-mass poly-γ-glutamate and regulation of its stereochemistry. Applied and environmental microbiology, 70(7), 4249-4255.
7. Ashiuchi, M., Soda, K., & Misono, H. (1999). Characterization of yrpC gene product of *Bacillus subtilis* IFO 3336 as glutamate racemase isozyme. Bioscience, biotechnology, and biochemistry, 63(5), 792-798.
8. Babu, R. P., O'connor, K., & Seeram, R. (2013). Current progress on bio-based polymers and their future trends. Progress in biomaterials, 2, 1-16.
9. Baharlouei, P., & Rahman, A. (2022). Chitin and chitosan: Prospective biomedical applications in drug delivery, cancer treatment, and wound healing. Marine Drugs, 20(7), 460.
10. Bajaj, I., & Singhal, R. (2011). Poly (glutamic acid)–an emerging biopolymer of commercial interest. Bioresource technology, 102(10), 5551-5561.
11. Bajestani, M. I., Kader, S., Monavarian, M., Mousavi, S. M., Jabbari, E., & Jafari, A. (2020). Material properties and cell compatibility of poly (γ-glutamic acid)-keratin hydrogels. International journal of biological macromolecules, 142, 790-802.
12. Birrer, G. A., Cromwick, A. M., & Gross, R. A. (1994). γ-Poly (glutamic acid) formation by Bacillus licheniformis 9945a: physiological and biochemical studies. International journal of biological macromolecules, 16(5), 265-275.

13. Browne, M. A., Crump, P., Niven, S. J., Teuten, E., Tonkin, A., Galloway, T., & Thompson, R. (2011). Accumulation of microplastic on shorelines woldwide: sources and sinks. Environmental science & technology, 45(21), 9175-9179.
14. Buescher, J. M., & Margaritis, A. (2007). Microbial biosynthesis of polyglutamic acid biopolymer and applications in the biopharmaceutical, biomedical and food industries. Critical reviews in biotechnology, 27(1), 1-19.
15. Bungenberg de Jong, H. G., & Kruyt, H. R. (1929). Coacervation (partial miscibility in colloid systems). In Proc. K. Ned. Akad. Wet (Vol. 32, pp. 849-856).
16. Cao, M., Feng, J., Sirisansaneeyakul, S., Song, C., & Chisti, Y. (2018). Genetic and metabolic engineering for microbial production of poly-γ-glutamic acid. Biotechnology advances, 36(5), 1424-1433.
17. Chen, Q., Gao, J., Yu, H., Su, H., Yang, Y., Cao, Y., ... & Liu, H. (2022). An emerging role of microplastics in the etiology of lung ground glass nodules. Environmental Sciences Europe, 34(1), 25.
18. Chen, X., Chen, S., Sun, M., & Yu, Z. (2005). High yield of poly-γ-glutamic acid from Bacillus subtilis by solid-state fermentation using swine manure as the basis of a solid substrate. Bioresource technology, 96(17), 1872-1879.
19. Chiesa, E., Genta, I., Dorati, R., Modena, T., & Conti, B. (2019). Poly (gamma-glutamic acid) based thermosetting hydrogels for injection: Rheology and functional parameters evaluation. Reactive and Functional Polymers, 140, 93-102.
20. Çobanoğlu, H., Belivermiş, M., Sıkdokur, E., Kılıç, Ö., & Çayır, A. (2021). Genotoxic and cytotoxic effects of polyethylene microplastics on human peripheral blood lymphocytes. Chemosphere, 272, 129805.
21. Cox, K. D., Covernton, G. A., Davies, H. L., Dower, J. F., Juanes, F., & Dudas, S. E. (2019). Human consumption of microplastics. Environmental science & technology, 53(12), 7068-7074.
22. Dexin, W., Hyangmi, K., Sungbeom, L., Dae-Hyuk, K., & Min-Ho, J. (2020). Simultaneous production of poly-γ-glutamic acid and 2, 3-butanediol by a newly isolated *Bacillus subtilis* CS13.
23. Do, J. H., Chang, H. N., & Lee, S. Y. (2001). Efficient recovery of γ-poly (glutamic acid) from highly viscous culture broth. Biotechnology and bioengineering, 76(3), 219-223.
24. Do, T. H., Suzuki, Y., Abe, N., Kaneko, J., Itoh, Y., & Kimura, K. (2011). Mutations suppressing the loss of DegQ function in Bacillus subtilis (natto) poly-γ-glutamate synthesis. Applied and environmental microbiology, 77(23), 8249-8258.
25. Ferdosian, F., Pan, Z., Gao, G., & Zhao, B. (2017). Bio-based adhesives and evaluation for wood composites application. Polymers, 9(2), 70.

26. Gajra, B., Pandya, S. S., Vidyasagar, G., Rabari, H., Dedania, R. R., & Rao, S. (2012). Poly vinyl alcohol hydrogel and its pharmaceutical and biomedical applications: A review. Int. J. Pharm. Res, 4, 2026.
27. Ghobril, C., & Grinstaff, M. W. (2015). The chemistry and engineering of polymeric hydrogel adhesives for wound closure: a tutorial. Chemical Society Reviews, 44(7), 1820-1835.
28. Giosafatto, C. V. L., & Porta, R. (2023). Advanced Biomaterials for Food Edible Coatings. International Journal of Molecular Sciences, 24(12), 9929.
29. Guan, E., Zhang, T., Wu, K., Yang, Y., & Bian, K. (2023). Physicochemical properties and gluten structures of frozen steamed bread dough under freeze–thaw treatment affected by gamma-polyglutamic acid. Food Hydrocolloids, 137, 108334.
30. Hejazi, S., Restaino, O. F., Sabbah, M., Zannini, D., Di Girolamo, R., Marotta, A., ... & Porta, R. (2023). Physicochemical Characterization of Chitosan/Poly-γ-Glutamic Acid Glass-like Materials. International Journal of Molecular Sciences, 24(15), 12495.
31. Ho, G. H., Ho, T. I., Hsieh, K. H., Su, Y. C., Lin, P. Y., Yang, J., ... & Yang, S. C. (2006). γ-Polyglutamic acid produced by Bacillus Subtilis (Natto): Structural characteristics, chemical properties and biological functionalities. Journal of the Chinese Chemical Society, 53(6), 1363-1384.
32. Horvatits, T., Tamminga, M., Liu, B., Sebode, M., Carambia, A., Fischer, L., ... & Fischer, E. K. (2022). Microplastics detected in cirrhotic liver tissue. EBioMedicine, 82.
33. Hwang, J., Choi, D., Han, S., Choi, J., & Hong, J. (2019). An assessment of the toxicity of polypropylene microplastics in human derived cells. Science of the Total Environment, 684, 657-669.
34. Ito, Yoshihito, Takeshi Tanaka, Tetsuo Ohmachi, and Yoshihiro Asada. (1996). Glutamic acid independent production of poly (γ-glutamic acid) by Bacillus subtilis TAM-4. Bioscience, biotechnology, and biochemistry 60, no. 8 1239-1242.
35. Ju, H. W., Lee, O. J., Moon, B. M., Sheikh, F. A., Lee, J. M., Kim, J. H., ... & Lee, H. R. (2014). Silk fibroin based hydrogel for regeneration of burn induced wounds. Tissue Engineering and Regenerative Medicine, 11, 203-210.
36. Kim, J. H., Lee, J. M., Jang, W. J., Park, H. D., Kim, Y. O., Kim, C. H., & Kong, I. S. (2019). Efficient production of poly γ-d-glutamic acid from the bloom-forming green macroalgae, Ulva sp., by Bacillus sp. SJ-10. Biotechnology and Bioengineering, 116(7), 1594-1603.
37. Kizilay, E., Kayitmazer, A. B., & Dubin, P. L. (2011). Complexation and coacervation of polyelectrolytes with oppositely charged colloids. Advances in colloid and interface science, 167(1-2), 24-37.

38. Koelmans, B., Pahl, S., Backhaus, T., Bessa, F., van Calster, G., Contzen, N., ... & Wright, S. (2019). A scientific perspective on microplastics in nature and society. SAPEA.
39. Kongklom, N., Luo, H., Shi, Z., Pechyen, C., Chisti, Y., & Sirisansaneeyakul, S. (2015). Production of poly-γ-glutamic acid by glutamic acid-independent Bacillus licheniformis TISTR 1010 using different feeding strategies. Biochemical Engineering Journal, 100, 67-75.
40. Kosuth, M., Mason, S. A., & Wattenberg, E. V. (2018). Anthropogenic contamination of tap water, beer, and sea salt. PloS one, 13(4), e0194970.
41. Kreyenschulte, D., Krull, R., & Margaritis, A. (2014). Recent advances in microbial biopolymer production and purification. Critical reviews in biotechnology, 34(1), 1-15.
42. Kubo, Y., Kobori, M., Nakagawa, R., Yoshiura, T., Asano, T., Takeda, A., & Noguchi, T. (2021). A high-accuracy method for quantifying poly-gamma-glutamic acid content in natto. Food Science and Technology Research, 27(3), 463-471.
43. Kumar, R., & Pal, P. (2015). Fermentative production of poly (γ-glutamic acid) from renewable carbon source and downstream purification through a continuous membrane-integrated hybrid process. Bioresource technology, 177, 141-148.
44. Kutralam-Muniasamy, G., Shruti, V. C., Pérez-Guevara, F., & Roy, P. D. (2023). Microplastic diagnostics in humans:“The 3Ps” Progress, problems, and prospects. Science of The Total Environment, 856, 159164.
45. Lazaridou, M., Bikiaris, D. N., & Lamprou, D. A. (2022). 3D bioprinted chitosan-based hydrogel scaffolds in tissue engineering and localised drug delivery. Pharmaceutics, 14(9), 1978.
46. Li, S., Qiu, Y., Xu, H., Wang, R., & Lei, P. (2022). Recent Advances in Poly-(γ-Glutamic Acid) Production by Microbial Fermentation. Microbial Production of High-Value Products, 237-269.
47. Lim, S. M., Kim, J., Shim, J. Y., Imm, B. Y., Sung, M. H., & Imm, J. Y. (2012). Effect of poly-γ-glutamic acids (PGA) on oil uptake and sensory quality in doughnuts. Food Science and Biotechnology, 21, 247-252.
48. Llorca, M., & Farré, M. (2021). Current insights into potential effects of micro-nanoplastics on human health by in-vitro tests. Frontiers in Toxicology, 3, 752140.
49. Luo, Z., Guo, Y., Liu, J., Qiu, H., Zhao, M., Zou, W., & Li, S. (2016). Microbial synthesis of poly-γ-glutamic acid: current progress, challenges, and future perspectives. Biotechnology for Biofuels, 9(1), 1-12.
50. Michaels, A. S. (1965). Polyelectrolyte complexes. Industrial & Engineering Chemistry, 57(10), 32-40.

51. Mitsui, N., Murasawa, H., & Sekiguchi, J. (2011). Disruption of the cell wall lytic enzyme CwlO affects the amount and molecular size of poly-γ-glutamic acid produced by Bacillus subtilis (natto). The Journal of general and applied microbiology, 57(1), 35-43.
52. Moeini, A., Cimmino, A., Dal Poggetto, G., Di Biase, M., Evidente, A., Masi, M., ... & Malinconico, M. (2018). Effect of pH and TPP concentration on chemico-physical properties, release kinetics and antifungal activity of Chitosan-TPP-Ungeremine microbeads. Carbohydrate polymers, 195, 631-641.
53. Mohanraj, R., Gnanamangai, B. M., Ramesh, K., Priya, P., Srisunmathi, R., Poornima, S., ... & Robinson, J. P. (2019). Optimized production of gamma poly glutamic acid (γ-PGA) using sago. Biocatalysis and Agricultural Biotechnology, 22, 101413.
54. Motiei, M., Mirahmadi-Zare, S. Z., & Nasr-Esfahani, M. H. (2021). Chemical stabilization of γ-polyglutamate by chitosan and the effect of co-solvents on the stability. Biophysical Chemistry, 275, 106605.
55. Mundo, J. L. M., Liu, J., Tan, Y., Zhou, H., Zhang, Z., & McClements, D. J. (2020). Characterization of electrostatic interactions and complex formation of ɣ-poly-glutamic acid (PGA) and ε-poly-l-lysine (PLL) in aqueous solutions. Food Research International, 128, 108781.
56. Nakajima, H., Dijkstra, P., & Loos, K. (2017). The recent developments in biobased polymers toward general and engineering applications: Polymers that are upgraded from biodegradable polymers, analogous to petroleum-derived polymers, and newly developed. Polymers, 9(10), 523.
57. Nordlund, P., & Eklund, H. (1995). Di-iron—carboxylate proteins. Current opinion in structural biology, 5(6), 758-766.
58. Ogunleye, Adetoro, Aditya Bhat, Victor U. Irorere, David Hill, Craig Williams, and Iza Radecka. (2015). Poly-γ-glutamic acid: production, properties and applications. Microbiology 161, 1-17.
59. Osera, C., Amati, G., Calvio, C., & Galizzi, A. (2009). SwrAA activates poly-γ-glutamate synthesis in addition to swarming in Bacillus subtilis. Microbiology, 155(7), 2282-2287.
60. Overbeek, J. T., & Voorn, M. J. (1957). Phase separation in polyelectrolyte solutions. Theory of complex coacervation. Journal of Cellular and Comparative Physiology, 49(S1), 7-26.
61. Paini, M., Aliakbarian, B., Casazza, A. A., Perego, P., Ruggiero, C., & Pastorino, L. (2015). Chitosan/dextran multilayer microcapsules for polyphenol co-delivery. Materials Science and Engineering: C, 46, 374-380.
62. Pakizeh, M., Moradi, A., & Ghassemi, T. (2021). Chemical extraction and modification of chitin and chitosan from shrimp shells. European Polymer Journal, 159, 110709.

63. Pang, X., Lei, P., Feng, X., Xu, Z., Xu, H., & Liu, K. (2018). Poly-γ-glutamic acid, a bio-chelator, alleviates the toxicity of Cd and Pb in the soil and promotes the establishment of healthy Cucumis sativus L. seedling. Environmental Science and Pollution Research, 25, 19975-19988.
64. Parati, M., Khalil, I., Tchuenbou-Magaia, F., Adamus, G., Mendrek, B., Hill, R., & Radecka, I. (2022). Building a circular economy around poly (D/L-γ-glutamic acid) a smart microbial biopolymer. Biotechnology Advances, 108049.
65. Park, S. B., Sung, M. H., Uyama, H., & Han, D. K. (2021). Poly (glutamic acid): Production, composites, and medical applications of the next-generation biopolymer. Progress in Polymer Science, 113, 101341.
66. Piao, Y. Z., & Chen, B. Q. (2015). Characterization, Formation Mechanisms, and pH-Sensitive Drug Release Behavior. Journal of Polymer Science Part B: Polymer Physics, 53(5), 356-367.
67. Pisani, S., Dorati, R., Scocozza, F., Mariotti, C., Chiesa, E., Bruni, G., ... & Conti, B. (2020). Preliminary investigation on a new natural based poly (gamma-glutamic acid)/Chitosan bioink. Journal of Biomedical Materials Research Part B: Applied Biomaterials, 108(7), 2718-2732.
68. Porcel, C. H., & Schlenoff, J. B. (2009). Compact polyelectrolyte complexes:“saloplastic” candidates for biomaterials. Biomacromolecules, 10(11), 2968-2975.
69. Porta, R. (2019). The plastics sunset and the bio-plastics sunrise. Coatings, 9(8), 526.
70. Rafalskiy, V. V., Zyubin, A. Y., Moiseeva, E. M., Kupriyanova, G. S., Mershiev, I. G., Kryukova, N. O., ... & Doktorova, S. A. (2022). Application of vibrational spectroscopy and nuclear magnetic resonance methods for drugs pharmacokinetics research. Drug Metabolism and Personalized Therapy, 38(1), 3-13.
71. Rehm, B. H., & Wibowo, D. (Eds.). (2022). Microbial Production of High-Value Products Springer Nature.
72. Restaino, O. F., Hejazi, S., Zannini, D., Giosafatto, C. V. L., Di Pierro, P., Cassese, E., ... & Porta, R. (2022). Exploiting Potential Biotechnological Applications of Poly-γ-glutamic Acid Low Molecular Weight Fractions Obtained by Membrane-Based Ultra-Filtration. Polymers, 14(6), 1190.
73. Rusnak, F., & Mertz, P. (2000). Calcineurin: form and function. Physiological reviews, 80(4), 1483-1521.
74. Sabbah, M., Di Pierro, P., Ruffo, F., Schiraldi, C., Alfano, A., Cammarota, M., & Porta, R. (2020). Glutamic acid as repeating building block for bio-based films. Polymers, 12(7), 1613.
75. Sakamoto, S., & Kawase, Y. (2016). Adsorption capacities of poly-γ-glutamic acid and its sodium salt for cesium removal from radioactive wastewaters. Journal of environmental radioactivity, 165, 151-158.

76. Sana, S. S., Dogiparthi, L. K., Gangadhar, L., Chakravorty, A., & Abhishek, N. (2020). Effects of microplastics and nanoplastics on marine environment and human health. Environmental Science and Pollution Research, 27, 44743-44756.
77. Santoni, I., & Pizzo, B. (2013). Evaluation of alternative vegetable proteins as wood adhesives. Industrial crops and products, 45, 148-154.
78. Scoffone, V., Dondi, D., Biino, G., Borghese, G., Pasini, D., Galizzi, A., & Calvio, C. (2013). Knockout of pgdS and ggt genes improves γ-PGA yield in B. subtilis. Biotechnology and Bioengineering, 110(7), 2006-2012.
79. Sha, Y., Sun, T., Qiu, Y., Zhu, Y., Zhan, Y., Zhang, Y., ... & Xu, H. (2019). Investigation of glutamate dependence mechanism for poly-γ-glutamic acid production in Bacillus subtilis on the basis of transcriptome analysis. Journal of agricultural and food chemistry, 67(22), 6263-6274.
80. Shi, Q., Tang, J., Liu, R., & Wang, L. (2022). Toxicity in vitro reveals potential impacts of microplastics and nanoplastics on human health: A review. Critical Reviews in Environmental Science and Technology, 52(21), 3863-3895.
81. Shih, L., & Van, Y. T. (2001). The production of poly- (γ-glutamic acid) from microorganisms and its various applications. Bioresource Technology, 79(3), 207-225.
82. Sirisansaneeyakul, S., Cao, M., Kongklom, N., Chuensangjun, C., Shi, Z., & Chisti, Y. (2017). Microbial production of poly-γ-glutamic acid. World Journal of Microbiology and Biotechnology, 33, 1-8.
83. Stephens, B., Azimi, P., El Orch, Z., & Ramos, T. (2013). Ultrafine particle emissions from desktop 3D printers. *Atmospheric Environment*, *79*, 334-339.
84. Sung, M. H., Park, C., Kim, C. J., Poo, H., Soda, K., & Ashiuchi, M. (2005). Natural and edible biopolymer poly-γ-glutamic acid: synthesis, production, and applications. The Chemical Record, 5(6), 352-366.
85. Tang, B., Lei, P., Xu, Z., Jiang, Y., Xu, Z., Liang, J., ... & Xu, H. (2015). Highly efficient rice straw utilization for poly-(γ-glutamic acid) production by Bacillus subtilis NX-2. Bioresource technology, 193, 370-376.
86. Tanimoto, H., Fox, T., Eagles, J., Satoh, H., Nozawa, H., Okiyama, A., ... & Fairweather-Tait, S. J. (2007). Acute effect of poly-γ-glutamic acid on calcium absorption in post-menopausal women. Journal of the American College of Nutrition, 26(6), 645-649.
87. Tanimoto, H., Mori, M., Motoki, M., Torii, K., Kadowaki, M., & Noguchi, T. (2001). Natto mucilage containing poly-γ-glutamic acid increases soluble calcium in the rat small intestine. Bioscience, biotechnology, and biochemistry, 65(3), 516-521.

88. Urushibata, Y., Tokuyama, S., & Tahara, Y. (2002). Difference in transcription levels of cap genes for γ-polyglutamic acid production between Bacillus subtilis IFO 16449 and Marburg 168. Journal of bioscience and bioengineering, 93(2), 252-254.
89. Visakh, P. M. (2014). Polyelectrolyte: thermodynamics and rheology: state of art, new challenges and opportunities. Polyelectrolytes: Thermodynamics and Rheology, 1-17.
90. Wang, L. L., Chen, J. T., Wang, L. F., Wu, S., Zhang, G. Z., Yu, H. Q., ... & Shi, Q. S. (2017). Conformations and molecular interactions of poly-γ-glutamic acid as a soluble microbial product in aqueous solutions. Scientific reports, 7(1), 12787.
91. Wang, Q., Chen, S., Zhang, J., Sun, M., Liu, Z., & Yu, Z. (2008). Co-producing lipopeptides and poly-γ-glutamic acid by solid-state fermentation of Bacillus subtilis using soybean and sweet potato residues and its biocontrol and fertilizer synergistic effects. Bioresource technology, 99(8), 3318-3323.
92. Wu, Q., Xu, H., Shi, N., Yao, J., Li, S., & Ouyang, P. (2008). Improvement of poly (γ-glutamic acid) biosynthesis and redistribution of metabolic flux with the presence of different additives in Bacillus subtilis CGMCC 0833. Applied microbiology and biotechnology, 79, 527-535.
93. Wu, Q., Xu, H., Xu, L., & Ouyang, P. (2006). Biosynthesis of poly (γ-glutamic acid) in *Bacillus subtilis* NX-2: regulation of stereochemical composition of poly (γ-glutamic acid). Process Biochemistry, 41(7), 1650-1655.
94. Yamashiro, D., Yoshioka, M., & Ashiuchi, M. (2011). Bacillus subtilis pgsE (Formerly ywtC) stimulates poly-γ-glutamate production in the presence of zinc. Biotechnology and bioengineering, 108(1), 226-230.
95. Yan, Z., Liu, Y., Zhang, T., Zhang, F., Ren, H., & Zhang, Y. (2021). Analysis of microplastics in human feces reveals a correlation between fecal microplastics and inflammatory bowel disease status. Environmental science & technology, 56(1), 414-421.
96. Yang, R., Huang, J., Zhang, W., Xue, W., Jiang, Y., Li, S., ... & Chi, B. (2021). Mechanoadaptive injectable hydrogel based on poly (γ-glutamic acid) and hyaluronic acid regulates fibroblast migration for wound healing. Carbohydrate Polymers, 273, 118607.
97. Zeng, W., Chen, G., Zhang, Y., Wu, K., & Liang, Z. (2012). Studies on the UV spectrum of poly (γ-glutamic acid) based on development of a simple quantitative method. International journal of biological macromolecules, 51(1-2), 83-90.
98. Zhang, D., Feng, X., Zhou, Z., Zhang, Y., & Xu, H. (2012). Economical production of poly (γ-glutamic acid) using untreated cane molasses and monosodium glutamate waste liquor by *Bacillus subtilis* NX-2. Bioresource technology, 114, 583-588.

99. Zhang, X., Li, H., Guo, Y., Ding, S., Chen, G., Liang, Z., & Zeng, W. (2021). An integrated strategy for recovery and purification of poly-γ-glutamic acid from fermentation broth and its techno-economic analysis. Separation and Purification Technology, 278, 119575.
100. Zhuang, H., Hong, Y., Gao, J., Chen, S., Ma, Y., & Wang, S. (2015). A poly (γ-glutamic acid)-based hydrogel loaded with superoxide dismutase for wound healing. Journal of Applied Polymer Science, 132(23).

Sitography

1. https://commission.europa.eu/strategy-and-policy_it (last accessed on 15 January 2024).
2. https://www.sigmaaldrich.com/IT/it/product/sigma/p4886(last accessed on 21 January 2024)

Chapter II

Exploiting Potential Biotechnological Applications of Poly-γ - Glutamic Acid Low Molecular Weight Fractions Obtained by Membrane-Based Ultra-Filtration

This chapter investigated the potential of low-molecular-weight poly-γ-glutamic acid (γ-PGA) from microbial and unexpensive commercial sources for bioplastic applications and therapeutic uses. To address the high cost of γ-PGA purification, two methods were evaluated: solvent precipitation and membrane-based ultra- and nano-filtration. These techniques successfully yielded size-specific γ-PGA fractions in large quantities. Subsequent characterization using size exclusion chromatography and ultra-high-performance liquid chromatography confirmed the molecular weight and concentration profiles of the γ-PGA fractions. Further investigations revealed that the purified γ-PGA might serve as bioplastic precursor, forming hydrocolloid films with desirable properties such as hydrophilicity, thermal stability, and mechanical strength. Additionally, these purified γ-PGA fractions demonstrated potential therapeutic effects by counteracting desiccation and oxidative stress in keratinocyte monolayers, suggesting their potential for alleviating oxidative stress-related diseases. These findings highlight the versatility of the obtained γ-PGA preparation in developing advanced biomaterials for various biomedical applications and support the use of environmentally friendly purification techniques, such as ultra-filtration, for large-scale production.

polymers

MDPI

Article

Exploiting Potential Biotechnological Applications of Poly-γ-Glutamic Acid Low Molecular Weight Fractions Obtained by Membrane-Based Ultra-Filtration

Odile Francesca Restaino [1], Sondos Hejazi [2], Domenico Zannini [3], Concetta Valeria Lucia Giosafatto [2], Prospero Di Pierro [4], Elisabetta Cassese [1], Sergio D'ambrosio [1], Gabriella Santagata [3], Chiara Schiraldi [1,*] and Raffaele Porta [2,*]

[1] Department of Experimental Medicine, Section of Biotechnology and Molecular Biology, University of Campania "Luigi Vanvitelli", 80138 Naples, Italy; odilefrancesca.restaino@unicampania.it (O.F.R.); eli.cassese@gmail.com (E.C.); sergio.dambrosio@unicampania.it (S.D.)
[2] Department of Chemical Sciences, University of Naples "Federico II", 80126 Naples, Italy; sondosmohammadhasan.hejazi@unina.it (S.H.); giosafat@unina.it (C.V.L.G.)
[3] Institute for Polymers, Composites and Biomaterials, National Council of Research, 80078 Pozzuoli, Italy; domenico.zannini@ipcb.cnr.it (D.Z.); santagata@ipcb.cnr.it (G.S.)
[4] Department of Agriculture, University of Naples "Federico II", 80055 Naples, Italy; dipierro@unina.it
* Correspondence: chiara.schiraldi@unicampania.it (C.S.); raffaele.porta@unina.it (R.P.); Tel.: +39-081-566-7654 (C.S.); +39-081-252-9470 (R.P.)

Abstract: Since the potentialities of applications of low molecular weight poly-γ-glutamic acid (γ-PGA) chains have been so far only partially explored, the separation of diverse molecular families of them, as well as their characterization for potential bioactivity and ability to form films, were investigated. Two different approaches based on organic solvent precipitation or on ultra- and nano-filtration membrane-based purification of inexpensive commercial material were employed to obtain size-specific γ-PGA fractions, further characterized by size exclusion chromatography equipped with a triple detector array and by ultra-high-performance liquid chromatography to assess their average molecular weight and their concentration. The γ-PGA low molecular weight fractions, purified by ultra-filtration, have been shown both to counteract the desiccation and the oxidative stress of keratinocyte monolayers. In addition, they were exploited to prepare novel hydrocolloid films by both solvent casting and thermal compression, in the presence of different concentrations of glycerol used as plasticizer. These biomaterials were characterized for their hydrophilicity, thermal and mechanical properties. The hot compression led to the attainment of less resistant but more extensible films. However, in all cases, an increase in elongation at break as a function of the glycerol content was observed. Besides, the thermal analyses of hot compressed materials demonstrated that thermal stability was increased with higher γ-PGA distribution po-lymer fractions. The obtained biomaterials might be potentially useful for applications in cosmetics and as vehicle of active molecules in the pharmaceutical field.

Keywords: poly-γ-glutamic acid; keratinocyte monolayers; oxidative stress; bio-based materials; hydrocolloid films

check for updates

Citation: Restaino, O.F.; Hejazi, S.; Zannini, D.; Giosafatto, C.V.L.; Di Pierro, P.; Cassese, E.; D'ambrosio, S.; Santagata, G.; Schiraldi, C.; Porta, R. Exploiting Potential Biotechnological Applications of Poly-γ-Glutamic Acid Low Molecular Weight Fractions Obtained by Membrane-Based Ultra-Filtration. *Polymers* **2022**, *14*, 1190. https://doi.org/10.3390/polym14061190

Academic Editor: Helmut Schlaad

Received: 25 January 2022
Accepted: 15 March 2022
Published: 16 March 2022

Publisher's Note: MDPI stays neutral with regard to jurisdictional claims in published maps and institutional affiliations.

1. Introduction

Poly-γ-glutamic acid (γ-PGA) is a poly-amino acid produced in nature by Gram-positive bacteria of the *Bacillus* genus (e.g., *Bacillus subtilis*, *B. subtilis subsp. natto*, *Bacillus licheniformis*), whose anionic polymeric structure is composed of D-glutamic acid and/or L-glutamic acid monomers linked by γ-amide bonds [1,2]. Nowadays, γ-PGA is considered a bio-homopolymer of high commercial interest, and it is already widely used in agriculture, environmental bioremediation, food industry, drug and cosmetic manufacturing, thanks to its biodegradable, edible, non-toxic, non-immunogenic and superabsorbent properties [2,3].

However, the different industrial applications of γ-PGA depend on its molecular weight (Mw), conformation, purity, solubility and pH conditions at which it is dissolved [2]. In water, at pH 7.0, γ-PGA solutions show high viscosity, whereas the homopolypeptide assumes an α-helix conformation in acidic conditions and a β-sheet-one at pH higher than 7.0 [4]. γ-PGA is also soluble in alcohols, but its solubility depends on the enantiomeric conformation. In fact, if the chains are composed of both D- and L-enantiomers, γ-PGA precipitates in ethanol, while if it contains only one type of enantiomer, it is soluble [3]. Furthermore, according to the microbial origin and to the culture conditions used in its fermentative production, the γ-PGA Mw ranges from less than 100 to 1000 kDa, and sometimes it can even reach 2000 kDa [1,5]. Ultra-high Mw γ-PGA chains (>1000–1500 kDa) can form colloids and could be used in the recycling of wastewater to remove heavy metals. Conversely, γ-PGA with a Mw > 700 kDa is widely used in cosmetics as skin moisturizing agent, being able to bind water in a proportion of 5000 times its weight, or in food industry as a thickener and cryoprotectant [1,5]. However, although both ultra-high and high Mw γ-PGA are quite exploited in industrial applications, their wider use is limited due to the high viscosity of their solutions at phy-siological pH values. Thus, in recent years, attention has been focused on the pre-paration of γ-PGA polymers of specific average sizes, mainly constituted from short Mw chains, that could be aimed at innovative commercial uses [2]. Oligomeric and low Mw (<100–200 kDa) γ-PGA have been used as drug carrier for tumor treatment [3] and, more recently, in the manufacturing of biodegradable films [6] potentially useful to produce materials with specific and tailored properties for applications in the pharmaceutical as well as cosmetic fields. Low Mw γ-PGA polymers are generally obtained by enzymatic digestion of those of high Mw chains of microbial origin, after their purification from the viscous fermentation broth.

The purification process has high costs and the recovery of the polymer can be hampered by the high viscosity of the fermentation broth [7,8]. The process generally includes centrifugation or sedimentation of the bacterial cells, γ-PGA recovery from the broth supernatant by alcohol precipitation (75–80% methanol or ethanol v/v) or addition of divalent copper salts. Ethanol precipitation did not assure the removal of proteins that precipitate along with PGA, thus further purification steps are required as concentration by ultrafiltration membranes, dialysis/diafiltration or chromatography to remove small molecules, such as salts, exhaust nutrients and even glutamate monomers [7–10]. Then, the purified product is dried by freeze drying or spray drying [7–10]. Recently, new strategies for the recovery and the purification of γ-PGA from the broth supernatant were reported that, for example, include four-unit operations, such as acidification, plate and frame filtration, cyclic ultra-filtration and freeze drying, in order to avoid any inefficient precipitation step and to reduce the purification costs [7]. In another case, a hybrid reactor system that integrated cross-flow microfiltration modules in a fermentation vessel was employed to continuously produce γ-PGA and directly purify it by using two-stage membrane treatments [10]. This approach assured continuous, high-yield production and productivity of γ-PGA by recycling of the bacterial cells and an efficient downstream process up to high product purity by removing any inhibiting fermentation products [10]. As the fermentative conditions influence the titer of γ-PGA production, as well as the Mw and polydispersity index of the homopolypeptide, and because the downstream purification process is a complex and not efficient procedure in which the different γ-PGA chain length populations are not separated, the commercial samples sold on the market often contain not pure, highly dispersed γ-PGA multiple forms with different Mw. As the Mw is critical for the γ-PGA applications, new downstream purification approaches are needed, as the classical precipitation procedures are not good in obtaining specific, highly homogenous Mw fractions, but only a mixture of different size populations. Therefore, the use of low Mw γ-PGA fractions for diverse biotechnological applications has been so far poorly investigated, particularly in the field of film manufacturing. So far, low Mw γ-PGA has been used to obtain films by formulating, casting and drying different film-forming solutions (FFSs) [6], while other methods, such as thermal compression of the polymer, have not been investigated yet.

In the present study, selected and highly homogenous γ-PGA fractions of low Mw were obtained on a large scale by a membrane-based purification process of ultra-filtration (UF), dia-filtration (DF) and nano-filtration (NF) from an inexpensive commercial source of γ-PGA (COM-PGA) and compared to a homopolypeptide preparation obtained from the same source by methanol precipitation (Figure 1). In order to quantify the γ-PGA concentration in all the samples, a new ultra-high-performance liquid chromatography (UHPLC) method was set up on the base of the L-glutamic acid monomer determination after acidic hydrolysis of the polymer. All the γ-PGA fractions were also characterized in terms of average Mw and poly-dispersity index by size exclusion chromatography coupled with a triple detector array (SEC-TDA) after determination, for the first time, of the γ-PGA dn·dc^{-1} value. Finally, the γ-PGA low Mw fractions obtained by UF, DF and NF and the homopolypeptide sample obtained by methanol precipitation (MET-PGA powder) were investigated for possible mammalian cell protection against dehydration and oxidative stress, as well as for the manufacturing of biomaterials potentially applicable in drug delivery systems and/or as dehydration masks in the cosmetic field. Manipulable γ-PGA films were produced not only by FFS casting but, for the first time, by hot compression of the powder samples and characterized in terms of mechanical, hydrophilic and thermal properties.

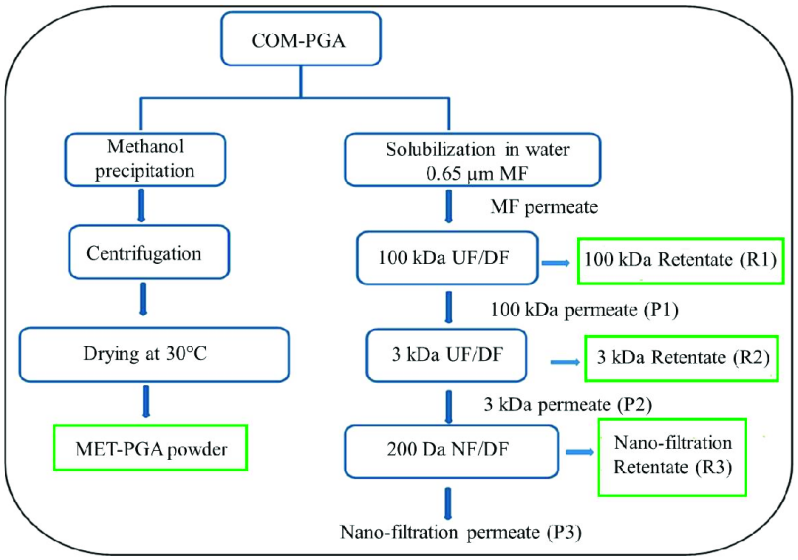

Figure 1. Flowchart of the processes for obtaining partially purified γ-PGA from COM-PGA by methanol precipitation (MET-PGA powder) or low Mw fractions of the homopolypeptide by membrane-based purification by micro-filtration (MF), ultra-(UF)/dia-filtration (DF) and nano-filtration (NF). The main γ-PGA fractions (MET-PGA powder, R1, R2 and R3), here reported in the green boxes, were then characterized and assayed for their properties.

2. Materials and Methods

2.1. Materials

COM-PGA of microbial origin was from Xi'an Fengzu Biological Technology Co., Ltd. (Xi'an, China). According to the manufacturer, this industrial bulk contained not purified γ-PGA obtained by microbial fermentation and suitable only for agriculture uses. Glycerol (GLY) (99.5%) was supplied from Carlo Erba Company (Milano, Italy), as well as methanol (99.9%) All other chemicals used for the buffer of SEC-TDA and UHPLC analyses and the standards were of analytical grade and from Sigma-Aldrich (St. Louis,

MO, USA). For the biological assays, the Dulbecco's modified eagle medium (DMEM), the heat-inactivated fetal bovine serum (FBS), the penicillin and the streptomycin, as well as the phosphate-buffered saline (PBS) and the trypsin, were all provided by Gibco Invitrogen (Milan, Italy).

2.2. Poly-γ-Glutamic Acid Purification by Organic Solvent Precipitation

Absolute methanol (1.2 L) was added to COM-PGA powder (300 g). The mixture was stirred by using a refrigerated incubator shaker (ISF-1-W, Kuhner, Birsfelden, Switzerland) for 12 h at 4 °C and then centrifuged at 10,000 rpm for 10 min (Avanti J-20 XP, Beckman Coulter, Brea, CA, USA). The supernatant was discarded, while the pellet was dried at 30 °C to remove the excess of methanol (left panel of Figure 1). The obtained powder (MET-PGA) was kept at 4 °C and used for film preparation and characterization.

2.3. Poly-γ-Glutamic Acid Fractionation by Ultra-Filtration and Nano-Filtration

COM-PGA (300 g) was dissolved overnight in 10 L of MilliQ water at room temperature under stirring conditions (600 rpm) and then microfiltered on a 0.65 μm polypropylene membrane (total filtering area of 0.05 m^2, Sartopure PP2 MidiCaps, Sartorius Group, Göttingen, Germany) to remove undissolved materials by using a non-automatic Sartoflow Alpha system (Sartorius Group, Göttingen, Germany). As illustrated in the right part of Figure 1, γ-PGA fractionation was performed in three steps by using two different UF membranes in sequence and then by using a NF membrane. The microfiltered solution was first treated on 100 kDa cut-off polyethersulfone cassette membranes (total filtering area of 0.1 m^2, Sartorius Group, Germany) and concentrated by using an automatic tangential flow filtration system (Uniflux 10, UNICORN, GE Healthcare, Chicago, IL, USA), equipped with a 10 L sample reservoir, feeding pumps, level sensors, pH and conductivity meters and connected to a software able both to control the process parameters and to collect data and process parameters continuously [11]. After that, 95.0% of the sample was filtered and a continuous DF was performed by adding two volumes of MilliQ water (with respect to the concentrated volume) to the 100 kDa retentate (R1). The 100 kDa permeate (P1) was then ultra-filtered on 3 kDa cut-off polyethersulfone cassette membranes (0.5 m^2 of total filtering area, Sartorius Group, Germany) and concentrated by using a non-automatic Sartoflow Alpha system (Sartorius Group, Germany). The obtained 3 kDa retentate (R2) was then dia-filtered with two volumes of MilliQ water (with respect to the concentrated volume), while the 3 kDa permeate (P2) was then nano-filtered on 200 Da polyethersulfone spiral membranes (0.3 m^2 of total filtering area, Fluxa Filtri, Milan, Italy) by using a non-automatic Sartoflow Alpha system (Sartorius Group, Germany). Finally, the nano-filtration retentate (R3) was dia-filtered with two volumes of MilliQ water (with respect to the concentrated volume) and concentrated, while the obtained nano-filtration permeate (P3) was discarded. During all the processes, data of the pressure and volumes were collected, while conductivity and pH of the solutions were measured. The trans-membrane pressure (TMP) was calculated by using the following formula:

$$\text{TMP} = [(\text{inlet pressure} - \text{retentate pressure})/2] \quad (1)$$

Fluxes were calculated as the volumes passed on a filtering area in 1 h (liter per square meter in 1 h, LMH). Samples were taken during each purification step to be freeze dried in order to determine their dry weight, the protein and inorganic material content and γ-PGA concentration. The selectivity of the membranes during the filtration processes was instead calculated on the base of the SEC-TDA analyses and on the dry weight of the samples according to the following formula:

$$\%\ \text{Selectivity} = [\gamma\text{-PGA amount in the retentate (g)}]/[\gamma\text{-PGA amount in the retentate (g)} + \gamma\text{-PGA amount in the permeate (g)}] \times 100 \quad (2)$$

2.4. Analytical Methods

2.4.1. Determination of the Dry Weight, Protein and Water Content of the Samples

Aliquots (10 mL) of samples of each step of the purification process, as well as the three collected retentate samples, were freeze dried (LIO 5P, 5Pascal, Milan, Italy) by using a previously reported method (18 h at −20 °C and 1.05 mbar and then 3 h at 20 °C and 0.04 mbar) [12] and weighted in order to determine their dry weight. The COM-PGA, the MET-PGA powder and the three retentate samples were also assayed to determine the percentage of total protein content with respect to the dry weight by using a colorimetric assay [13] and the bovine serum albumin (BSA) as standard (Bio-Rad Laboratories Inc., Hercules, CA, USA). The total protein percentage of the samples was calculated according to the following formula:

$$\%\ \text{Protein/dry weight} = \%\ [(\text{Protein sample(g)/dry weight sample (g)}) \times 100] \quad (3)$$

The water content of the COM-PGA, MET-PGA powder and of the three retentate samples was also investigated according to the method described by Shankar et al. [14].

2.4.2. γ-PGA Concentration Analyses by Ultra-High-Performance Liquid Chromatography

γ-PGA concentration analyses were performed by ultra-high-performance liquid chromatography (UHPLC) after setting up a new method that exploited a previously reported analytical procedure for organic acid determination [12] and an acidic hydrolysis protocol previously used to depolymerize different polysaccharide chains and lignin–carbohydrate complexes [15–17]. The COM-PGA, the MET-PGA powder and all the other freeze-dried samples of the purification process were hydrolyzed with 5 M HCl, at a concentration of 2.5 $g \cdot L^{-1}$, for 6 h at 100 °C and 600 rpm (Thermomixer comfort, Eppendorf, Germany) to obtain L-glutamic acid monomers. Runs were performed by using an ultra-high-performance chromatography system (Ultimate 3000, Thermofisher-Dionex, Sunnyvale, CA, USA), by injecting 10 µL of the sample on a ion-exclusion column (Rezex ROA-organic acid H^+, 300 × 78 mm, Phenomenex, Torrance, CA, USA) and by eluting in isocratic conditions with 0.1% H_2SO_4 for 25 min at 0.8 $mL \cdot min^{-1}$ and at 40 °C with detection at 200 nm. A calibration curve of the γ-PGA standard after hydrolysis was built in the range from 0.025 to 0.100 $g \cdot L^{-1}$ on the base of the L-glutamic acid monomer area. The peak area values of this calibration curve were compared with the ones of the L-glutamic acid standard curve, built after hydrolysis in the same range, and the percentage of the γ-PGA recovery after reaction was calculated. The values of the γ-PGA concentrations, obtained by UHPLC analyses, were multiplied for the sample volumes to calculate the total amount (g) of the polymer in each sample of the purification process. The percentage of γ-PGA recovery in each sample of the purification process, with respect to the COM-PGA content, was calculated according to the following formula:

$$\%\ \gamma\text{-PGA recovery/COM-PGA sample} = \%[\gamma\text{-PGAsample (g)/COM-PGA sample (g)}] \times 100 \quad (4)$$

The percentage of γ-PGA content in the COM-PGA, in the MET-PGA powder and in the three retentate samples with respect to their dry weight was calculated according to the following formula:

$$\%\ \gamma\text{-PGA/dry weight} = \%\ (\gamma\text{-PGA sample (g)/dry weight sample (g)}] \times 100 \quad (5)$$

The mass yield values were calculated as percentage ratio of the mass value of each sample on the mass value of the initial sample.

2.4.3. γ-PGA Molecular Weight Analyses by Size Exclusion Chromatography with Triple Detector Array

Mw analyses of the COM-PGA sample, of the MET-PGA powder and of the three retentate samples were performed by using a SEC-TDA instrument (Viscotek, Malvern, Italy) equipped with a triple detector array, including a refractive index (RI) detector, a four-bridge viscosimeter (VIS) and two laser detectors of right-angle (RALS) and low-angle light scattering (LALS). Runs were performed by using two gel-permeation columns put in series (TSK-GEL GMPWXL, 7.8 × 30.0 cm, Tosoh Bioscience, Turin, Italy), equipped with a guard column, at pH 7.0 and at 40 °C and by eluting with 0.1 M $NaNO_3$ at a flow rate of 0.6 mL·min^{-1}, according to a previously reported method [6,18]. The instrument was calibrated by using a polyethylene oxide (PEO) standard (22 kDa PolyCAL, Viscotek, Malvern, Italy). All the retentate samples were analyzed in duplicate to determine the γ-PGA average Mw, the poly-dispersity index (Mw/Mn) and the intrinsic viscosity (IV) on the base of the detector signals and on the base of the γ-PGA dn·dc^{-1} value by applying the equations reported by the manufacturer:

$$\text{RI signal} = \text{kRI} \cdot \text{dn·dc}^{-1} \cdot \text{C} \quad (6a)$$

$$\text{VIS signal} = \text{kVIS} \cdot \text{IV} \cdot \text{C} \quad (6b)$$

$$\text{LALS signal} = \text{kLALS} \cdot \text{Mw} \cdot (\text{dn·dc}^{-1})^2 \cdot \text{C} \quad (6c)$$

where IV is the intrinsic viscosity (dL·g^{-1}); C is the concentration (mg·mL^{-1}); dn·dc^{-1} is the refractive index increment (mL·g^{-1}); and kRI, kVIS and kLALS are instrumental constants obtained by the universal calibration with PEO, performed according to the manufacturer's procedure (Viscotek, information available from http://www.viscotek.com, accessed date 10 March 2022).

The γ-PGA dn·dc^{-1} value was never reported in the literature so far, and it was experimentally determined after injection in triplicate solutions of the commercial γ-PGA standard in a concentration range from 0.1 to 0.5 g·L^{-1}, as previously described [18]. The commercial γ-PGA standard average Mw was 580 kDa ± 2 with a poly-dispersity index of 1.1 ± 0.1, as experimentally determined by using our instrument. By plotting the different γ-PGA concentrations versus the peak areas obtained from the RI signal, the γ-PGA dn·dc^{-1} value was calculated according to the following formula:

$$\text{dn·dc}^{-1} = (\text{Area RI/g·L}^{-1}\text{·1000})/(\text{kRI·injection volume})\text{·RI of the solvent} \quad (7)$$

where the injection volume was 0.1 mL; the RI of the solvent was 1.33; the constant kRI was 9.72 × 10^7. The representative of each peak was calculated as the percentage ratio bet-ween the single peak RI area divided by the sum of the RI areas of all the peaks in each chromatogram [18]. In the retentate samples, the percentages of representativity of the Mw populations were also determined by dividing the populations in four different ranges in order to calculate the selectivity of the membranes, as reported above: Fraction A—between 150 and 50 kDa, Fraction B—between 50 and 20 kDa, Fraction C—between 20 and 3 kDa, and Fraction D—lower than 3 kDa.

2.5. Biological Activity Assay

2.5.1. Dehydration Assay

COM-PGA, MET-PGA powder and the three retentate samples were tested for their ability to counteract dehydration in a cell-based assay. The dehydration assay was performed by using a spontaneously transformed, non-tumorigenic human keratinocyte cell line (HaCaT) provided by Istituto Zooprofilattico (Brescia, Italy). The cells were cultured in DMEM medium supplemented with 10% (*v*/*v*) FBS, 100 U·mL^{-1} of penicillin and 100 μg·mL^{-1} of streptomycin, in 24-multiwell plates (5 × 104/well) until a 70% cell confluence was reached (157,000 ± 10 cells/well). At this point, the culture medium was removed, a wash with PBS was performed, and the keratinocyte cell monolayers were

treated for 2 h with solutions of the COM-PGA sample, MET-PGA powder and of the three retentate samples at a concentration of 1.5 g·L^{-1} in DMEM. All experiments were performed in triplicate. The negative control (−CTR), instead, was carried out in triplicate simply by diluting the culture medium in PBS without any treatment with γ-PGA samples. After 2 h treatment, the samples and the negative control were dehydrated by removal of the medium and incubated at 37 °C until a stress response, in terms of morphological changes detected by using an optical microscope (100-fold magnification) (Axiovert, Zeiss, Oberkochen, Germany), was observed. The positive control (+CTR) of the experiment was constituted by cell mono layers not subjected to dehydration and kept in the presence of the medium during the whole experiment. Cell viability was determined by assessing cell metabolism through the NAD(P)H-dependent cellular oxidoreductase enzyme activity by a colorimetric assay. Cells were incubated for 3 h with the 3-(4,5-dimethylthiazol-2-yl)-2,5-diphenyltetrazolium bromide (MTT) reagent (Cell proliferation Kit I, MTT, Merck, Rome, Italy) at 37 °C and then treated with 0.1 M HCl in isopropanol (Sigma-Aldrich, St. Louis, MO, USA) for 15 min at room temperature. The NAD(P)H oxidoreductase activity was evaluated by measuring the absorbance at 570 nm (PA800, Beckman Coulter, Brea, CA, USA), and the percentage cell viability in the γ-PGA treated samples was compared to the cell viability in the negative control.

2.5.2. Oxidative Stress Assay

COM-PGA, MET-PGA powder and the three retentate samples were compared for their ability to counteract the H_2O_2 oxidative stress in a cell-mediated test (HaCaT) as rescuing agents. In the experiments 150,000 cell/well were seeded in 24-multiwell plates and cultivated for 24 h until a 40% cell confluence was reached (90,000 ± 10 cells/well). Then, the medium was removed, a wash with PBS was performed and 50 μM H_2O_2 (Sigma-Aldrich, USA) was added. After 30 min, the samples were observed by using the optical microscope in order to evaluate the eventual morphological changes due to the oxidative stress. Then, the H_2O_2 solution was removed, a wash with PBS was performed, and the keratinocyte mono layer cells were treated for 24 h in triplicate with solutions of COM-PGA, MET-PGA powder and of the three retentate samples at a concentration of 1.5 g·L^{-1} in DMEM (except for the CTR samples). The MTT viability assay was performed after 24 h, as previously described, and the percentage of cell viability of the samples was compared with the negative control. The negative control was simply prepared by diluting the culture medium in PBS and then performing the oxidative stress, while the positive control was not subjected to treatment with H_2O_2, and the cells were simply kept in the presence of the medium during the whole experiment.

2.6. Film Preparation and Characterization

2.6.1. Preparation of Films by Casting

Different FFSs (30 mL) containing 800 mg of either MET-PGA powder or retentates containing different γ-PGA fractions obtained by UF (R1, 55 kDa, R2, 18 kDa and R3, 6 kDa), were prepared by adjusting the pH to different values (2.0, 2.5, 3.0, 3.5, 4.0) by addition of 2.0 N HCl. All the FFSs were ultrasonicated (Bandelin SONOPULS ultrasonic homogenizers, Binder, Tuttlingen, Germany) for 20 min at 85% power by using 2 × 10% cycle. The FFSs were prepared in the absence or presence of different concentrations of GLY (1–10%, *w*/*w* γ-PGA). FFSs were poured into 60 × 15 mm polystyrene Petri dishes and left to dry in climatic chamber (25 °C and 45% relative humidity (RH) for 48 h). Dried films were conditioned at 25 °C and 50% RH for 2 h before the peeling and characterization.

2.6.2. Preparation of Films by Thermal Compression

Films of quite uniform thickness (≈500 μm) were prepared by compression molding in a Carver lab press (Carver Inc., No. 4122-12-12H, Wabash, IN, USA). Prior to film production, 2 g of γ-PGA powder samples (COM-PGA, MET-PGA, R1 and R2) were homogeneously mixed with 5% or 10% GLY (*w*/*w* of γ-PGA) in a mortar by pestle. Each

single dough obtained was finally shaped into small spherical pellets, then subjected to thermal compression. The samples were sandwiched between two flats of polytetrafluoroethylene foils and heated between the plates of the press up to 150 °C for 2 min at 500 PSI. Then, the samples were removed from the hot press and cooled down to room temperature before the film peeling. Films were always conditioned at 25 °C and 50% RH for 2 h before their characterization.

2.6.3. Film Moisture Content and Solubility

For the determination of the moisture content (MC) of the films, small pieces of them (≈2 × 2 cm) were weighted, put in aluminum dishes and dried in an oven at 105 °C for 24 h. The weight before and after drying was recorded to calculate the MC by the following equation:

$$\% \text{ MC} = [(\text{Wi} - \text{Wd})/\text{Wi}] \times 100 \quad (8)$$

where Wi and Wd represent the weights of the initial and dried film, respectively.

Water solubility (WS) of the films was instead calculated by determining the initial weight (Wi) of the film samples after oven drying at 105 °C for 24 h and by immersing the dried specimens in 50 mL of distilled water continuously shaken for 24 h at 25 °C. Then, the insoluble film pieces were oven dried again at 105 °C to obtain the final dry weight (Wf) [19]. Film WS (%) was calculated according to equation

$$\% \text{ WS} = [\text{Wi} \times 100]/\text{Wf} \quad (9)$$

2.6.4. Film Mechanical Properties

All handleable films were cut into 1 cm × 8 cm strips and analyzed for their mechanical properties (tensile strength, TS; elongation at break, EB; Young's module, YM) by means of a dynamometer Instron (Engineering Corp., Norwood, MA, USA), according to the procedure described in ASTM D882–10 [20]. Five specimens of each film sample were analyzed (5 cm gage length, 1 kN load and 20 mm/min speed) taking into consideration film thickness that was measured in five different points with a micrometer with a sensitivity of 0.001 mm (Electronic digital micrometer, DC-516, Alpa, Albiate Monza e Brianza, Italy).

2.6.5. Film Thermal Properties

Thermogravimetric analysis of MET-PGA-, R1- and R2-derived films was performed using a thermogravimetric analyzer TGA/DTG Perkin-Elmer PyrisDiamond, equipped with gas station. Samples (3–4 mg) were placed in an open ceramic crucible and heated from 25 °C to 600 °C at a speed rate of 10 °C·min^{-1}, under nitrogen flow of 30 mL·min^{-1}. Before testing, samples were conditioned for 24 h at 25 °C and 50% RH. Thermal properties of MET-PGA-, R1- and R2-derived films were investigated by using a Q2000 T zero differential scanning calorimeter (DSC), TA Instrument (New Castle, DE, USA), equipped with a liquid nitrogen accessory for fast cooling. The calorimeter was calibrated in temperature and energy using indium. Dry nitrogen was used as purge gas at a rate of 30 mL·min^{-1}. Samples (3–4 mg) were weighed and placed individually in aluminum pans; an empty pan was then used as reference. DSC measurements were performed in double heating run; the first one, occurring from 50 to 200 °C, at 10 C·min^{-1}, could reproduce the thermal history of the samples. After an isothermal step of one min, non-isothermal crystallization experiments were performed by cooling the specimens up to −50 °C, at a rate of 10 C·min^{-1}. Finally, a second heating ramp from −50 °C to 250 °C at 10 °C·min^{-1} was recorded. Before testing, the samples were conditioned for 24 h at 25 °C and 50% RH.

2.7. Statistical Analysis

For cell viability analyses, data were reported as averaged values of three replicates with their standard deviation values and were statistically analyzed by using Excel program (Microsoft, Redmond, WA, USA), using the Student's *t*-test, considering statistically significant differences between data with $p < 0.05$. In terms of film characterization, in order

to determine a significant difference between treatments, one-way analysis of variance (ANOVA) and Duncan's multiple range tests ($p < 0.05$) were performed using the Statistical Package for the Social Sciences (SPSS19, SPSS Inc., Chicago, IL, USA) software.

3. Results

3.1. γ-PGA Quantitative Determination by UHPLC and Purification by Organic Solvent Precipitation

In order to determine the γ-PGA concentration in the commercial material and in all the purified samples, a new UHPLC method was set up on the base of the L-glutamic acid monomer determination after acidic hydrolysis of the homopolypeptide. The L-glutamic acid standard shows a peak at 5.5 min, as well as the γ-PGA standard after acidic hydrolysis (92.5% of the γ-PGA standard was recovered after reaction). Therefore, a calibration curve was built in the linearity range from 0.025 to 0.100 $g \cdot L^{-1}$ (Figure S1). The obtained results indicate that the commercial dry sample contained only 51.5% of γ-PGA. Thus, 300 g of COM-PGA, containing around 154 g of γ-PGA, was mixed with methanol, and the obtained precipitated material (250 g) was dried overnight in the oven at 37 °C to eliminate methanol. Afterward, the dry material was grinded to obtain a powder (MET-PGA powder) that was further characterized and used for film preparation. At the end of this treatment, only 83% of the original powder was recovered (250 g) with a consequent γ-PGA content of 128.2 g. A similar percentage of recovery was previously reported by Manocha and Margaritis [21] by using ethanol to precipitate γ-PGA. The conductivity and the pH of the MET-PGA powder, when dissolved in water, were 13 $mS \cdot cm^{-1}$ and pH 6.4, respectively.

3.2. γ-PGA Purification by Using Filtration Membranes and Characterization

The COM-PGA was purified on different cut-off membranes, as illustrated in the right panel of Figure 1, with the aim to recover fractions with the highest polymer concentration and of homogeneous averaged Mw size. The entire process is summarized in Table 1 and Figure 2. An amount of 300 g of the COM-PGA was first solubilized in water (10 L), but 9.2% of the sample remained insoluble.

Table 1. Summarized data of the γ-PGA filtration membrane-based purification process. (ND, not determined). Mass yield values were calculated as percentage ratio of the mass value of each sample on the mass value of the initial sample.

Sample	Volume (L)	pH	Conductivity (mS/cm)	Dry Weight (g)	Total γ-PGA (g)	% γ-PGA Recovery/Initial Sample	Mass Yield (%)
γ-PGA	10.0	6.2	14.0	272.5	140.3	-	-
Microfiltered γ-PGA	9.3	6.2	14.0	233.7	120.3	85.7	85.7
100 kDa Retentate (R1)	0.7	6.3	4.5	31.3	21.8	15.5	11.4
100 kDa Permeate (P1)	11.6	6.3	8.8	187.7	94.5	67.4	68.9
3 kDa Retentate (R2)	1.0	6.5	5.8	27.1	15.9	11.3	10.0
3 kDa Permeate (P2)	11.6	6.3	7.6	152.5	76.6	54.6	56.0
Nano-filtration Retentate (R3)	2.6	6.4	4.0	110.0	70.7	50.4	40.4
Nano-filtration Permetate (P3)	8.7	6.4	7.0	36.2	4.6	3.3	13.3

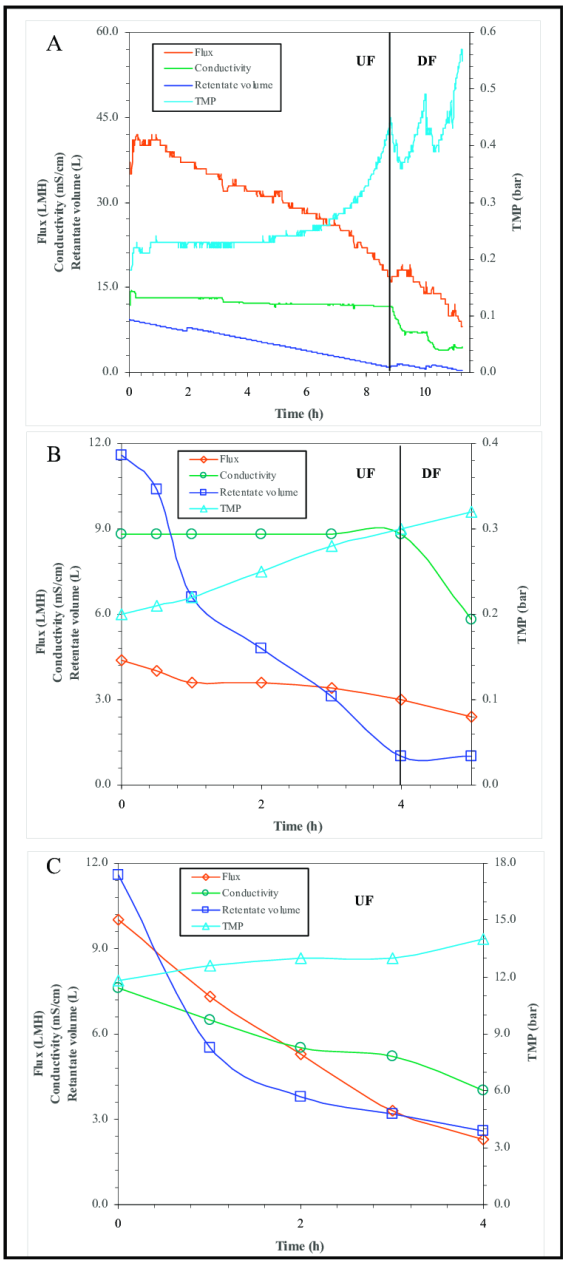

Figure 2. γ-PGA ultra-filtration (UF) and dia-filtration (DF) phases of 100 kDa (**A**), 3 kDa (**B**) membrane processes and the ultra-filtration phase of the nano-filtration purification (**C**), as indicated in the graphs. The curves of TMP, flux, conductivity and retentate volume during the processes are reported.

Thus, a micro-filtration step was performed to remove other insoluble material contained in the starting sample. A total of 85.7% of the initial γ-PGA was recovered in the microfiltered permeate that was initially concentrated and dia-filtered on 100 kDa membranes. The process parameters are reported in Figure 2A.

The 100 kDa retentate (R1) had a concentration factor of 13.3, and it contained 15.5% of the initial material. The resulting permeate sample (P1) was then concentrated and dia-filtered on 3 kDa membranes (Figure 2B), achieving a conductivity decrease from 8.8 to 5.8 $mS \cdot cm^{-1}$. The corresponding retentate (R2) was 11.6-fold concentrated, and it contained 12.3% of the initial COM-PGA. The resulting permeate (P2) was then treated on the nano-filtration membranes (Figure 2C), and during the process, conductivity decreased up to 4.0 $mS \cdot cm^{-1}$. The high TMP values reached did not permit a further dia-filtration step. The nano-filtration process allowed a recovery of 50.4% of the initial γ-PGA in the retentate (R3) (concentration factor of 4.4), while the remaining 3.3% was found in the nano-filtration permeate (P3). The selectivity values were 18.8%, 16.6%, 93.9% for the three steps of purification, respectively. In conclusion, the total γ-PGA recovery of the whole membrane process in the three retentate samples was 77.3%; the three retentate fractions were freeze dried, and their γ-PGA content resulted in an increase compared to the COM-PGA, since the γ-PGA content on the dry weight, also considering a water percentage of the freeze-dried samples between 6.0 and 10.0%, was 69.5%, 58.6% and 64.3%, respectively. The percentage protein concentrations on the recovered freeze-dried material of the three retentate samples was very low, between 0.3 and 3.2%.

3.3. γ-PGA Molecular Weight Analysis by SEC-TDA

To perform the SEC-TDA analyses of the samples, the $dn \cdot dc^{-1}$ value of the γ-PGA standard was experimentally determined for the first time, and it emerged as 0.183 $mL \cdot g^{-1}$ (Figure S1). COM-PGA, MET-PGA and the three obtained retentates were analyzed (Figure 3A). In Figure S2, their complete chromatograms showed the diverse bio-polymer families that corresponded to the average Mw values reported and highlighted in Figure 3B. Analyses showed the presence of three different populations of γ-PGA with low and ultra-low averaged Mw(between 78.3 and 5.6 kDa, with a poly-dispersity index between 1.07 and 2.73). The lowest Mw (5.6 kDa) fraction of γ-PGA constituted the main peak of the commercial sample with a representativity of 64.5%. The precipitation of the COM-PGA by methanol roughly halved the ultra-low Mw population, since the SEC-TDA analysis showed the presence of three peaks, with averaged Mw values like the values of the commercial sample (between 64.0 and 3.0 kDa) but with different representativity. Conversely, the representativity of the other two populations with higher Mw (64 and 20.6 kDa) increased by about 1.6- and 1.9-fold. The membrane-based purification process allowed for obtaining γ-PGA fraction samples that were more homogeneous in size. More specifically, R1 contained a homopolypeptide fraction with an average Mw of 54.7 kDa, a poly-dispersity index of 1.56 and a representativity of 98.5%. In R2, the main peak of 17.9 kDa with a representativity of 87.4% was found (Figure 3), together with a higher Mw peak of 52.7 kDa, accounting for the 12.6% of γ-PGA. Finally, γ-PGA chains with Mw values lower than 10 kDa were collected only in R3. It is worthy to note that γ-PGA of average 3000 kDa Mw (between 2761 and 3254 kDa) was found in very small percentages (up to 1.5% of representativity) in all the analyzed samples.

A

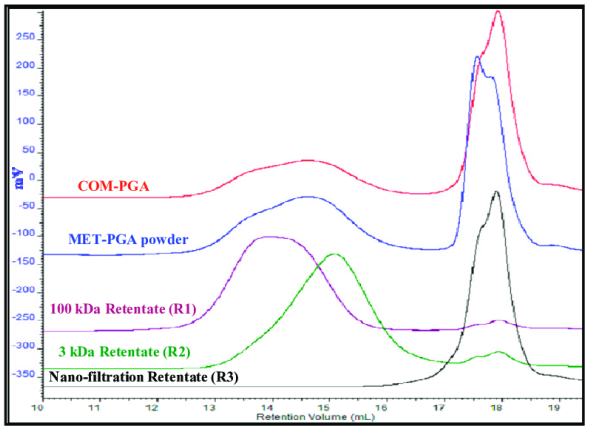

B

Sample	Mw (kDa)	Mw/Mn	IV (dL/g)	Representativity (%)
COM-PGA	78.3	1.25	1.46	12.7
	23.1	1.07	0.48	22.0
	5.6	2.73	0.05	64.5
MET-PGA powder	64.0	1.19	1.36	20.1
	20.6	1.07	0.40	41.7
	3.0	2.33	0.05	37.1
R1	54.7	1.56	1.23	98.5
R2	52.7	1.20	1.27	12.6
	17.9	1.38	0.35	87.4
R3	6.6	2.37	0.05	99.5

Figure 3. Overlaid SEC-TDA chromatograms of the different γ-PGA samples: refractive index signals of the COM-PGA (red line), MET-PGA powder (blue line), as well as of the R1 (purple line), R2 (green line) and R3 (black line) fractions (**A**). Average Mw, poly-dispersity index (Mw/Mn), intrinsic viscosity (IV) and percentage representativity of each γ-PGA fraction analyzed by SEC-TDA (**B**).

3.4. Biological Activity: Dehydration and Oxidative Stress Assays

The biological activity of COM-PGA, MET-PGA powder and of the γ-PGA-containing R1, R2 and R3 fractions was investigated using HaCaT cells by an in vitro model for challenging both dehydration and oxidative stress. The dehydration test showed an 80% decrease in viability of the negative control, and a similar effect was observed in the presence of the COM-PGA sample (Figure 4A). Conversely, the addition of all the other γ-PGA samples was able to restore cell viability to various extents. In particular, R1 and R2 γ-PGA-containing fractions caused a marked improvement, with a recovery higher than 2.5-fold, whereas cell viability increased by less than 30% and 40% by employing R3 and MET-PGA powder (normalized to the positive control), respectively (Figure 4A).

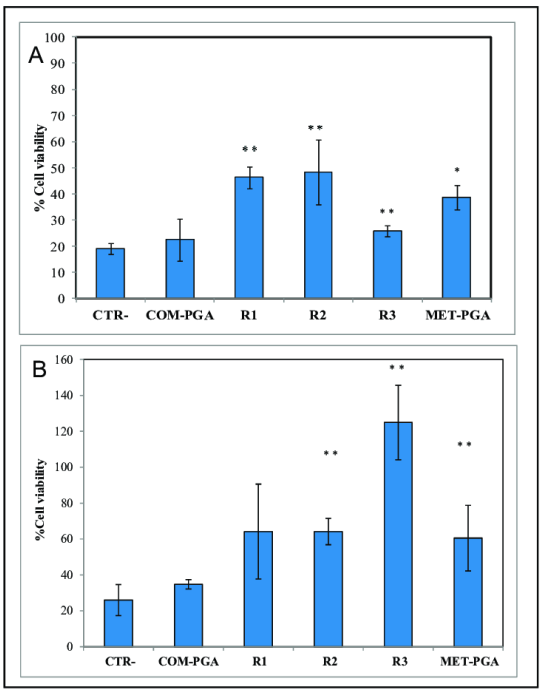

Figure 4. Dehydration assay (**A**) and oxidative stress assay (**B**) on HaCat cells as rescue effect of COM-PGA, MET-PGA and of γ-PGA-containing R1, R2 and R3 fractions, normalized over the positive control and compared to the negative control. (Statistical analysis: * $p < 0.05$ and ** $p < 0.01$ compared to the negative control).

As far as the oxidative stress applied to HaCat monolayers is concerned, it reduced cell viability by about 70% compared to the positive control, while all γ-PGA-containing fractions were found to determine a significant rescue of the cell metabolism when added after the oxygen peroxide treatment (Figure 4B). In fact, while the COM-PGA seemed unable to improve cell viability, both MET-PGA powder and all the γ-PGA fractions obtained by ultra-filtration had a marked enhancing effect and, among them, the R3 fraction showed by far the best performance.

3.5. γ-PGA Film Preparation by FFS Casting/Drying and by Hot Compression

γ-PGA-based films were prepared by two different procedures, either by casting and drying of the FFSs containing 800 mg of the homopolypeptide and GLY at two different concentrations (5 and 10%, *w*/*w* of γ-PGA) or by hot compression for 2 min at 150 °C and 500 p.s.i. of the powders (2 g) of the different γ-PGA fractions, obtained by methanol precipitation or by ultra-filtration, after their mixing with GLY (5% *w*/*w* of γ-PGA). As it is possible to see from panel A of Figure 5, all the films obtained by the FFS casting appeared brownish, and only the MET-PGA-based FFS containing 10% GLY and all the R3-based FFSs, prepared both in the absence or presence of GLY [22], did not allow for obtaining any manipulable films after casting and drying.

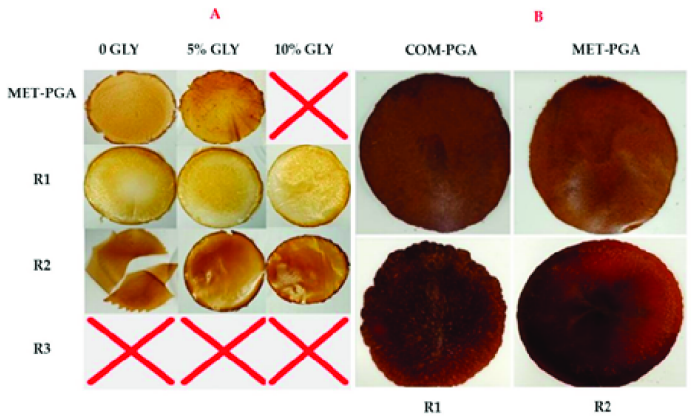

Figure 5. Films obtained by casting film forming solutions prepared with 800 mg of MET-PGA, R1, R2 and R3 γ-PGA fractions in the absence or presence of two different glycerol (GLY) concentrations; x, unhandleable sticky material (**A**). Films obtained by hot compression of 2 g of COM-PGA (γ-PGA), MET-PGA, R1 and R2 powders mixed with 5% GLY (**B**). Further experimental details are given in the text.

In contrast, all the films prepared with the R1 γ-PGA fraction (55 kDa), both in the absence and in the presence of the two different GLY concentrations, were easy to be peeled off from the plates and were very manipulable, even though they presented some spots on their surface. Finally, the R2 γ-PGA fraction (18 kDa) gave rise to brittle films when prepared either in the absence or presence of 5% GLY; conversely, brown and transparent films without any irregularities were obtained in the presence of 10% of GLY.

Panel B of Figure 5 shows the films obtained by hot compression of the γ-PGA powders (COM-PGA, MET-PGA, R1 and R2 γ-PGA fractions) previously mixed with 5% GLY, as described in Materials and Methods. These films showed a dark brown color and were handleable and quite homogenous, whereas no manipulable films were obtained by hot compression of the R3 γ-PGA powder, similarly to what occurred after casting and drying of the FFS containing R3 γ-PGA fraction.

3.6. Film Characterization for Mechanical and Hydrophylicity Properties

All the films prepared with the two different procedures were analyzed according to their mechanical (TS, EB and YM) and hydrophilicity (MC and WS) properties, and the detected results, reported in Table 2, were compared. It was possible to analyze only the peelable and well-shaped materials, since unmanipulable films (either * sticky or ** brittle) were obtained by casting and drying the FFSs containing COM-PGA, with or without GLY, or MET-PGA and 10% GLY (both originating sticky materials) and R2 γ-PGA fraction prepared in the absence or presence of 5% GLY (originating brittle materials). Moreover, similar unmanipulable materials were obtained in the attempt to prepare γ-PGA films by hot compression from COM-PGA and 10% GLY or from MET-PGA in the absence of GLY, which gave rise to sticky and brittle materials, respectively. Finally, not even R3 γ-PGA fraction was able to produce manipulable films, both in the absence or presence of GLY, neither by casting and drying nor by hot compression of its powder. It is worthy to note that the thickness values of the films obtained by hot compression were markedly higher (2–4 times) as a consequence of the higher amount of the homopolypeptide used (2 g with respect to 0.8 g occurring in the cast FFSs) and that the effect of the presence of GLY in increasing film thickness was observed only when the films were prepared by casting and drying the γ-PGA FFSs.

Table 2. Mechanical and hydrophilicity properties of the films obtained by either casting or hot compression of the different γ-PGA samples (ND, not detectable values because of the unmanipulable (either * sticky or ** brittle) material obtained or because of *** the very low tensile strength (TS) values (<1.0 MPa) detected. Different small letters (a–g) indicate significant differences among the values reported in each column for each procedure ($p < 0.05$). Further experimental details are given in the text.

Procedure	Sample	GLY (%)	T (μm)	TS MPa	EB (%)	YM (MPa)	MC (%)	WS (%)
Casting/Drying	COM-PGA	0	ND *					
		5	ND *					
		10	ND *					
	MET-PGA	0	128 ± 4^{a}	1.1 ± 0.1^{a}	20 ± 3^{a}	302 ± 20^{a}	15 ± 1^{a}	82 ± 1^{a}
		5	143 ± 9^{b}	<1.0	56 ± 5^{b}	ND ***	17 ± 1^{a}	84 ± 2^{a}
		10	ND *					
	R1	0	149 ± 1^{b}	7.3 ± 2.0^{b}	0.5 ± 0.1^{c}	1927 ± 176^{b}	16 ± 1^{a}	99 ± 1^{b}
		5	178 ± 2^{c}	6.1 ± 0.5^{b}	13 ± 1^{a}	678 ± 29^{c}	16 ± 1^{a}	99 ± 1^{b}
		10	193 ± 4^{d}	1.2 ± 0.4^{a}	100 ± 27^{d}	230 ± 80^{a}	16 ± 1^{a}	99 ± 1^{b}
	R2	0	ND **					
		5	ND **					
		10	89 ± 1^{d}	1.1 ± 0.2^{a}	58 ± 1^{b}	318 ± 45^{a}	13 ± 1^{a}	99 ± 1^{b}
Procedure	**Sample**	**GLY (%)**	**T (μm)**	**TS MPa**	**EB (%)**	**YM (MPa)**	**MC (%)**	**S (%)**
Hot compression	COM-PGA	0	364 ± 61^{a}	<1.0	8 ± 1^{a}	ND ***	8 ± 1^{a}	92 ± 2^{a}
		5	421 ± 20^{a}	<1.0	17 ± 3^{b}	ND ***	11 ± 1^{b}	96 ± 1^{a}
		10	ND *					
	MET-PGA	0	ND **					
		5	472 ± 17^{b}	<1.0	8 ± 1^{a}	ND ***	7 ± 1^{a}	91 ± 1^{a}
		10	591 ± 17^{c}	<1.0	10 ± 1^{a}	ND ***	9 ± 1^{ab}	99 ± 1^{a}
	R1	0	499 ± 10^{b}	<1.0	38 ± 2^{c}	ND ***	11 ± 1^{b}	62 ± 1^{b}
		5	537 ± 32^{bc}	<1.0	113 ± 6^{d}	ND ***	11 ± 1^{b}	71 ± 1^{c}
		10	454 ± 10^{ab}	<1.0	159 ± 8^{e}	ND ***	11 ± 1^{b}	99 ± 1^{a}
	R2	0	463 ± 13^{b}	<1.0	31 ± 9^{c}	ND ***	12 ± 2^{b}	99 ± 1^{a}
		5	415 ± 10^{a}	<1.0	77 ± 1^{f}	ND ***	12 ± 2^{b}	99 ± 1^{a}
		10	430 ± 14^{ab}	<1.0	785 ± 20^{g}	ND ***	13 ± 2^{b}	99 ± 1^{a}

The analyses of the mechanical properties showed a marked plasticizing effect of GLY in the films prepared by both procedures with all the different γ-PGA samples, as TS and YM always decreased, and EB values concurrently increased, as a function of GLY concentration enhancement. In particular, it deserves to be highlighted that both R1 and R2 γ-PGA films prepared in the presence of GLY (especially R2-derived film with 10% GLY) were endowed with a remarkably high extensibility. Conversely, the films obtained by hot compression of all the γ-PGA powder samples exhibited very low TS values (<1.0 MPa) and, as a consequence, undetectable YM values. Thus, it seems that the hot compression procedure led to production of less resistant but much more extensible films.

The films were also analyzed for their MC and WS after immersing the samples in distilled water for 24 h. As shown in Table 2, the materials seemed to behave in a very similar way regardless of the method used for their manufacture. In fact, all the films showed a WS higher than 80%, except for R1-based films prepared by means of

thermal compression in the absence or presence of 5% GLY, the WS of which was 62 and 71%, respectively. However, the hot compressed materials were found to possess a lower amount of water, as the measured MC was lower than that of the respective cast films prepared under the same conditions, with the only exception of the R2 γ-PGA films manufactured with 10% GLY.

3.7. Thermal Properties of γ-PGA Different Samples and of the Derived Films Manufactured by Hot Compression

The thermal properties of both MET-PGA and R1 and R2 powders, as well as of the derived films manufactured in the absence or presence of 10% GLY by hot compression, were evaluated by both thermogravimetric analysis and differential scanning calorimetry (DSC). However, it is worth considering that, in general, γ-PGA could exhibit different thermal characteristics depending on the microorganism used for fermentation and the fermentation conditions, which can in turn influence the Mw and, consequently, the physicochemical properties of the analyzed homopolypeptide sample [23].

3.7.1. Thermogravimetric Analysis

The thermogravimetric (TGA) and the differential thermogravimetric (DTG) curves of MET-PGA, R1 and R2 γ-PGA films, without and with glycerol, are reported in Figure 6A,B and Figure 6D,E, respectively. All curves were normalized with respect to the starting sample size.

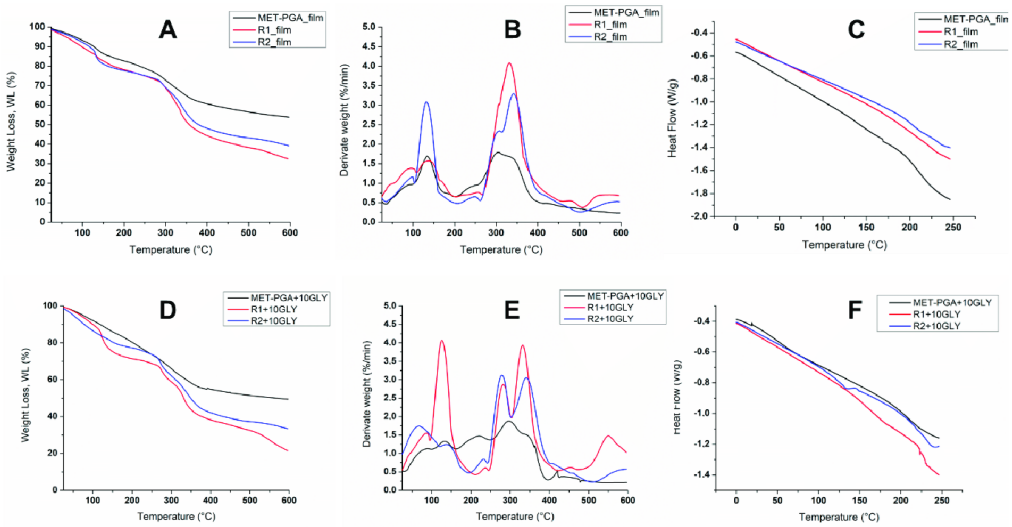

Figure 6. Thermogravimetric (**A**,**D**), differential thermogravimetric (**B**,**E**) and differential scanning calorimetric (second heating ramp) (**C**,**F**) thermograms of MET-PGA, R1 γ-PGA and R2 γ-PGA films, without (**A**–**C**) and with (**D**–**F**) 10% glycerol (10GLY).

In order not to overburden the paper content, finalized to mainly emphasize the role of films, all the thermal analysis of powder-based samples, together with their interpretation and discussion, were postponed to the Supplementary Material file (Section S1, Figure S3A,B). In Figure 6A,B,D,E, the thermograms of neat and GLY-doped films are reported. Generally, from the analysis of weight loss curves (Figure 6A,D), different mass evolution steps could be detected, highlighting the complex pattern of film thermal degradation profiles. This outcome was better highlighted by analyzing the DTG curves of all the films. Specifically, for all neat samples (Figure 6B), at least three different regions of

water evolutions could be found with their corresponding maxima peaks at around 50, 100 and 150 °C. In fact, as widely reported in the literature, the investigated region can be ascribed to free, bound and strongly bound water release, mostly if hydrophilic and hygroscopic polymers are concerned. It should be considered that γ-PGA-based samples are characterized by the presence of many polar groups, such as amino, carboxyl and hydroxyl residues, mostly involved in hydrogen bonding with water and, in any case, able to absorb and/or entrap water molecules in their three-dimensional networks. These findings, likewise well documented in the literature by some of the authors of the current paper [6], could also be explained by considering the thermal processing undergone by the films (compression molding), during which strong hydrogen bonds between water molecules and polymer polar residues occurred, responsible for water entrapment inside the polymer matrix network, releasable only at high temperature. Similar results were also found in the presence of GLY (Figure 6D,E); in these samples, the presence of two main regions of water evolution is well evident. The first one, up to 100 °C, was likely associated with the free and weakly bound water release, whereas the second temperature range between 100 and 200 °C was likely due to water evaporation coming from GLY-rich region, in which hydrogen bonding occurred. In fact, it is worthy to mention that water released at high temperature also came from the condensation reactions following polymer thermal degradation. Sabbah et al. [6] found that γ-PGA underwent the first depolymerization process at around 200 °C, consisting of an end-of-chain unzipping cyclodepolymerization reaction, leading to pyroglutamic acid. The short chains formed upon heating could depolymerize at around 250 °C, as shown by the small shoulder peak in both neat and doped films, whereas the main degradation process of high molecular weight polymers occurred in the wide range of 280–500 °C. From the comparison of DTG thermograms reported in Figure 6B,E, it is worthy to note that in the presence of GLY, a clear splitting of the different γ-PGA Mw fractions degradation rate occurred [24]. Specifically, as shown in Table 3 and Figure 6E, the lower molecular weight fractions, likely involved in hydrogen bonding with GLY, showed a maximum degradation rate peak at around 280 °C, about 20 °C lower with the analogous chain fractions of the neat polymers, degrading at 300 °C (Figure 6B) [25]. This result was ascribed to the increase in free volume and macromolecular mobility of the plasticized systems, as widely reported in the literature [26]. It was also likely that the thermal depolymerization of lower Mw macromolecular chains occurred simultaneously with GLYdegradation, thus explaining the higher peak intensity of this region. The third thermal peak, related to the higher γ-PGA molecular weight decomposition, occurred at 330 °C in all the samples, thus confirming both that the effect of the plasticizer was mainly marked in smaller Mw γ-PGA polymer residues and that a phase separation occurred during hot compression molding between regions of different molecular weights [27,28]. The final step of decomposition, observed by ana-lyzing the film samples in 450–550 °C range, was likely associated with the decarboxylation process leading to unsaturated chain fragments, non-volatile compounds in inert atmosphere (nitrogen).

Table 3. Glass transition temperatures (Tg) and the starting endothermic peak (Tpeak) of all the films.

Samples	(DSC) Tg (°C)	(TGA) Tpeak (°C)
MET-PGA	125	300–350
MET-PGA+10%GLY	50	300–350
R1 γ-PGA	163	300–330
R1 γ-PGA +10%GLY	60	280–330
R2 γ-PGA	82	300–340
R2 γ-PGA +10%GLY	56	280–340

3.7.2. Differential Scanning Calorimetry

DSC thermograms, related to the second heating ramp of MET-PGA, R1 and R2 films, are reported in Figure 6C,F. Apart from the expected chemical reaction, the first thermal heating of polymers by DSC analysis erases their thermal history (Figure S3D–F), while the second thermal run accounts for the real polymer properties at mole-cular level, evidencing all the involved transition phenomena [29]. In fact, due to the instrument limiting upper value of temperature, it was not possible to take a suitable guess related to the starting endothermic peaks visible for all samples at around 250 °C. In any event, from the differential thermal analysis (DTA) (Figure S4A,B), detectable by the same thermogravimetric analyzer used for TGA/DTG analysis in the range of 25–600 °C, and able to provide qualitative information on liable polymer transitions, no peaks could be found, apart from the ones related to polymer thermal degradation, better highlighted by DTG thermograms, as previously discussed. Thus, from DSC profiles, the starting endothermic peak found at 250 °C could likely be due to polymer degradation events. Nevertheless, from DSC analysis of the second heating run, it was possible to detect the glass transition temperature (Tg) of all the samples. The results, reported in Table 3, demonstrated the plasticizing action of GLY, as the Tg decreased for all the tested films [30].

4. Discussion

Up to now, the use of different low Mw γ-PGA chains as natural and biodegradable sources for diverse biotechnological applications has been poorly investigated [6]. In particular, little exists in the literature on the specific application of low Mw fractions of the homopolypeptide as cosmeceutical agent or to produce biodegradable films. As the γ-PGA functions change according to the size, their homogeneous low Mw fractions might potentially exhibit different properties compared to both high or very high Mw γ-PGA or to the mixtures of different Mw chains of the homopolypeptide. Thus, a key point in assessing specific polymer properties and potential functions is the necessity to find new protocols to purify and prepare γ-PGA size-specific fractions and to characte-rize them in terms of concentration and Mw [2]. So far, the γ-PGA quantitative determination has been performed by spectrophotometric assays (e.g., colorimetric test of safradin-induced precipitation, or after cetyltrimethylammonium bromide precipitation, or UV absorbance) [31,32]. Although these methods are apparently rapid, most of them require extensive purification of the samples before the analyses to avoid interference of other components in the estimation of the real titer. Zeng et al. [32] used an HPLC method for the γ-PGA determination after a strong hydrolysis (i.e., 105 °C for 8 h). In the present study, a new UHPLC method was set up to precisely quantify γ-PGA, occurring even in raw samples, on the base of the L-glutamic acid amount after milder acidic hydrolysis of the samples and ion-exchange chromatography separation. This hydrolysis procedure, which already proved to be effective for the quantitative determination of other macromolecules [16–18], emerged as highly reliable (92% of recovery) also in evaluating the amount of γ-PGA. Besides, so far, γ-PGA molecular weight analyses have been performed by using methods such as SDS-PAGE (with methylene blue or alcian blue staining, as well as with densitometry band detection) and gel-permeation chromatography with RI detection [32]. In the present study, instead, we used SEC-TDA analyses that also involve the contemporary detection by light scattering signals and intrinsic viscosity, thus obtaining a more reliable determination of the γ-PGA Mw and poly-dispersity index. In fact, improving our previous results [6], the γ-PGA $dn \cdot dc^{-1}$ value was also experimentally determined for the first time, since in the literature, only the increment of the calculated, and not experimental, value of L-glutamic acid is reported [33]. Furthermore, improved procedures for γ-PGA purification are needed for a better characterization of the homopolypeptide. Alcohol precipitation is one of the main methods reported. However, it is not specific, and undesired polysaccharide and protein impurities contained in the fermentation broth generally remain in the γ-PGA samples and must then be removed with following acid or protease treatments [31]. Moreover, this method involves the consumption of high volumes of solvent, which raises environmental

concerns, especially in large-scale production of the homopolypeptide [10]. Finally, alcohol precipitation does not fractionize γ-PGA in homogeneous Mw samples. In this respect, various methods, such as alkaline or enzymatic hydrolysis and ultrasonic irradiation, have been used to degrade the ultra-high and high Mw γ-PGA, obtained by fermentation, into low Mw homopolypeptide chains [31]. However, even these methods have limits, by degrading the polymer producing highly poly-dispersed molecular species. Size-specific γ-PGA samples (between 13 and 1300 kDa) have been previously obtained by using a hydrophilic silica-based anion exchange [31] or by gel-permeation chromatography [34]. However, these kinds of chromatographic methods are not applicable for large-scale γ-PGA preparations [34]. Therefore, membrane-based purification appeared more selective than alcohol-based precipitation and easy to scale up [11]. In the literature, ultra-filtration with polyethersulfone hollow fiber membranes (cut-off of 500 kDa, 300 kDa and 30 kDa) have been previously used to concentrate γ-PGA from a highly viscous culture broth and to reduce the amount of alcohol to be used in a second step of recovery [10]. An ultra-filtration process (with plate and frame cassettes of 10 and 100 kDa), coupled with nano-filtration was instead used in a previous work on lab scale to purify a small amount of γ-PGA (25 g). In this paper, we attempted a scale up of the previously developed tangential flow-based ultra-filtration process [6], to better recover some of the fractions with slight modifications of ultra-filtration membrane size in the second step, in order to purify a larger amount of COM-PGA (300 g) that contained a mixture of three different low Mw γ-PGA populations. The fractions were then compared with the sample obtained from the same raw material by methanol precipitation. This last procedure partially removed the very low Mw chains (<6.0 kDa) of the homopolypeptide from the COM-PGA, thus increasing the representativity of the other two macromolecular species and delivering high γ-PGA recovery percentages, but without an extensive purification of the commercial sample or selecting a precise size population of the homopolypeptide. The membrane-based process, instead, allowed for obtaining fractions with quite homogeneous sizes (54.7 and 17.9 kDa) and a higher purity grade. These fractions showed biological properties in terms of rescue effect against dehydration and oxidative stress. In fact, COM-PGA was not able to preserve the viability of the HaCaT cell monolayers, whereas the γ-PGA fractions with specific Mw sizes, such as R1 (54.7 kDa) and R2 (18.0 kDa), protected the cells from the dehydration stress and were rescuing the detrimental effect of oxygen peroxide treatment, with a significant outcome also by the R3 (6 KDa) γ-PGA fraction. The homopolypeptide size was shown to also affect the properties of the homopolymer-derived biomaterials. It is inte-resting to note that R3, containing very low Mw species of γ-PGA, was not able to produce any kind of films, neither in the absence nor presence of plasticizer, while COM-PGA, MET-PGA and the two retentate samples, R1 and R2, allowed for obtaining, under selected experimental conditions (i.e., pH and GLY concentration), manipulable films by casting/drying of FFSs or by hot compression of the sample powders. The mechanical properties of the manufactured γ-PGA-based materials demonstrated that GLY was able to promote a marked extensibility of these films, reducing contextually their TS and YM. These findings suggest a potential cosmetic application aimed at the preparation of hydration masks where the ability to stretch the skin is a prerequisite of paramount importance. In particular, an extraordinary extensibility (EB value of 785%) of the R2-based films when manufactured by hot compression and plasticized with 10% GLY was demonstrated. This behavior might be due to the fact that the thermal pressing at 150 °C of R2 powder mixed with 10% GLY led to an extensive esterification reaction between the carboxyl groups of the low Mw species of γ-PGA occurring in R2 sample and the hydroxyl groups of GLY that, in turn, improved the extensibility of the films as a consequence of the formation of a high number of covalent stable bonds between the plasticizer and the polymer matrix [35].

Finally, the thermal characterization of the materials obtained by hot compression showed an increase in their thermal stability corresponding to the enhancement of the Mw of γ-PGA molecular species. The thermogravimetric analyses of the different γ-PGA samples indicated at around 330 °C the peak of the thermal decomposition of the higher

Mw species of γ-PGA (54.7 kDa) contained in R1 fraction, whereas the peak corresponding to the decomposition of the lower Mw species of γ-PGA (17.9 kDa) present in the R2 samples occurred just below 300 °C. In addition, from DSC analyses, it was possible to assess that R2 sample evidenced the lower glass transition temperature, as expected, given its lower molecular weight. Moreover, a worthy plasticizing effect of GLY was extended to all the films, thus confirming, at molecular level, the previous improvement of mechanical properties for all the GLY-doped samples. A recent study of Lee et al. [35] on the design of films from cellulose graft copolymers obtained by carver press demonstrated that the hot compression really led to an evident thermos-plasticizing effect. In conclusion, fractionated γ-PGA may be used for film formation with diverse possible uses, among which the bioactivity data here reported suggest some cosmeceutical applications. It is worth to mention that, for the first time, γ-PGA was used to prepare biomaterials by both casting and hot compression method. Although casting is the most successful technique for preparing homogeneous materials, it is less suitable for a large-scale process. In fact, the hot compression requires less time to produce materials and, therefore, it has been demonstrated to be a promising method for packaging ma-nufacture. Besides, the thermally obtained films ensure a superior processability and may also be proposed for packaging purposes. In the future, emphasis should be given to scale up experimentation on this hot compression method for the commercialization of γ-PGA-based biomaterials. However, further attempts are necessary in order to increase the very low TS found for the films prepared by means of this method (Table 2).

5. Conclusions

The potential of γ-PGA as raw ingredient for ready-to-use market products has been extensively explored so far, even though the majority of the commercially inexpensive preparations of the homopolypeptide seem to result in low quality and purity. To better highlight the potential use of specific homogenous low molecular size populations of γ-PGA obtained by fermentation, a specific three-step membrane process was developed up to 300 g scale of the commercial product and compared to γ-PGA obtained from the same original source after precipitation by methanol. The retentate fractions, also characterized by new analytical methods, permitted the obtaining of films by both casting and hot compression with good technological properties and diverse potential applications. Furthermore, since the results obtained by two skin damage experimental models showed that the low Mw forms of the homopolypeptide were able to counteract the desiccation and the oxidative stress of keratinocyte monolayers, all these data suggest possible applications of the γ-PGA-based films also as protective co-smeceutical devices.

Supplementary Materials: The following supporting information can be downloaded at: https://www.mdpi.com/article/10.3390/polym14061190/s1, Section S1. Thermal analysis of MET-PGA, R1 and R2 powder based films Figure S1. UHPLC chromatogram of a standard (std) sample of γ-PGA (black line), analysed on the base of its L-glutamic acid content after acidic hydrolysis of the polymer, in comparison with the chromatogram of a representative γ-PGA sample (blue line) from the membrane purification process (A). RI chromatograms of SEC-TDA analyses of the different γ-PGA standards used to determine the $dn \cdot dc^{-1}$ value (B). Figure S2: Complete SEC-TDA chromatograms of the different γ-PGA samples with the signals of RI (red line), of the viscosimeter (blue line) and of the right angle (green) and low angle light scattering (black line): Commercial γ-PGA, MET-PGA powder, 100 kDa retentate (R1), 3 kDa retentate (R2) and of the nano-filtration retentate (R3). The dot blue lines indicate how were integrated the different species. Figure S3. Thermogravimetric TGA (A), differential thermogravimetric DTG (B) and differential scanning calorimetric analysis DSC (second heating run C) of powder samples. DSC first heating run of powders (D), neat films (E) and glycerol doped films (F). Figure S4. Derivative Thermogravimetry (DTG) and Differential Thermal Analysis (DTA) of MET-PGA, R1 and R2 neat films (A) and glycerol doped films (B).

Author Contributions: Conceptualization, C.S. and R.P.; methodology, O.F.R., S.H., C.V.L.G., E.C., S.D., G.S., D.Z. and P.D.P.; formal analysis, O.F.R., S.H., C.V.L.G., E.C., S.D., G.S., D.Z. and P.D.P.; investigation, O.F.R., S.H., C.V.L.G., E.C. and S.D.; writing—original draft preparation, O.F.R., S.H.

and C.V.L.G.; writing—review and editing, C.S. and R.P.; funding acquisition, C.S. and R.P. All authors have read and agreed to the published version of the manuscript.

Funding: This research was funded by Contratto di sviluppo "Altergon Italia" (CdS000463), and by the grant PRIN: Progetti di Ricerca di Interesse Nazionale—Bando 2017—"CARDoon valorisation by InteGrAted biorefiNery (CARDIGAN)" of Italian Ministero dell'Università e della Ricerca (COD. 2017KBTK93). In addition, O.F.R. fellowship was granted by MUR PON01_2464.

Data Availability Statement: The data that support the findings of this study are available on request from the corresponding author.

Acknowledgments: We thank Rocco Di Girolamo (Department of Chemical Sciences, University of Naples Federico II) for his helpful technical assistance in preparing films by carver press.

Conflicts of Interest: The authors declare no conflict of interest.

References

1. Bajaj, I.; Singhal, R. Poly(glutamic acid)-An emerging biopolymer of commercial interest. *Bioresour. Technol.* **2011**, *102*, 5551–5561. [CrossRef] [PubMed]
2. Jiang, S.; Fan, L.; Zhao, M.; Qiu, Y.; Zhao, L. Enhanced low molecular weight poly-γ-glutammic acid production in recombinant *Bacillus subtilis* 1A751 with zinc ion. *Appl. Biochem. Biotechnol.* **2019**, *189*, 411–423. [CrossRef] [PubMed]
3. Luo, Z.; Guo, Y.; Liu, J.; Qiu, H.; Zhao, M.; Zou, W.; Li, S. Microbial synthesis of poly-γ-glutamic acid: Current progress, challenges, and future perspectives. *Biotechnol. Biofuels* **2016**, *9*, 134. [CrossRef] [PubMed]
4. Wang, L.-L.; Chen, J.-T.; Wang, L.-F.; Wu, S.; Zhang, G.-Z.; Yu, H.-Q.; Ye, X.-D.; Shi, Q.-S. Conformations and molecular interactions of poly-γ-glutamic acid as soluble microbial product in aqueous solutions. *Sci. Rep.* **2017**, *7*, 12787. [CrossRef] [PubMed]
5. Hsueh, Y.-H.; Huang, K.-Y.; Kunene, S.C.; Lee, T.-Y. Poly-glutamic acid synthesis, gene regulation, phylogenetic relationship, and role in fermentation. *Int. J. Mol. Sci.* **2017**, *18*, 2644. [CrossRef] [PubMed]
6. Sabbah, M.; Di Pierro, P.; Ruffo, F.; Schiraldi, C.; Alfano, A.; Cammarota, M.; Porta, R. Glutamic acid as repeating building block for bio-based films. *Polymers* **2020**, *12*, 1613. [CrossRef] [PubMed]
7. Zhang, X.; Li, H.; Guo, Y.; Ding, S.; Chen, G.; Liang, Z.; Zeng, W. An integrated strategy for recovery and purification of poly-γ-glutamic acid from fermentation broth and its techno-economic analysis. *Sep. Purif. Technol.* **2022**, *278*, 119575. [CrossRef]
8. Do, J.H.; Chang, H.N.; Lee, S.Y. Efficient recovery of γ-poly (glutamic acid) from highly viscous culture broth. *Biotechnol. Bioeng.* **2001**, *6*, 219–223. [CrossRef]
9. Kreyenschulte, D.; Krull, R.; Margaritis, A. Recent advances in microbial biopolymer production and purification. *Crit. Rev. Biotechnol.* **2014**, *34*, 1–15. [CrossRef] [PubMed]
10. Kumar, R.; Pal, P. Fermentative production of poly (γ-glutamic acid) from renewable carbon source and downstream purification through a continuous membrane-integrated hybrid process. *Bioresour. Technol.* **2015**, *177*, 141–148. [CrossRef]
11. Schiraldi, C.; Alfano, A.; Cimini, D.; De Rosa, M.; Panariello, A.; Restaino, O.F.; De Rosa, M. Application of a 22L scale membrane bioreactor and cross-flow ultrafiltration to obtain purified chondroitin. *Biotechnol. Prog.* **2012**, *28*, 1012–1018. [CrossRef] [PubMed]
12. Restaino, O.F.; Borzacchiello, M.G.; Scognamiglio, I.; Fedele, L.; Alfano, A.; Porzio, E.; Manco, G.; Donatiello, C.; De Rosa, M.; Schiraldi, C. High yield production and purification of two recombinant thermostable phosphotriesterase-like lactonases from *Sulfolobus acidocaldarius* and *Sulfolobus solfataricus* useful as bioremediation tools and bioscavengers. *BMC Biotechnol.* **2018**, *18*, 18. [CrossRef] [PubMed]
13. Bradford, M.M. A rapid and sensitive method for the quantitation of microgram quantities of protein utilizing the principle of protein-dye binding. *Anal. Biochem.* **1976**, *72*, 248–254. [CrossRef]
14. Shankar, S.; Teng, X.; Rhim, J.-W. Properties and characterization of agar/CuNP bionanocomposite films prepared with different copper salts and reducing agents. *Carbohydr. Polym.* **2014**, *114*, 484–492. [CrossRef] [PubMed]
15. Restaino, O.F.; Finamore, R.; Stellavato, A.; Diana, P.; Bedini, E.; Trifuoggi, M.; De Rosa, M.; Schiraldi, C. European chondroitin sulfate and glucosamine food supplements: A systematic quality and quantity assessment compared to pharmaceuticals. *Carbohydr. Polym.* **2019**, *222*, 114984. [CrossRef] [PubMed]
16. Squillaci, G.; Finamore, R.; Diana, P.; Restaino, O.F.; Schiraldi, C.; Arbucci, S.; Ionata, E.; La Cara, F.; Morana, A. Production and properties of an exopolysaccharide synthesized by the estreme halophilic archaeon *Haloterrigena turkmenica*. *Appl. Microbiol. Biotechnol.* **2015**, *100*, 613–623. [CrossRef]
17. Mirpoor, S.F.; Restaino, O.F.; Schiraldi, C.; Giosafatto, C.V.L.; Ruffo, F.; Porta, R. Lignin/carbohydrate complex isolated from *Posidonia oceanica* sea balls (Egagropili): Characterization and antioxidant reinforcement of protein-based films. *Int. J. Mol. Sci.* **2021**, *22*, 9147. [CrossRef]
18. Restaino, O.F.; D'Ambrosio, S.; Cassese, E.; Barbuto Ferraiuolo, S.; Alfano, A.; Ventriglia, R.; Marrazzo, A.; Schiraldi, C.; Cimini, D. Molecular weight determination of heparosan- and chondroitin-like capsular polysaccharides: Figuring out differences between wild-type and engineered *Escherichia coli* strains. *Appl. Microbiol. Biotechnol.* **2019**, *103*, 6771–6782. [CrossRef]
19. Roy, S.; Rhim, J.-W. Preparation of carbohydrate-based functional composite films incorporated with curcumin. *Food Hydrocoll.* **2020**, *98*, 105302. [CrossRef]

Chapter III

Physicochemical Characterization of Chitosan/Poly-γ-Glutamic Acid Glass-like Materials

This chapter introduces a novel method for preparing non-covalently crosslinked bio-composites by blending poly-γ-glutamic acid (γ-PGA) of microbial origin and CH through polyelectrolyte complexation. The materials exhibited a remarkable dual nature, initially appearing as soft, moldable hydrogels and transforming into exceptionally hard, glass-like materials upon dehydration. Structural, physicochemical, and thermal analyses revealed strong physical interactions between the polysaccharide and the homopolypeptide chains, mediated by electrostatic attraction and hydrogen bonding. The bio-composites exhibited both crystalline and amorphous structures, demonstrating excellent thermal stability and biodegradability. Their unique blend of properties, including thermoplasticity and saloplasticity, opens vast possibilities in the field of polyelectrolyte complexes (PECs). This versatility renders them highly promising candidates for diverse applications in regenerative medicine, biomedical devices, food packaging, and 3D printing.

International Journal of
Molecular Sciences

MDPI

Article

Physicochemical Characterization of Chitosan/Poly-γ-Glutamic Acid Glass-like Materials

Sondos Hejazi [1], Odile Francesca Restaino [1], Mohammed Sabbah [2], Domenico Zannini [1,3], Rocco Di Girolamo [1], Angela Marotta [4], Sergio D'Ambrosio [5], Irene Russo Krauss [1,6], C. Valeria L. Giosafatto [1], Gabriella Santagata [3], Chiara Schiraldi [5] and Raffaele Porta [1,*]

1 Department of Chemical Sciences, University of Naples "Federico II", 80126 Naples, Italy; sondosmohammadhasan.hejazi@unina.it (S.H.); odilefrancesca.restaino@unina.it (O.F.R.); domenico.zannini@unina.it or domenico.zannini@ipcb.cnr.it (D.Z.); rocco.digirolamo@unina.it (R.D.G.); irene.russokrauss@unina.it (I.R.K.); giosafat@unina.it (C.V.L.G.)
2 Department of Nutrition and Food Technology, An-Najah National University, Nablus P400, Palestine; m.sabbah@najah.edu
3 Institute for Polymers, Composites, and Biomaterials, National Council of Research, 80078 Pozzuoli, Italy; gabriella.santagata@ipcb.cnr.it
4 Department of Chemical, Materials and Production Engineering (DICMaPI), University of Naples "Federico II", 80126 Naples, Italy; angela.marotta@unina.it
5 Department of Experimental Medicine, Section of Biotechnology and Molecular Biology, University of Campania "Luigi Vanvitelli", 80138 Naples, Italy; sergio.d'ambrosio@unicampania.it (S.D.); chiara.schiraldi@unicampania.it (C.S.)
6 Consorzio per lo Sviluppo dei Sistemi a Grande Interfase, 50019 Florence, Italy
* Correspondence: raffaele.porta@unina.it

Abstract: This paper sets up a new route for producing non-covalently crosslinked bio-composites by blending poly-γ-glutamic acid (γ-PGA) of microbial origin and chitosan (CH) through polyelectrolyte complexation under specific experimental conditions. CH and two different molecular weight γ-PGA fractions have been blended at different mass ratios (1/9, 2/8 and 3/7) under acidic pH. The developed materials seemed to behave like moldable hydrogels with a soft rubbery consistency. However, after dehydration, they became exceedingly hard, glass-like materials completely insoluble in water and organic solvents. The native biopolymers and their blends underwent comprehensive structural, physicochemical, and thermal analyses. The study confirmed strong physical interactions between polysaccharide and polyamide chains, facilitated by electrostatic attraction and hydrogen bonding. The materials exhibited both crystalline and amorphous structures and demonstrated good thermal stability and degradability. Described as thermoplastic and saloplastic, these bio-composites offer vast opportunities in the realm of polyelectrolyte complexes (PECs). This unique combination of properties allowed the bio-composites to function as glass-like materials, making them highly versatile for potential applications in various fields. They hold potential for use in regenerative medicine, biomedical devices, food packaging, and 3D printing. Their environmentally friendly properties make them attractive candidates for sustainable material development in various industries.

Keywords: chitosan; poly-γ-glutamic acid; polyelectrolytes complexation; crosslinked materials; glass-like materials; bioplastics; physicochemical characterization

check for updates

Citation: Hejazi, S.; Restaino, O.F.; Sabbah, M.; Zannini, D.; Di Girolamo, R.; Marotta, A.; D'Ambrosio, S.; Krauss, I.R.; Giosafatto, C.V.L.; Santagata, G.; et al. Physicochemical Characterization of Chitosan/Poly-γ-Glutamic Acid Glass-like Materials. *Int. J. Mol. Sci.* **2023**, *24*, 12495. https://doi.org/10.3390/ijms241512495

Academic Editor: Andrea Salis

Received: 18 July 2023
Revised: 3 August 2023
Accepted: 4 August 2023
Published: 6 August 2023

1. Introduction

The rapid emergence of innovative technologies at reduced costs has created a matrix of potential challenges to find new sustainable alternatives to plastic pollution. Only one-fourth of fossil-based materials are recycled [1], making the turn to eco-sustainable, biodegradable polymers unavoidable. Bioplastics produced from renewable sources gained a huge interest as possible replacements for oil-based plastics [2]. In fact, the European

Sustainable Development agenda aims to achieve a wider use of bioplastics by 2030 [3]. Traditional plastics are constituted by polymers of specific repeating units that determine their properties. These features, common not only to polyethylene, polypropylene, polystyrene, and polyvinyl chloride but also to biopolymers such as polylactic acid, starch, or cellulose derivatives, appear to confer to plastic materials key properties [4]. Despite several research efforts dedicated to biopolymers in recent years, little is known about the ability of polypeptides or homopolypeptides to give rise to materials with specific plastic-like properties [5]. Among these, poly-γ-glutamic acid (γ-PGA), a natural, anionic homopolyamide (molecular weight (Mw) from 20 to 2000 kDa), is made of D- and/or L-glutamic acid units that are linked by amide linkages between the α-amino group and γ-carboxylic acid [6]. It is widely used in medicine and food industry applications, and can potentially replace synthetic plastics, being both non-toxic and biodegradable [4,5]. γ-PGA is produced by *Bacillus* strain fermentation [6,7], but as a pure powder, it is expensive, according to the Merck price list (100 mg costs 291 €) [8], due to low production yields and complex purification procedures [9]. Cheaper bulks, having low γ-PGA content and pureness, are also present on the market but need to be purified [10] before being employed [10,11]. However, the use of food by-products offers a promising solution in terms of cost and sustainability, as shown by Hisada and Kawase (2017), who have explored the utilization of wasted natto mucilage as a fermentation source for industrial-scale production of γ-PGA [12]. Chitosan (CH), instead, is a polysaccharide made of β-1,4-linked glucosamine, partially acetylated (≤25%), derived from the chitin of shell shrimps [13]. CH is soluble in aqueous acidic solutions, where the amine groups are protonated [14], making it form polyelectrolyte complexes with highly negatively charged polymers, such as γ-PGA [15]. Thus, crosslinked materials were prepared in this paper by physical blending of γ-PGA and CH. Their physicochemical properties, thermal behavior, and degradability were evaluated and compared with those displayed by the native biopolymers.

2. Results and Discussion

2.1. Poly-γ-Glutamic Acid and Chitosan Molecular Weight Determination

A commercial γ-PGA sample (COM-PGA) was employed, the pureness of which was 51.8 ± 0.5% on the dry weight (water content was 8.7 ± 0.2%), as analyzed by ultra-high performance liquid chromatography (UHPLC) [10]. It was ultrafiltered (UF) after being dissolved in MilliQ water (18.7 ± 0.8% of the sample remained insoluble) on 100 and 3 kDa cut-off membranes. The 100 kDa (R1) and 3 kDa (R2) retentates contained 8.7 ± 0.7% and 10.6 ± 0.5% of the initial γ-PGA amount with a purity of 72.4 ± 0.8% and 73.9 ± 0.5% on the dry weight, respectively, which was similar to previous results [10]. During the process, the mass recoveries of R1 plus the 100 kDa permeate (P1) and of R2 plus the 3 kDa permeate (P2) were 90.8% and 99.0%, respectively (Appendix A Table A1). The COM-PGA Mw distribution, determined by size-exclusion chromatography with triple detector array (SEC-TDA), showed three peaks of 77.4, 20.6, and 2.92 kDa average Mw. These populations were separated by UF in R1 and R2, which showed 59.4 and 20.1 kDa Mw with a representativity of 93.2% and 93.6%, respectively, and were then used to prepare the materials (Figure 1a,b). Previous data demonstrated that COM-PGA lowest Mw fraction (2.92 kDa) was not suitable to prepare materials [10]. Conversely, CH showed a main peak (75.0% of representativity) of about 285.5 kDa with a dispersity (Mw/Mn) of 1.6 (Figure 1a,b).

a

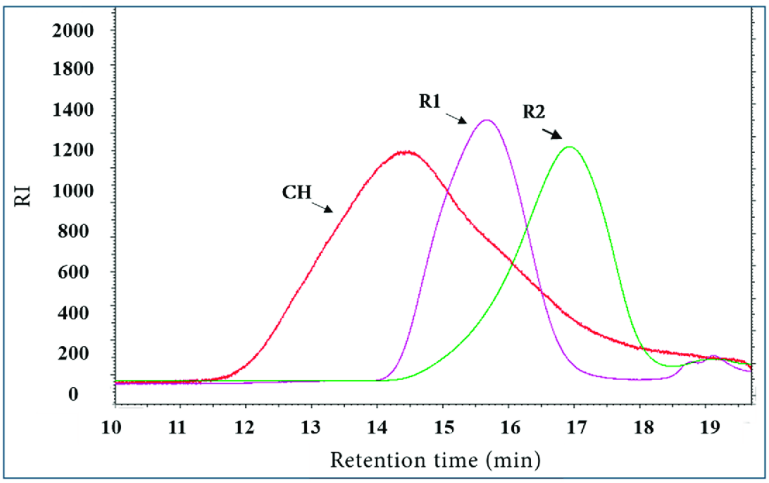

b

Sample	Mw (kDa)	Mw/Mn	IV (dL/g)	Representativity (%)
COM-PGA	77.4	1.3	1.03	10.0
	20.6	1.2	0.34	23.0
	2.92	2.1	0.96	67.0
R1	59.4	1.4	0.77	93.2
	29.1	1.2	1.00	5.1
R2	20.1	1.4	0.37	93.6
CH	285.5	1.6	5.85	75.0

Figure 1. (**a**) Overlay chromatograms of SEC-TDA analyses of chitosan (CH), R1, and R2 ultrafiltrated fractions of poly-γ-glutamic acid (COM-PGA). (**b**) Average molecular weight (Mw), dispersity (Mw/Mn), intrinsic viscosity (IV), and representativity of the main peaks.

2.2. *Hydrophilicity and Solubility*

Crosslinked materials were prepared by blending solutions of CH and of the two γ-PGA fractions (R1 and R2) at pH 3.5 and weight ratios of 1/9, 2/8, 3/7 CH/R1, or CH/R2. The precipitated materials separated first by decantation and then by centrifugation after several washings with the same solvent resulted in soft, rubbery, easy-to-manipulate materials that were moldable in a wet state.

Astonishingly, once dehydrated at ambient temperature, they turned into extremely hard and glass-like materials. Comparable findings were published, describing rubbery hydrogels obtained by blending CH with carrageenan [16]. Since its rubbery consistency resembles soft living tissues, this kind of hydrogel might interest the scientific and medical fields for its ability to trap water and solutes, forming a solid gel structure. Thus, the blending of polycationic and polyanionic biopolymers must be carried out in a water solution, where the pH becomes a key factor as the different charged groups can be more or less ionized, and their interactions affect the physical properties of the matrix [17]. As γ-PGA pKa is about 4.86 and CH pKas are 6.2 and 7.0 [11,17] a pH of 3.5 was optimal for the blending, as at this value, both biopolymers were charged and, consequently, rapidly

bind to each other through strong electrostatic interactions and lead to the precipitation of the supramolecular complex. It is worth noting that the variation in CH/γ-PGA ratios and pH values made it impossible to obtain any precipitated material. The resulting glass-like materials were characterized in terms of their solubility both in water and in several organic solvents as well as under different stressing temperatures (70 °C) pH (3.5, 7.0, and 10.0) and mechano-physic (sonication, stirring) conditions. All the glass-like materials tested were insoluble, thus highlighting that, during the ion complex forming and dehydration process, very strong physical crosslinking occurred among the biopolymer chains. It was shown that after 24 h of different solvents, the material samples preserved their physical integrity. In addition, it was observed that the glass-like materials immersed in water rehydrated, whereas those immersed in organic solvents kept their toughness and a glass-like structure, thereby confirming the physical strength of the three-dimensional network that developed [18]. Only hydrogen peroxide at pH 4.0 and 10.0 was found to disintegrate the blended materials due to CH precipitation at a very basic pH and oxidative degradation of polyamide [19] (Figure 2). The pioneering study by Fuoss and Sadek in 1949 explored the interaction between a strongly acidic polyanion (sodium polystyrene sulfonate) and a strongly basic polycation (poly (vinyl methyl pyridinium) chloride) in an aqueous solution [20]. They observed that this interaction led to a colloidal precipitate and the formation of a stable, infusible, and insoluble precipitate, and the reaction occurred rapidly, resulting in a product with nearly stoichiometric equivalents of the component polyions. Shamoun et al. (2012) further investigated stoichiometric polyelectrolyte complexes (PECs) [21] and introduced the term "saloplastics" to describe the materials formed by combining polycations and polyanions, and they demonstrated the compaction of PECs using ultracentrifugation at room temperature with the addition of extensive salt. The study demonstrated the successful creation of stoichiometric PECs in various shapes using an extruder [21].

Solvents	Water			H_2O_2		Chloroform	DMSO	Acetic acid	Methanol	Toluene
pH	3.5	7	10	4	10	-	-	-	-	-

Figure 2. Images of CHR1(2/8) sample immersed in distilled water at different pH values (3.5, 7.0, and 10.0), or in 30% (*w*/*v*) of H_2O_2 at different pH 4.0 and 10.0, or in different organic solvents.

In light of these findings, our materials can be described as thermoplastic and saloplastic, signifying vast applications in the field of PECs, including the creation of 3D forms, PEC micro-chambers (opening up new possibilities for innovative uses), and further explorations in the realm of polyelectrolyte complexes [22,23].

2.3. Structural Analyses and Dynamic Mechanical Analysis

Figure 3a,b show Fourier transform infrared (FTIR) spectra of crosslinked materials (CHR1 and CHR2) and neat biopolymers of CH, R1, and R2. The characteristic peaks of neat CH appeared at 3439, 1659, 1550, 1320, 1593, 1420, and 1378 cm^{-1} corresponding to the stretching vibration of N-H and O-H groups engaged in intramolecular and intermolecular hydrogen bonds, C=O stretching of amide I, N-H bending of amide II, C-N stretching of amide III, N-H bending of the primary amine, CH_2 bending, and CH_3 symmetrical deformations [19], respectively. Finally, the absorption band at 1154 cm^{-1} can be attributed to asymmetric stretching of the C-O-C glycosidic bridge bond [24]. Regarding R1 and R2, the characteristic peaks observed at 3400, 1727, 1645, 1557, and 1410 cm^{-1} correspond to N–H bonds, C=O stretching vibration of the carboxylic acid, C=O of amide I, C–N stretching modes vibration, and CH_2 bending deformations, respectively. Notably, the prominent

peaks at 1129 cm^{-1} could be related to the melanoidin C-O bending bands [25]. The complexation between the two biopolymers was investigated by comparing the infrared spectra of CHR1 and CHR2 with the neat biopolymers (CH, R1, and R2). Results referred to only physical interactions, as no chemical reactions occurred during the formation of the supramolecular complex [14]. The first evidence of CH complexation with either R1 or R2 was found in the reduction of the intensity of the γ-PGA carboxyl group at 1726 cm^{-1}, following its electrostatic and hydrogen bonding engagements with the polar residues of CH (Figure 3). Furthermore, the γ-PGA amide I peak at around 1645 cm^{-1}, both in CHR1 (Figure 3a) and in CHR2 (Figure 3b) blends, shifted towards a lower frequency with the increase in CH mass percentage, which evidenced the even stronger physical interaction between the polar residues of the two biopolymers through hydrogen bonding. It has been widely reported in the literature that hydrogen bonding reduces the vibration frequency energy of functional groups engaged in that kind of interaction [26]. The same trend was observed for CH stretching vibration at around 1420 cm^{-1} attributed to the NH_3^+ of CH complexing with $-COO^-$ of γ-PGA [27]. The FTIR study confirmed successful CH/γ-PGA complex formation via electrostatic attractions between γ-PGA negative charged polar groups and CH protonated amine residues as well as hydrogen bonding interactions.

X-ray diffraction (XRD) profiles of CH, R1, and R2 are shown in Figure 3c. CH diffraction peaks at 2θ 10.5° and 20.5° were recorded. XRD patterns indicated the presence of CH crystallinity structure, whereas both R1 and R2 showed a typical amorphous pattern characterized by a broad amorphous halo centered at 2θ~22°. XRD profiles of CHR1 or CHR2 blends (Figure 3c) indicated amorphous characteristics of the supramolecular complexes, since only amorphous haloes at 2θ~22° and a shoulder at 2θ~40° were visible [28,29].

Far-UV circular dichroism (CD) spectroscopy was used to investigate CH, R1, and R2 features in solutions. CH exhibited a spectrum (Appendix A Figure A1) with a deep minimum at 211 nm, indicative of an acetylated amine chromophore on a glycosidic ring in an acidic solution. This signal is related to the acetyl content of the CH, and it is independent of the α, β anomeric equilibrium, the chain length beyond two residues, the ionic strength and pH, and the polymer conformation [30]. R1 and R2 fractions have comparable spectra, showing a deep minimum at about 218 nm when analyzed at pH 6.0, indicating a predominant presence of β-sheet structures in both samples. Decreasing the pH to 3.5 leads to a shift towards 215 nm, with a significant intensity increase (Appendix A Figure A1). This change is typically associated with β-sheets, but the change of intensity associated with the pH change suggests that conformational changes occurred, and a higher content of alpha-helices can be hypothesized considering that the CD spectra of alpha helices are much more intense than those of β-sheets. The limited purity of R1 and R2 prevented the exact determination of secondary structure content via spectrum deconvolution. It is noteworthy that in no case does γ-PGA adopt a random coil conformation. This finding confirms the exclusive presence of γ-PGA in both samples. Its α-helix content increased as pH decreased from 7.0 to 3.0, while β-sheet and random coil contents decreased. On the other hand, α-PGA is mostly a random coil at pH $\geq$ 6 and α-helical in strongly acid conditions [31]. Furthermore, to streamline the study and gain valuable insights into the behavior of the polymer blends, we focused on one specific type of blended material (CHR1, 1/9) for CD spectra recording. Additionally, DMA analysis was performed on a dry sample CHR1 (3/7) as a representative example for all of the other prepared blended ratios. The CD spectra revealed an intense minimum intermediate between CH and γ-PGA, suggesting that the interaction between the two polymers does not cause significant conformational changes (Figure 3d).

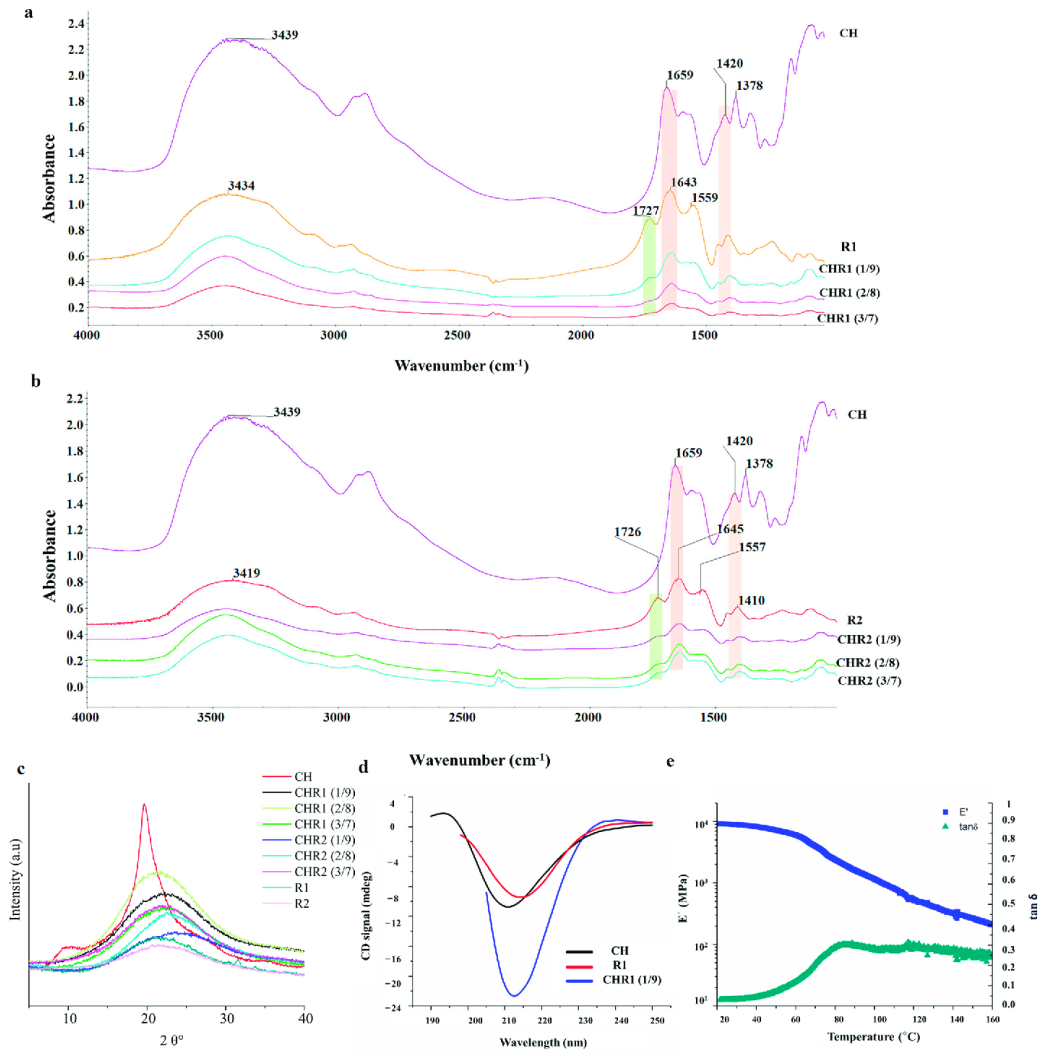

Figure 3. (**a**) Fourier transform infrared spectroscopy (FTIR) spectra of CHR1. (**b**) FTIR spectra of CHR2 blends. (**c**) X-ray diffractograms of CHR1 and CHR2 using three different ratios CH/R1 or CH/R2 (1/9, 2/8 and 3/7) in comparison with the single biopolymers of chitosan (CH) and poly-γ-glutamic acid (γ-PGA) fractions (R1 and R2). (**d**) Circular dichroism spectra of CHR1 (1/9 ratio) in comparison with CH and γ-PGA R1 fraction. (**e**) Storage modulus (E′) and tan δ values by DMA analysis of the crosslinked materials of CHR1 (3/7).

The DMA analysis of the dry sample CHR1 (3/7) indicated the formation of a crystalline phase after water removal. The storage modulus exhibited a smooth and wide drop, indicating the presence of crystalline fractions relaxing at different times (Figure 3e). Notably, the material demonstrated a high glassy storage modulus, surpassing analogous CH/γ-PGA materials produced through extrusion and the addition of additives [32]. It also showed comparable properties to pristine γ-PGA [33] or CH [34]. Moreover, the glass transition temperature (Tg) of 84.4 °C was higher than the Tg of the reference material [32].

According to the XRD and DMA results, the materials studied exhibit both crystalline and amorphous phases. These findings align with the mechanical model proposed by Takayanagi, which supports the viscoelastic behavior of crystalline polymers by connecting the crystalline and amorphous regions in series and parallel elements [35].

2.4. Thermal Analyses

Thermogravimetric (TG) and differential thermogravimetric (DTG) analyses of CH, R1, and R2 were carried out and the obtained curves were normalized to the initial sample size (Figure 4a–d). The TG results showed that weakly bound water evaporated from 50 °C up to about 200 °C [36]. CH lost 25% of water while R1 and R2 15%, confirming the obtained moisture uptake and the content data. Glass-like materials showed minimal water loss due to their crosslinked structures. The absence of very low intense decomposition peaks in the region of water evolution in the differential thermograms was consistent with the findings discussed earlier regarding glass-like materials. The decomposition temperatures of CH (215.0 °C), R1 (257.7–306.0 °C), and R2 (291.1 °C) were aligned with the previous thermal characterization of the same biopolymers [27]. The depolymerization of γ-PGA started at around 200 °C, according to an unzipping cyclo-depolymerization mechanism generating pyroglutamic acid and methyl pyroglutamate, with the decomposition of the ionic complex [11]. Both R1 and R2 showed greater stability than CH as their main polymer degradation occurred at higher temperatures. R1 showed two thermal degradation peaks, likely associated with the thermal depolymerization of γ-PGA with different Mw. TG and DTG curves obtained from the analyses of CHR1 and CHR2 blends prepared at different CH/γ-PGA ratios are also shown in Figure 4a–d. The main polymer degradation phenomena of all the blends were faster than those observed with R1 and R2 but slower than that of CH. These findings highlighted the strong physical links occurring inside the supramolecular complexes due to both electrostatic interactions between the amino groups of CH and the carboxyl group of γ-PGA as well as the intermolecular hydrogen bonding [37]. Although γ-PGA represents the main polymer matrix of the crosslinked materials, the thermal degradation was significantly influenced by the presence of even low amounts of CH, as shown by the shifting of the observed T_{onset} towards lower temperatures. The peaks corresponding to the maximum degradation rate of the polymers (T_{max}) overlapped at the value of CH T_{max}. This could be due to the higher Mw of CH and to its reactive protonated amine groups being able to strongly attract the negatively charged γ-PGA chains [38]. The lower Mw of γ-PGA contained in the R2 fraction could be responsible for different structural networks, as shown by the presence of at least three degradation kinetics [10]. The last decomposition step observed between 400–500 °C, particularly marked in R2-based materials, was likely associated with the decarboxylation process leading to unsaturated chain fragments and non-volatile compounds in an inert atmosphere (nitrogen).

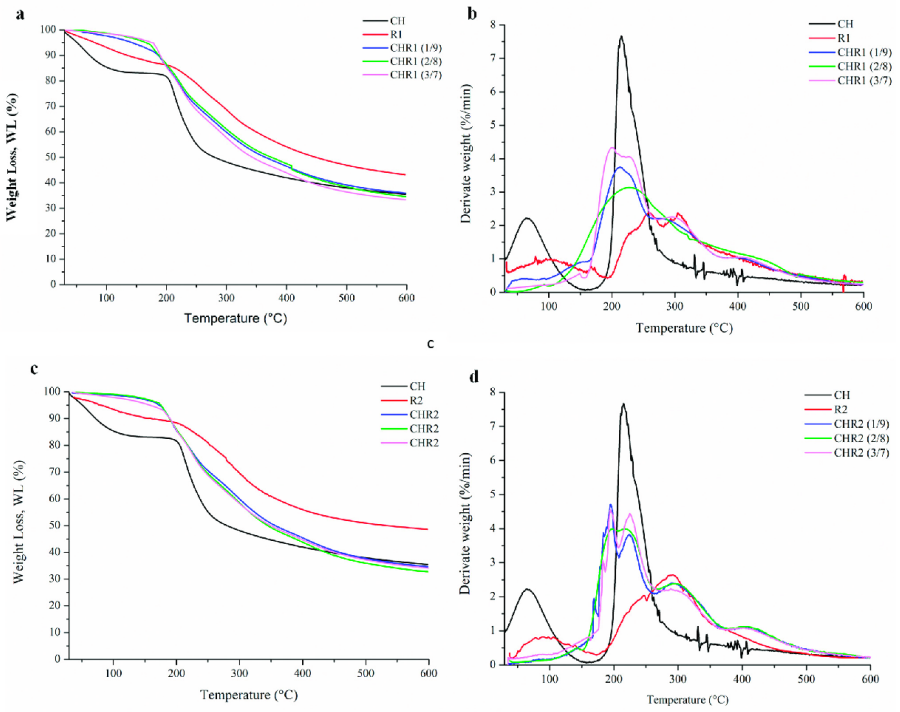

Figure 4. Thermogravimetric (TG) (**a**,**c**) and differential thermogravimetric (DTG) (**b**,**d**) analyses of CHR1 and CHR2 blends, obtained with three different CH/R1 or CH/R2 ratios (1/9, 2/8 and 3/7). The curves were compared to the single biopolymers of chitosan (CH) and poly-γ-glutamic acid fractions (R1 and R2).

2.5. Morphological Analysis and Disintegration Test

Scanning electron microscope (SEM) analyses of CH, R1, and R2 powders revealed a heterogeneous morphology for biopolymers with irregular particles (100–200 mm) (Figure 5a). As far as R1, elongated/fibrillar structures (200–300 mm) were also present. In addition, SEM images showed a flat and homogeneous structure for all of the glass-like materials prepared at all CH/R1 and CH/R2 ratios (Figure 5b). The observed structure demonstrated that complexation between the oppositely charged biopolymers produced a smoothed surface as well as the absence of voids and/or other morphological defects. Moreover, SEM images confirmed the absence of phase separation between CH and R1 or R2 in all of the blend ratios. Finally, Figure 5c-1,c-2 shows some preliminary results on the disintegration of the glass-like materials. The results show marked changes in the weight over time when samples were buried in the soil [39]. It is well known that as water diffuses from the soil into the polymer samples, their swelling and degradation increases because of the role played by water as a carrier of soil microorganisms able to depolymerize and transform the biopolymers in biomass, CO_2, and water [40]. All of the sample weights gradually decreased during the experiment. The samples showed low disintegration after 5 days with a loss of weight of 3.0–8.0%, while the degradability increased after 15 days as the mass reached 25.0%. Finally, the degradability further increased in the next 25 days, and the weight loss of the samples was between 13.0 and 85.0% and, in particular, was 62.0% for CHR1 (3/7 ratio) and even higher (85.0%) for CHR2 (3/7 ratio). These results suggest that these materials are degradable in soil under open-air environmental conditions.

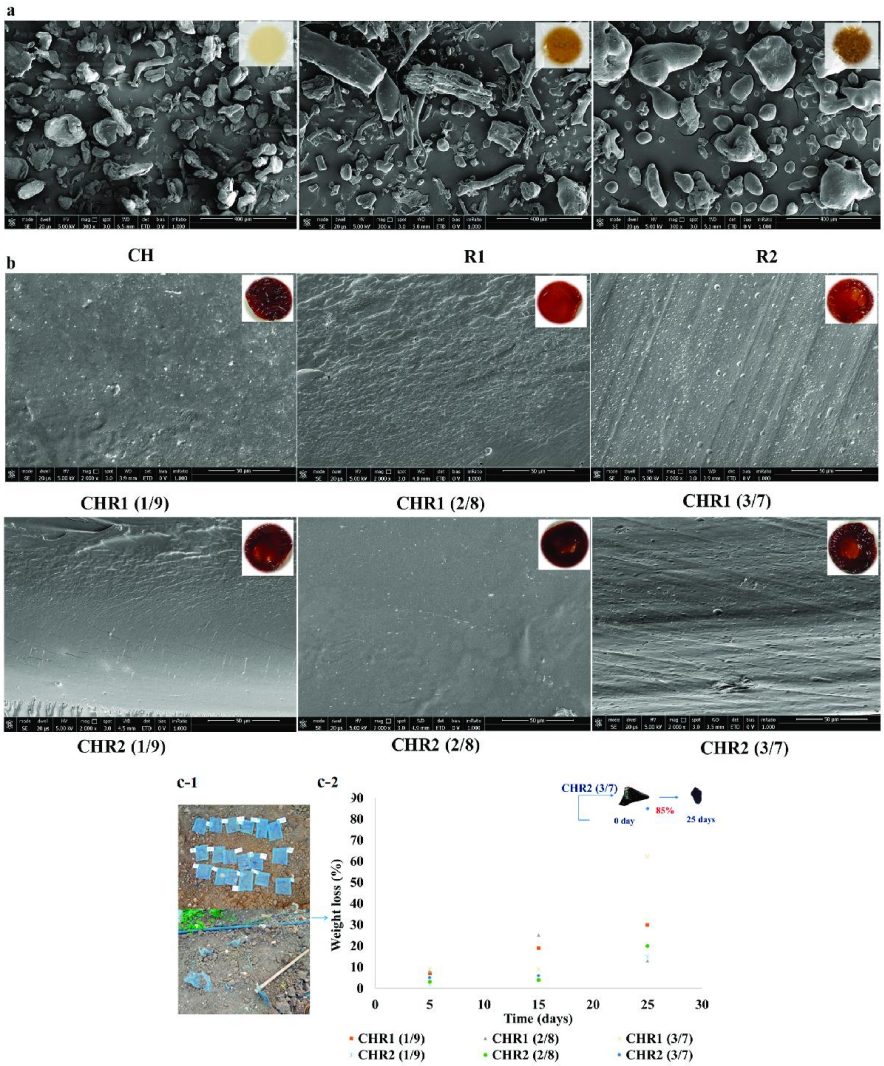

Figure 5. (**a**) Scanning electron microscopy (SEM) images of chitosan (CH) and of poly-γ-glutamic acid fractions (R1 and R2) captured at magnitude 2000× (the scale bar was 400 μm); the inserts represent the visual aspect of the three analysed powders. (**b**) SEM images (cross-section) of glass-like materials (CHR1, upper panels; CHR2, lower panels) obtained using the three different CH/R1 or CH/R2 ratios (1/9, 2/8, and 3/7) at magnitude 2000× (scale bar was 50 μm). The inserts represent the visual aspect of the three analysed glass-like materials. (**c-1**) Pictures of the blended materials buried in the soil. (**c-2**) Degree of disintegration, expressed as % weight loss, of CHR1 and CHR2 blends obtained at three different CH/R1 or CH/R2 ratios (1/9, 2/8, and 3/7) buried in the soil (orange square for CHR1 (1/9), grey triangle for CHR1 (2/8), yellow cross for CHR1 (3/7); blue cross for CHR2 (1/9), green circle for CHR2 (2/8), blue circle for CHR2 (3/7). Blended material at the beginning (T0) and after 25 days (T25) of degradation is shown in the insert of the panel.

3. Materials and Method

3.1. Materials and Chemicals

A not pure poly-γ-glutamic acid (COM-PGA, 50% purity) bulk, produced by microbial fermentation, was purchased by Xi'an Fengzu Biological Technology Co., Ltd. (Xi'an City, Shaanxi Province, China). Chitosan (CH) (75–85% deacetylated chitin, poly-D-glucosamine, 50,000–190,000 Da) was purchased by Sigma Aldrich, St. Louis, MO, USA, hydrogen peroxide (30% H_2O_2), acetic acid 96%, toluene, dimethyl sulfoxide 99.9% (DMSO) methanol, 99.9%, and chloroform,99.9% was purchased by CARLO ERBA (Emmendingen, Germany). All of the reagents used to prepare the buffers and the standards employed in UHPLC and SEC-TDA analyses were purchased from Sigma-Aldrich, St. Louis, MO, USA.

3.2. Fractionation of Commercial Poly-γ-Glutamic Acid by Membrane-Based Ultra-Filtration

Two γ-PGA fractions were prepared by UF from the COM-PGA, as previously reported [10]. Briefly, the COM-PGA sample (300 g) was dissolved in MilliQ water (10.0 L), stirred at 600 rpm for 18 h, and then centrifuged at 6500 rpm (4 °C) for 20 min (Avanti J-20XP, Beckman Coulter, USA) to remove insoluble material. The dissolved, centrifuged sample was micro-filtrated with a 0.65 µm polypropylene membrane (total filtering area of 0.05 m^2, Sartopure PP2 MidiCaps, Sartorius Group, Germany) and a non-automatic Sartoflow Alpha system (Sartorius Group, Göttingen, Germany). After this step, it was ultra-filtered and diafiltered with two volumes of MilliQ water by using two 100 kDa cut-off polyethersulfone cassette membranes (total filtering area of 0.1 m^2, Sartorius Group, Germany) and an automatic tangential flow filtration system (Uniflux 10, UNICORN, GE Healthcare, Chicago, IL, USA). The 100 kDa retentate sample (R1) was collected while the 100 kDa permeate (P1) was further ultra-filtered and diafiltered with two volumes of MilliQ water by using two 3 kDa cut-off polyethersulfone cassette membranes (0.5 m^2 of total filtering area, Sartorius Group, Germany) and the abovementioned system. The 3 kDa retentate sample (R2) was recovered while the 3 kDa permeate (P2) was discarded. During the process, samples were taken to determine the dry weight and the γ-PGA concentration. Data on pressure, volumes, conductivity, and the pH of the samples were also collected during the processes.

3.3. Determination of the Dry Weight and Water Content of the Samples

Aliquots (10 mL) of the UF samples were freeze-dried (LIO 5P, 5Pascal, Italy, Milan) (18 h at −20 °C and 1.05 mbar, and then 3 h at 20 °C and 0.04 mbar) [41] and then weighed to determine their dry weight. The water content of CH, COM-PGA, R1, and R2 was also determined as previously described [10].

3.4. Poly-γ-Glutamic Acid Quantitative Determination by Ultra-High Performance Liquid Chromatography

Analyses of the γ-PGA quantity present in the initial COM-PGA sample and in R1 and R2 were performed by UHPLC (Ultimate 3000, Dionex, Sunnyval, CA, USA) using a previously reported method [10]. Briefly, the samples were first hydrolyzed at 2.5 $g{\cdot}L^{-1}$ with 5 M HCl at 100 °C and 600 rpm for 6 h (Thermomixer comfort, Eppendorf, Germany) and then analyzed by using an ion-exclusion column (Rezex ROA-organic acid H^+, 300 × 78 mm, Phenomenex, Torrance, CA, USA) and an ultra-high-performance chromatographer (Ultimate 3000, Dionex, Sunnyvale, CA, USA), injecting 10 µL and eluting with 0.1% H_2SO_4 for 25 min at 0.8 $mL{\cdot}min^{-1}$ at 40 °C and detecting at 200 nm. The determined γ-PGA concentrations were then multiplied for the volumes of the samples to calculate the total amount (g) of the polymer in each fraction. These amount values were then divided by the polymer content in the initial COM-PGA sample to calculate the percentage of γ-PGA recovery in the UF process according to Equation (1):

$$\%\ \gamma\text{-PGA recovery/COM-PGA sample} = \%\ [\gamma\text{-PGA sample (g)/COM-PGA sample (g)}] \times 100 \quad (1)$$

Furthermore, in all of the samples, the percentage of the γ-PGA amount concerning the sample dry weight was calculated according to Equation (2):

$$\%\ \gamma\text{-PGA/dry weight} = \%\ (\gamma\text{-PGA sample (g)/dry weight sample (g)}] \times 100 \quad (2)$$

3.5. Chitosan and Poly-γ-Glutamic Acid Molecular Weight Determination by Size Exclusion Chromatography with Triple Detector Array

Mw analyses of CH, COM-PGA, and R1 and R2 were performed by using two gel-permeation columns (TSK-GEL GMPWXL, 7.8 × 30.0 cm, Tosoh Bioscience, Italy), put in series in a SEC-TDA instrument (Viscotek, Malvern, Italy), and equipped with a triple detector array with a refractive index (RI), a four-bridge viscosimeter (VIS), and two laser detectors of right-angle (RALS) and low-angle light scattering (LALS). The calibration of the instrument was performed with polyethylene oxide (PEO) standard (22 kDa PolyCAL, Viscotek, Malvern, Italy). CH and γ-PGA were analyzed by using two different methods. CH analyses were run using a buffer made of 0.15 M acetic acid, 0.1 M sodium acetate, and 0.4 mM sodium azide at pH 4.5 and 40 °C with a flow rate of 0.6 mL·min^{-1}, as previously described (Nguyen, Winnik, and Buschmann, 2009) [42]. γ-PGA was eluted with 0.1 M sodium nitrate at pH 7.0 and 40 °C, with a flow rate of 0.6 mL·min^{-1}, as previously described [43]. The CH and γ-PGA average Mw values, their dispersity (Mw/Mn), and their intrinsic viscosity (IV) were determined in duplicate on the base of the detector signals and the specific dn·dc^{-1} values by applying Equations (3)–(5), as reported by the manufacturer:

$$\text{RI signal} = \text{kRI} \cdot \text{dn·dc}^{-1} \quad (3)$$

$$\text{VIS signal} = \text{kVIS} \cdot \text{IV} \cdot \text{C} \quad (4)$$

$$\text{LALS signal} = \text{kLALS} \cdot \text{Mw} \cdot (\text{dn·dc}^{-1})^2 \cdot \text{C} \quad (5)$$

where IV is the intrinsic viscosity (dl × g^{-1}), C is the concentration (mg·mL^{-1}), dn·dc^{-1} is the refractive index increment (mL × g^{-1}), and kRI, kVIS, and kLALS are instrumental constants obtained by the universal calibration with PEO (Viscotek; information available from http://www.viscotek.com (accessed on 2 May 2023) [44]. The γ-PGA dn·dc^{-1} value used for the analyses was 0.183 mL·g^{-1}, as experimentally determined in a previous paper [10]. The CH dn·dc^{-1} value was 0.192 mL·g^{-1}, as reported in the literature [43]. In the analyses, the representativity of each peak was calculated as the percentage ratio of the RI area of a single peak divided by the sum of the RI areas of all the peaks in the chromatogram [41].

3.6. Preparation of Chitosan and Poly-γ-Glutamic Acid Crosslinked Materials (CH/γ-PGA)

First, aqueous solutions of CH (20 mg/mL *w*/*v* in 0.1 M HCl) and the γ-PGA fractions (R1 and R2, 50 mg/mL) were prepared at pH 3.5. Then, R1 and/or R2 solutions were added to CH solutions in different mass ratios (1/9, 2/8, and 3/7; *w*/*w*, CH/R1 or CH/R2), and the resulting mixtures were adjusted at pH 3.5 and stirred at 800 rpm at 25 °C for 60 min. This addition led precipitates to form, which were collected first by decantation and then by centrifugation at 10,000 rpm for 10 min at 4 °C (Avanti J-20 XP, Beckman Coulter, Brea, CA, USA) after being washed three times with distilled water at pH 3.5. The collected materials were in a dried state for characterization. In addition, separate aqueous solutions of R1, R2, and CH at pH 3.5 were lyophilized (Thermo Savant Modulyo Benchtop, USA) in order to characterize the neat polymers.

3.7. Hydrophilicity and Solubility

Solubility qualitative studies were carried out on glass-like materials focusing on the sample CHR1 (2/8 ratio) as a representative material. Briefly, about 10 mg of glass-like materials were immersed for 24 h in 600 µL of water at different pHs (3.5, 7.0, and

10.0) as well as in 600 µL of different solvents at pH 4.0 and pH 10.0 (in 30% hydrogen peroxide (*w*/*v*), chloroform, DMSO, acetic acid, methanol, and toluene). The samples were also further treated by ultrasonication (Bandelin SONOPULS ultrasonic homogenizers, Binder, Tuttlingen, Germany) followed by stirring for 2 h at 70 °C in a water bath to check the insolubility.

3.8. Structural Analyses

Fourier Transform Infrared Spectroscopy Analysis (FTIR)

Spectra were recorded by an FTIR instrument (NICOLET 5700, Australia) and 64 scans interferogram was collected with a variable path length cell and KBr windows. 1 mg of CH, R1, and R2 samples, and of the CHR1 and CHR2 blends were ground into powder using Ball Mills (Retch-PM 100 CM, UK Ltd., Hope Valley, UK) combined with 100 mg dry KBr. The grounded mixture was then pressed into a transparent disc and dried at 60 °C for 24 h before analysis. The spectra were recorded at a straight baseline of 400–4000 cm^{-1}.

X-ray Diffraction Analysis

Wide angle X-ray scattering measurements (WAXS) of CH, R1, and R2 samples as well as the CHR1 and CHR2 blends were obtained using nickel-filtered CuKα radiation with a Philips automatic diffractometer (Empyrean by Panalytical, Monza, Italy).

Circular Dichroism

CD spectra of CH, R1 and R2, as well as that of the CHR1 (1/9) blend, were recorded at 20 °C using a Jasco J-1500 spectropolarimeter equipped with a Peltier thermostatic cell holder (Model PTC-348WI). CD measurements were carried out in the 250−200 nm range, using a 0.1 cm path length cell. A total of 0.1 mg mL^{-1} CH solutions at pH 3.5 of 0.5 mg mL^{-1} of R1 and R2 solutions, either at pH 6.0 or 3.5 and 0.5 mg mL^{-1} CHR1 (1/9 ratio) blend suspension at pH 3.5, were analyzed with 0.5 nm data pitch, 2 nm bandwidth, and 20 nm min^{-1} scanning speed. Each spectrum was obtained as the average of three measurements and corrected for solvent signal.

3.9. Dynamic Mechanical Properties Analysis (DMA)

The mechanical properties of the blends were evaluated by dynamic mechanical analysis (DMA) performed with a Tritec 2000 DMA (Triton technology, London, UK). Hydrogels of CHR1 (3/7) were dried and formed in the shape of bars with a rectangular section (10 × 1 mm^2). Tests were conducted at 1 Hz with a displacement of 0.01 mm and heated at 2 °C min^{-1} starting from room temperature.

3.10. Thermal Analyses

Thermogravimetric analyses of CH, R1, and R2, as well as of CHR1 and CHR2 glass-like materials, were performed using a thermogravimetric analyzer (TGA/DTA, Perkinelmer pyrisdiamond) equipped with a gas station. An amount of 3–4 mg of each sample was placed in an open ceramic crucible and heated from 25 °C up to 600 °C at a speed rate of 10 °C/min under a nitrogen flow of 30 mL/min. Before testing, the samples were conditioned for 24 h at 25 °C and 50% RH.

3.11. Scanning Electron Microscopy

The morphological structure of the CH, R1, and R2 powders, as well as the cross-section fracture of CHR1 and CHR2 glass-like materials, were analyzed by SEM (Nova NanoSem 450-FEI-Thermo Fisher, Scientific, Waltham, MA, USA). The cryo-fractured samples were coated with thin layers of gold/palladium alloy using a sputter, and the images were then taken at an accelerating voltage of 5 kV.

3.12. Disintegration Test

All of the glass-like materials were dried at 105 °C, weighed, and buried in agricultural clay soil at the Faculty of Agriculture and Veterinary Medicine farm at An Najah National University in Tulkarm, Palestine. Properly labeled steel meshes were used to insert the samples inside the soil in 15 cm deep holes and to recollect them more easily in order to measure the weight loss. Before and after burying the samples, the soil was sifted to remove large clumps and plant debris. The soil moisture was controlled using a moisture indicator (IRROMETER. REG. US PAT. OFF) and kept at about 20% during the study by adding water whenever necessary. The buried samples were dug out once every 10 days, washed in distilled water, dried in the oven at 105 ± 2 °C for 6 h, and equilibrated in a desiccator for at least one day. The samples were then weighed, and the weight loss (%) was expressed according to Equation (6):

$$\text{Weight loss (\%)} = \text{Degraded sample weight(g)/Initial sample weight} \times 100 \quad (6)$$

3.13. Statistical Analysis

All the results are presented as mean ± standard deviations of the three replicates. Statistical analyses were performed with Microsoft Excel software (Microsoft Office 2017). The obtained data were tested for significant differences through the *t*-test, and data with $p < 0.05$ were considered to have statistical significance.

4. Conclusions

Advanced bio-composites made of CH and low Mw γ-PGA fractions were prepared by a process based on mixing distinct solutions of the two biopolymers at specific ratios and at acidic pH. The sedimented supramolecular complexes appeared as rubbery hydrogels that, when dehydrated, gave rise to glass-like materials endowed with advantageous physical characteristics and thermal stability as well as the amorphous and crystalline structure of the obtained glass-like material. This opens a window for the potential use of these new bio-composites in diverse fields.

Their applications could span regenerative medicine, biomedical devices, food packaging, and even 3D printing. The non-toxicity of the constituent biopolymers further enhances their suitability for these applications [45–47]. Due to its protein-like effects, this polymer composite holds significant potential, and may even outperform conventional polymers, thereby making it suitable for particular applications in regenerative medicine, such as the restoration of segmental bone defects [48].

In summary, the successful development of these advanced bio-composites opens up vast possibilities and represents a promising step towards sustainable and innovative materials for a wide range of applications in different industries. Further exploration and refinement of these materials will undoubtedly unveil even more exciting opportunities for their utilization in various fields.

Author Contributions: Conceptualization, S.H., R.P., M.S., C.V.L.G. and C.S.; methodology, O.F.R., S.H., G.S., D.Z., I.R.K., R.D.G. and A.M.; software, D.Z., S.H., O.F.R. and R.D.G.; validation, S.H., R.P., C.V.L.G. and C.S.; formal analysis, D.Z., S.H., G.S., S.D., A.M. and I.R.K., investigation, R.P., C.S., S.H. and M.S.; resources, S.H.; writing—original draft preparation, S.H., M.S. and C.V.L.G.; writing—review and editing, C.V.L.G., O.F.R. and R.P.; supervision, R.P., G.S. and C.S. All authors have read and agreed to the published version of the manuscript.

Funding: This research received no external funding.

Institutional Review Board Statement: Not applicable.

Informed Consent Statement: Not applicable.

Data Availability Statement: Not applicable.

Acknowledgments: We thank Elisabetta Cassese, Department of Experimental Medicine, University of Campania "Luigi Vanvitelli", 80138 Naples, for her technical assistance in determining molecular weight using SEC-TDA.

Conflicts of Interest: The authors declare no conflict of interest.

Appendix A

Table A1. Poly-γ-glutamic acid (γ-PGA) ultra-filtration process data: volume, pH, conductivity, protein content, dry weight, and mass yield recovery of the main fractions.

Sample	Volume (L)	pH	Conductivity (MicroS/cm)	Protein Content (g/L)	Dry Weight (g)	Mass Yield (%)
γ-PGA	10.0	6.27	13.17	0.209	301.7	-
Microfiltered γ-PGA	10.5	6.26	12.46	0.165	257.5	85.3
100 kDa Retentate (R1)	1.3	6.41	4.83	0.400	37.8	14.6
100 kDa Permeate (P1)	9.2	6.34	11.24	0.067	196.4	76.2
3 kDa Retentate (R2)	0.96	6.83	4.52	0.294	21.0	8.1
3 kDa Permeate (P2)	10.2	6.47	10.40	0.036	175.5	68.1

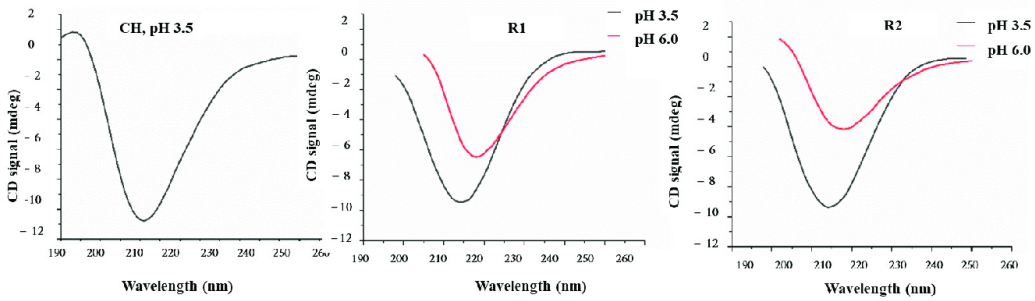

Figure A1. Circular dichroism (CD) spectra of chitosan (CH) at pH 3.5, poly-γ-glutamic acid fractions R1 at pH 3.5 and 6, and poly-γ-glutamic acid fractions R2 at pH 3.5 and pH 6.

References

1. Closing the Loop-An EU Action Plan for the Circular Economy COM/2015/0614. Available online: https://www.eea.europa.eu/en/topics/in-depth/sustainability-challenges (accessed on 12 February 2023).
2. Kumar, R.; Verma, A.; Shome, A.; Sinha, R.; Sinha, S.; Jha, P.K.; Kumar, R.; Kumar, P.; Shubham; Das, S.; et al. Impacts of Plastic Pollution on Ecosystem Services, Sustainable Development Goals, and Need to Focus on Circular Economy and Policy Interventions. *Sustainability* **2021**, *13*, 9963. [CrossRef]
3. European Commission. Communication from the Commission to the European Parliament, the Council, the European Economic and Social Committee and the Committee of the Regions Closing the Loop—An EUAction Plan for the Circular Economy. Available online: https://eur-lex.europa.eu/legal-content/EN (accessed on 12 February 2023).
4. Porta, R. The Plastics Sunset and the Bio-Plastics Sunrise. *Coatings* **2019**, *9*, 526. [CrossRef]
5. Nakajima, H.; Dijkstra, P.; Loos, K. The Recent Developments in Biobased Polymers toward General and Engineering Applications: Polymers that are Upgraded from Biodegradable Polymers, Analogous to Petroleum-Derived Polymers, and Newly Developed. *Polymers* **2017**, *9*, 523. [CrossRef]
6. Hu, Z.Z.; Sha, X.M.; Huang, T.; Zhang, L.; Wang, G.Y.; Tu, Z.C. Microbial transglutaminase (MTGase) modified fish gelatin-γ-polyglutamic acid (γ-PGA): Rheological behavior, gelling properties, and structure. *Food Chem.* **2021**, *348*, 129093. [CrossRef]
7. Wang, J.Q.; Zhao, J.; Xia, J.Y. γ-PGA Fermentation by Bacillus subtilis PG-001 with glucose feedback control pH-stat strategy. *Appl. Biochem. Biotechnol.* **2022**, *194*, 1871–1880. [CrossRef] [PubMed]
8. Poly-L-γ-Glutamic Acid Sodium Salt. Available online: https://www.sigmaaldrich.com (accessed on 17 February 2023).
9. Nair, P.; Navale, G.R.; Dharne, M.S. Poly-gamma-glutamic acid biopolymer: A sleeping giant with diverse applications and unique opportunities for commercialization. *Biomass-Convers. Biorefinery* **2021**, *13*, 4555–4573. [CrossRef]

10. Restaino, O.F.; Hejazi, S.; Zannini, D.; Giosafatto, C.V.L.; Di Pierro, P.; Cassese, E.; D'ambrosio, S.; Santagata, G.; Schiraldi, C.; Porta, R. Exploiting Potential Biotechnological Applications of Poly-γ-glutamic Acid Low Molecular Weight Fractions Obtained by Membrane-Based Ultra-Filtration. *Polymers* **2022**, *14*, 1190. [CrossRef]
11. Sabbah, M.; Di Pierro, P.; Ruffo, F.; Schiraldi, C.; Alfano, A.; Cammarota, M.; Porta, R. Glutamic Acid as Repeating Building Block for Bio-Based Films. *Polymers* **2020**, *12*, 1613. [CrossRef]
12. Hisada, M.; Kawase, Y. Mucilage extracted from wasted natto (fermented soybeans) as a low-cost poly-γ-glutamic acid based biosorbent: Removal of rare-earth metal Nd from aqueous solutions. *J. Environ. Chem. Eng.* **2017**, *5*, 6061–6069. [CrossRef]
13. Moeini, A.; Cimmino, A.; Poggetto, G.D.; Di Biase, M.; Evidente, A.; Masi, M.; Lavermicocca, P.; Valerio, F.; Leone, A.; Santagata, G.; et al. Effect of pH and TPP concentration on chemico-physical properties, release kinetics and antifungal activity of Chitosan-TPP-Ungeremine microbeads. *Carbohydr. Polym.* **2018**, *195*, 631–641. [CrossRef]
14. Motiei, M.; Mirahmadi-Zare, S.Z.; Nasr-Esfahani, M.H. Chemical stabilization of γ-polyglutamate by chitosan and the effect of co-solvents on the stability. *Biophys. Chem.* **2021**, *275*, 106605. [CrossRef] [PubMed]
15. Paini, M.; Aliakbarian, B.; Casazza, A.A.; Perego, P.; Ruggiero, C.; Pastorino, L. Chitosan/dextran multilayer microcapsules for polyphenol co-delivery. *Mater. Sci. Eng. C* **2015**, *46*, 374–380. [CrossRef] [PubMed]
16. Liang, X.; Wang, X.; Xu, Q.; Lu, Y.; Zhang, Y.; Xia, H.; Lu, A.; Zhang, L. Rubbery Chitosan/Carrageenan Hydrogels Constructed through an Electroneutrality System and Their Potential Application as Cartilage Scaffolds. *Biomacromolecules* **2018**, *19*, 340–352. [CrossRef] [PubMed]
17. Wang, L.-L.; Chen, J.-T.; Wang, L.-F.; Wu, S.; Zhang, G.-Z.; Yu, H.-Q.; Ye, X.-D.; Shi, Q.-S. Conformations and molecular interactions of poly-γ-glutamic acid as a soluble microbial product in aqueous solutions. *Sci. Rep.* **2017**, *7*, 12787. [CrossRef] [PubMed]
18. Puppi, D.; Migone, C.; Morelli, A.; Bartoli, C.; Gazzarri, M.; Pasini, D.; Chiellini, F. Microstructured chitosan/poly (γ-glutamic acid) polyelectrolyte complex hydrogels by computer-aided wet-spinning for biomedical three-dimensional scaffolds. *J. Bioact. Compat. Polym.* **2016**, *31*, 531–549. [CrossRef]
19. Zhou, X.; Wang, Y.; Ren, L.; Wang, L. Novel biomimetic composite based on collagen and poly (γ-benzyl l-glutamate) -co-poly (glutamic acid). *Polym. Adv. Technol.* **2008**, *19*, 244–249. [CrossRef]
20. Michaels, A. SPolyelectrolyte complexes. *Ind. Eng. Chem.* **1965**, *57*, 32–40. [CrossRef]
21. Shamoun, R.F.; Reisch, A.; Schlenoff, J.B. Extruded Saloplastic Polyelectrolyte Complexes. *Adv. Funct. Mater.* **2012**, *22*, 1923–1931. [CrossRef]
22. Gai, M.; Frueh, J.; Kudryavtseva, V.L.; Mao, R.; Kiryukhin, M.V.; Sukhorukov, G.B. Patterned Microstructure Fabrication: Polyelectrolyte Complexes vs Polyelectrolyte Multilayers. *Sci. Rep.* **2016**, *6*, 37000. [CrossRef]
23. Zhang, J.; Gai, M.; Ignatov, A.V.; Dyakov, S.A.; Wang, J.; Gippius, N.A.; Frueh, J.; Sukhorukov, G.B. Stimuli-Responsive Microarray Films for Real-Time Sensing of Surrounding Media, Temperature, and Solution Properties via Diffraction Patterns. *ACS Appl. Mater. Interfaces* **2020**, *12*, 19080–19091. [CrossRef]
24. Duarte, M.L.; Ferreira, M.C.; Marvao, M.R.; Rocha, J. An optimized method to determine the degree of acetylation of chitin and chitosan by FTIR spectroscopy. *Int. J. Biol. Macromol* **2002**, *31*, 1–8. [CrossRef] [PubMed]
25. Zhang, W.; Tang, R.-C. Application of the Products from the Maillard Reaction of Polyglutamic Acid and Glucose to Prepare Colored and Bioactive Silk. *Polymers* **2018**, *10*, 648. [CrossRef] [PubMed]
26. Mallardo, S.; De Vito, V.; Malinconico, M.; Volpe, M.G.; Santagata, G.; Di Lorenzo, M.L. Poly(butylene succinate)-based composites containing β-cyclodextrin/d-limonene inclusion complex. *Eur. Polym. J.* **2016**, *79*, 82–96. [CrossRef]
27. Tsao, C.T.; Chang, C.H.; Lin, Y.Y.; Wu, M.F.; Wang, J.L.; Young, T.H.; Han, J.L.; Hsieh, K.H. Evaluation of chitosan/γ-poly(glutamic acid) polyelectrolyte complex for wound dressing materials. *Carbohydr. Polym.* **2011**, *84*, 812–819. [CrossRef]
28. Qiao, C.; Ma, X.; Zhang, J.; Yao, J. Effect of hydration on water state, glass transition dynamics and crystalline structure in chitosan films. *Carbohydr. Polym.* **2019**, *206*, 602–608. [CrossRef]
29. Di Girolamo, R.; Cicolella, A.; Talarico, G.; Scoti, M.; De Stefano, F.; Giordano, A.; Malafronte, A.; De Rosa, C. Structure and Morphology of Crystalline Syndiotactic Polypropylene-Polyethylene Block Copolymers. *Polymers* **2022**, *14*, 1534. [CrossRef]
30. Zhang, H.; Neau, S.H. In vitro degradation of chitosan by a commercial enzyme preparation: Effect of molecular weight and degree of deacetylation. *Biomaterials* **2001**, *22*, 1653–1658. [CrossRef]
31. Agresti, C.; Tu, Z.; Ng, C.; Yang, Y.; Liang, J.F. Specific interactions between diphenhydramine and α-helical poly (glutamic acid)—A new ion-pairing complex for taste masking and pH-controlled diphenhydramine release. *Eur. J. Pharm. Biopharm.* **2008**, *70*, 226–233. [CrossRef]
32. Yu, Z.; Liu, W.; Huo, P. Preparation, characterization, and antimicrobial activity of poly (γ-glutamic acid)/chitosan blends. *Polym. Bull.* **2019**, *76*, 2163–2178. [CrossRef]
33. Niu, D.; Xu, P.; Sun, Z.; Yang, W.; Dong, W.; Ji, Y.; Liu, T.; Du, M.; Lemstra, P.J.; Ma, P. Superior toughened bio-compostable Poly(glycolic acid)-based blends with enhanced melt strength via selective interfacial localization of in-situ grafted copolymers. *Polymer* **2021**, *235*, 124269. [CrossRef]
34. Madian, N.G.; Mohamed, N. Enhancement of the dynamic mechanical properties of chitosan thin films by crosslinking with greenly synthesized silver nanoparticles. *J. Mater. Res. Technol.* **2020**, *9*, 12970–12975. [CrossRef]
35. Takayanagi, M.; Imada, K.; Kajiyama, T. Mechanical properties and fine structure of drawn polymers. *J. Polym. Sci. Part C Polym. Symp.* **1967**, *15*, 263–281. [CrossRef]

36. Turco, R.; Zannini, D.; Mallardo, S.; Poggetto, G.D.; Tesser, R.; Santagata, G.; Malinconico, M.; Di Serio, M. Biocomposites based on Poly(lactic acid), Cynara Cardunculus seed oil and fibrous presscake: A novel eco-friendly approach to hasten PLA biodegradation in common soil. *Polym. Degrad. Stab.* **2021**, *188*, 109576. [CrossRef]
37. Nisar, S.; Pandit, A.H.; Nadeem, M.; Pandit, A.H.; Rizvi, M.M.A.; Rattan, S. γ-Radiation induced L-glutamic acid grafted highly porous, pH-responsive chitosan hydrogel beads: A smart and biocompatible vehicle for controlled anti-cancer drug delivery. *Int. J. Biol. Macromol.* **2021**, *182*, 37–50. [CrossRef] [PubMed]
38. Pereira, A.; Sandoval-Herrera, I.; Zavala-Betancourt, S.; Oliveira, H.; Ledezma-Pérez, A.; Romero, J.; Fraceto, L. γ-Polyglutamic acid/chitosan nanoparticles for the plant growth regulator gibberellic acid: Characterization and evaluation of biological activity. *Carbohydr. Polym.* **2017**, *157*, 1862–1873. [CrossRef] [PubMed]
39. Adamcová, D.; Zloch, J.; Brtnický, M.; Vaverková, M.D. Biodegradation/disintegration of selected range of polymers: Impact on the compost quality. *J. Polym. Environ.* **2019**, *27*, 892–899. [CrossRef]
40. Merino, D.; Mansilla, A.Y.; Casalongué, C.A.; Alvarez, V.A. Effect of Nanoclay Addition on the Biodegradability and Performance of Starch-Based Nanocomposites as Mulch Films. *J. Polym. Environ.* **2019**, *27*, 1959–1970. [CrossRef]
41. Restaino, O.F.; Borzacchiello, M.G.; Scognamiglio, I.; Fedele, L.; Alfano, A.; Porzio, E.; Manco, G.; De Rosa, M.; Schiraldi, C. High yield production and purification of two recombinant thermostable phosphotriesterase-like lactonases from Sulfolobus acidocaldarius and Sulfolobus solfataricus useful as bioremediation tools and bioscavengers. *BMC Biotechnol.* **2018**, *18*, 18. [CrossRef] [PubMed]
42. Nguyen, S.; Winnik, F.M.; Buschmann, M.D. Improved reproducibility in the determination of the molecular weight of chitosan by analytical size exclusion chromatography. *Carbohydr. Polym.* **2009**, *75*, 528–533. [CrossRef]
43. Restaino, O.F.; D'ambrosio, S.; Cassese, E.; Ferraiuolo, S.B.; Alfano, A.; Ventriglia, R.; Marrazzo, A.; Schiraldi, C.; Cimini, D. Molecular weight determination of heparosan- and chondroitin-like capsular polysaccharides: Figuring out differences between wild -type and engineered Escherichia coli strains. *Appl. Microbiol. Biotechnol.* **2019**, *103*, 6771–6782. [CrossRef]
44. Available online: http://www.viscotek.com (accessed on 10 February 2023).
45. Ma, Z.; Yao, J.; Wang, Y.; Jia, J.; Liu, F.; Liu, X. Polysaccharide-based delivery system for curcumin: Fabrication and characterization of carboxymethylated corn fiber gum/chitosan biopolymer particles. *Food Hydrocoll.* **2022**, *125*, 107367. [CrossRef]
46. Wu, C.-S. Modulation, functionality, and cytocompatibility of three-dimensional printing materials made from chitosan-based polysaccharide composites. *Mater. Sci. Eng. C* **2016**, *69*, 27–36. [CrossRef] [PubMed]
47. Frey, M.; Biffi, G.; Adobes-Vidal, M.; Zirkelbach, M.; Wang, Y.; Tu, K.; Hirt, A.M.; Masania, K.; Burgert, I.; Keplinger, T. Tunable wood by reversible interlocking and bioinspired mechanical gradients. *Adv. Sci.* **2019**, *6*, 1802190. [CrossRef]
48. Popkov, A.; Kononovich, N.; Dubinenko, G.; Gorbach, E.; Shastov, A.; Tverdokhlebov, S.; Popkov, D. Long Bone Defect Filling with Bioactive Degradable 3D-Implant: Experimental Study. *Biomimetics* **2023**, *8*, 138. [CrossRef] [PubMed]

Chapter IV

Chitosan/Poly-γ-Glutamic Acid Crosslinked Hydrogels: Characterization and their Application as Bio-Glues

This chapter shed light into the potential of CH/γ-PGA hydrogels, distinguished by their unique three-dimensional structure and remarkable versatility. By combining CH obtained from crustacean shrimp shells (molecular weight of 285 kDa) with two fractions of microbial γ-PGA having low molecular weights (R1=59 kDa; R2=20 kDa), six different hydrogels were developed using sustainable physical blending techniques. These hydrogels, categorized as CHR1 and CHR2, were found to act as effective bio-glues for specific applications, including wood and aluminum, and their mechanical and morphological characteristics were compared to those of commercial glues, namely vinyl (V1) and acetovinyl (V2). Thanks to their adhesive properties, the prepared hydrogels might be suitable for diverse applications, including biomedical such as wound healing.

Chitosan/poly-γ-glutamic acid crosslinked hydrogels: characterization and application as bio-glues

Sondos Hejazi[a], Andrea Carpentieri[a], Angela Marotta[b], Odile Francesca Restaino[a], Antonella Giarra[a], Ilaria Solimeno[c], Domenico Zannini[a,d], Loredana Mariniello[a], C. Valeria L. Giosafatto [a*], and Raffaele Porta[a]

[a]Department of Chemical Sciences, University of Naples "Federico II", 80126 Naples, Italy
[b]Department of Chemical, Materials and Production Engineering (DICMaPI), University of Naples "Federico II", 80126 Naples, Italy
[c]University Suor Orsola Benincasa, Department of Humanities, Via Santa Caterina da Siena, 32, Naples, 80132, Italy
[d]Institute for Polymers, Composites, and Biomaterials, National Council of Research, 80078 Pozzuoli, Italy
Corresponding author at Department of Chemical Sciences, University of Naples "Federico II", 80126 Naples, Italy

[Submitted paper]

A B S T R A C T

Ecofriendly hydrogels made of chitosan (CH = 285 kDa) from shrimp chitin and two fractions of low molecular weights microbial poly-γ-glutamic acid (γ-PGA) (R1 = 59 kDa; R2 = 20 kDa) were prepared by sustainable physical blending using three CH/γ-PGA mass ratios (1/9, 2/8 and 3/7). The six resulting CHR1 and CHR2 hydrogels were physico-chemically characterized and the most abundant of them (CH/R1 and CH/R2 ratio of 3/7) were analysed for rheological, morphological, and mechanical properties, as well as shown to act as effective bio-glues by using both wood and aluminum substrates compared to commercial vinyl- (V1) and acetovinyl (V2) glues. Lap shear analyses of CH/R1 and CH/R2 blends exhibited adhesive strength on wood, as well as adhesive/cohesive failure like that of V1 and V2. Conversely, CHR2 had higher adhesive strength and adhesive/cohesive failure on aluminum, while CHR1 showed an adhesion strength with adhesive failure on the metal similar to that of V1 and V2. Scanning electron microscopy revealed the formation of strong bonds between the produced hydrogels and both substrates. Beyond their use as bio-glues, the properties of these hydrogels make them suitable for further applications in paint, coating, and adhesive even in heritage preservation as well as in medical field for wound dressing.
Keywords: poly-γ-glutamic acid/chitosan, biodegradable hydrogels, bio-glue

1. Introduction

Hydrogels are materials offering promising applications in various fields thanks to their three-dimensional polymer network structure capable of retaining substantial amounts of water in a swollen state. The swelling behavior of hydrogels is finely tuned by a balance between hydration

forces and counteracting forces exerted by the crosslinked polymer chains that resist expansion [1]. Polymer crosslinking can be achieved through chemical covalent bonds, non-covalent interactions between the chains, or by a combination of both. Synthetic polymers such as polyacrylamide, poly (ethylene glycol)-polyester block copolymers, and several biodegradable naturally occurring polymers, such as alginate, hyaluronic acid, gelatin, chitosan (CH), poly-γ-glutamic acid (γ-PGA), have been extensively explored to produce different hydrogels [2-6].
γ-PGA is an extracellularly secreted polymer in which glutamic acid units are linked by peptide bonds. Synthesized by strains of *Bacillus* species, it is a biopolymer with attributes, like water-solubility, biodegradability, and non-toxicity, suitable for diverse applications [7-9]. On the other hand, CH is a polysaccharide made of β-(1→4)-D-glucosamine and N-acetyl-D-glucosamine units and derived from chitin, the most abundant polysaccharide occurring in nature after cellulose, through an alkaline treatment of diacylation [10]. CH exhibits biodegradability, biocompatibility, non-toxicity, as well as non-immunogenicity [11]. Since both CH and γ-PGA derived from renewable resources, they represent attractive biomacromolecules for a myriad of applications, including bio-adhesives, wound healing factors, bio-inks, 3D printing, scaffolding, immunotherapeutic agents against cancer, drug delivery and food packaging components [6,12-15]. Under acidic pH, CH and γ-PGA are positively and negatively charged, respectively. Hence, they could be eventually employed for the preparation of new hydrogel materials based on electrostatic interactions [16,17]. In the pursuit of sustainable development of bio-based materials with novel applications, CH and γ-PGA-based hydrogels might also be potentially exploited as bio-adhesive materials in the heritage restoration and renovation fields. Over 1000 years, Egyptians, Greeks, and Romans employed a variety of natural adhesives, including semiliquid balsams, wet lime, tree resins, collagen, and animal-based glues derived from fish and other natural sources to join materials like ceramics, to make marquetry, and to link wooden plies [18]. Nowadays, adhesive products (i.e. glues) have become indispensable in modern life, playing a vital role in assembling and spanning various applications from construction and engineering to medicine and biotechnology [19]. Nevertheless, commercial glues such as formaldehyde, phenolic resin, and synthetic polyvinyl-based glues are a major concern due to their toxicity, carcinogenicity and airborne pollutants [20]. Therefore, biodegradable adhesives derived from natural sources such as plants, animals, or microorganisms, emerge as a promising solution, offering several advantages over

petroleum-based counterparts. In recent times hydrophilic adhesives have garnered attention from both researchers and consumers due to their compatibility, environmentally friendly nature and user-friendly applications. Santoni & Pizzo investigated various protein sources and two different soy (*Glycine max L.*) protein-based products, untreated or treated with alkali, were found suitable to produce wood adhesives for indoor applications [21]. In this paper, a novel bio-glue was prepared by a polyelectrolyte complexation between CH and γ-PGA. To this purpose, six hydrogels were first prepared by physical blending by using CH (285 kDa) and two γ-PGA fractions with low molecular weight (R1= 55 kDa, R2= 20 kDa) obtained by ultrafiltration of a commercial product of microbial origin [22]. R1 and R2 were crosslinked with CH at three different mass ratios (CH/γ-PGA = 1/9, 2/8 and 3/7) and at pH 3.5 as previously described by Hejazi et al. [16]. The structural, rheological, morphological and thermal properties of the obtained biodegradable hydrogels were studied and their potential applications as bio-glues were investigated on the surfaces of two different materials, i.e. wood and aluminum.

2. Materials and methods

2.1. Materials

A commercial γ-PGA bulk of microbial origin (COM-PGA, 50% purity) was purchased from Xi'an Fengzu Biological Technology Co., Ltd. (Xi'an City, Shaanxi Province, China). CH (75–85% deacetylated chitin, poly-D-glucosamine, Mw=285 kDa) was purchased by Sigma Aldrich, St. Louis, MO, USA. Two commercial vinyl-based glues were used as reference: Pattex® universal vinyl glue (V1) and Flashbond Acetovinyl glue (V2) were purchased from a local store in Naples. Wood panels were prepared from oak, whereas the aluminium samples were from 6082-T6 alloy. All the reagents used for analyses and the material characterization were of analytical grade unless specified.

2.2. Preparation of CH/γ-PGA hydrogels

For preparing the hydrogels, COM-PGA was first purified by ultrafiltration in two distinct retentate fractions (R1 and R2) as described previously [22]. The molecular weight of CH (285 kDa), R1 (55 kDa) and R2 (20 kDa) were also formerly determined by size exclusion chromatography with a triple detector array [23]. The preparation of

CH/γ-PGA hydrogels followed the protocol described in Hejazi et al. [16]. Aqueous solutions of CH and the γ-PGA fractions (R1 and R2) were prepared at a pH of 3.5 in 0.1 M HCl. The CH solution had a concentration of 20 mg/mL (w/v), while the R1 and R2 solutions were prepared at a concentration of 50 mg/mL. Subsequently, the R1 or R2 solutions were added to the CH solution to obtain three diverse CH/γ-PGA mass ratio (1/9, 2/8, or 3/7) blends. The resulting mixtures were adjusted to a pH of 3.5 again and stirred at 800 rpm at 25°C for 60 minutes. It is worth noting that, as previously reported [16], any further increase of CH/γ-PGA ratio made it impossible to obtain any precipitated material. In fact, when the amount of CH in the mixture increased to CH/R1 and CH/R2 ratios of 4/6 or 5/5, milky colloidal suspensions rather than sedimented hydrogels were formed (Fig.1). The latter phenomenon was likely due to the ability of higher amounts of free $–NH_3^+$ groups of CH to completely neutralize the negative charges of free $–COO^-$ groups of γ-PGA by forming CH-γ-PGA complexes able to remain in suspension. Therefore, six different amounts of precipitated hydrogels were obtained at CH/R1 or CH/R2 mass ratios of 1/9, 2/8, and 3/7, respectively. The six sediments were first collected by decantation and then centrifuged at 10,000 rpm for 10 minutes at 4°C (Avanti J-20 XP centrifuge, Beckman Coulter, Brea, CA, USA).

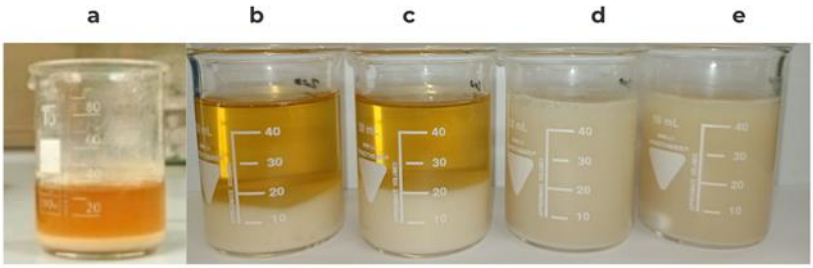

Fig. 1. Increasing amounts of sedimented hydrogels obtained by blending CH with either R1 or R2 γ-PGA fractions at 1/9 (a), 2/8 (b) and 3/7 (c) CH/γ-PGA mass ratios, and colloidal suspensions obtained by blending the two biopolymers at 4/6 d) and 5/5 ratios (e). Further experimental details are reported in the text.

The obtained sediments were finally washed three times with distilled water at pH 3.5 and then analyzed for their ash and metal content, as well as for swelling and thermal features. Two of the six samples, those obtained at CH/R1 and CH/R2 mass ratio of 3/7, resulting the most abundant sedimented hydrogels (Table 1), were also characterized for

their rheological and morphological properties, and tested as bio-adhesives on both wood and aluminum surfaces.

Table 1. Amounts of CH/R1 and CH/R2 sedimented hydrogels produced at different CH/γ-PGA mass ratios. Experimental details are reported in the text.

CH/γ-PGA ratio	Amount of each polymer (mg)		Sedimented hydrogel produced (mg)
	CH	R1 or R2 γ-PGA fraction	
CH/R1 (1/9)	200	1800	1700
CH/R1 (2/8)	400	1600	3200
CH/R1 (3/7)	600	1400	3300
CH/R2 (1/9)	200	1800	1600
CH/R2 (2/8)	400	1600	2700
CH/R2 (3/7)	600	1400	3000

Video 1 shows the manipulability of one of the six hydrogels obtained (CH/R1, 3/7 w/w) which all take on, during the evaporation of the solvent, a non-sticky plastic gum consistency such as to become easily mouldable material. Conversely, when the solvent was completely removed, the stratified material took on a glassy consistency so rigid and hard that it could be compared to Bakelite (Fig. 2).

VIDEO 1

https://watch.wave.video/bDgzs3WWcH9xu0k3

Fig. 2. Sheet of the biodegradable material obtained by drying the hydrogels produced with CH/R1 or CH/R2 at 3/7 mass ratio.

2.3. Ash and metal content analysis

Ash content was used as preliminary analysis to assess the purity and composition of the six obtained hydrogels. About 500 mg of dried samples were weighed into a pre-weighed heated porcelain crucible. The crucibles were then placed in a muffle furnace and heated to 600°C for 6 hours until all the carbonaceous material disappeared. After the furnace was cooled, the residue in the crucibles was weighed. The ash content was then calculated as follows:

$$\text{Ash content (\%)} = \textit{(weight of residue/weight of initial sample)} \times \textit{100} \quad (2)$$

Metal content analysis for the determination of the Ca^{2+} and Mg^{2+} ions was performed by subjecting 0.2 g of each sample to oxidative acid digestion with 2 mL of HNO_3 (≥ 69%, v/v) (Sigma Aldrich, St. Louis, MO, USA) in a tube kept in the thermostatic bath at about 90°C for 3 hours. The six mineralized samples were recovered with ultrapure water up to a volume of 10 mL to determine Ca^{2+} and Mg^{2+} ions and finally analysed by MP-AES (Microwave Plasma-Atomic Emission Spectrometry). A calibration curve was obtained for each analysed ion from a certified standard solution (Ultrascientific, Bologna, Italy).

2.4. Differential scanning calorimeter (DSC)

The thermal properties of all six samples were determined by using a Q2000 T zero differential scanning calorimeter (DSC), TA Instrument (New Castle, DE, USA), equipped with a liquid nitrogen accessory for fast cooling. The calorimeter was calibrated for temperature and energy using indium. Dry nitrogen was used as purge gas at a rate of 30 mL/min. Samples (3-4 mg each) were placed in aluminum pans and an empty pan was used as a reference. DSC measurements were performed in a double heating run; the first one, occurring from 50 to 200°C, at 10°C·min^{-1}, reproduced the thermal history of the samples. After an isothermal step of one-minute, non-isothermal cooling runs were performed up to -50 °C, at a rate of 10°C·min^{-1}. Finally, a second heating ramp from -50°C to 250°C at 10°C·min^{-1} was recorded. Before testing, the samples were conditioned for 24 h at 25°C and 50% RH.

2.5. Rheological properties

A stress-controlled rotational rheometer (ARG2, TA Instruments, New Castle, Delaware, USA), equipped with a cone-plate geometry (diameter 40 mm, angle 2°) and a Peltier base for the control of the temperature, was used to assess the viscoelastic properties of the CHR1 (3/7) and CHR2 (3/7) hydrogel samples. Frequency sweep tests were conducted at 25°C from 100 to 1 rad/s, applying 5% strain.

2.6. Swelling ratio

Swelling studies were performed in triplicate by using CHR1 and CHR2 samples prepared at 3/7 mass ratio. Each dried material (Wi = 140 mg), previously equilibrated at 25°C for 30 min in a chamber at a relative humidity of 6%, was immersed in distilled water at 25°C for different times (18, 24, 42, and 48 hours). At the end of the incubation, the hydrogels were removed and placed on filter paper to remove surface water and then, their wet weight was recorded as Wf. The swelling ratio was calculated using the following formula:

$$\% \text{ swelling ratio} = (Wf - Wi) / Wi \quad (1)$$

2.7. Lap shear test of the adhesives

The adhesive performance of CHR1 (3/7) and CHR2 (3/7) hydrogel samples (0.83 mg/cm^2 for wood and 0.62 mg/cm^2 for aluminum) was analyzed with a lap shear test by using wood bars and aluminum films as two different substrates. For comparison, two commercial types of glue, a vinyl- and an acetovinyl-based one (0.16 mg/cm^2 for wood and 0.12 mg/cm^2 for aluminum) were also applied on the same different substrates. Two pieces of wood with dimensions of 80 mm × 25 mm × 1.5 mm were bonded together overlapping the substrate on a joint area of 12 mm × 25 mm. Analogously, two aluminum strips of 80 mm x 20 mm and thick 150 µm were bonded over a joint area of 20 mm x 20 mm. For each substrate/adhesive combination, 5 lap joint samples were obtained and let dry at ambient conditions for 24 h under slight pressure (200 g). The adhesive strength of bio-glues and commercial glues was evaluated by performing lap shear tests to failure with a universal testing machine Tensometer 2020 at a crosshead speed of 1mm/min for the aluminum joint and 5 mm/min for the wood, so that the joint failure of all samples happens in 60 ± 20 sec, as suggested by the standard EN 1465. The adhesive strength was evaluated by dividing the maximum load by the adhesive overlap area and the adhesive strength values reported are means of five replications [24].

2.8. Microscopic examination of adhesives

Scanning electron microscopy (SEM) was performed to investigate the adhesive penetration of the CHR1 (3/7) and CHR2 (3/7) hydrogel samples on wood bars and aluminum films by using an SEM instrument (Nova NanoSem 450-FEI-Thermo Fisher, Scientific, Waltham, MA, USA). Cryo-fractured samples were coated with a thin layer of gold/palladium alloy using a sputter coater. SEM images were then taken at an accelerating voltage of 5 kV.

3. Results and discussion

3.1. Ash and metal content

The results reported in Table 2 show that the blended materials with a higher γ-PGA content gave rise to a significantly higher ash content (4%).

Table 2. Ash and metal content of chitosan (CH), R1 and R2 poly-γ-glutamic acid fractions and in the derived hydrogels (CHR1 and CHR2) blended at three different CH/γ-PGA mass ratios. Significant differences ($p < 0.05$) were found between the R1 and CHR1 materials and R2 and CHR2 materials as indicated by small subscript letters. Further experimental details are reported in the text.

Sample	Ash (%)	Ca^{2+} (mg/g)	Mg^{2+} (mg/g)
CH	0.0	0.44±0.37	0.10±0.06
R1	26±0.80	3.87±2.80	12.70±1.30
R2	26±0.70	3.05±2.70	10.80±3.50
CH/R1 (1/9)	4±0.14	1.78±0.01	$3.96±0.38^{a}$
CH/R1 (2/8)	2±0.07	1.80±0.30	$3.80±0.50^{a}$
CH/R1 (3/7)	0.8±0.07	0.64±0.12	$1.40±0.12^{a}$
CH/R2 (1/9)	4±0.30	1.55±0.30	$3.11±0.09^{b}$
CH/R2 (2/8)	1±0.06	0.92±0.28	$2.25± 0.40^{b}$
CH/R2 (3/7)	0.7±0.10	0.65±0.08	$1.55± 0.01^{b}$

Moreover, the amount of Ca^{2+} and Mg^{2+} ions in the blended materials was measured to understand if they play a role in the CH/γ-PGA crosslinking. In fact, the free α-carboxyl group of glutamic acid residues occurring in the γ-PGA chain confers to the homopolypeptide highly anionic features, allowing the possible electrostatic binding with cations. It is worth mentioning that Ca^{2+} and Mg^{2+} are also generally supplemented to the growth medium to biotechnologically produce γ-PGA by bacterial fermentation [26]. The results shown in Table 2 indicate that the content of both Ca^{2+} and Mg^{2+} was significantly lower in CHR1 and CHR2 than in R1 and R2 γ-PGA fractions and that their amount was lower decreasing the amounts of γ-PGA in the blended materials. The lower content of Ca^{2+} and Mg^{2+} observed in the crosslinked materials was probably due to the small amount of cations co-precipitated with the blends, while most of them remained in the supernatants [27].

3.2. Differential scanning calorimetry (DSC) analyses

DSC thermogram, related to the second heating ramp of samples, was reported in Fig. 3a and b. Generally, the first heating of polymer analysis erases their thermal history, while the second thermal run accounts for the real polymer properties at the molecular level, evidencing all the involved transition phenomena [28]. CH showed a glass transition temperature (T_g) at 210°C, which is a value close to that reported in literature, i.e. ~196°C [29] whereas it was not possible to observe the endothermic peak for CH at 292°C reported in the literature [30,31] corresponding to the thermal decomposition of the polymeric backbone. As reported in previous studies, R1 and R2 samples could not take a suitable guess related to the starting endothermic peaks visible for all samples at around 250°C [22]. The T_g of R1 and R2 were latent at decomposition at 224.6°C and 219.6°C, respectively [32]. Concerning DSC results of the CHR1 and CHR2 blends obtained at different ratios and pH 3.5, DSC thermograms suggested that both blends behaved like CH, evidencing the same degradative pattern particularly shifted at lower temperatures in R2-based systems [33].

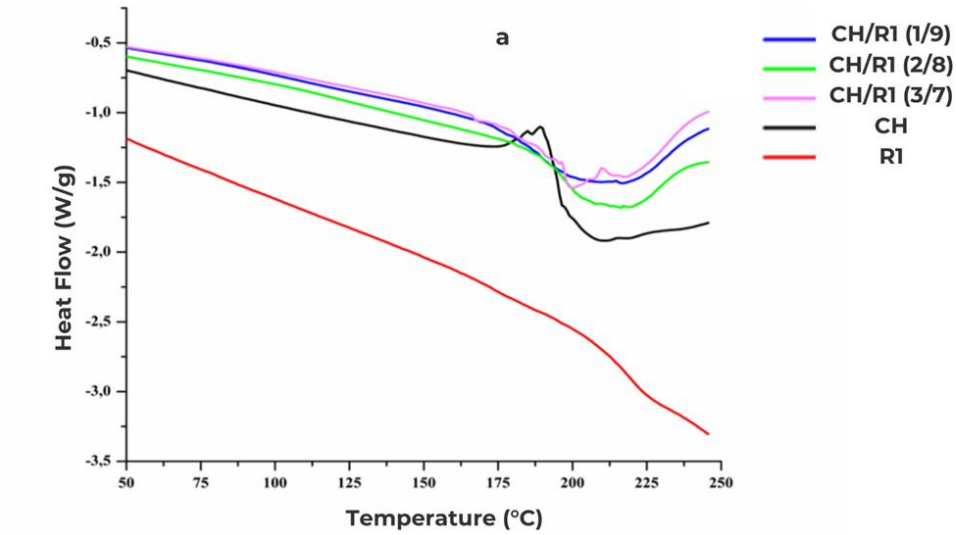

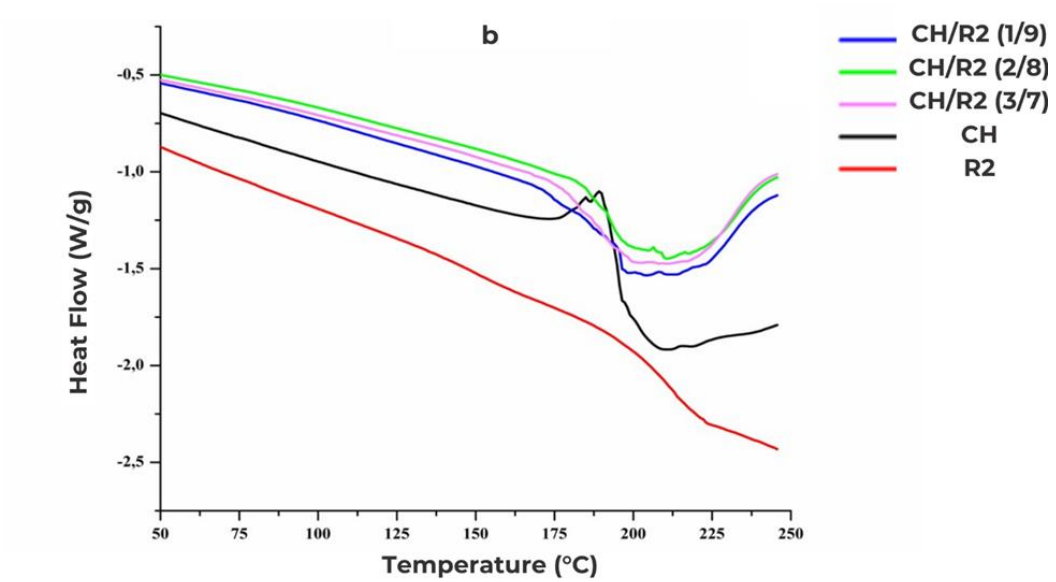

Fig. 3. Differential scanning calorimetric (second heating ramp) thermograms of chitosan (CH), poly-γ-glutamic acid R1 and R2 fractions and their crosslinked blends prepared at different CH/R1 (a) and CH/R2 (b) mass ratios (1/9, 2/8, and 3/7). Further experimental details are reported in the text.

In this case, it can be observed that the shifting of the T_g for CHR1 and CHR2 hydrogels towards a lower value (200-215°C) was due to the lower thermal stability of glutamic-acid moieties linked to the CH backbone [34]. This phenomenon was more marked in the R2-containing hydrogels in which the lower molecular weight of γ-PGA chains probably move more freely compared to the R1-based hydrogels containing higher molecular weight γ-PGA chains [35,36]

3.3. Rheological and swelling properties

The rheological behavior of hydrogels was tested by measuring their storage modulus (G') and loss modulus (G") as a function of the angular frequency. The variations of G′ and G″ vs. ω of the hydrogels prepared with the two different γ-PGA fractions (R1 and R2) at 3/7 mass ratio are reported in Fig. 4. None of the samples exhibited the gel point in the range of analyzed frequencies. Specifically, the material prepared starting from CH and the γ-PGA fraction having higher molecular weight (CHR1) showed a G' value higher than G" at angular frequencies lower than 100 rad/s, indicating that the gel point could be encountered at higher frequencies. When the elastic modulus prevails, it means that high stability of the formed complexes was reached, and the materials behave like solids with strong physical interactions

between the CH and γ-PGA chains [37]. On the other side, the presence of the lower molecular weight γ-PGA fraction (R2) led to the formation of less strong hydrogels with a significantly lower elastic modulus and a liquid-like behavior. In this case, it is likely that the gel point would have been encountered at frequencies lower than 1 rad/s.

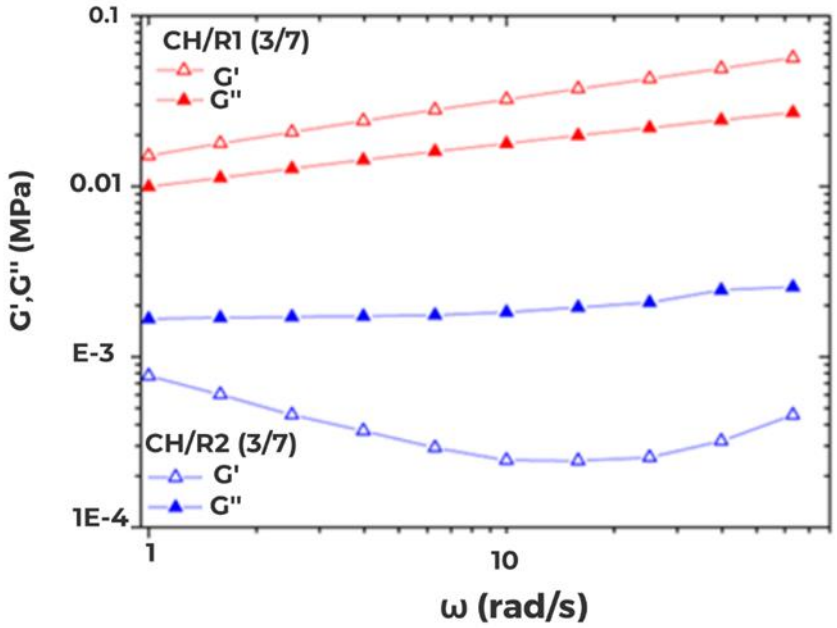

Fig. 4. Rheological properties of CHR1 (blue) and CHR2 (red) hydrogels. Experimental details are reported in the text.

Fig. 5 revealed a significant disparity also in swelling ratio over time (18-48 hours) between CHR1 and CHR2 hydrogels prepared at 3/7 mass ratio. Despite both containing highly hydrophilic CH and γ-PGA, CHR1 exhibited a markedly higher swelling ratio, nearly five times the value observed at 48 hours, compared to that of CHR2. These differences, in addition to those already detected in their rheological properties, undoubtedly depend on the different molecular weight of γ-PGA fraction contained in the two blended hydrogels, that contributes to their hydrophilicity, pore size and final network structure [22,25].

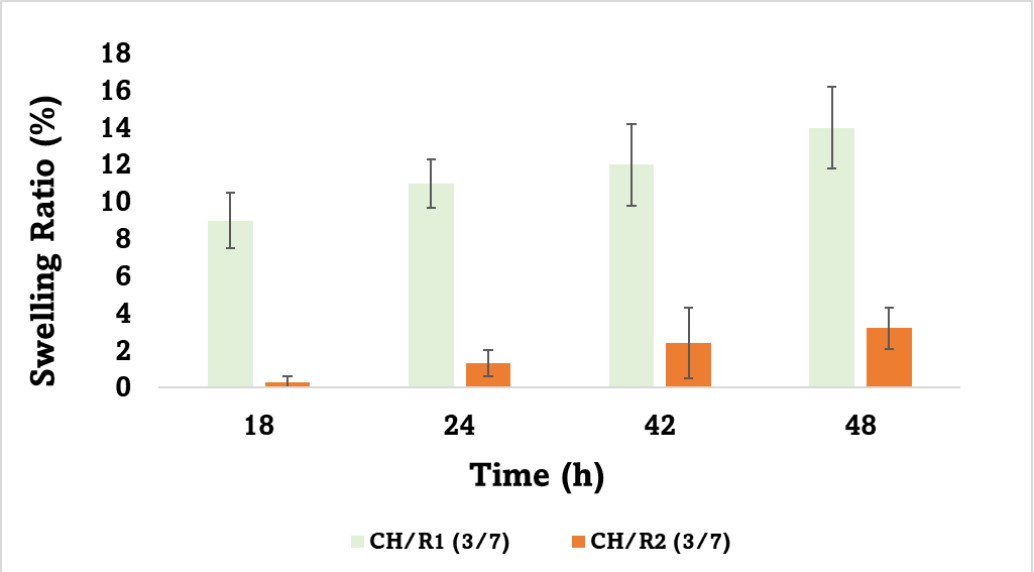

Fig. 5. Swelling ratio of crosslinked CH/R1 and CH/R2 blends prepared 3/7 mass ratio over four time points (18 h, 24 h, 42 h, and 48 h). Further experimental details are reported in the text.

3.4. Adhesion strength of hydrogels as bio-glues

The potentiality as bio-glue of CHR1 and CHR2 hydrogel samples, prepared at 3/7 mass ratio, was tested by using two different substrates and measuring the adhesive strength with a lap-shear test. The putative bio-glue samples were stratified on two pieces of either wood or aluminum and let to dry under slight pressure (clamps or weights can be equally used). The resulting joints were capable of bearing stresses comparable to those of joints glued with vinyl- (V1) and acetovinyl-based (V2) commercial products (Table 3 and Fig. 6). In particular, when used on wood, all six CH/R1 and CH/R2 hydrogel samples prepared, regardless of the CH/γ-PGA ratio, showed similar adhesive strength values and showed mainly adhesive/cohesive failure, bearing the stress up to substrate failure (data not shown). Compared to V1 and V2 commercial glues, which failed always in a cohesive way (Fig. 6), CHR1 and CHR2 hydrogels exhibited an adhesive strength slightly lower than V1 but, interestingly, higher than V2 (Table 3).

Table 3. Adhesive strength values of CH/R1 and CH/R2 hydrogel samples (3/7, mass ratio), tested on wood or aluminum substrates, compared to the vinyl- or acetovinyl-based glues. Further experimental details are reported in the text.

TYPE OF GLUE	ADHESIVE STRENGTH [PA]	
	Wood	Aluminum
CHR1	3.54 ± 0.37	0.71 ± 0.08
CHR2	3.17 ± 0.67	0.75 ± 0.05
V1	4.25 ±1.72	0.26 ± 0.11
V2	1.92 ± 1.56	0.12 ± 0.05

Conversely, when tested on aluminum substrates, both bio-glues showed an adhesive strength higher than that of V1 and V2, even though CHR1 underwent adhesive failure (Table 3 and Fig. 6). Moreover, when attached with the bio-glues, the aluminum substrates deformed before the glue failure, even though this deformation did not lead to a macroscopic substrate failure (Fig. 6). On the metallic substrate, thus, the CH/R1 and CH/R2 hydrogels might be valuable substitutes for the commercial glues showing significantly lower adhesion strength and cohesive failure.

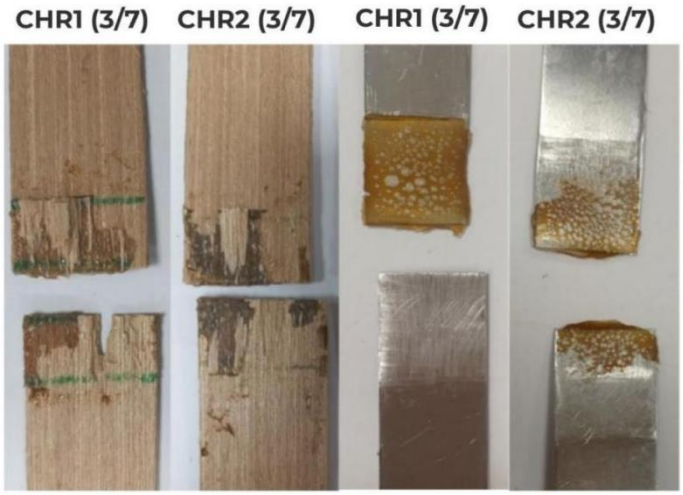

Fig. 6. Images of the wood and aluminum areas glued by CH/R1 or CH/R2 hydrogels after the lap-shear test. Further experimental details are given in the text.

3.5. Microscopic examination of adhesives

Panel a and panel b of Fig. 7 clearly show the areas of the wood substrate glued by V1 and V2, respectively, even though in panel b it is possible to observe a more extensive coverage of the wood surface indicating a thicker adhesive layer. Moreover, the morphology of the wood substrates glued by CHR1 (Fig. 7, panel c) and CHR2 (Fig. 7, panel d) reveals a noticeable partially or fully interlacing between the glue and the wood fibers. More in particular, CHR1 (panel c) seems to exhibit more penetration into the wood surface compared to CHR2 (panel d), by forming bridged fibril bundles within the interpenetrating channels of the 3D polymer network and leading to an uniform distribution in the matrix. These findings are in agreement with the rheological behavior of CHR1, substantiating that CHR1 possesses a higher viscosity (Fig. 4) that facilitates the formation of a crosslinked network creating stronger adhesiveness and the swelling ratio results (Fig. 5). Furthermore, in contrast to the findings previously reported by Yusoh et al. [38] regarding the impact of glue-line thickness on wood adhesion, the present SEM micrographs demonstrated significant variations in adhesive penetration. A thicker glue line suggested a reduced adhesive penetration into the wood cell. Conversely, the SEM images obtained with samples of aluminum substrate treated with all types of glue, either commercial (panels e-f) or bio-glues (panels g-h), showed strong adhesion with the material surface, as evidenced by clear joint formation. It is worthy to note that, although Zheng et al. [39]. previously explored the effects of an acrylic-modified epoxy adhesive on aluminum substrates and through SEM revealed a strong bonding with minimal visible gaps or inconsistencies, this is the first time that a bio-based material prepared from renewable sources is proposed as glue for such a material.

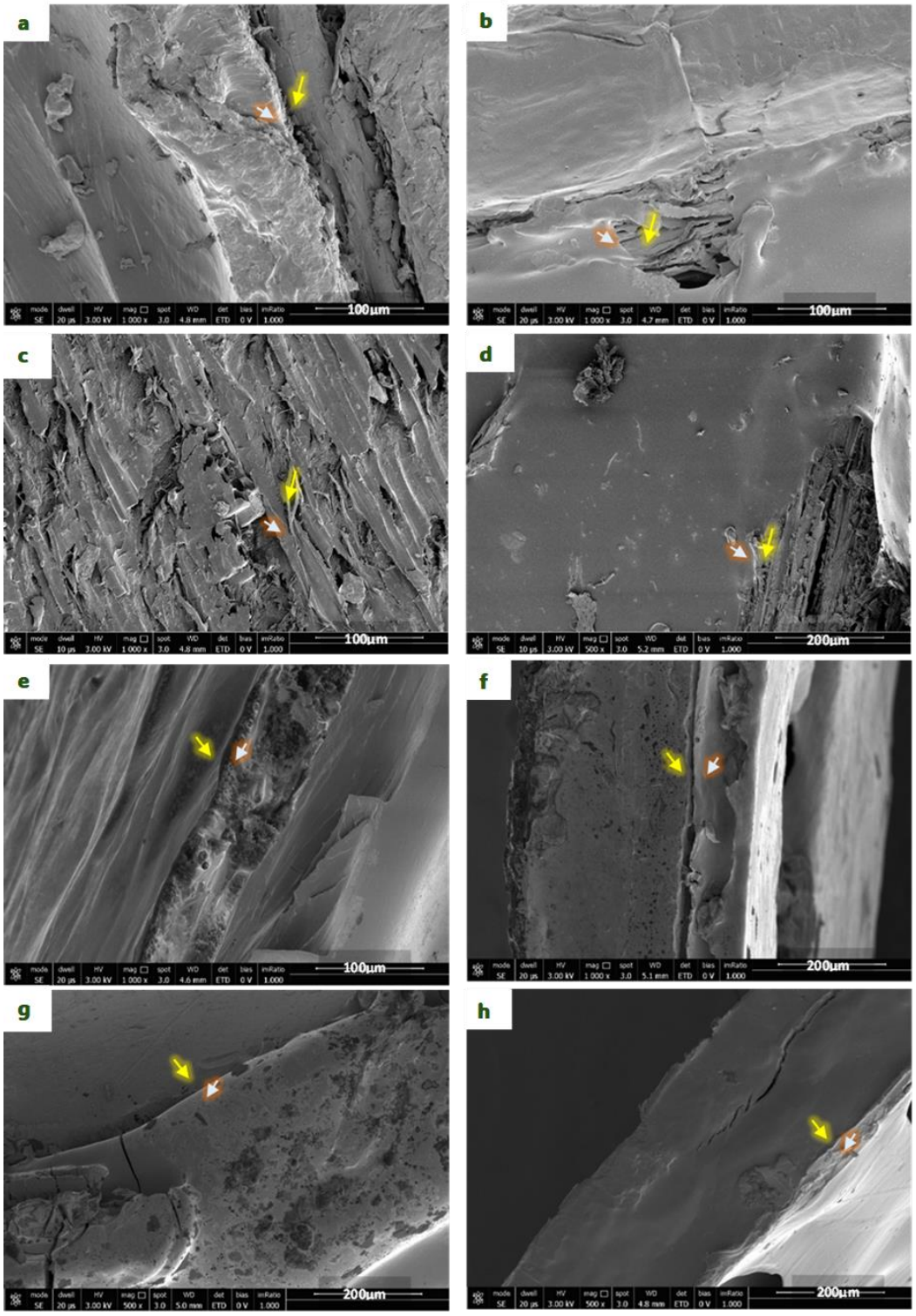
a
100µm
b
100µm
c
100µm
d
200µm
e
100µm
f
200µm
g
200µm
h
200µm

Fig. 7. SEM images of wood (panels 4-d) and aluminum (panels e-h) substrates attached by either CHR1 and CHR2 hydrogel samples (3/7 mass ratio) or vinyl- and acetovinyl-based glues. Panels a and e, b and f, c and g, d and h refer to V1, V2, CHR1 and CHR2 on wood, respectively. The yellow arrows indicate the substrate whereas the orange arrows indicate the glue. Further experimental details are reported in the text.

4. Conclusions

This study marked a significant advancement in the field of biodegradable materials, demonstrating the successful preparation of bio-hydrogels, endowed with thermal stability and promising properties, through a sustainable physical blending of two different biopolymers. It has been demonstrated that the blending of chitosan, derived from chitin, the second most abundant polysaccharide occurring in nature, with a biosynthesized homopolypeptide derived from glutamic acid, give rise, under specific experimental conditions, to easily mouldable hydrogels. A comprehensive range of rheological, swelling, morphological, mechanical, and thermal analyses allowed the characterization of the produced new biomaterial. Among its features, the dried samples were shown to possess marked adhesive properties on both wood and aluminum, comparable to well-known synthetic glues, assuming a glassy consistency so rigid and hard that it could be compared to Bakelite. Therefore, this eco-friendly material is a potential candidate to produce alternatives to the conventional synthetic adhesives for various applications, such as painting, coatings, and cultural heritage preservation. In addition, its biodegradability and biocompatibility make it a promising tool in the medical and surgical field as wound healing agent.

Author statement

All authors confirm that they have read and approved the final version of this manuscript. We warrant that this work is our original research and has not been previously published or submitted for publication elsewhere.

CRediT authorship contribution statement

Sondos Hejazi, Angela Marotta, Domenico Zanninia, Antonella Giarra: Data curation, Formal analysis, Investigation, Methodology, Writing – original draft; **Sondos Hejazi, Ilaria Solimeno, C. Valeria L. Giosafatto, and Raffaele Porta**: Conceptualization; **Andrea Carpentieri, Loredana Mariniello:** Visualization, Validation; **Odile**

Francesca Restaino, **C. Valeria L. Giosafatto, and Raffaele Porta**: Review & Editing**; C. Valeria L. Giosafatto, and Raffaele Porta**: Supervision.

Declaration of competing interest

The authors declare no competing interests.

Acknowledgments

We thank Maria Toscanesi for her technical support in performing mineral analysis.

References

[1] Chiesa, E., Genta, I., Dorati, R., Modena, T., & Conti, B., Poly (gamma-glutamic acid) based thermosetting hydrogels for injection: Rheology and functional parameters evaluation. React Funct Polym, 140 (2019), 93-102., https://doi.org/10.1016/j.reactfunctpolym.2019.03.021.

[2] Y. Piao, B. Chen, Self-assembled graphene oxide–gelatin nanocomposite hydrogels: characterization, formation mechanisms, and pH-sensitive drug release behavior, J. Polym. Sci. B Polym. Phys. 53 (2015) 356–367, https://doi.org/10.1002/polb.23636.

[3] D. Zhang, W. Zhou, B. Wei, X. Wang, R. Tang, J. Nie, et al., Carboxyl-modified poly (vinyl alcohol)-crosslinked chitosan hydrogel films for potential wound dressing, Carbohydr. Polym. 125 (2015) 189–199, https://doi.org/10.1016/j.carbpol.2015.02.034.

[4] H.W. Ju, O.J. Lee, B.M. Moon, F.A. Sheikh, J.M. Lee, J.H. Kim, et al., Silk fibroin based hydrogel for regeneration of burn-induced wounds, Tissue Eng. Regen. Med. 11 (2014) 203–210, https://doi.org/10.1007/s13770-014-0010-2.

[5] C. Ghobril, M.W. Grinstaff, The chemistry and engineering of polymeric hydrogel adhesives for wound closure: a tutorial, Chem. Soc. Rev. 44 (2015) 1820–1835, 10.1039/C4CS00332B.

[6] H. Zhuang, Y. Hong, J. Gao, S. Chen, Y. Ma, S. Wang, A poly (γ-glutamic acid)-based hydrogel loaded with superoxide dismutase for wound healing, J. Appl. Polym. Sci.132 (2015), https://doi.org/10.1002/app.42033.

[7] Ashiuchi, M., Occurrence and biosynthetic mechanism of poly-gamma-glutamic acid. In: Amino-Acid Homopolymers Occurring in Nature, Springer Berlin, Heidelberg, 2010, pp. 77–93, https://doi.org/10.1007/978-3-642-12453-2_5.

[8] Ogunleye, A., Bhat, A., Irorere, V.U., Hill, D., Williams, C., Radecka, I., Poly- γ-glutamic acid: production, properties and applications, Microbiology 161 (2015),1–17, https://doi.org/10.1099/mic.0.081448-0.

[9] Luo, Z., Guo, Y., Liu, J., Qiu, H., Zhao, M., Zou, W., Li, S., Microbial synthesis of poly-γ-glutamic acid: current progress, challenges, and future perspectives. BIOTECHNOL BIOFUELS 9 (2016), https://doi.org/10.1186/s13068-016-0537-7.

[10] Pakizeh, M., Moradi, A., & Ghassemi, T., Chemical extraction and modification of chitin and chitosan from shrimp shells, Eur. Polym. J., 159 (2021), 110709, https://doi.org/10.1016/j.eurpolymj.2021.110709/

[11] Moeini, A.; Cimmino, A.; Poggetto, G.D.; Di Biase, M.; Evidente, A.; Masi, M.; Lavermicocca, P.; Valerio, F.; Leone, A.; Santagata, G.; et al., Effect of pH and TPP concentration on chemico-physical properties, release kinetics and antifungal activity of Chitosan- TPP-Ungeremine microbeads. Carbohydr. Polym., 195 (2018), 631–641, https://doi.org/10.1016/j.carbpol.2018.05.005.

[12] Lazaridou, M., Bikiaris, D. N., & Lamprou, D. A., 3D bioprinted chitosan-based hydrogel scaffolds in tissue engineering and localised drug delivery, Pharmaceutics, 14(2022), 1978, https://doi.org/10.3390/pharmaceutics14091978.

[13] Baharlouei, P., & Rahman, A., Chitin and chitosan: Prospective biomedical applications in drug delivery, cancer treatment, and wound healing. Mar Drugs., 20 (2022), 460, 10.3390/md20070460.

[14] Lima, B. V., Oliveira, M. J., Barbosa, M. A., Goncalves, R. M., & Castro, F., Harnessing chitosan and poly- (γ-glutamic acid)-based biomaterials towards cancer immunotherapy. Mater. Today, Adv., 15 (2022), 100252, https://doi.org/10.1016/j.mtadv.2022.100252.

[15] Chang, C. H., Lin, Y. H., Yeh, C. L., Chen, Y. C., Chiou, S. F., Hsu, Y. M., ... & Wang, C. C., Nanoparticles incorporated in pH-sensitive hydrogels as amoxicillin delivery for eradication of Helicobacter pylori. Biomacromolecules, 11(2010), 133-142, 10.1021/bm900985h.

[16] Hejazi, S., Restaino, O. F., Sabbah, M., Zannini, D., Di Girolamo, R., Marotta, A., ... & Porta, R., Physicochemical Characterization of Chitosan/Poly-γ-Glutamic Acid Glass-like Materials, Int. J. Mol. Sci., 24 (2023), 12495, https://doi.org/10.3390/ijms241512495.

[17] Motiei, M.; Mirahmadi-Zare, S.Z.; Nasr-Esfahani, M.H. Chemical stabilization of polyglutamate by chitosan and the effect of co-solvents on the stability. Biophys. Chem. 275 (2021), 106605, https://doi.org/10.1016/j.bpc.2021.106605.

[18] Ramesh, Manickam, and L. Rajesh Kumar, "Bioadhesives." Green Adhesives: Preparation, Properties and Applications 2020, pp.145-164, https://doi.org/10.1002/9781119655053.ch7.

[19] Ferdosian, F., Pan, Z., Gao, G., & Zhao, B., Bio-based adhesives and evaluation for wood composites application. Polymers, 9 (2017), 70., https://doi.org/10.3390/polym9020070.

[20] Mwiiri, F. K., Brandner, J. M., & Daniels, R. Electrospun bioactive wound dressing containing colloidal dispersions of birch bark dry extract. Pharmaceutics, 12(2020), 70, https://doi.org/10.3390/pharmaceutics12080770.

[21] Santoni, I., & Pizzo, B., Evaluation of alternative vegetable proteins as wood adhesives. Ind Crops Prod., 45 (2013), 148-154, https://doi.org/10.1016/j.indcrop.2012.12.016.

[22] Restaino, O. F., Hejazi, S., Zannini, D., Giosafatto, C. V. L., Di Pierro, P., Cassese, E., ... & Porta, R., Exploiting Potential Biotechnological Applications of Poly-γ-glutamic Acid Low Molecular Weight Fractions Obtained by Membrane-Based Ultra-Filtration. Polymers, 14 (2022), 1190, https://doi.org/10.3390/polym14061190.

[23] Restaino O.F., D'ambrosio S., Cassese E., Barbuto Ferraiuolo S., Alfano A., Ventriglia R., Marrazzo A., Schiraldi C., Cimini D., Molecular weight determination of heparosan- and chondroitin-like capsular polysaccharides: figuring out differences between wild-type and engineered Escherichia coli strains". Appl. Microbiol. Biotechnol. 103 (2019), 6771-6782, https://doi.org/10.1007/s00253-019-09969-8.

[24] EN 1465 Adhesives Lap Shear Bond Strength of Rigid-to-Rigid Assemblies (2009).

[25] Nair, P., Navale, G. R., & Dharne, M. S., Poly-gamma-glutamic acid biopolymer: A sleeping giant with diverse applications and unique opportunities for commercialization, Biomass Conversion and Biorefinery, 13(2023), 4555-4573, https://doi.org/10.1007/s13399-021-01467-0.

[26] Mohanraj, R., Gnanamangai, B. M., Ramesh, K., Priya, P., Srisunmathi, R., Poornima, S., ... & Robinson, J. P., Optimized production of gamma polyglutamic acid (γ-PGA) using sago, Biocatal. Agric. Biotechnol., 22 (2019), https://doi.org/10.1002/bab.1879.

[27] Guibal, E. Interactions of metal ions with chitosan-based sorbents: a review. Sep. Purif. Technol., 38(2004), 43-74, https://doi.org/10.1016/j.seppur.2003.10.004.

[28] Eyholzer, C., Borges de Couraça, A., Duc, F., Bourban, P. E., Tingaut, P., Zimmermann, T., ... & Oksman, K., Biocomposite hydrogels with carboxymethylated, nanofibrillated cellulose powder for replacement of the nucleus pulposus. Biomacromolecules, 12(2011), 1419-1427, 10.1021/bm101131b.

[29] Wersig, T., Hacker, M. C., Kressler, J., & Mäder, K., Poly (glycerol adipate)–indomethacin drug conjugates–synthesis and in vitro characterization, Int. J. Pharm, 531(2017), 225-234, https://doi.org/10.1016/j.ijpharm.2017.08.093.

[30] Pal, A. K., & Katiyar, V., Nanoamphiphilic chitosan dispersed poly (lactic acid) bionanocomposite films with improved thermal, mechanical, and gas barrier properties. Biomacromolecules, 17(2016), 2603-2618, https://doi.org/10.1021/acs.biomac.6b00619.

[31] Pereira, A. E. S., Sandoval-Herrera, I. E., Zavala-Betancourt, S. A., Oliveira, H. C., Ledezma-Pérez, A. S., Romero, J., & Fraceto, L. F., γ-Polyglutamic

acid/chitosan nanoparticles for the plant growth regulator gibberellic acid: Characterization and evaluation of biological activity. Carbohydr. Polym 157 (2017), 1862-1873, https://doi.org/10.1016/j.carbpol.2016.11.073.

[32] Marcasuzaa, P., Reynaud, S., Ehrenfeld, F., Khoukh, A., & Desbrieres, J., Chitosan-graft-polyaniline-based hydrogels: elaboration and properties. Biomacromolecules, 11(2010), 1684-1691, https://doi.org/10.1021/bm100379z.

[33] Yu, Z., Liu, W., & Huo, P., Preparation, characterization, and antimicrobial activity of poly (γ-glutamic acid)/chitosan blends. Polym. Bull, 76 (2019), 2163-2178, https://doi.org/10.1007/s00289-018-2485-9.

[34] Lin, W. C., Yu, D. G., & Yang, M. C., Blood compatibility of novel poly (γ-glutamic acid)/polyvinyl alcohol hydrogels, Colloids Surf.B,47 (2006), 43-49, https://doi.org/10.1016/j.colsurfb.2005.11.013.

[35] Wu, H., Reeves-McLaren, N., Jones, S., Ristic, R. I., Fairclough, J. P. A., & West, A. R., Phase transformations of glutamic acid and its decomposition products. Cryst. Growth Des., 10 (2010), 988-994, https://pubs.acs.org/doi/10.1021/cg901303a.

[36] Nisar, S., Pandit, A. H., Nadeem, M., Pandit, A. H., Rizvi, M. M. A., & Rattan, S., γ-Radiation induced L-glutamic acid grafted highly porous, pH-responsive chitosan hydrogel beads: A smart and biocompatible vehicle for controlled anti-cancer drug delivery. Int. J. Biol. Macromol, 182 (2021), 37-50, https://doi.org/10.1016/j.ijbiomac.2021.03.134.

[37] Chen, Y., Yan, X., Zhao, J., Feng, H., Li, P., Tong, Z., Yang, Z., Li, S., Yang, J. & Jin, S., Preparation of the chitosan/poly (glutamic acid)/alginate polyelectrolyte complexing hydrogel and study on its drug releasing property,

Carbohydr. Polym., 191 (2018), 8-16, https://doi.org/10.1016/j.carbpol.2018.02.065.

[38] Yusoh, A. S., Tahir, P. M., Uyup, M. K. A., Lee, S. H., Husain, H., & Khaidzir, M. O., Effect of wood species, clamping pressure and glue spread rate on the bonding properties of cross-laminated timber (CLT) manufactured from tropical hardwoods, Constr Build Mater., 273 (2021), 121721, https://doi.org/10.1016/j.conbuildmat.2020.121721.

[39] Zheng, R., Lin, J., Wang, P. C., Zhu, C., & Wu, Y., Effect of adhesive characteristics on static strength of adhesive-bonded aluminum alloys, Int J Adhes Adhes, 57 (2015)., 85-94, https://doi.org/10.1016/j.ijadhadh.2014.10.007.

Tables

Table 1. Amounts of CH/R1 and CH/R2 sedimented hydrogels produced at different CH/γ-PGA mass ratios. Experimental details are reported in the text.

Table 2. Ash and metal content of chitosan (CH), R1 and R2 poly-γ-glutamic acid fractions and in the derived hydrogels (CHR1 and CHR2) blended at three different CH/γ-PGA mass ratios. Significant differences ($p < 0.05$) were found between the R1 and CHR1 materials and R2 and CHR2 materials as indicated by small subscript letters. Further experimental details are reported in the text.

Table 3. Adhesive strength values of CH/R1 and CH/R2 hydrogel samples (3/7, mass ratio), tested on wood or aluminum substrates, compared to the vinyl- or acetovinyl-based glues. Further experimental details are reported in the text.

Figures

Fig. 1. Increasing amounts of sedimented hydrogels obtained by blending CH with either R1 or R2 γ-PGA fractions at 1/9 (a), 2/8 (b) and 3/7 (c) CH/γ-PGA mass ratios, and colloidal suspensions obtained by

blending the two biopolymers at 4/6 d) and 5/5 ratios (e). Further experimental details are reported in the text.

Fig. 2. Sheet of the biodegradable material obtained by drying the hydrogels produced with CH/R1 or CH/R2 at 3/7 mass ratio.

Fig. 3. Differential scanning calorimetric (second heating ramp) thermograms of chitosan (CH), poly-γ-glutamic acid R1 and R2 fractions and their crosslinked blends prepared at different CH/R1 (a) and CH/R2 (b) mass ratios (1/9, 2/8, and 3/7). Further experimental details are reported in the text.

Fig. 4. Rheological properties of CHR1 (blue) and CHR2 (red) hydrogels. Experimental details are reported in the text.

Fig. 5. Swelling ratio of crosslinked CH/R1 and CH/R2 blends prepared 3/7 mass ratio over four time points (18 h, 24 h, 42 h, and 48 h). Further experimental details are reported in the text.

Fig. 6. Images of the wood and aluminum areas glued by CH/R1 or CH/R2 hydrogels after the lap-shear test. Further experimental details are given in the text.

Fig. 7. SEM images of wood (panels 4-d) and aluminum (panels e-h) substrates attached by either CHR1 and CHR2 hydrogel samples (3/7 mass ratio) or vinyl- and acetovinyl-based glues. Panels a and e, b and f, c and g, d and h refer to V1, V2, CHR1 and CHR2 on wood, respectively. The yellow arrows indicate the substrate whereas the orange arrows indicate the glue. Further experimental details are reported in the text.

Unpublished Data on Bio-glue Supporting the Findings of [Chitosan/poly-γ-glutamic acid crosslinked hydrogels: characterization and application as bio-glues]

Hydrogel Cost Estimation:

This section outlines the estimation of the production cost for the produced hydrogel bio-glue based on a techno-economic assessment (TEA). The TEA employs the Technology Readiness Level (TRL) metric, which ranges from 1 (basic principles observed) to 9 (actual system proven in operational use). We consider our product to be TRL 4: Technology validation at laboratory level. The cost calculations were performed considering the current market price of γ-PGA from a reputable supplier, Xi'an Fengzu Biological Technology Co., Ltd. (China), where 500g of γ-PGA costs €10. Additionally, considering the readily available and inexpensive nature of CH derived from shrimp waste, we sourced a reference price of €0.001/gram from a Chinese company's website. Based on these costs and our manufacturing process, we calculated the production cost of 1 gram of our hydrogel bio-glue to be €0.08/gram, as detailed in the table below.

Table 1S: Estimated cost price for the final bio-glue (3/7 w/w CH/ γ-PGA) using commercial γ-PGA from the Chinese company Xi'an Fengzu Biological Technology Co., Ltd considering that the actual yield after ultrafiltration: 25g.

Cost Component	Cost Calculation
Material Costs:	
γ-PGA	0.17 euro/g
Chitosan	0.0003 euro/g
Total Material Cost	**0.08 euro/g**
Rabit glue (as a commercial bio-glue reference)	0.04 euro/g

Preliminary Findings: CHR1/CHR2 Bio-Glue Shows Promise for Ceramic

The application of hydrogels as bio-glue transcends traditional materials like wood and aluminum, presenting opportunities for biomedical use, particularly in wound healing. Studies have investigated hydrogel wound dressings for wet dressings, with examples such as Zhang et al. (2018) developing hydrogels with antioxidants, CH (Mw = 600 kDa), heparin (Mw = 6-20 kDa), and γ-PGA (Mw = 440 kDa) for wound healing in diabetic patients. Tang et al. (2023) introduced a novel bioactive wound dressing sponge made from carboxymethyl chitosan, γ-PGA, and platelet-rich plasma, promoting hemostasis and wound healing. The potential of hydrogels in wound care is promising, ushering in a new era of patient-friendly closure procedures as research in this field advances. Our experiments with the bio-glue (CHR1 or CHR2) on various surfaces have yielded encouraging results, indicating its potential as a versatile adhesive (Fig.1S). We extended our evaluation to ceramic and metal observing strong bonding capabilities when attaching ceramic and metal (Fig. 1S, A and B). Notably, limited research exists on adhesives for ceramic, stone, or marble repair. Alonso-Villar et al. (2019) explored the efficacy of Araldite AY 103-1 (epoxy resin) and Fluoline A (acrylic resin) with and without a Paraloid B-72 intervention layer on stone substrates, demonstrating their effectiveness. Similarly, Jorjani et al. (2008) investigated thermoplastic resins and polaroids for marble bonding, finding satisfactory bonding strength, especially on Carrara marble. However, trials on plastics, specifically poly-lactic acid (PLA) and poly-methyl methacrylate (PMM), indicated poor adhesion, possibly due to the smooth plastic surfaces lacking sufficient mechanical interlocking for the glue to form a strong bond (Winther et al., 2013). While our preliminary findings are promising, further investigation is needed for a comprehensive understanding of the bio-glue's performance in ceramic, stone, and marble applications. These insights could potentially offer an alternative to traditional adhesives in marble sculpture repair, restoration, and archaeological conservation.

Fig.1S. Bio-glue composed of chitosan (CH) and poly-γ-glutamic acid (γ-PGA) (CHR1 or CHR2) applied to various sculptures (A and B), demonstrating its effectiveness in bonding stone to stone and stone to metal. The arrows highlight the bonded surfaces.

References

1. Alonso-Villar, E. M., Rivas, T., & Pozo-Antonio, J. S., Adhesives applied to granite cultural heritage: Effectiveness, harmful effects and reversibility. Construction and Building Materials, 223 (2019), 951-964.
2. Jorjani, M., Wheeler, G., Riccardelli, C., Soboyejo, W. O., & Rahbar, N., An evaluation of potential adhesives for marble repair, Objects Specialty Group Postprints, Volume Fifteen, 15 (2208), 95-107.
3. Tang, J., Yi, W., Yan, J., Chen, Z., Fan, H., Zaldivar-Silva, D., ... & Wang, S. (2023). Highly absorbent bio-sponge based on carboxymethyl chitosan/poly-γ-glutamic acid/platelet-rich plasma for hemostasis and wound healing. International Journal of Biological Macromolecules, 247, 125754.
4. Winther, T., Bannerman, J., Skogstad, H., Johansson, M. K., Jacobson, K., & Samuelsson, J., Adhesives for adhering polystyrene plastic and their long-term effect, Studies in Conservation, 60(2015), 107-120.
5. Zhang, L., Ma, Y., Pan, X., Chen, S., Zhuang, H., & Wang, S. (2018). A composite hydrogel of chitosan/heparin/poly (γ-glutamic acid) loaded with superoxide dismutase for wound healing. Carbohydrate polymers, 180, 168-174.

Chapter V

Production and Characterization of Poly-γ-Glutamic Acid from *Bacillus subtilis* Engineering Strains: Towards Novel Biomaterials Applications

This section delves into the core of the project, which involves exploring γ-PGA production by fermentation process using genetically engineered bacteria to increase the yield of the γ-PGA biosynthesis. In collaboration with Dr. Cinzia Calvio from the University of Pavia (Department of Biology and Biotechnology), it was investigated the production of γ-PGA using two engineered *Bacillus* strains (PB5523 and PB5390). Strain PB5390 presented a mutation within the *degS* gene, denoted as the Hy mutation, and a wild-type copy of the *swrA* allele (*swrA+ degS200* (Hy)). In addition to the above characteristics, PB5523 underwent the knockout of the *pgdS* and *ggt* genes, which are involved in γ-PGA degradation (*swrA+ degS200*(Hy) *ΔpgdS Δggt*). The γ-PGA produced by the two strains was characterized by NMR and its molecular weight was determined. Following the production of γ-PGA, it was explored the feasibility of physically blending the homopolypeptide with CH to create hydrogels and dried materials for their potential application in biomedical field (e.g. wound healing).

Production and Characterization of Poly-γ-Glutamic Acid from *Bacillus Subtilis* Engineering Strains: Towards Novel Biomaterials Applications

[Manuscript in preparation]

Introduction

In the pursuit of improving γ-PGA production, generally the main routes involve identifying novel producer strains and optimizing fermentation conditions. However, a less explored approach involves controlling the degradation of γ-PGA by inhibiting specific enzymes. Among the bacterial species suitable for γ-PGA production, *Bacillus subtilis* stands out for its rapid growth and ease of genetic manipulation. Studies by Ashiuchi et al. (2003) and Yao et al. (2009) identified PgdS, an endopeptidase belonging to the DL-endopeptidase II family, as the key enzyme responsible for degrading γ-PGA into smaller fragments (Ashiuchi et al., 2003; Yao et al., 2009). PgdS is encoded by the *pgdS* gene and is located downstream of the *pgs* operon, which comprises four genes (*pgsB*, *pgsC*, *pgsAA*, and *pgsE*) responsible for γ-PGA synthesis (Scoffoni et al., 2013), and is essential for the degradation of γ-PGA by the γ-glutamyl transferase GGT (an exopeptidase that cleaves off glutamic acid monomers from the end of the polymer) (Yao et al., 2009). In a study published in 2009, Osera et al. investigated the correlation between genetic traits, *swrA* and *degU*, which enable a variant of the domestic strain *Bacillus subtiliis* JH642 to exhibit a mucoid colony morphology on LB agar plates due to the production of γ-PGA. The complete activation of the *pgs* operon was shown to be dependent on the co-presence of SwrA and the phosphorylated form of DegU (DegU~P), which can either be obtained through the degU32(Hy) or degS200 (Hy) mutations. In their study they showed that the corporation of these two proteins SwrA and DegU are necessary for γ-PGA production. Therefore, one of the strains they obtained was designated PB5390, which exhibited this mutation: [*degS200*(hy)*swrAA*+]. This strain PB5390 is the one we are studying in this chapter, and further characterizations have been made. Scoffoni et al. (2013) further investigated the effect of inactivating by double knockout the *pgdS* and *ggt* genes (Δ*pgdS* Δ*ggt*) in vivo, by evaluating γ-PGA production and recovery in deletion mutant strains carrying the

degU32(Hy) allele. In the Δ*pgdS* Δ*ggt* strain, the absence of the main degradative enzymes allows accumulation of substantial amounts of γ-PGA, remarkably improving polymer yield up to more than 40 g/L. Here in, the same approach was used to obtain PB5523 (still unpublished strain, engineered by Dr. Cinzia Calvio) in which the *degS200* (Hy) mutation substituted the *degU32*(Hy) in the *swrA*$^{+}$, Δ*pgdS* Δ*ggt* genetic background. This chapter also presents the employment of two previously engineered *Bacillus subtilis* strains, PB5390 and PB5523, for enhancing γ-PGA production and properties characterization. Additionally, efforts were made to develop hydrogel biomaterials by blending chitosan (CH) and γ-PGA for potential various medical applications, such as wound healing. Further trials were conducted to enhance the properties of the hydrogels by incorporating bacterial melanin particles (MNPs), which were prepared using ion gelation techniques. Melanin, a versatile biopolymer with antioxidant, antimicrobial, and conductive properties, holds promise as an effective component of wound healing biomaterials due to it is good biocompatibility and biostability, no cytotoxicity, and no antigenic response (Delevoye, 2014; Mostert 2021; Restaino et al., 2022). Restaino et al. (2024) obtained melanin from a bacterial source as *Streptomycetes nashvillensis*. Here we proposed a novel hydrogel-based system composed of γ-PGA and CH carrying melanin for their potential wound closure and enhanced healing.

Materials ad Methods

Materials

Chitosan (CH) (75–85% deacetylated chitin, poly-D-glucosamine,50–190kDa), glycerol (GLY), sodium tripolyphosphate (STPP), Tween 80, and 2,2-diphenyl-1-picrylhydrazyl (DPPH) deuterium oxide (D_2O) and sodium 3-nitrobenzenesulfonate (CAS Number: 127-68-4) were purchased by Sigma Aldrich, St. Louis, MO, USA.

Microscopy

Strains PB5390 and PB5523 were observed using an inverted microscope (Carl Zeiss Axiovert 25 Feasterville-Trevose, USA). Cells were first grown in LB broth and then collected by centrifugation. Pellets were washed twice in deionized water and dissolved in an appropriate volume of fresh LB. 100 µL was spotted on LB agar and incubated at

37°C for 24 hours. After incubation, the cells were spotted onto clean glass slides and mixed with 0.9 g/L NaCl. The slides were allowed to dry for 15 minutes, and then a coverslip was sealed onto the slide. The morphology of the cells was observed at 20X magnification using the inverted microscope, and images were captured using a phone camera.

Poly-γ-glutamic acid production by two types of *Bacillus subtilis* mutant strains PB5390 and PB5523

In a collaborative study with Dr Cinzia Calvio from Pavia University, we delved into the production of γ-PGA utilizing two *B. subtilis* strains, PB5390 and PB5523. Strain PB5390 possesses a mutation within the *degS* gene, known as the Hy mutation, and the wild-type copy of the swrA allele (*swrA+ degS200* (Hy)), as reported by Osera et al. (2009) and Ermoli et al. (2021). The other strain, PB5523, is identical to the previous one, but in addition it underwent the knockout strain of the genes *pgdS* and *ggt*, which play a role in γ-PGA degradation (*swrA+ degS200* (Hy) Δ*pgdS* Δ*ggt*). This strain has not yet been published, but a similar strain, PB5522, has been reported in Scoffone et al. (2013). The fermentation process was conducted using shake flasks. First, *B. subtilis* cultures were grown on LB agar plates at 37°C for 24 hours to revitalize the spores. A few distinct colonies were used to prepare precultures in 20 mL of E-medium in a 100 mL flask capacity (Table 1) and incubated for 8 hours at 37°C in an orbital shaker rotating at 180 rpm. From each preculture, 1mL (OD= 2) was transferred into 200 mL of E-medium in a 2 L shake flask and incubated for 36 hours at 37°C. After fermentation, the cells were separated from the fermented broth by centrifugation for 20 minutes at 10,000x*g* (Avanti J-20 XP, Beckman Coulter, USA). The culture supernatant was precipitated using 3 volumes of cold methanol and kept overnight at 4°C. The γ-PGA pellet was collected by centrifugation for 5 minutes and resuspended in distilled water. The suspension was then acidified to a pH of 2 to remove contaminants, including proteins and cell debris. After acidification, the suspension was again centrifuged, and the supernatant was dialyzed using a 3 kDa membrane tube for overnight dialysis at 4°C. Then the materials were freeze dried (Thermo Savant Modulyo Benchtop, USA).

Table 1: E-medium used for Poly-γ-glutamic acid production using a shake flask fermentation process.

E-medium	Concentration
$CaCl_2$ $2H_2O$	0.15 g/L
$MnSO_4$ H_2O	0.104 g/L
$FeCl_3$	0.04 g/L
Glucose	8%
K-glutamate	4%
Trp and Phe	50 ug/mL
Citric acid	12 g/L
$MgSO_4$ $7H_2O$	0,5 g/L
K_2HPO_4	0,5 g/L
NH_4Cl	7 g/L

Molecular weight determination using Gel Permeation Chromatography (GPC)

Evaluation of molecular weights of γ-PGA samples produced using two different *Bacillus* strains 5523 and 5390 was determined through GPC. The apparatus consisted of a Malvern/Viscotek GPC MAX (Malvern, UK), equipped with a Triple detector array (TDA 305). The latter was composed of the following detectors: Refractive Index (RI), Viscometer (IV), Right-Angle Light Scattering (RALS), and Low Angle Light Scattering (LALS). The column set was composed of a pre-column TSK (Tosoh Corporation), PolySep-GFC-P5000, and PolySep-GFC-P3000 (Phenomenex) Samples were prepared and eluted in H_2O (0.02% NaN_3 and 0.1 M $NaNO_3$). After complete dissolution, samples were filtered on nylon membranes of 0.22 µm porosity. The injection volume was 75 µl, and the flow rate was 0.8 ml/min. The chosen method of analysis was a triple point, calibrated with a pullulan standard, provided by Viscotek, having a narrow molecular weight distribution. The measurements carried out at 35°C according to the temperatures of columns and detectors, were run for 50 min in duplicate.

Synthesis of chitosan/poly-γ-glutamic acid crosslinked materials using poly-γ-glutamic acid produced by *Bacillus* strain PB5390

This experiment was performed as described by Hejazi et al. (2023) for synthesizing CH/γ-PGA crosslinked materials using physical blending, where we employed purer γ-PGA. γ-PGA produced by *Bacillus* strains PB5390 was used to prepare hydrogels and dehydrated materials.

Aqueous separate solutions of CH and γ-PGA were prepared at pH of 3.5 using 0.1 M HCl. The γ-PGA solutions were then added to the CH solutions in a weight ratio of 3:7 (Hejazi et al., 2023). γ-PGA aqueous solution was added to CH solution, the mixtures were then adjusted to a pH of 3.5 and stirred at 800 rpm at 25°C for 60 minutes. The resulting precipitates were collected through decantation and centrifugation, followed by washing with distilled water at pH 3.5. The washed hydrogels were dried at room temperature to obtain dried material.
A second hydrogel material was prepared using a similar blending procedure but incorporating chitosan nanoparticles carrying biotechnologically produced melanin (CHMNPs) with γ-PGA from PB5523 strain. Melanin was produced using a bacterial fermentation method as described Restaino et al. (2022 and 2024), whereas the MNPs were produced by means of ion gelation method as outlined by Malik (2018). Firstly, 10 mg of melanin were dissolved in phosphate buffer (pH 7) and subjected to sonication for 10 minutes to ensure thorough dispersion. Subsequently, an aqueous phase was prepared by dissolving CH (20mg/mL) in a 0.1M HCl solution and adjusting the pH to 3.5. Tween 80 was then added as a surfactant and the mixture was stirred for 30 minutes at 45°C to achieve homogeneity. Melanin solution was added dropwise into the CH aqueous solution. Next, a STPP solution (0.3% w/v) was prepared in distilled water and added to the emulsions to induce crosslinking, resulting in the formation of CHMNPs. The particles were then isolated by centrifugation (Avanti J-20 XP, Beckman Coulter, Brea, CA, USA)) at 10,000×g for 35 minutes at 4°C, washed multiple times with a 1% (v/v) aqueous Tween 80 solution. Ultrasonication (Bandelin SONOPULS ultrasonic homogenizers, Binder, Tuttlingen, Germany) was applied to homogenize the dispersion, ensuring a uniform distribution of CHMNPs. The collected pellet was subjected to freeze drying (Thermo Savant Modulyo Benchtop, USA). The resulting pellet was then suspended in 0.1M HCl, adjusted to pH 3.5, and γ-PGA solutions were added to form a hydrogel material loaded with CHMNPs/γ-PGA.

Nuclear magnetic resonance (NMR) spectroscopy

High-resolution NMR spectra were obtained using Bruker Avance Ultrashield 400 and Varian 500 Oxford NMR spectrometers operating at proton frequencies of 400 and 500 MHz, respectively. The experiments were conducted at a temperature of 298 K. Chemical shifts were reported in parts per million (ppm) relative to the solvent peak of D_2O (1H NMR δ = 4.79 ppm). NMR multiplicities were denoted

as follows: t for triplet, b for broad, and m for multiple in cases where the splitting pattern was unclear. Coupling constants were expressed in Hertz (Hz). A relative quantification was performed involved dissolving an accurate amount of sample in 500 µL of deuterium oxide (D_2O) and adding 100 µL of a 0.039 M solution of sodium 3-nitro benzene sulfonate (CAS Number: 127-68-4) in D_2O. The internal standard sodium 3-nitrobenzenesulfonate was selected for quantification due to its distinct NMR spectral region compared to the samples.

Size and zeta potential

Size and zeta potential of samples were analyzed using the Zetasizer Nano-ZSP 202 (Malvern®, Worcestershire, UK). The Zetasizer Nano combines different techniques of light scattering (DLS) to obtain a complete characterization of a colloidal system. Three independent measurements were carried out on each sample, diluted to have a final concentration of 1 mg/mL.

Results and discussions

Culture observations

Fig.1. shows microscopic images of rod-shaped cells observed for both *Bacillus subtills* strains (PB5390 and PB5523).

Fig.1. Inverted microscopy images of *Bacillus subtilis* strains PB5390 and PB5523 at 20x magnification.

Poly-γ-glutamic acid production by *Bacillus* stains and purification

γ-PGA was produced by two strains of *Bacillus*, PB5523 and PB5390, differing for the yield of polymer production (higher for PB5523) using 200 mL of E-medium (**Table 1**) at 37°C for 36 hours. The γ-PGA was purified by first precipitating it with cold methanol. The precipitated materials were then suspended in water, forming a highly viscous material. The γ-PGA produced exhibited a pinkish color due to the presence of manganese and iron in the fermentation medium. Next, the solution was acidified to a pH of 2 to reduce the viscosity of the γ-PGA and to eliminate any remaining protein contaminants from the bacterial cells. Finally, dialysis using a 3 kDa cutoff membrane was performed to further purify the γ-PGA. The resulting acidified and dialyzed solution was freeze-dried (**Fig. 2**), yielding 0.448 g and 0.404 g of γ-PGA for strains PB5390 and PB5523, respectively.

Fig.2. Poly-γ-glutamic acid produced by PB5390 and PB5523 *B. subtilis* strains with E-medium after methanol precipitation (left panel) and after dialysis and freeze drying (right panel).

Nuclear magnetic resonance (NMR) spectroscopy

NMR spectroscopy was employed to confirm the presence γ-PGA and for its relative quantification. The NMR spectra of 5390, 5523 exhibit characteristic peaks at δ [1H NMR (500 MHz, D_2O)] of ~4.25 (b, 1H), ~2.4 (b, 2H), ~2.2 (b, 1H), and ~2.0 (b, 1H), respectively. These peaks are similar/identical to those observed in the NMR spectrum of cosmetic standard γ-PGA, confirming the presence of γ-PGA in the samples. However, slight shifts in the positions of these peaks may be attributed to the variations in pH conditions. The results revealed that the content of γ-PGA was 0.794 g/g for the sample obtained using PB5390 strain, and 0.644 g/g for the sample derived from PB5523

strain. The quantification procedure involved dissolving an accurate amount of sample in 500 µL of deuterium oxide (D_2O) and adding 100 µL of a 0.039 M solution of sodium 3-nitrobenzenesulfonate (CAS Number: 127-68-4) in D_2O. The internal standard sodium 3-nitrobenzenesulfonate was selected for quantification due to its distinct NMR spectral region compared to the samples.

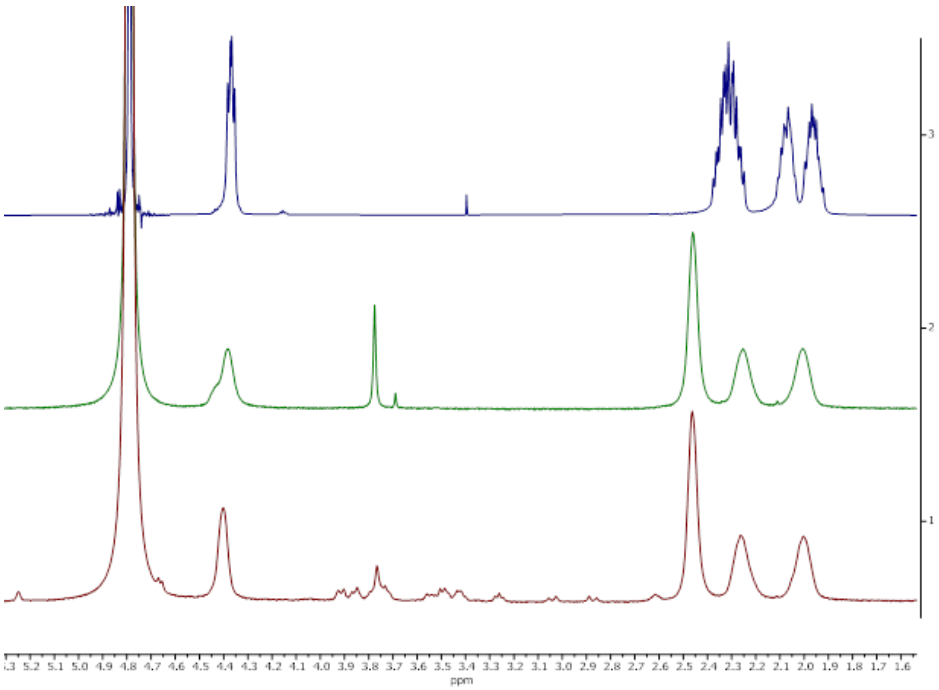

Fig.3. NMR analysis of poly-γ-glutamic acid (γ-PGA) produced using two different *B. subtilis* strains, PB5390 (second panel) and PB5523 (third panel), compared to sigma Aldrich γ-PGA (first panel).

Molecular weight determination using gel permeation chromatography/ size exclusion chromatography (GPC/SEC)

Fig. 4. presents superimposed chromatograms at the RI detector for γ-PGA produced by 5390 and 5523, along with distributions of molecular weights and viscosities (**Fig. 4C**.). For γ-PGA produced by 5523, resulted in shifted maximum peaks towards the left side (**Fig. 4A**) (smaller retention volumes). Multimodal distribution is observed for both samples. In sample 5390, it is possible to notice around 13 ml of a higher fraction at a lower retention volume (higher molecular weights) compared to another one at 19 ml (lower molecular weight) meanwhile in sample 5523 those fractions are almost similar. Moreover, as

possible to notice in **Fig. 4.,** fractions at 19 ml do not respond to the IV detector suggesting oligomeric species at this retention volume. These behaviors suggest a higher polymerization degree in samples 5390 and 5523.

A

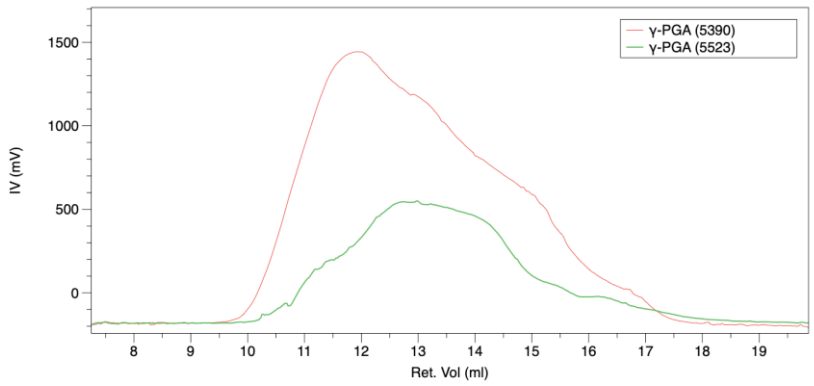

B

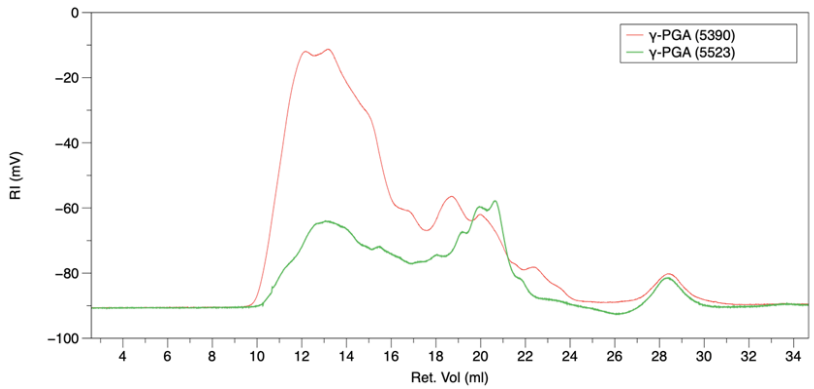

C

Sample	Mw (Da)	Mn (Da)	IV (dL/g)
γ-PGA (5390)	105469	87503	30.58
γ-PGA (5523)	132966	105345	41.41

Fig. 4. Superimposed chromatograms at RI (A) and IV (B) detector of injected samples. (C) Molecular weight, polydispersity index, and intrinsic viscosity as instrument output of RI detector of injected samples.

Crosslinked materials of chitosan and poly-γ-glutamic acid (PB5390, PB5523)

In this study, we confirmed our former method for producing hydrogel/dehydrated materials using a physical blending technique under special conditions. However, we employed a purer form of γ-PGA, produced using E-medium and a knockout *Bacillus* strain

PB5390. The CH and γ-PGA were blended at a ratio of 3:7 (w/w) at pH 3.5. Unlike the previous study by Hejazi et al. (2023), which employed a 70% pure γ-PGA to prepare blends with a 3:7 CH/ γ-PGA ratio and a final amount of 1 g, herein it was utilized a 100% pure γ-PGA, as assumed by the extensive purification methods involving i) methanol precipitation; ii) acidification; iii) dialysis over 48 hours. The resulting material exhibited hydrogel properties in a hydrated state, characterized by strong and intriguing compact and bonded behavior (**Fig. 5**). Upon drying, the material transitioned to a glass-like form with an exceptionally light pink hue like human skin (**Fig. 5**). The resulting hydrogel was also loaded with CHMNPs (10 mg) prepared using an ion gelation method (Malik et al., 2018).

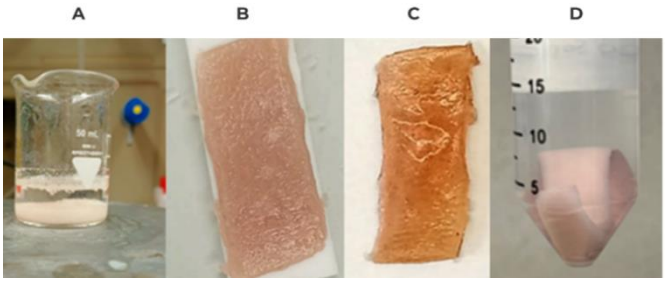

Fig. 5. Depicts of crosslinked materials synthesized using CH/γ-PGA (3:7 w/w) and loaded or not with melanin. The panels showcase the materials process from precipitation to drying. The pictures show: precipitated material obtained by blending CH and γ-PGA before (Panel A) and after centrifugation (Panel B); the above materials after drying (Panel C); hydrogels obtained through blending of chitosan/melanin nanoparticles (CHMNPs) with γ-PGA (Panel D).

Size and zeta potential

The size and zeta potential of γ-PGA produced by the two *B. subtilis* strains were investigated under different pH conditions (3.5 and 7.0) (**Table 2**).

Table 2: Size and zeta potential of purified poly-γ-glutamic from PB5390 and PB5523 strains in acid aqueous solution at pH 3.5 and 7 and their crosslinked materials.

Sample	pH	Zeta potential (mV)	Size (d.nm)	PDI
γ-PGA PB5390	7.0	-34.1±0.8	4130±488	0.20±0.01
γ-PGA PB5390	3.5	-28.0±0.8	3105±320	0.31±0.05
γ-PGA PB5523	7.0	-29.1±1.1	3403±346	0.31±0.01
γ-PGA PB5523	3.5	-22.2±1.5	3376±392	0.72±0.01
CH	3.5	+67.1±1.5	1271±170	0.51±0.01
Melanin	7.0	-53.1±3.0	532±18	0.40±0.01
CHMNPs /STPP	3.5	-9.0±0.3	5444±509	0.71±0.02
CHMNPs/ γ-PGA(PB5523) hydrogel	3.5	2.5±0.4	2870±343	0.50±0.04

At pH 7 the negative surface charge was higher than at acidic pH (3.5). This is due to the complete ionization of the carboxyl groups on the side chain (Sabbah et al., 2020). The zeta potential at pH 3.5 was more stable for γ-PGA obtained by the PB5390 fermentation, with a value of -22 mV, while for γ-PGA produced by PB5523, it was -28 mV. However, the size of the particles was smaller for γ-PGA produced by PB5390, with an average size of 3105 ± 320 nm, compared to 3376 ± 392 nm for γ-PGA produced by PB5523. DLS results revealed the formation of a complex, as evidenced by a significant change in surface charge. The final resultant hydrogel (CHMNPs/γ-PGA) exhibited a positive net charge of +2.5 ± 0.4, compared to -53 ± 3 for melanin prepared in phosphate buffer and -9 ± 0.3 mV for the matrix of CH, melanin, and STPP. The formation of a complex between melanin and γ-PGA was also evidenced by the particle size distribution of the hydrogels. The size of the resultant hydrogel was found to be 2870 ± 343 nm, significantly smaller than the size of the CH/STPP/melanin matrix (5444 ± 509 nm) at pH 3.5. This reduction in particle size is likely due to the formation of a network of entangled γ-PGA chains around the melanin particles. It is crucial to emphasize that after crosslinking CH with melanin using STPP, the resulting pellet is dissolved in 0.1M HCl. This acidic environment dissociates the STPP molecules, enabling them to serve as bridges between the CH and γ-PGA molecules. Although the resulting pellet is dissolved in 0.1M HCl to facilitate

physical blending with γ-PGA, melanin is likely to remain loaded within the CH matrix due to its strong negative charge (zeta potential of -53 in phosphate buffer) and electrostatic interactions with CH and STPP. While this was a preliminary trial, more comprehensive analysis is warranted (in future) to precisely ascertain the encapsulation efficiency and melanin loading capacity.

Conclusions

To investigate the enhancement production of γ-PGA using two genetically modified *Bacillus subtilis* strains, E-medium (a medium dependent on L-glutamic acid) was employed, followed by purification using methanol precipitation and dialysis. The γ-PGA produced by PB5523 exhibited a higher molecular weight (MW) of 135 kDa compared to that produced by PB5390 (MW of 105 kDa), while maintaining similar yields based on both freeze-dried weight (0.404 g and 0.448 g, respectively) and NMR analysis (0.644 g and 0.794 g, respectively). This suggests that the double knockout of *pgdS* and *ggt* genes, along with the Hy mutant of the *swrA* allele, which are involved in γ-PGA degradation, contributed to the enhanced MW of the γ-PGA produced by PB5523. In a preliminary experiment, γ-PGA was blended with CH to form hydrogels. The successful preparation of hydrogels (CH/γ-PGA) using both γ-PGA variants (PB5390 and PB5523) demonstrates the versatility of this polymer in hydrogel production, even when using a lower amount of material. The reduced amount (500 mg) was possible due to the higher molecular weight (105 kDa and 135 kDa for PB5390 and PB5523, respectively) and purity of the γ-PGA, compared to the lower molecular weight (R1=59 kDa, R2=20 kDa) and lower purity (70%) γ-PGA fractions used in the previous study by Hejazi et al. (2023). Furthermore, melanin-loaded hydrogels were synthesized by encapsulating melanin within a chitosan matrix and subsequently blending the composite with γ-PGA sourced from PB5523. While initial findings indicate the potential of melanin-loaded hydrogels for biomedical applications, rigorous *in vitro* and *in vivo* evaluations are warranted to unequivocally determine their encapsulation efficacy, melanin loading capacity, and associated biological effects.

Reference

1. Ashiuchi, M., Nakamura, H., Yamamoto, T., Kamei, T., Soda, K., Park, C., ... & Misono, H. (2003). Poly-γ-glutamate depolymerase of Bacillus subtilis: production, simple purification and substrate selectivity. Journal of Molecular Catalysis B: Enzymatic, 23(2-6), 249-255.
2. Delevoye, C. (2014). Melanin transfer: the keratinocytes are more than gluttons. Journal of Investigative Dermatology, 134(4), 877-879.
3. Ermoli, F., Bontà, V., Vitali, G., & Calvio, C. (2021). SwrA as global modulator of the two-component system DegSU in Bacillus subtilis. *Research in Microbiology*, *172*(6), 103877.
4. Malik, A., Gupta, M., Mani, R., Gogoi, H., & Bhatnagar, R. (2018). Trimethyl chitosan nanoparticles encapsulated protective antigen protects the mice against anthrax. Frontiers in immunology, 9, 562.
5. Hejazi, S., Restaino, O. F., Sabbah, M., Zannini, D., Di Girolamo, R., Marotta, A., ... & Porta, R. (2023). Physicochemical Characterization of Chitosan/Poly-γ-Glutamic Acid Glass-like Materials. International Journal of Molecular Sciences, 24(15), 12495.
6. Mostert, A. B. (2021). Melanin, the what, the why and the how: An introductory review for materials scientists interested in flexible and versatile polymers. Polymers, 13(10), 1670.
7. Osera, C., Amati, G., Calvio, C., & Galizzi, A. (2009). SwrAA activates poly-γ-glutamate synthesis in addition to swarming in Bacillus subtilis. Microbiology, 155(7), 2282-2287.
8. Restaino, O. F., Scognamiglio, M., Mirpoor, S. F., Cammarota, M., Ventriglia, R., Giosafatto, C. V. L., ... & Schiraldi, C. (2022). Enhanced Streptomyces roseochromogenes melanin production by using the marine renewable source Posidonia oceanica egagropili. Applied Microbiology and Biotechnology, 106(21), 7265-7283.
9. Restaino, O. F., Manini, P., Kordjazi, T., Alfieri, M.L., Rippa, M., Mariniello, L., and Porta, R., (2024). Biotechnological Production and Characterization of Extracellular Melanin by *Streptomyces nashvillensis* Microorganisms.

10. Sabbah, M., Di Pierro, P., Ruffo, F., Schiraldi, C., Alfano, A., Cammarota, M., & Porta, R. (2020). Glutamic acid as repeating building block for bio-based films. Polymers, 12(7), 1613.
11. Scoffone, V., Dondi, D., Biino, G., Borghese, G., Pasini, D., Galizzi, A., & Calvio, C. (2013). Knockout of pgdS and ggt genes improves γ-PGA yield in B. subtilis. Biotechnology and Bioengineering, 110(7), 2006-2012.
12. Wang, D., Fu, X., Zhou, D., Gao, J., & Bai, W. (2022). Engineering of a newly isolated Bacillus tequilensis BL01 for poly-γ-glutamic acid production from citric acid. Microbial Cell Factories, 21(1), 276.
13. Yao, J., Jing, J., Xu, H., Liang, J., Wu, Q., Feng, X., & Ouyang, P. (2009). Investigation on enzymatic degradation of γ-polyglutamic acid from *Bacillus subtilis* NX-2. Journal of Molecular Catalysis B: Enzymatic, 56(2-3), 158-164.

Chapter VI

Comprehensive Approach to Poly-γ-Glutamic Acid Production: Screening Honey-Isolated Bacterial Strains, Characterization, Their Production Capabilities Evaluation and Developing a Novel Ninhydrin-Based Quantification Method

Herein, screening different bacterial strains isolated from Polish honey for their ability to produce γ-PGA using various assessment methods was investigated. Out of eight strains tested, only two were found to be able to produce γ-PGA: MMS4 and MMS6. These strains produced γ-PGA when grown in LB medium supplemented with copper or zinc. A preliminary optimization study was conducted using these strains to determine the optimal time for maximum γ-PGA production. A natural source medium based on beetroot molasses was used supplemented with L-glutamic acid, salts, and ammonium, but it resulted in γ-PGA hydrolysis. These initial results indicated that the medium first required optimization to enhance γ-PGA production. To further enhance the quantification of γ-PGA production, we developed a novel ninhydrin-based spectrophotometric method, demonstrating its reliability and accuracy in measuring γ-PGA levels. However, to fully establish the robustness and validity of this method, further validation using more sophisticated techniques, such as high-performance liquid chromatography (HPLC), must be warranted. This novel method offers a promising alternative to existing γ-PGA quantification methods, providing a rapid, sensitive, and cost-effective approach for evaluating γ-PGA production. With further validation and optimization, this method could play a significant role in advancing γ-PGA research and its practical applications.

Comprehensive Approach to Poly-γ-Glutamic Acid Production: Screening Honey-Isolated Bacterial Strains, Characterization, Production Capabilities Evaluation and Developing a Novel Ninhydrin-Based Quantification Method

[Manuscript in preparation]

Introduction

Identifying bacteria that can produce poly-γ-glutamic acid (γ-PGA), especially those that do not require L-glutamic acid as a substrate, is challenging. Due to the unique properties of honey that make it difficult for bacteria to grow, including its antimicrobial activity, acidic pH (3-6), and high sugar content. As a result, most of the microorganisms found in honey are yeasts and spore-forming bacteria (Snowdon 1996). *Bacillus* spp. are Gram-positive, spore-forming bacteria that are ubiquitous in soil and plants. However, their spore-forming characteristics, which allow them to withstand acidic pH conditions, also enable them to colonize a variety of environments, including honey (Sanders et al., 2003). A study by Amin et al. (2020) et al. successfully isolated two *Bacillus* strains, *B. amyloliquefaciens HTI-19* and *B. subtilis HTI-23*, from stingless bee honey serving as potential candidates for use as probiotics and fermentation starter cultures (Zulkhairi Amin et al., 2020). Hamdy et al (2020) were able to isolate two *Bacillus subtilis* strains, HMNig-2 and MENO2 from honey and honeybee gut microbiomes. These strains have high homology and exhibit promising probiotic characteristics, including levansucrase production, biofilm formation, adhesion, free radical scavenging activity, antimicrobial activity, and prebiotic effect (Hamdy et al., 2020). A study by Lukasiewicz et al. (2015) examined the antimicrobial and antioxidant properties of various types of honey. They analyzed five types of herb honeys: nettle, chokeberry, pine, hawthorn, and aloe, as well as three types of natural honeys: buckwheat, acacia, and honeydew. They found that nettle herb honey exhibited the strongest antimicrobial activity, particularly against *Escherichia coli* and *Proteus myxofaciens*. However, no detectable antimicrobial activity was observed against *Bacillus subtilis* for any of the samples tested (Lukasiewicz et al., 2015). In this study, the isolated strains were obtained from the same types of honeys that were previously analyzed. While there is no existing study demonstrating the potential of using honey-isolated strains for γ-PGA production, here we have initiated a study to screen different strains isolated from Polish honeys for their γ-

PGA production. Mucoid assessment is a simple method for evaluating γ-PGA production in isolated strains, which we adopted in this chapter. *Bacillus subtilis* is a model organism for studying biofilm formation and extracellular polymeric substance (EPS) production. There is growing evidence that zinc and copper homeostasis are linked to the effectiveness of EPS production (Vlamakis et al., 2013). EPS is composed of polysaccharides, proteins, nucleic acids, and γ-PGA (Vlamakis et al., 2013). γ-PGA is known for its role in virulence, survival in harsh environments, and the sequestration of toxic metal ions (Ogunleye et al., 2015). In *B. subtilis*, the γ-PGA biosynthesis machinery is encoded by the *pgsBCAE* operon (Yamashiro et al., 2011). In some bacteria, such as *B. subtilis*, γ-PGA is secreted and released from the cell surface. In others, such as *B. anthracis* and *S. pneumoniae*, it is attached to the cell surface as a capsule (Ezzell et al., 1999). As a result, when γ-PGA is produced and secreted by *B. subtilis*, the colonies produce a mucoid slime layer. Since zinc supplementation is known to increase γ-PGA production, mucoid colony phenotype could be attributed to γ-PGA. Deol et al. (2022) conducted a study to investigate the effects of zinc and copper on γ-PGA production in *B. subtilis*. They found that zinc and copper decreased biofilm hydrophobicity, which increased antibiotic susceptibility and demonstrated that the mucoid phenotype was due to the production of the secreted polymer, γ-PGA which acts as protects for *B. subtilis* from zinc and copper intoxication. Additionally, they provided evidence that the small protein *PgsE* mediates zinc and copper-dependent γ-PGA production at the posttranscriptional level (Deol et al.,2022). Furthermore, optimizing the fermentation medium is a crucial strategy for maximizing γ-PGA production. Additionally, sourcing L-glutamic acid precursors, carbon sources, and ammonium sources from natural sources presents a significant challenge in γ-PGA production. Nair and Dahrn (2023) explored the production of γ-PGA from molasses, a sustainable and cost-effective method. They focused on the ability of *Bacillus paralicheniformis* NCIM 5769 to produce γ-PGA from molasses with minimal nutrients. Their findings revealed that a 30% molasses concentration combined with 2% ammonium nitrate established the optimal medium for γ-PGA synthesis. This synthesized γ-PGA exhibited anti-drought properties, significantly enhancing shoot length, biomass content, and germination rate in wheat plants compared to the control group (Nair & Dharne, 2023). This chapter further investigates the utilization of beetroot molasses combined with minimal nutrients for γ-PGA production using strains isolated from honey. Moreover, finding simple method for γ-PGA quantification is

crucial. In fact, traditional methods that involved measuring γ-PGA in aqueous solution, with a maximum absorption wavelength occurring at 216 nm require pure samples and may be influenced by other polysaccharides (Zeng et al., 2012). In addition, this chapter introduces a reliable UV-spectrophotometric technique based on the ninhydrin reaction for quantifying γ-PGA. A developed method based on a UV-spectrophotometric approach was adopted and optimized for γ-PGA quantification. The ninhydrin method was introduced in the late 1940s and remains indispensable in various scientific disciplines. Its enduring popularity is attributed to its simplicity, cost-effectiveness, and suitability for analyzing large sample sets without the need for expensive equipment. Ninhydrin's principle lies in its reaction with primary amines, specifically amino acids, ammonia, and proteins. When Ninhydrin ($C_9H_6O_4$) interacts with a free amino group it triggers a chemical reaction that oxidizes the compound. This leads to the formation of colored ninhydrin chromophore-colored compounds (Friedman et al., 2004), commonly referred to as "Rahman's color." The intensity of the coloration is directly proportional to the amount of primary amines present in the sample. Over the years, efforts to enhance the method have included crucial modifications. Notable improvements include the substitution of flammable cellulose acetate with dimethyl sulfoxide (DMSO), making the method safer and more convenient. However, varying experimental conditions, such as heating times, temperatures, buffer systems, pH values, and solvent choices for ninhydrin, have resulted in complexity and discrepancies across studies (Lamothe & McCormick in 1972; Sun et al.,2006; Wellington 1952). Overall, this chapter presents a comprehensive overview of screening methods for identifying γ-PGA-producing bacteria from honey, as well as efforts to improve γ-PGA production using beetroot molasses and optimize ninhydrin methods for γ-PGA quantification.

Materials and methods

Materials

L-glutamic acid (molecular weight = 147.13 Da) was from Bioshop, Canada Inc. (Canada), n-propanol, HCl (36.46 g/mol), citric acid monohydrate (210 g/mol), and sodium phosphate dibasic dihydrate (177.99 g/mol) were purchased from Firma Chempur (Poland). Ethanol 96% was from Honeywell (Poland), ninhydrin (Mw 178.16 g/mol) was from POCH SA Gliwice (Poland), dimethyl sulfoxide (99.9%) was from

Bioshop (Canada) while Tin Chloride Dihydrate was purchased from Merck (Warszawa, Poland). Honey samples from local beekeeping cooperatives (Bartnik Sadecki, Poland) were collected, including herb honey (nettle-*Urtica dioica*, *chokeberry*, *pine*, *hawthorn*, and *aloe*) and natural kinds of honey (*buckwheat*, *acacia*, and *honeydew*). The botanical origin of each honey was confirmed by the producers.

Screening bacterial strains for poly-γ-glutamic acid production

Samples of various Polish honey varieties were analyzed. Initially, 5 ml of each honey sample was suspended in sterile 0.9% NaCl solution until a uniform liquid consistency was achieved. The suspensions were then subjected to agitation for 2 hours at room temperature. From each suspension, 100 µL was taken and spread onto solid LB medium plates. These plates were incubated at 37°C and 50°C for 24 hours, allowing bacterial colonies to grow. After this incubation period, selected colonies exhibiting vigorous growth at both temperatures were further evaluated by plating onto fresh LB agar plates. These plates were also incubated at 37°C and 50°C for 18-24 hours, colonies demonstrating robust growth at both temperatures were selected for further analysis. Subsequently, six promising bacterial isolates were selected for further evaluation to assess their mucoidal production, a characteristic indicative of γ-PGA production potential.

Colony mucoid assessment

To evaluate the colony mucoid phenotype, strains from the well plate containing the bacterial cultures in the presence or absence of zinc or copper were spotted onto freshly poured LB agar. The mucoid appearance of the colonies was assessed and recorded.

The influence of zinc sulfate and copper sulfate salts on the optical density (OD) and growth of bacterial strains

To investigate the effects of salt supplementation, the bacterial strains were grown in 10 mL of LB broth and incubated for 24 hours at 37°C. A 96-well plate was prepared to measure the OD of the strains in the presence or absence of salts using a Tecan Sunrise microplate reader (Tecan Trading AG, Switzerland). The strains were added to a 1:100 dilution of LB medium, with or without the addition of $ZnSO_4$ (250 µM) or $CuSO_4$ (100 µM). The plate was then incubated in the Tecan Sunrise microplate reader with continuous shaking (shaking frequency 180 rpm, 37°C), and the OD at 620 nm was measured every 30 minutes for 24 hours. Each experiment was conducted with 5 replicates.

Screening of bacterial strains for their ability to produce poly-γ-glutamic acid

Six strains (MMS1, MMS2, MMS4, MMS6, MMS9, MMS13, MMS20 and MMS21) were selected for further analysis of potential γ-PGA production. The production assessment was conducted using three different media: LB alone, LB with 100 µM $CuSO_4$ and LB with 250 µM $ZnSO_4$. To initiate the production process, cells of the selected strains were cultured in 15 mL LB broth or minimum media containing $ZnSO_4$ or $CuSO_4$. The cultures were incubated in 100 mL flasks at 37°C for 16–18 hours. After incubation, cells were collected from 15 mL of culture through centrifugation at 10000 × g for 30 minutes at 4°C. The resulting supernatant was retained for further processing. To isolate the γ-PGA, 30 mL of 96% ethanol was added to the supernatant and allowed to incubate at 4°C overnight with shaking at 200rpm. The precipitated γ-PGA was then collected by centrifugation at 10000 × g for 10 minutes at 4°C. The obtained pellet was resuspended in 2 mL of distilled water. Then was freeze-dried for NMR analysis and subsequent analysis.

Culture observations

Strains MMS4 and MMS6 were observed under a cover glass using an inverted microscope (Carl Zeiss Axiovert 25 Feasterville-Trevose, USA). For visualization, bacterial colonies grown on LB agar plates were transferred onto separate microscope slides. Each slide was mounted with a drop of immersion NaCl and sealed with a coverslip. Morphological changes were observed at 20X magnification and images were captured using a phone camera.

Time optimizing for poly-γ-glutamic acid production using beet molasses medium

Two strains, namely MMS4 and MMS6, were investigated using a medium composed mainly of beet molasses over 24, 48 and 72 hours. The medium was composed primarily of beet molasses, a natural source of carbon and nitrogen sources as amino acids, including glutamic acid. A preliminary attempt with 6.2% molasses was used, incorporating 80% dry matter and 50% sucrose, as specified by the supplier (Nordzucker Polska; Czarnkow). The medium was further supplemented with a 1% of K-glutamic acid as a precursor and source of nitrogen, ammonium chloride, and salts essential for γ-PGA synthesis (**Table 1**).

Table 1: Beetroot molasses-based medium used for time optimizing for poly-γ-glutamic acid production

Component	Concentrations
Beetroot Molasses	6.2%
K-glutamic acid	1%
Copper sulfate	100µM
Zinc sulfate	250 µM
Manganese sulfate	0.104 g/L
Magnesium sulfate	0.05%
Ammonium chloride	1.5%
Citric acid	1%

The fermentation process was conducted using shake flasks. First, MMS4, MMS6 cultures were grown on LB agar plates at 37°C for 24 hours to revitalize the spores. A few distinct colonies were used to prepare precultures in 10 mL on LB broth in a 100 mL flask capacity and incubated for 16 hours at 37°C in an orbital shaker rotating at 180 rpm. From each preculture, 2-3 mL (OD600 = 6±1) was transferred into 300 mL beetroot molasses based medium in a 300mL shake flask and incubated for different time interval at 37°C. an overlapping experimental design was implemented, wherein each strain was inoculated into 50 mL of medium at pH 7 (**Table 2**), and duplicates were generated for each condition. At each specific time interval, four samples were harvested. After fermentation, following the designated time points, each sample underwent purification treatment process. Initially, the samples were subjected to centrifugation to separate the cells10,000 xg (Avanti J-20 XP, Beckman Coulter, USA). Subsequently, ethanol was introduced into the supernatant, and the samples were left to shake overnight at 4°C. Afterward, another round of centrifugation was performed, and the precipitated material was re-suspended in 10 mL of distilled water. To further purify the suspension, acidification was carried out until a pH of 2 was achieved. Following acidification, another centrifugation ensued, followed by dialysis of the supernatant against 5 liters of distilled water. The dialysis was conducted using a 3kDa membrane tube and left to occur overnight at 4°C**.** Then the materials were freeze-dried (Thermo Savant Modulyo Benchtop, USA). The obtained samples were then evaluated by NMR to detect the presence of γ-PGA.

Table 2: Glutamic acid monomer amount that was detected by NMR and relatively quantify from the samples that obtained after fermentation process using beetroot molasses-based medium.

Sample	Fermentation time (h)	Monomer (g/g)
MMS4	24	0.0404
	48	0.0767
	72	0.0420
	96	0.0631
MMS6	24	0.0358
	48	0.0344
	72	0.0153
	96	0.0730

Developing a spectrophotometric method based on ninhydrin for poly-γ-glutamic acid quantification

To quantify γ-PGA, a ninhydrin method was developed. A buffer solution was prepared using sodium phosphate dibasic dihydrate and citric acid monohydrate, and the pH was adjusted to 5.5 using 1 M potassium hydroxide. To prevent oxidation, tin chloride ($SnCl_2$) was added to the ninhydrin solution. Ninhydrin solution was freshly prepared at a concentration of 1.5% w/v in DMSO. Cosmetic-grade γ-PGA is subjected to hydrolysis using 6M hydrochloric acid and then heated in a water bath for six hours. The resulting samples were freeze-dried and used to prepare a standard curve. Hydrolyzed γ-PGA samples within a range of 5-9 µg/mL were combined with 1 mL of buffer and 1 mL of freshly prepared ninhydrin solution. The mixtures were vortexed for 30 seconds and then incubated in a water bath at 100°C for 20 minutes. After cooling to room temperature, 3 mL of 60% ethanol was added to each sample, and the vertexing was repeated for 30 seconds. All samples were analyzed spectrophotometrically at a wavelength of 570 nm using a visible spectrophotometer (OMC ENVAG, HACH). Duplicate measurements were performed, and a blank sample containing only buffer was used for reference. The resulting standard curve was plotted, and an equation was generated. To validate the analytical methods, a second standard curve was constructed using glutamic acid monomer (Sigma Aldrich, USA) and compared with the hydrolyzed γ-PGA standard curve. Samples of γ-PGA produced using simple LB medium in the presence of salts were also analyzed. These samples underwent hydrolysis and were treated in the same manner as the standard samples.

Nuclear magnetic resonance (NMR)

High-resolution NMR spectra were obtained using Bruker Avance Ultrashield 400 and Varian 500 Oxford NMR spectrometers operating at proton frequencies of 400 and 500 MHz, respectively. The experiments were conducted at a temperature of 298 K. Chemical shifts were reported in parts per million (ppm) relative to the solvent peak of D_2O (1H NMR δ = 4.79 ppm). NMR multiplicities were denoted as follows: t for triplet, b for broad, and m for multiple in cases where the splitting pattern was unclear. Coupling constants were expressed in Hertz (Hz). A relative quantification was performed involved dissolving an accurate amount of sample in 500 µL of deuterium oxide (D_2O) and adding 100 µL of a 0.039 M solution of sodium 3-nitro benzene sulfonate (CAS Number: 127-68-4) in D_2O. The internal standard sodium 3- 3-nitro benzene sulfonate was selected for quantification due to its distinct NMR spectral region compared to the samples.

Results and discussion

Screening different types of stains for their poly-γ-glutamic acid production

Preliminary experiments were conducted to evaluate the mucoidal production potential of the isolated strains and select potential γ-PGA producers without engaging in DNA or mRNA sequencing or strain identification techniques. A variety of *Bacillus* strains isolated from different types of Polish local honey, coded as MMS1, MMS2, MMS4, MMS6, MMS9, MMS13, MMS20 and MMS21 was cultured on LB agar and incubated at 37°C for 24 hours (**Fig. 1)**.

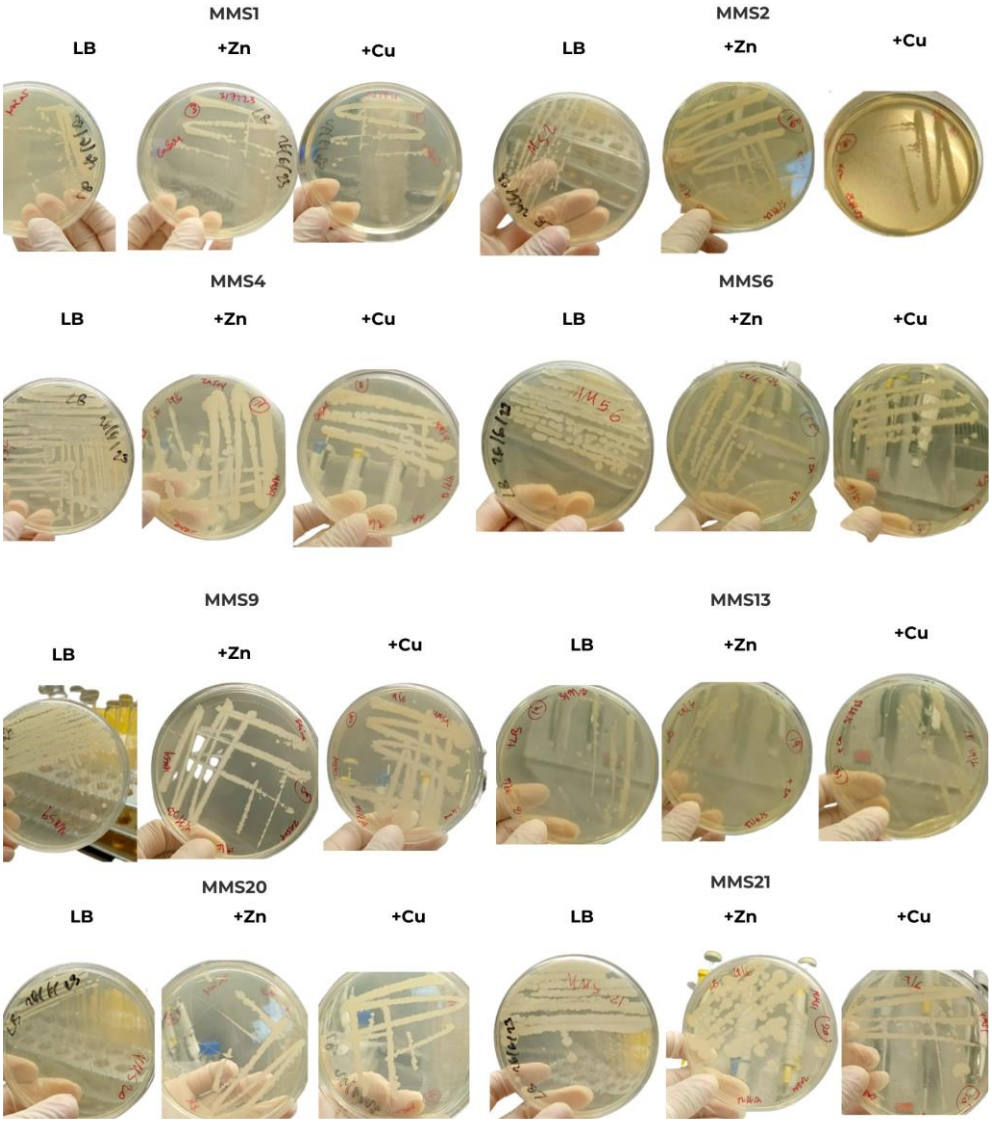

Fig. 1. Morphological observation of various strains isolated from different Polish honey samples on LB Agar in presence and absence of copper and zinc after 24 hours of incubation.

This was done to determine their ability to produce mucoid colonies, which could be an indication of γ-PGA production, as the production of γ-PGA by some *Bacillus* strains contributes to the mucoid or slimy texture of the colonies and is known to contribute to biofilm formation and protection against environmental stresses. Therefore, when these strains display a mucoid phenotype, it likely means that they are actively synthesizing γ-PGA (Qiu et al. 2019).

The strains exhibited different colony morphologies. Some strains appeared irregular, rough, and opaque, while others were round, small, and opaque. Notably, most strains appeared dry and did not produce mucoid characteristics. Conversely, strains MMS4, MMS6, MMS21 and MMS9 were identified with a mucoid phenotype, suggesting that they were actively synthesizing γ-PGA.

Strain growth patterns through optical density measurements over 24 hours

The relationship between various strain types incubated at 37°C and their corresponding optical density (OD) values within 24 hours is presented in **Fig. 2.** The experiment was conducted to evaluate the impact of different conditions on strain growth, including the presence or absence of $ZnSO_4$ and $CuSO_4$ in LB medium. According to the OD pattern, the addition of $ZnSO_4$ appears to negatively affect the growth of certain strains, such as MMS2, MMS6, and MS13. In contrast, the highest growth is observed in the LB medium alone, as expected. For example, MMS2 exhibited the highest growth without any salts, with an OD value of 1.7 after 900 minutes. The addition of copper reduced the OD value to approximately 1.4 after 900 minutes, and the presence of zinc resulted in an OD value of 1.5 after 700 minutes. Generally, the log phase of the growth was around 600 minutes, and the stationary phase seems to initiate around 800 minutes for most of the strains. It is worth noting that for strain MMS4, the addition of $ZnSO_4$ resulted in delayed growth, starting after 200 minutes. MMS4 exhibited slow growth in the addition of zinc and a peak OD of around 1 after 500 minutes. Interestingly, this toxicity can induce stress in *Bacillus*, thereby stimulating γ-PGA synthesis. Zinc and copper are essential micronutrients, and their toxicity at elevated concentrations aligns with the mucoidal observations in **Fig. 1**. Deol et al. (2022) proposed that *Bacillus subtilis* produces the extracellular polymeric substance γ-PGA as a protective response to excess zinc and copper. This corresponds with the findings in **Fig. 2**, where the addition of $ZnSO_4$ affects the growth of certain strains and potentially triggers the production of γ-PGA. Moreover, they highlight that zinc and copper-dependent γ-PGA production in *Bacillus* subtilis is regulated at a posttranscriptional level through the involvement of a small protein called *PgsE*. This sheds light on the regulatory mechanisms governing bacterial γ-PGA biosynthesis.

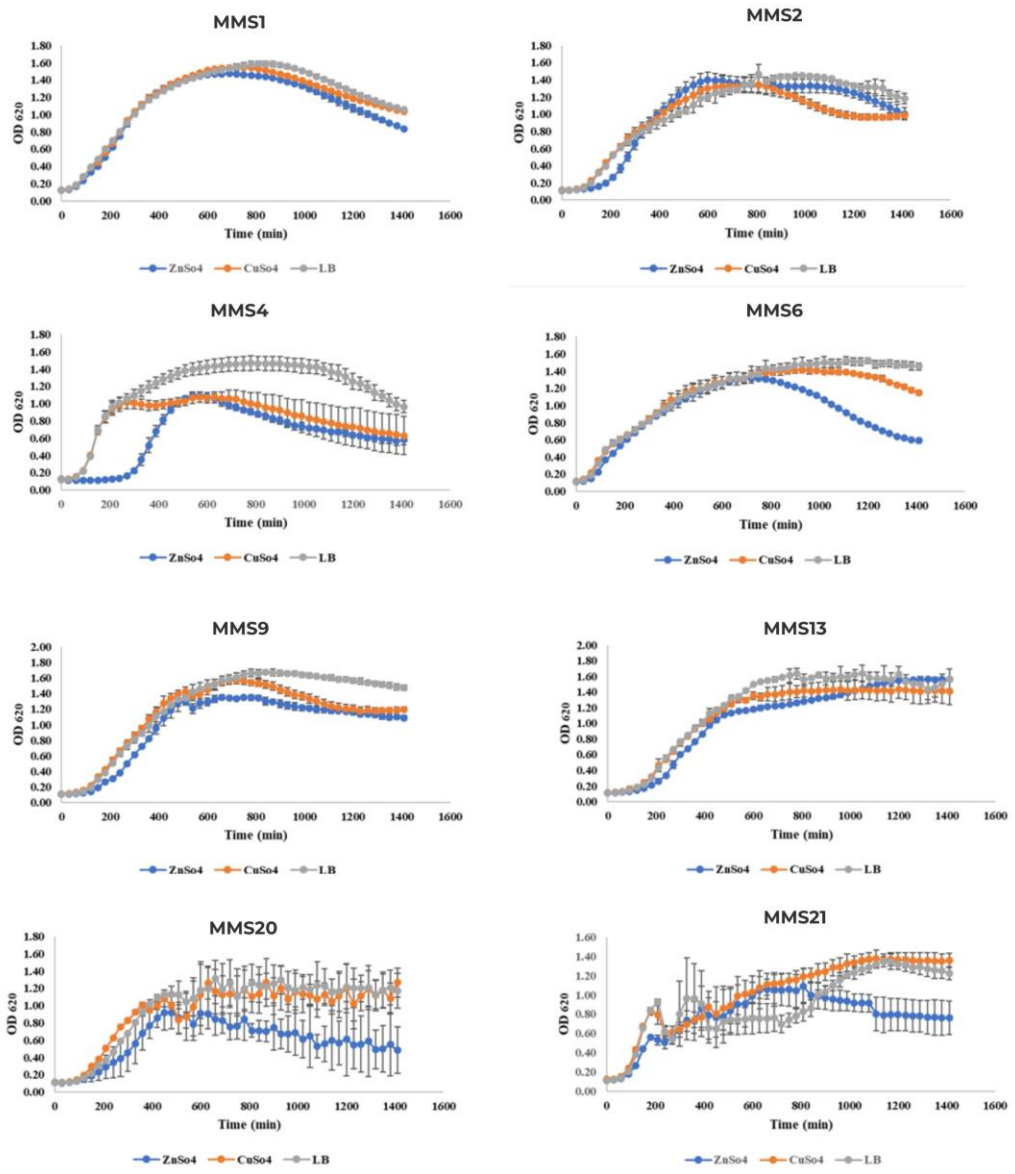

Fig.2. Optical density measurements of various strains isolated from Polish honey samples and cultivated in LB medium alone (gray line), with the addition of copper (orange line) or zinc (blue line) after 24 hours incubation at 37°C.

The presence of precipitates, possibly formed by biofilms of spores from certain strains (MMS20, MMS21), might explain the fluctuating OD pattern, which could help the bacteria adapt to challenging environments. Overall, the results demonstrate that the addition of zinc has a diverse impact on strain growth. While some strains exhibit

resistance and continue to grow steadily, others experience inhibited growth or even toxicity.

NMR analysis

NMR spectroscopy was employed to confirm the presence of γ-PGA and to quantify its relative abundance. γ-PGA was ducted by MMS4 and MMS6 strains grown in LB medium supplemented with various salts which were isolated from Gąski honey (nettle -*Urtica dioica*). **Fig. 3,** NMR spectra of MMS6 cultures grown in LB medium supplemented with copper (**A**) and zinc (**B**) exhibited characteristic peaks indicative of γ-PGA production. The presence of γ-PGA was also confirmed in MMS4 cultures grown in LB medium supplemented with zinc (**C**). The characteristic peaks for γ-PGA were observed at 4.15 ppm (broad), 2.4 ppm (broad), 2.1 ppm (broad), and 1.95 ppm (broad), which are in line with the published literature for γ-PGA (^{1}H NMR, 500 MHz, D_2O: ~4.15 (b, 1H), ~2.4 (b, 2H), ~2.1 (b, 1H), ~1.95 (b, 1H)). These peaks are in close agreement with those observed in the NMR spectrum of a Sigma Aldrich γ-PGA standard, confirming the presence of γ-PGA in the samples. In contrast, NMR spectra of samples prepared using beetroot molasses medium revealed only the presence of monomer peaks, indicating hydrolysis of γ-PGA (**Fig. 4)**. The presence of glutamic acid monomer peaks at δ [^{1}H NMR (500 MHz, D_2O)] of ~2.53 (multiplet, 2H) and ~2.13 (multiplet, 2H) further confirms the degradation of γ-PGA to glutamic acid. Other peaks observed in the NMR spectra were partially obscured by other signals. Based on the NMR analysis and the amount of internal standard added to each sample, the monomer concentrations in MMS4 (24 h) and MMS6 (24 h) were determined to be 0.0404 g/g and 0.0358 g/g, respectively, with an estimated error of approximately 2%. Samples of MMS4 (48h, 72h), and MMS6 (48h, 72h), do not indicate γ-PGA. While a broad peak was observed in MMS4 (72h), its chemical shift deviates from the expected value for γ-PGA, suggesting an external impurity. The major peaks at δ [^{1}H NMR (500 MHz, D_2O)] ~2.54 (m, 2H) and ~2.13 (m, 2H) confirm the presence of glutamic acid in all samples.

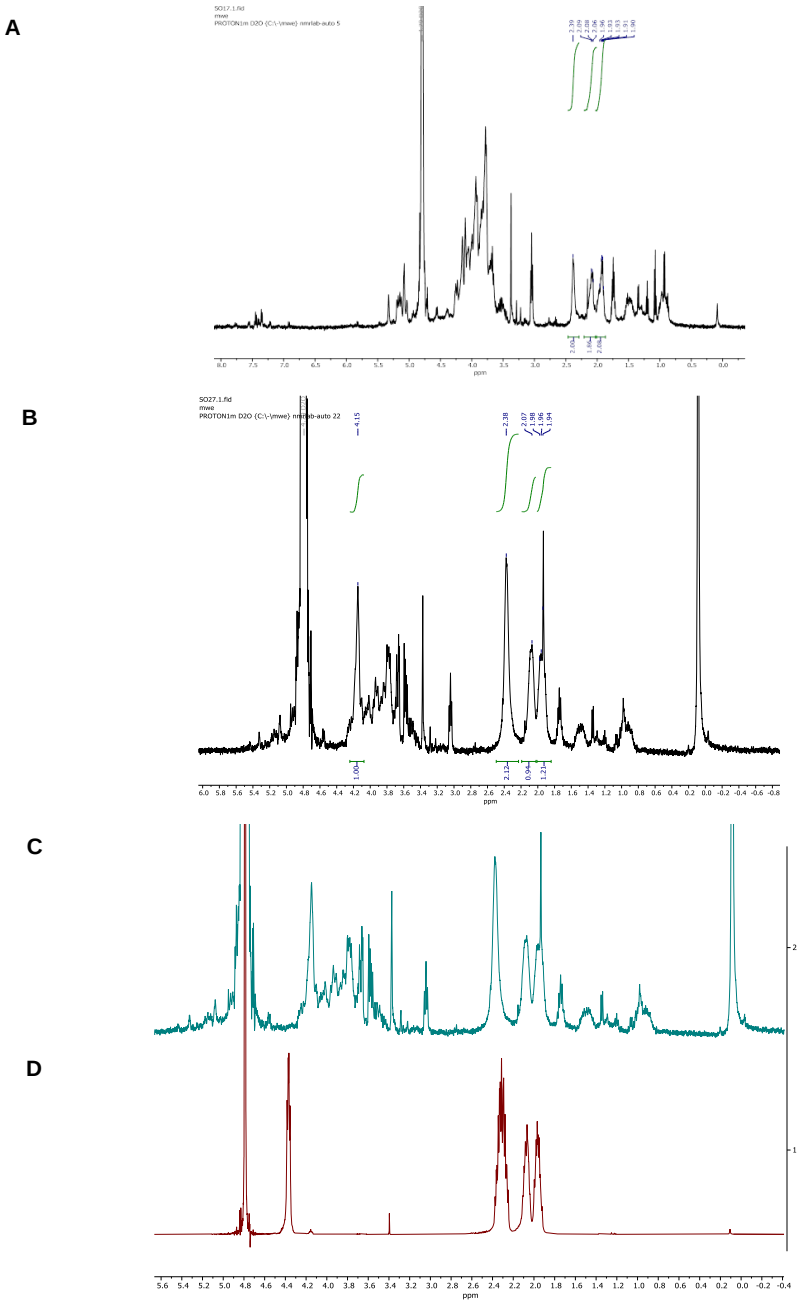

Fig.3. ^{1}H-NMR spectra of γ-PGA production (A), ^{1}H-NMR spectra of γ-PGA produced from MMS6 with copper (B), MMS6 with zinc and (C) MMS4 with zinc after 24 hours of fermentation in LB medium supplemented with salts. (D) The spectrum of γ-PGA standard is also shown for comparison.

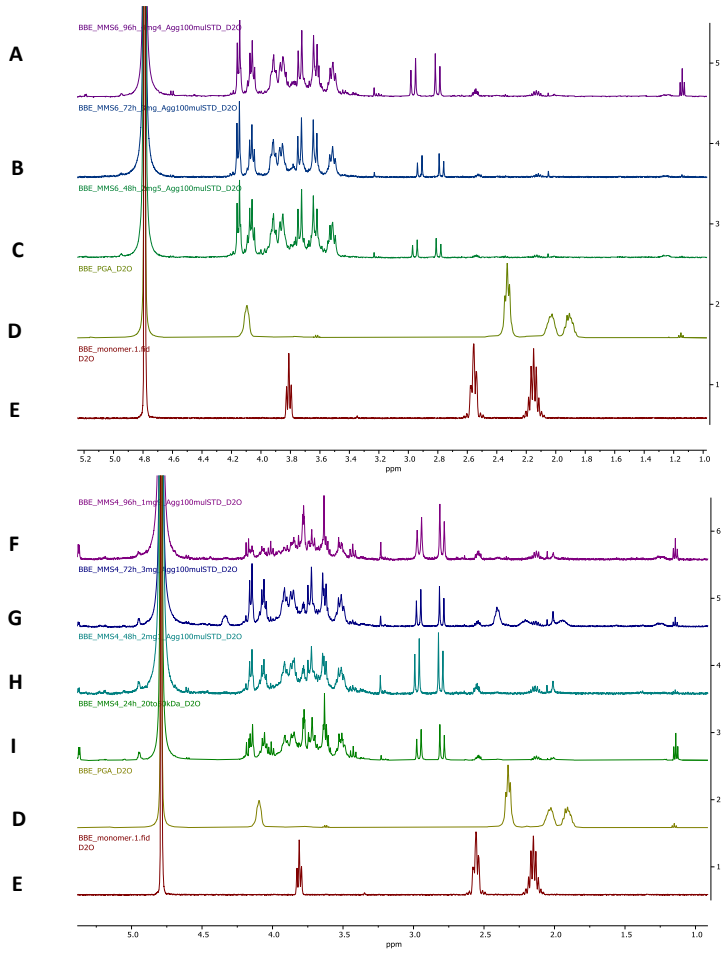

Fig.4. Overlay of ^{1}H-NMR spectra of glutamic acid monomers detected from MMS4 and MMS6 strains using beetroot molasses based medium overtime (24-96h). The γ-PGA standard and L-glutamic acid standard are also shown for comparison (Panels D and E, respectively). MMS6 overtime (48-96h) is shown in Panels A-C, while MMS4 overtime (24-96h) is shown in Panels F-I. The γ-PGA peak is absent in all the MMS4 and MMS6 samples.

These findings indicate a trace hydrolysis of γ-PGA in these samples. By incorporating an internal standard and employing the same analytical protocol as before, the monomer content was quantified in these samples. The data show that the number of monomers in all samples decreases from 48 to 72 hours and then increases again. This suggests that there may be two processes occurring: one that breaks down γ-PGA into monomers and another that polymerizes monomers into γ-PGA. The relative rates of these two processes may change over time, leading to the observed zig-zag trend.

Overall, this hydrolysis could be attributed to several factors, including the relatively low nitrogen content of the molasses-based medium, which may have prompted the strains to utilize γ-PGA as a nitrogen source.

Culture observations

Based on microscopic examination, the isolates revealed rod-shaped (**Fig.5**) shows microscopic images of shape cells as well as coccoid shaped cells were observed for MMS4 and MMS6 suggesting they belong to the *Bacillus* genus. These isolates exhibited distinct colony morphologies, with Isolate displaying slimy, transparent white colonies. This study highlights the potential of honey as a rich source of spore-forming bacteria and provides insights into the diversity of these bacteria in different honey types.

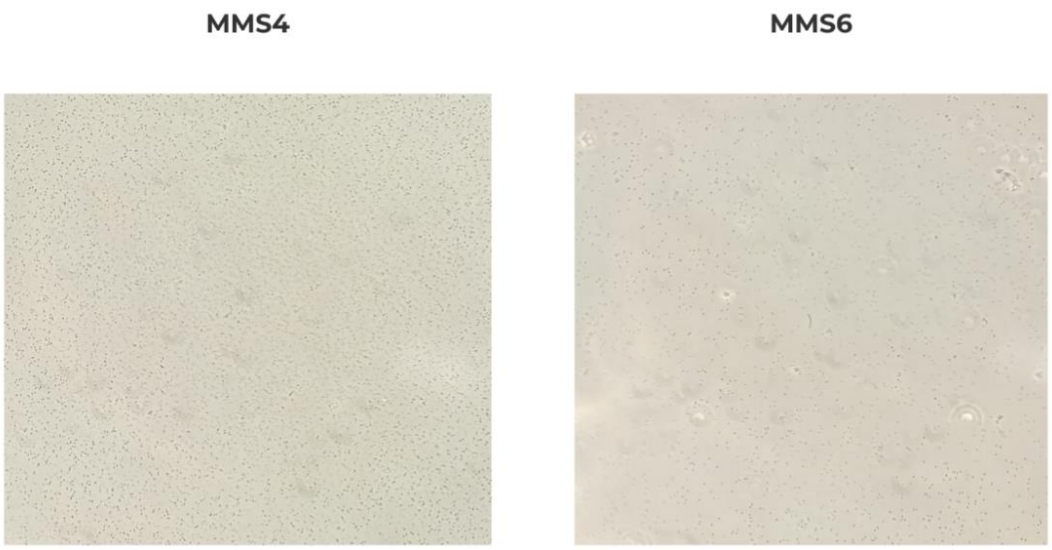

Fig.5. Inverted microscopy images of MMS4 and MMS6 strains under cover glass culture, isolated from honey, at 20x magnification.

Optimization of ninhydrin method for γ-PGA quantification

A UV-spectrophotometric approach was adopted and developed for γ-PGA quantification based on ninhydrin reaction. Herein, we present a reliable and efficient UV-spectrophotometric method for γ-PGA quantification based on the ninhydrin reaction. The ninhydrin method is a classic and widely used technique for amino acid analysis due to its simplicity, cost-effectiveness, and suitability for large-scale sample

analysis. Our optimization efforts focused on: buffer system as we utilized citrate phosphate buffer (pH 5.5) to maintain a stable pH environment, which is critical for efficient ninhydrin reaction and accurate quantification. A concentration of 1.5% w/v ninhydrin in dimethyl sulfoxide (DMSO) was found to be optimal, providing a balance between reaction efficiency and reagent stability. The addition of Tin Chloride ($SnCl_2$) was incorporated into the ninhydrin reagent to act as a reducing agent, preventing the reagent's oxidation and preserving its reactive properties. Samples were purified using ultrafiltration to remove impurities and ensure the presence of only glutamic acid. In this method, Ninhydrin, typically used for amino acid quantification, was adapted for γ-PGA analysis by hydrolyzing the purified γ-PGA to yield its monomer, L-glutamic acid. Following hydrolysis, the samples were freeze-dried and re-suspended in 1 mL citrate phosphate buffer (pH 5.5). Subsequently, a 50 µL sample was mixed with 1 mL of Ninhydrin reagent (1.5% w/v in DMSO), ensuring the reaction reached the optimal pH of 5.2, as described by Paul J. Lamothe and Patrick G. McCormick in 1972. The samples were vortexed and subjected to a boiling water bath, resulting in the formation of a characteristic purple color indicating the completion of the reaction.

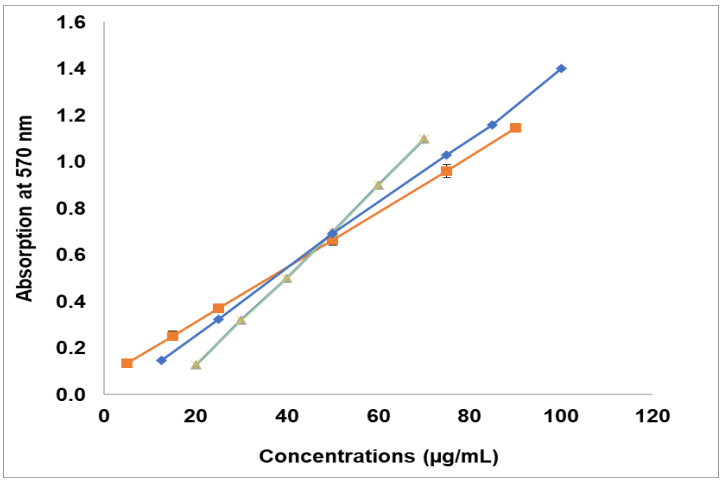

Fig.6. Calibration curve for the quantification of γ-PGA using the optimized ninhydrin assay. The curve was generated using two sets of measurements, one with concentrations ranging from 12.5 to 100 µg/mL (orange line) and the other with concentrations ranging from 5 to 90 µg/mL (blue line). For comparison, a calibration curve for glutamic acid was also generated using concentrations ranging from 10 to 80 µg/mL (green line).

Three standard curves were constructed to quantify the concentrations of hydrolyzed γ-PGA and glutamic acid in the fermentation samples. The hydrolyzed γ-PGA standard curve, prepared within concentrations ranging from 5 to 90 µg/mL, yielded a linear equation of y = 0.0119 + 0.0731 (R^2 = 1), indicating excellent correlation. A second standard curve, built using hydrolyzed γ-PGA within concentrations ranging from 5 to 30 µg/mL, produced a linear equation of y=0.0142+0.0302 (R^2=0.999), showcasing high reliability. AA third standard curve, constructed using glutamic acid prepared within concentrations ranging from 20 to 70 µg/mL, produced a linear equation of y = 0.0194 + 0.265 (R^2 = 0.997), demonstrating high reliability. These results validate the use of both standard curves for accurately quantifying the concentrations of hydrolyzed γ-PGA and glutamic acid in the fermentation samples (**Fig.6.**).

A preliminary analysis was conducted to determine the γ-PGA concentrations produced by MMS4 and MMS6 in the presence of copper and zinc sulfate (**Table 3**). MMS4 grown in LB medium supplemented with copper exhibited a γ-PGA concentration of 2.8±0.001 mg/L, while MMS6 in LB supplemented with copper yielded 3.8±0.15 mg/L. Notably, MMS6 cultivated in LB medium containing zinc sulfate (LB+ZnSO4) produced significantly higher amounts of γ-PGA, reaching 9.3±0.39 mg/L, far surpassing the γ-PGA production of the other strains.

Table 3: Concentrations of γ-PGA (µg/mL) for different strains cultivated from a shake-flask of 15 mL of LB containing $CuSO_4$ and $ZnSO_4$.The quantification of γ-PGA concentrations was carried out using the Ninhydrin assay spectrophotometric assay at 570 nm.

Samples	PGA concentrations (µg/mL)
LB+$CuSO_4$ (MMS4)	2.8±0.001
LB+$CuSO_4$ (MMS6)	3.8±0.15
LB+$ZnSO_4$ (MMS6)	9.3±0.39

Conclusion

In this study, we investigated the γ-PGA production capabilities of eight strains isolated from Polish honey. We employed a simple mucoid assessment method to screen the strains for their γ-PGA production potential. The results indicated that certain strains, particularly MMS4 and MMS6, exhibited γ-PGA production in LB medium. NMR spectroscopy confirmed the presence of γ-PGA in these media. However, when a beetroot molasses medium supplemented with minimal glutamic acid, ammonium source, and salts was employed for time optimization experiments, NMR analysis revealed that only the monomer of γ-PGA was detected over a period of 96 hours. These findings suggest either an insufficient nitrogen source leading to γ-PGA hydrolysis or the presence of hydrolysis enzymes within the strains. Furthermore, we developed a novel spectrophotometric method based on the ninhydrin reaction for γ-PGA quantification. This method proved to be reliable and accurate for measuring γ-PGA production. However, further validation using more sophisticated methods such as HPLC is warranted to establish its robustness. Overall, this study highlights the potential of honey-derived bacterial strains for γ-PGA production. Further optimization of media composition, salt conditions, and the development of improved cultivation strategies are essential to harness the full potential of these microorganisms for γ-PGA production and its applications in various fields.

References:

1. Deol, R., Louis, A., Glazer, H. L., Hosseinion, W., Bagley, A., & Chandrangsu, P. (2022). Poly-Gamma-Glutamic acid secretion protects *bacillus* subtilis from zinc and copper intoxication. *Microbiology Spectrum*, *10*(2), e01329-21.
2. Ezzell Jr, J. W., & Welkos, S. L. (1999). The capsule of Bacillus anthracis, a review. Journal of applied microbiology, 87(2), 250-250.
3. Fall, R., Kinsinger, R. F., & Wheeler, K. A. (2004). A simple method to isolate biofilm-forming Bacillus subtilis and related species from plant roots. Systematic and applied microbiology, 27(3), 372-379.
4. Friedman, M. (2004). Applications of the ninhydrin reaction for analysis of amino acids, peptides, and proteins to agricultural

and biomedical sciences. Journal of agricultural and food chemistry, 52(3), 385-406.

5. Galus, S.; Kadzinska, J.Moisture sensitivity optical mechanical and structural properties of whey protein-based edible films incorporated with rapeseed oil. Food Technol. Biotechnol. 2016, 54, 78–89.
6. Halmschlag, B., Putri, S. P., Fukusaki, E., & Blank, L. M. (2020). Identification of key metabolites in poly-γ-glutamic acid production by tuning γ-PGA synthetase expression. *Frontiers in Bioengineering and Biotechnology*, 8, 38.
7. Hamdy, A. A., Esawy, M. A., Elattal, N. A., Amin, M. A., Ali, A. E., Awad, G. E., ... & Mansour, N. M. (2020). Complete genome sequence and comparative analysis of two potential probiotics Bacillus subtilis isolated from honey and honeybee microbiomes. Journal of Genetic Engineering and Biotechnology, 18(1), 1-8.
8. Lamothe, P. J., & McCormick, P. G. (1972). Influence of acidity on the reaction of ninhydrin with amino acids. Analytical Chemistry, 44(4), 821-825.
9. Li, D., Hou, L., Gao, Y., Tian, Z., Fan, B., Wang, F., & Li, S. (2022). Recent advances in microbial synthesis of poly-γ-glutamic acid: a review. *Foods*, *11*(5), 739.
10. Li, M., Zhang, Z., Li, S., Tian, Z., & Ma, X. (2021). Study on the mechanism of production of γ-PGA and nattokinase in *Bacillus subtilis natto* based on RNA-seq analysis. *Microbial Cell Factories*, *20*, 1-15.
11. Lukasiewicz, M., Kowalski, S., & Makarewicz, M. (2015). Antimicrobial an antioxidant activity of selected Polish herbhoneys. LWT-Food Science and Technology, 64(2), 547-553.
12. M, Zhang Z, Li S, Tian Z, Ma X. 2021. Study on the mechanism of production of γ-PGA and nattokinase in Bacillus subtilis natto based on RNA-seq analysis. Microb Cell Fact 20:83.
13. Nair, P. G., & Dharne, M. S. (2023). Effective valorization of blackstrap molasses to poly gamma glutamic acid (γ-PGA) using L-glutamic acid independent feeding approach and its significance as drought mitigator in wheat plant. Industrial Crops and Products, 202, 116985.

14. Ogunleye, Adetoro, Aditya Bhat, Victor U. Irorere, David Hill, Craig Williams, and Iza Radecka. "Poly-γ-glutamic acid: production, properties and applications." Microbiology 161, no. 1 (2015): 1-17.
15. Qiu, Y., Zhu, Y., Zhang, Y., Sha, Y., Xu, Z., Li, S., ... & Xu, H. (2019). Characterization of a Regulator pgsR on Endogenous Plasmid p2Sip and Its Complementation for Poly (γ-glutamic acid) Accumulation in *Bacillus* amyloliquefaciens. *Journal of Agricultural and food chemistry*, *67*(13), 3711-3722.
16. S. Jacobs (1959). Determination of nitrogen in proteins by means of indanetrione hydrate, Nature, vol. 183, p. 262.
17. Sabbah, M., Di Pierro, P., Ruffo, F., Schiraldi, C., Alfano, A., Cammarota, M., & Porta, R. (2020). Glutamic acid as repeating building block for bio-based films. Polymers, 12(7), 1613.
18. Sanders, M. E., Morelli, L., & Tompkins, T. A. (2003). Sporeformers as human probiotics: *Bacillus, Sporolactobacillus*, and *Brevibacillus*. Comprehensive reviews in food science and food safety, 2(3), 101-110.
19. Snowdon, J. A., & Cliver, D. O. (1996). Microorganisms in honey. International journal of food microbiology, 31(1-3), 1-26.
20. Sun, S. W., Lin, Y. C., Weng, Y. M., & Chen, M. J. (2006). Efficiency improvements on ninhydrin method for amino acid quantification. Journal of food composition and analysis, 19(2-3), 112-117.
21. Tiwari, A. (2015). Practical Biochemistry: A Student Companion. LAP Lambert Academic Publishing.
22. Vlamakis, H., Chai, Y., Beauregard, P., Losick, R., & Kolter, R. (2013). Sticking together: building a biofilm the Bacillus subtilis way. Nature Reviews Microbiology, 11(3), 157-168.
23. Wellington, E. F. (1952). An ultramicro method for quantitative determination of amino acids. Canadian Journal of C.
24. Yamashiro, D., Yoshioka, M., & Ashiuchi, M. (2011). Bacillus subtilis pgsE (Formerly ywtC) stimulates poly-γ-glutamate production in the presence of zinc. Biotechnology and bioengineering, 108(1), 226-230.
25. Zeng, W., Chen, G., Zhang, Y., Wu, K., & Liang, Z. (2012). Studies on the UV spectrum of poly (γ-glutamic acid) based on development of a simple quantitative method. International journal of biological macromolecules, 51(1-2), 83-90.

26. Zulkhairi Amin, F. A., Sabri, S., Ismail, M., Chan, K. W., Ismail, N., Mohd Esa, N., ... & Zawawi, N. (2020). Probiotic properties of Bacillus strains isolated from stingless bee (Heterotrigona itama) honey collected across Malaysia. International journal of environmental research and public health, 17(1), 278.

General conclusions

This project has demonstrated promising advancements in the purification of pure and unexpensive γ-PGA of microbial origin, readily available in the market. Using eco-friendly ultrafiltration methods and an industrial-scale amount of 300 g, we successfully fractionated this polymer into distinct molecular weight (Mw) ranges: R1 (55-59 kDa) and R2 (20 kDa). The proposed purification methods hold immense promise for industrial-scale production and commercialization, requiring only a straightforward process involving centrifugation, microfiltration, and ultrafiltration. Additionally, they offer significant cost-effectiveness, providing a truly promising solution to a challenging problem. Building upon our successful fractionation of γ-PGA, we further explored the potential of these retentate fractions for bioplastics production. We employed both traditional casting methods and a thermal pressing approach, which involved simply mixing a specific amount of the fractions (R1 or R2) with glycerol and then subjecting the mixture to thermal pressing at 150°C for 2 min. The resulting films were characterized comprehensively, revealing promising properties such as good thermal stability and favorable mechanical properties, particularly in terms of extensibility.

These findings pave the way for potential applications of these γ-PGA-based films in food packaging, particularly given the biodegradability and edibility of γ-PGA. Additionally, the γ-PGA films, particularly those derived from the low-molecular-weight fractions, exhibited promising properties in mitigating oxidative stress, which suggest their potential application in wound healing and other biomedical applications. Purified γ-PGA fractions have also demonstrated the ability to counteract desiccation and oxidative stress in keratinocyte monolayers, suggesting a potential therapeutic option for oxidative stress-related diseases and modulating antioxidant defense pathways. These findings further highlight the potential of γ-PGA fractions for developing advanced biomaterials for various biomedical applications, including wound healing, tissue engineering, and regenerative medicine. Intriguingly, we further investigated the potential of the previously mentioned purified γ-PGA low mol. wt fractions (R1 and R2) to produce additional blended bioplastics. In fact, by blending CH with R1 or R2, under specific experimental conditions and employed only eco-friendly approaches, we produced a promising bio-composite

crosslinked material. Comprehensive characterization was performed for these inspiring materials, which the sedimented supramolecular complexes formed rubbery hydrogels that, upon dehydration, gave rise to glass-like materials endowed with advantageous physical characteristics and thermal stability, as well as an amorphous and crystalline structure. These findings open up new possibilities for the potential use of these new bio-composites in diverse fields. Their applications could span regenerative medicine, biomedical devices, food packaging, and even 3D printing.

Furthermore, the hydrogel state was also characterized, and the rheological analysis revealed that CHR1 exhibited gelation properties. The resulting hydrogel was initially tested as a bio-glue for various purposes, targeting its use as a material for restoration and cultural heritage preservation. Successful results were obtained when this potential adhesive biomaterial was applied to wood and aluminum, exhibiting properties comparable with those of commercially vinyl-based available glue. More in particular, the bio-glue performed comparably to commercial glue on wood, while exhibited superior adhesive strength when tested on aluminum substrates. This indicates the cohesive/adhesive failure mode, confirming its effectiveness, durability, and strength. However, these findings could be further explored for applications in paints and coatings, as well as in depth for biomedical applications such as wound dressing.

Delving into the heart of the project, we further explored the γ-PGA production, employing a molecular engineering approach by using *Bacillus subtilis* strains (PB5523 and PB 5390). To utilize the power of these modified bacteria, we cultivated them in an E-medium (???) enriched with L-glutamic acid. Following meticulous purification using methanol precipitation and dialysis, PB5523 yielded γ-PGA of high molecular weight (135 kDa) and PB5390 (105 kDa) while maintaining comparable yields. This breakthrough can be attributed to the double knockout of *pgdS* and *ggt* genes, along with the Hy mutant of the *swrA* allele, which act as γ-PGA degradation inhibitors. In a thrilling experiment, we delved into the intriguing realm of γ-PGA-based hydrogels, blending it with CH to form a synergistic composite. This versatile combination, using either PB5390 or PB5523-derived γ-PGA, proved remarkably efficient, even when employing a reduced quantity of material. The ability to achieve hydrogel formation with as little as 500 mg is a testament to the interesting properties of PB5523- and PB5390-derived γ-PGA, surpassing the lower molecular weight

(R1=59 kDa, R2=20 kDa) and relative purity (70%) γ-PGA fractions employed in previous studies.
Our quest for biomedical applications led us to create melanin-loaded hydrogels, a new objective of the bio-engineering. Thus, by encapsulating melanin within a CH matrix, it was synthesized a biocomposite that, when further blended with γ-PGA from PB5523, revealed to be promising for biomedical applications. While these initial findings paint a hopeful picture, *in vitro* and *in vivo* evaluations are now essential to unequivocally determine the encapsulation efficacy, melanin loading capacity, and associated biological effects of these melanin-loaded hydrogels. This groundbreaking research unveils the remarkable potential of γ-PGA and its derivatives, paving the way for a future brimming with innovative biotechnological applications.
Our further exploration for γ-PGA production continued during the research stay at Wroclaw university, where experiments of γ-PGA biosynthesis by using *Bacillus* strains isolated from Polish honey were carried out. In this respect, a novel reliable and accurate ninhydrin-based spectrophotometric method was developed to quantify the amount of γ-PGA produced. In addition, this research utilized eight different *Bacillus* strains and explored the influence of media composition, metal additives, and salt conditions on their growth patterns and γ-PGA production capabilities. The results revealed that the distint strains exhibited variable responses to these factors, demonstrating different growth characteristics and γ-PGA production profiles, the strains MMS4 and MMS6 isolated from Gąski honey (nettle - *Urtica dioica*) being of particular interest. In particular, NMR spectroscopy indicated the presence of γ-PGA in LB medium and the enhancement of homopolypeptide production was observed upon addition of copper. Therefore, these results highlighted the potential of these specific strains for γ-PGA production and suggested further investigations for the optimization of their γ-PGA biosynthetic capability. A preliminary study in this direction was carried out to determine the optimal time to obtain the maximum amount of γ-PGA. A natural source medium based on beetroot molasses, supplemented with L-glutamic acid, salts, and ammonium, was used but, unfortunately, this experiment resulted in γ-PGA hydrolysis. Thus, these initial results suggested the requirement of a preliminary optimization of the medium to enhance γ-PGA production.

List of publications and communications

Published articles:

1. **Hejazi, S.,** Restaino, O. F., Sabbah, M., Zannini, D., Di Girolamo, R., Marotta, A., ... & Porta, R. (2023). Physicochemical Characterization of Chitosan/Poly-γ-Glutamic Acid Glass-like Materials. International Journal of Molecular Sciences, 24(15), 12495.

2. Restaino OF., **Hejazi S.**, Zannini D., Giosafatto C.V.L., Di Pierro P., Cassese E., D'ambrosio S., Santagata G, Schiraldi C, Porta R. (2022). Exploiting Potential Biotechnological Applications of Poly-γ-glutamic Acid Low Molecular Weight Fractions Obtained by Membrane-Based Ultra-Filtration. Polymers. 14(6),1190.

3. Restaino, O. F., Giosafatto, C. V. L., Mirpoor, S. F., Cammarota, M., **Hejazi, S**., Mariniello, L., ... & Porta, R. (2023). Sustainable Exploitation of Posidonia oceanica Sea Balls (Egagropili): A Review. International Journal of Molecular Sciences, 24(8), 7301.

Virtual congresses and meetings:

1. 61° SIB 2021 Congress Virtual Edition, 23-24 September 2021 "**Innovative bio-composite materials manufactured with chitosan and poly-γ-glutamic acid**" **Sondos Hejazi**, Raffaele Porta, Valeria L. Giosafatto, and Prospero Di Pierro.

2. BRALLO DI PREGOLA (Pavia) 13 - 16 September 2021 32nd"A. Castellani"Meeting of PhD students in biochemical sciences, poster entitiled "**Poly-γ-glutamic acid based film" Sondos Hejazi**, Prospero Di Pierro, C. Valeri, L. Giosafatto, Raffaele Porta.

Oral communications:

1. Invited speaker at Paint and Coating Congress about "**Sustainable Production of Poly-γ-glutamic Acid Biodegradable Materials**" in Milan (17-18 October 2023)

2. Flash presentation at FISV Congress in Portici-University of Naples Federico II about "**Bio-inspired materials manufactured with poly-γ-glutamic acid and chitosan**". **Sondos Hejazi**, O.F. Restaino, C.V.L. Giosafatto, C. Schiraldi, G. Santagata, R. Porta (14-16 September 2022)

Poster communications:

1. **Clove Essential Oil Encapsulated by Chitosan-Based Systems: Future Outlook**. **Sondos Hejazi**, Valeria Scala, Nicoletta Pucci,

Raffaele Porta, Mohammed Sabbah, Loredana Mariniello, C. Valeria L. Giosafatto at **62°congress of the Italian Society of Biochemistry National (SIB) at Florance** (September 2023)

2. **Potential Therapeutic Applications of Poly-Ɣ-Glutamic Acid in Oxidative Stress-Related Disease. Sondos Hejazi**, Odile Francesca Restaino, Concetta Valeria Lucia Giosafatto, Elisabetta Cassese, Sergio D'ambrosio, Chiara Schiraldi* and Raffaele Porta* at BIOPROSYS JOINT MEETING at Luigi Vavetilli University in Naples, Italy on May 18-19, 2023

3. **Evaluation of novel bio-composite materials made of polyglutamic acid and chitosan Evaluation of novel bio-composite materials made of polyglutamic acid and chitosan**. **S. Hejazi**, O.F. Restaino, C.V.L. Giosafatto, C. Schiraldi, G. Santagata3, R. Porta of the Italian Society of Biochemistry National meeting (SIB) at the University of Naples Federico II -Naples (October 2022)

4. **Potential Biotechnological Applications of Low Molecular Weight Poly-γ-Glutamic Acid Fractions**. **Sondos Hejazi**, Odile Francesca Restaino, C. Valeria L. Giosafatto, Sergio D'Ambrosio, Chiara Schiraldi, Domenico Zannini, Gabriella Santagata, and Raffaele Porta, at Congress IUBMB-FEBS-PABMB 2022 in Lisbon-Portugal (9-14 July 2022)

Awards and grants:

1. Best Poster Award for participation at the BIOPROSYS JOINT MEETING at Luigi Vanvitelli University in Naples, Italy on May 18-19, 2023. The poster was titled "Exploring the Therapeutic Potential of Poly- γ -glutamic Acid in Oxidative Stress-Related Diseases." (18-19 May 2023).

2. Scholarship for participation in the IUBMBFEBS-PABMB 2022 Congress. Lisbon-Portugal. The abstract that was selected for this award was titled "Potential biotechnological applications of low molecular weight poly-gamma-glutamic acid fractions" (9-14 July 2022).

3. Grant for participation in FEBS Young Scientists' Forum 2024 (YSF 2024) to be held in Pavia, Italy, 26–29 June 2024 and 48th FEBS Congress in Milano 29 June-3rd July 2024 the abstract that was selected for this award was titled "Chitosan/poly-γ-glutamic acid blends: characterization of the produced hydrogels and their application as biodegradable glues".

Two experiences in foreign laboratories were made during the three years PhD course. The first at **Wroclaw university** in Poland, at the **Department of Biotransformation** of the University of Wroclaw, the second in North Italy at the **Department of Biology and Biotechnology** of the **University of Pavia**.

Uniwersytet Wrocławski

Prof. dr hab. inż.Marcin Łukaszewicz
Department of Biotransformation,
Faculty of Biotechnology,
University of Wroclaw
Poland

Aprile 28th 2023

RE: Invitation letter for Sondos Mohammad Hasan Hejazi

TO WHOM IT MAY CONCERN:

It is my pleasure to invite Sondos Mohammad Hasan Hejazi (University of Federico II, Naples, Italy) as a visiting student in the Department of Biotechnology at the University of Wroclaw. Her research activities will be focused on poly-γ-glutamic acid production and application as bio-based materials.

This research stay will take place from June 1st, 2023, to September 30th under my supervision.

With this invitation letter, we grant access to Sondos Mohammad Hasan Hejazi to the installations and laboratories of the Department of Biotransformation, Faculty of Biotechnology at the University of Wroclaw. The use of laboratory equipment and basic consumables will be granted free of cost. The University of Wroclaw will participate in any publication resulting from the research undertaken here.

Sincerely yours,
Marcin Łukaszewicz.
University of Wroclaw.
Poland

UNIVERSITÀ DI PAVIA
Dipartimento di
Biologia e Biotecnologie
"Lazzaro Spallanzani"

Pavia, 18/01/2023

A CHI DI COMPETENZA

Con la presente dichiaro che la dottoranda **Sondos Hejazi** è stata ospite nel laboratorio di Genetica dei Microrganismi da me diretto, presso il Dipartimento di Biologia e Biotecnologie *L. Spallanzani*, Università degli Studi di Pavia, Via Ferrata 9, 27100 Pavia, **dal giorno 11 al giorno 19 gennaio 2023**.

La visita ha previsto attività sperimentali utili per la realizzazione degli obiettivi scientifici che la Dott.ssa Hejazi si prefigge di raggiungere per la sua tesi di dottorato in Biotecnologie, in svolgimento presso l'Università Federico II di Napoli.

In fede

UNIVERSITA' DEGLI STUDI DI PAVIA
DIPARTIMENTO di BIOLOGIA E BIOTECNOLOGIE

Dott.ssa Cinzia Calvio
Ricercatore Universitario presso il
Dipartimento di Biologia e Biotecnologie "L. Spallanzani"
dell'Università degli Studi di Pavia

Università di Pavia - - Dipartimento di Biologia e Biotecnologie "L. Spallanzani"
Via A. Ferrata, 9 - 27100 Pavia (Italia)
Tel.: +39 0382 98 6288 - http://dbb.unipv.it/ - emdip08@unipv.it
Partita IVA: IT00462870189 - C.F.: 80007270186

DBB Dipartimento di Biologia e Biotecnologie "L. Spallanzani"

Additional papers

During the three years of PhD course, some scientific collaborations with researchers working at the Department of Chemical Sciences on scientific issues related to that of the present thesis have been possible and successfully carried out. These studies have been object of one Review and one Article, the first published and the second under submission on qualified international Journals.

International Journal of *Molecular Sciences*

MDPI

Review

Sustainable Exploitation of *Posidonia oceanica* Sea Balls (Egagropili): A Review

Odile Francesca Restaino [1], Concetta Valeria L. Giosafatto [1], Seyedeh Fatemeh Mirpoor [1], Marcella Cammarota [2], Sondos Hejazi [1], Loredana Mariniello [1], Chiara Schiraldi [2] and Raffaele Porta [1,*]

[1] Department of Chemical Sciences, University of Naples "Federico II", Montesantangelo Campus, Via Cinthia 4, 80126 Naples, Italy; odilefrancesca.restaino@unina.it (O.F.R.); giosafat@unina.it (C.V.L.G.); seyedehfatemeh.mirpoor@unina.it (S.F.M.); sondosmohammadhasan.hejazi@unina.it (S.H.); loredana.mariniello@unina.it (L.M.)

[2] Department of Experimental Medicine, University of Campania "Luigi Vanvitelli", Via De Crecchio 7, 80138 Naples, Italy; marcella.cammarota@unicampania.it (M.C.); chiara.schiraldi@unicampania.it (C.S.)

* Correspondence: raffaele.porta@unina.it

Abstract: *Posidonia oceanica* (L.) Delile is the main seagrass plant in the Mediterranean basin that forms huge underwater meadows. Its leaves, when decomposed, are transported to the coasts, where they create huge banquettes that protect the beaches from sea erosion. Its roots and rhizome fragments, instead, aggregate into fibrous sea balls, called egagropili, that are shaped and accumulated by the waves along the shoreline. Their presence on the beach is generally disliked by tourists, and, thus, local communities commonly treat them as waste to remove and discard. *Posidonia oceanica* egagropili might represent a vegetable lignocellulose biomass to be valorized as a renewable substrate to produce added value molecules in biotechnological processes, as bio-absorbents in environmental decontamination, to prepare new bioplastics and biocomposites, or as insulating and reinforcement materials for construction and building. In this review, the structural characteristics, and the biological role of *Posidonia oceanica* egagropili are described, as well as their applications in different fields as reported in scientific papers published in recent years.

Keywords: cellulose; egagropili; holocellulose; lignin; marine waste; *Posidonia oceanica*

Citation: Restaino, O.F.; Giosafatto, C.V.L.; Mirpoor, S.F.; Cammarota, M.; Hejazi, S.; Mariniello, L.; Schiraldi, C.; Porta, R. Sustainable Exploitation of *Posidonia oceanica* Sea Balls (Egagropili): A Review. *Int. J. Mol. Sci.* **2023**, *24*, 7301. https://doi.org/10.3390/ijms24087301

Academic Editor: Francesco Trotta

Received: 21 March 2023
Revised: 9 April 2023
Accepted: 12 April 2023
Published: 14 April 2023

1. Introduction

1.1. Biological Role of Posidonia oceanica and Derived Egagropili

Posidonia oceanica (L.) Delile (PO) is an aquatic plant that is a dominant and endemic sea grass of the Mediterranean basin belonging to the *Posidoniaceas* family [1], and therefore, it is not an alga, despite still being frequently and wrongly defined as such in numerous scientific papers [1]. PO is a slow-growing plant that might live for millennia, and it forms huge underwater meadows that are estimated to cover more than 2.0% of the Mediterranean seabed (for a total of more than 12,000 km^2) and that could extend from the sea surface up to 40 m of depth [1,2]. PO mainly spreads itself by sexual reproduction, although asexual reproduction might also occur by stem extension. The sexual annual reproductive cycle starts in the fall with pollination, and after a period of six to nine months, its mature fruits release seeds that reach the seabed and can develop roots and produce a new plant [3]. In only one year, the meadows of PO produce a huge amount of debris as leaves (leaf blades and sheaths), rhizomes, and roots that could constitute a biological sediment on the seabed and, eventually, might be either degraded by macro-organisms, microorganisms, and abiotic factors, or being subjected to the hydrodynamic action of the sea and rolled on its floor or ripple marks, or transported by the waves on the coasts where they accumulate [3]. The leaves, in particular the portions called leaf blades, fall from the plant after 5–8 months of existence and, generally, at higher rates in the autumn, as in this season, a lower amount of sunlight reaches the sea, and many strong storms occur. Conversely, the leaf sheaths

usually remain attached to the rhizomes. The leaves, that reach the seashore transported by the waves and deposited on the beaches by the winds, usually form huge banquettes with thickness ranging from a few centimeters up to 2.5 m [3,4]. The annual total amount of PO leaves that reach the coast is in the range of 5 to 50 million tons, and nowadays the banquettes are estimated to cover about 50,000 km^2 of sandy shores in the Mediterranean areas [1–3,5]. They are generally composed of wet and dried brown PO leaves, and they play an important ecological role in preserving the ecosystem and the biodiversity. In fact, they represent a favorable habitat for many species, promote sediment entrapment and stabilization, regulate the CO_2 absorption of the sea and of the atmosphere, as well as water oxygenation, and protect the coasts from erosion by acting as a barrier [2,4–6]. PO roots and rhizome fragments, instead, might naturally be entangled by the constant rolling of the sea motions and aggregate as ball-shaped materials that are then delivered by the waves on the coasts, where they dried under the sun and the wind action [2,4]. These brown dried fibrous balls are generally known as PO egagropili (POEG), also spelled egagropilia, egagropoli, or aegagropiles, and reported as sea balls, sea rissoles, sea potatoes, beach balls, Neptune balls, or Kedron balls. The name "aegagropiles" derives from the ancient Greek words of αίγαγρος (wild goat) and πῖλος (fur), as the shape of these sea balls is reminiscent of the ones that are generally regurgitated by goats [4]. Figure 1 shows a re-presentative image of some POEG samples collected by the authors on the beach of Marzamemi, Sicily, Italy; 36°44′34″ N, 15°7′1″ E, and Figure 2 indicates the map of the sites in the Mediterranean Sea where the POEGs mentioned in this review were collected [2,5]. As with theleaves, every year millions of POEGs are delivered on the beaches by the winds, mainly in the period between October and March and especially after strong sea storms [3,5]. In some cases, POEG deposition could constitute a characteristic geomorphological feature of the landscape, such as along the southeastern Gulf of Sirte, in Libya, near the coastal town of Brega (30°26′06″ N, 19°40′01″ E) (Figure 2). Here the POEGs are deposited by the action of westerly winds, while the hot and arid wind of Ghibli, from the south, carries huge amounts of Sahara sand, thus forming peculiar POEG sandy sheets and dunes that are considered paleoenvironmentally interesting to study in our Holocene era [5]. Indeed, POEGs have been frequently studied in integrated archaeological and geological investigations as a sign of the coastal barrier evolution in different Mediterranean areas as well as of the stratification and of the climate changes during the Holocene (e.g., the studies on the Mistras coastal barrier system in central Sardinia, Italy [7]).

1.2. POEG Structural Characteristics

POEGs have specific physical characteristics such as a texture of rough felt, oval shapes (ball-shape), spherical or subspherical, or sometimes also elongated ellipsoidal shapes (egg-shape) and have different sizes with diameter values from millimeters to centimeters up to 20 cm (Figure 1). They have a very light weight, so they easily float freely in the sea water [2,3,5]. Their shape and their geometrical and mechanical properties are conserved, although they are formed in the open sea and under not-constant environmental conditions. For these reasons, POEGs have been considered a natural archetype of fiber networks and studied as models to understand fundamental aspects of the clustering mechanisms and of the aggregation dynamic forces in the networking processes [4]. Indeed, the natural processes and forces, as well as the sequence of events that drives POEG formation, are not easy to decipher, and in the literature, there are only a few studies on their origin, properties, and structural composition. In a recent paper, the determination of the average mass, average size, in terms of length and radius, and of the volume was performed on 2000 POEG samples collected in two beaches in France, at Six Fours (43°63′06″ N, 5°49′20″ E) and at Porquerrolles Island (43°00′02″ N, 6°13′38″ E) (Figure 2) [4]. X-ray tomography analyses were used to determine the POEG average density and density profile, their internal structure, and their fiber orientation. The sea balls showed an average density of 128 $kg \cdot m^{-3}$ and an inhomogeneous fiber alignment, at least in the dense outward shell, in which the fibers had low orthoradial orientation [4]. Studies on the fiber

properties by using scanning electron microscopy (SEM) analyses were also performed to study the nature of the constituent fibers of the sea balls and thus decipher their connectivity and mechanical responses, which in general depend not only on the properties of the fibers themselves but also on their density and their organization in the cluster. Figure 3A, B report representative SEM images of the POEG fibers. Images of the outer and near-surface areas of the sea balls showed fibers to be very smooth and straightly slender with a cross-section of 100 μm with length values between 0.5 and 20 mm, and a predominance of short fibers with a weighted average length of 7.7 mm [4]. Analyses also showed that the connectivity and the cohesion mechanism between the fibers were due to their elasticity and inter-fiber friction contacts. The very dense structure and the high inhomogeneity of the fiber organization might be responsible for the high stiffness of POEGs that allows them to resist finger pressure. Based on all these data, the authors formulate the hypothesis that the sea balls are generally formed underwater, in submarine hollows, by isotropic mixing of randomly oriented smooth fibers and by aggregation mechanisms due to the action of friction forces from repeated collisions with the seabed and not by simple compaction processes due to hydrodynamic forces [4]. The hypothesis of POEG formation by aggregation mechanisms of litter fibers was also supported by the studies of Lefebvre and coworkers that collected 159 POEGs on the beach of Calvi (Corsica, France; 42°35′04″ N, 008°43′39″ E) (Figure 2). These authors performed deeper studies and formulated broader conclusions on the POEG formation process. In fact, the 159 samples were analyzed from a macroscopical point of view, in terms of shape, size, and density, but also in their microscopic aspects, performing sections of the balls by sli-cing them, studying both their external and internal layers, and carefully disassembling the POEG network to analyze the fibers at different strata [3]. Between the collected samples, only 21% had a ball-shaped form, while the rest showed an egg-shaped form. They had density values between 100 and 400 $kg \cdot m^{-3}$ with an average of 220 ± 40 $kg \cdot m^{-3}$ [3]. Thanks to stereo-microscope photographs and X-ray projections, the authors were able to classify the sea balls into three types: a heterogeneous type with a white, distinct nucleus that contains inside a piece of rhizome (58% of heterogeneous samples were egg-shaped, ellipsoidal POEGs), a homogeneous type without a distinct nucleus (mainly ball-shaped, spheroidal POEGs), in which the nucleus was probably degraded, and an intermediate type in which the nucleus contained clusters of dark pieces or fibers. Besides the nucleus (that, if present, might constitute 17% of the POEG architecture), all three types of POEGs showed three different concentric layers with diverse thickness and fiber composition: the superficial layer (14% of the POEGs), the median layer (25% of the POEGs), and the deep layer (44% of the POEGs). In the external, superficial layer, the fibers were poorly organized, as previously described by Verhillea and co-workers [4]. The median layer appeared fiber-rich, while in the deeper layer, many particles of sand contributed to a more whitish color. In fact, these round-shaped conglomerations contain not only fibers from the roots and rhizomes of PO meadows but also 10–20% of their weight as water and some minerals, such as aluminum-silicate particles and calcium carbonate salts, probably coming from the seabed sediments and included in the POEG network during their formation (Figure 3C) [3]. Sometimes calcified fragments of marine organisms, such as diatoms, might be easily detected in the POEG network too, not only by using X-rays but also by SEM analyses, as reported also by Restaino and co-workers [8] for samples collected in Poetto (Sardinia, Italy; 39°12′00″ N, 9°09′33″ E, Figures 2 and 3D). Independently from the POEG type, the nucleus and the three layers always showed thickness values that increased gradually from the external portions to the internal parts, ranging from 2.35 to 7.95 mm. The fiber density and the presence of mineral particles also increase when mo-ving from the external to the internal part of the POEG network. Fibers ranged from 12.0 ± 2.0% of the section surface of fiber/unit of section surface in the superficial zone to 18.0 ± 4.0% in the median and deeper layers, while minerals ranged from 1.2 ± 0.9% of the section surface of mineral/unit of section surface to 7.0 ± 2.0%. In a heterogeneous POEG, the nucleus is the denser part (about 26.0 ± 4.0%), and it sometimes also contains woody pieces and minerals. This

central zone, if present, also contains larger fibers. In fact, the determination of the width of 960 fibers in the three layers and of the nucleus of the different types of POEGs allowed the authors to classify them into thin, flat, and wide fibers. The thin fibers (0.142 ± 0.051 mm) were mainly present in the superficial layer (70% and 55% of the superficial layer fibers were thin in the homogenous and heterogeneous types, respectively), similarly to what had previously been reported by Verhillea and co-workers [4]. In the median layer, a mixture of tin, flat (0.462 ± 0.095 mm), and wide (2.295 ± 1.380 mm) fibers was detected. In the deep layer, a higher percentage of wider fibers was detected in heterogeneous POEGs (24%), compared to the homogeneous type (5%) [3]. All the fiber types were flexible, especially the thinner ones. Based on all these results, the authors proposed that the formation of the POEGs follows several steps in which an initial roll of fibers and sand starts to aggregate in the seabed on ripple marks, then this roll grows and breaks down into small balls by mechanical and/or microbial degradation [3]. Structural characterization of the POEG fibers showed a chemical composition typical of the lignocellulosic materials, thus made of lignin groups bound to a holocellulose structure that includes cellulose and hemicellulose chains (Figure 3E,F) [2]. The composition of the POEGs was first reported as being made of 29.8% lignin, 61.8% holocellulose (21.8% hemicellulose, and 40% cellulose), and then ashes [6]. But then more accurate analyses were performed; acidic hydrolysis and HPAE-PAD analyses were used to determine the monosaccharide composition of untreated POEG fiber samples collected in Poetto. They were neutral sugars, such as fucose (Fuc), arabinose (Arab), rhamnose (Rham), galactose (Gal), glucose (Glc), and xylose (Xyl), as well as an amino sugar, such as glucosamine (GlcN), and an uronic acid, such as GlcA. The representativity of these sugars ranged from 51.0% of Glc to 0.6% of Fuc, for a total carbohydrate content of 28.3% of the dry weight of the fibers. Monosaccharides such as Fuc, Arab, Rham, Gal, Glc, Xyl, and GlcA were also found in the water extracts of PO leaves, together with mannose (Man) and galacturonic acid (GalA), but with a relative abundance that ranged from 80% for Gal to 50% and 45% for Glc and Xyl, respectively [9]. In another paper, aqueous fractions were extracted from samples of POEG, collected in Tunisia (the specific place was not mentioned), and then analyzed by GC-FID/MS and by colorimetric assay for the monosaccharide composition, by the permethylation method for the identification of glycosidic linkages, and by elemental analyses [10]. These authors found the same monosaccharide composition described in the previous paper (Fuc, Arab, Rham, Gal, Glc, Xyl) and detected the presence of uronic acid by colorimetric assay, but they found that xylose was the most representative sugar, which may be because they analyzed the water extracts of POEGs and not the fibers directly [10]. Linkages of 1,2-, 1,3, 1,4-types were found by the permethylation method for the Arab, Rham, and Xyl monosaccharides, but the complete structure of the carbohydrate sequence was not determined. Both cellulose and hemicellulose fractions were isolated from POEG fibers mainly by u-sing protocols that first removed the lignin portion. In the literature, different methods have been used to isolate the lignin-containing fraction from POEGs after an initial washing step, and the samples were processed through grinding or knife milling. In the first protocol, the powder was extensively extracted by using the Soxhlet method and then with a dioxane–water solution to remove plant cell-wall components and recover a total content of acid-soluble and acid-insoluble lignin [11]. In the second protocol, instead, the powder was treated using a 1.7% sodium chloride oxidation at pH 3.5 and then dewaxed by employing a toluene/ethanol solution (2:1 *v*/*v*) [2]. The total lignin content was estimated to be around 8–12% of the initial weight in the POEG samples collected in Portlligat Bay (Girona, Spain; 42°17′37″ N, 3°17′7.2″ E, Figure 2) that were extracted with the first protocol [11], or about 15% of the initial weight in the case of POEG samples collected in Poetto Beach (Sardinia, Italy; 39°12′00″ N, 9°09′33″ E, Figure 2) and extracted with the se-cond method [2,12] (Figure 3E). The analyses of the lignin of the egagropili collected in Portlligat, performed through derivatization that was followed by the reductive cleavage (DFRC) degradation method, and by GC/MS analyses after pyrolysis and by bidimensional NMR analyses, showed the presence of few syringyl units and numerous guaiacyl units that were also

frequently bounded to a highly acetylated 4-hydroxybenzoic acid [11]. The presence of a high degree of p-hydroxy benzoylation in both guaiacyl (73%) and syringyl (61%) lignin units in *P. oceanica* tissues was the highest ever reported, so far, in a plant, and explained the higher capacity of this species to store carbon dioxide, compared to other species, such as *Poseidonia australis* [13]. Furthermore, gel permeation chromatography analyses determined the molecular weight of this lignin fraction that was found to be 6100 Da, with a polydisperdity of 2.2, thus indicating a low molecular weight aromatic polymeric structure, made of dimers, trimers, or tetramers. Instead, by using the second protocol of extraction, a water soluble, brown colored lignin-containing fraction was isolated that showed high absorbance in wavelength range from 250 to 400 nm, due to the presence of aromatic rings. This presence was also confirmed by broad peaks in the aromatic regions (6.5–7.5 ppm) in ^{1}H NMR analyses [12]. In the alkoxide regions (3.5–4.5 ppm), the signals of -OCH_3 groups indicated the presence of the syringyl and guaiacyl units. After determination of the total phenol content by the Folin–Ciocalteu method, 22% of flavonoids and 10% of anthocyanins were identified using an aluminum chloride co-lorimetric assay [12]. The sodium chloride oxidation method allowed the extraction of the part of the hemicellulose chains that remained attached to the lignin portion, as demonstrated by the presence of alkoxy signals in the ^{1}H NMR spectrum. This lignin–carbohydrate complex showed a molecular weight (Mw) of about 35 kDa and a monosaccharide composition made of the eight different sugars (fucose, arabinose, rhamnose, galactose, glucose, xylose, glucosamine, and glucuronic acid) that was found in the POEG fiber mo-nosaccharide composition as well, but, of course, with different ratios as the glucose pre-sence due to the cellulose chain, was greatly reduced by the carbohydrate extraction [12].

Figure 1. Pictures of POEGs of both oval and elongated shapes of different sizes, with a ruler used as a reference. They were collected by the authors on the beach of Marzamemi (Sicily, Italy; 36°44′34″ N, 15°7′1″ E).

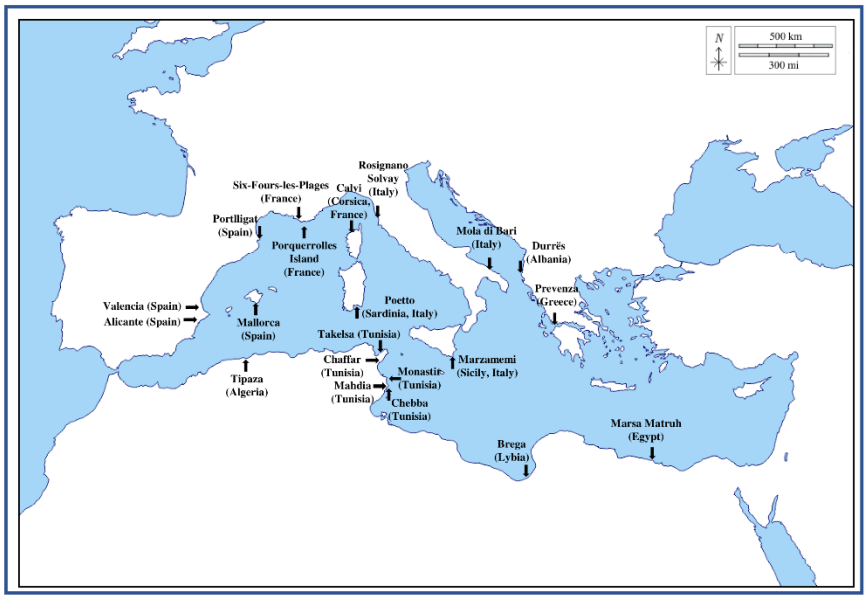

Figure 2. Map of the sites in the Mediterranean Sea where the POEG samples mentioned in this review were collected.

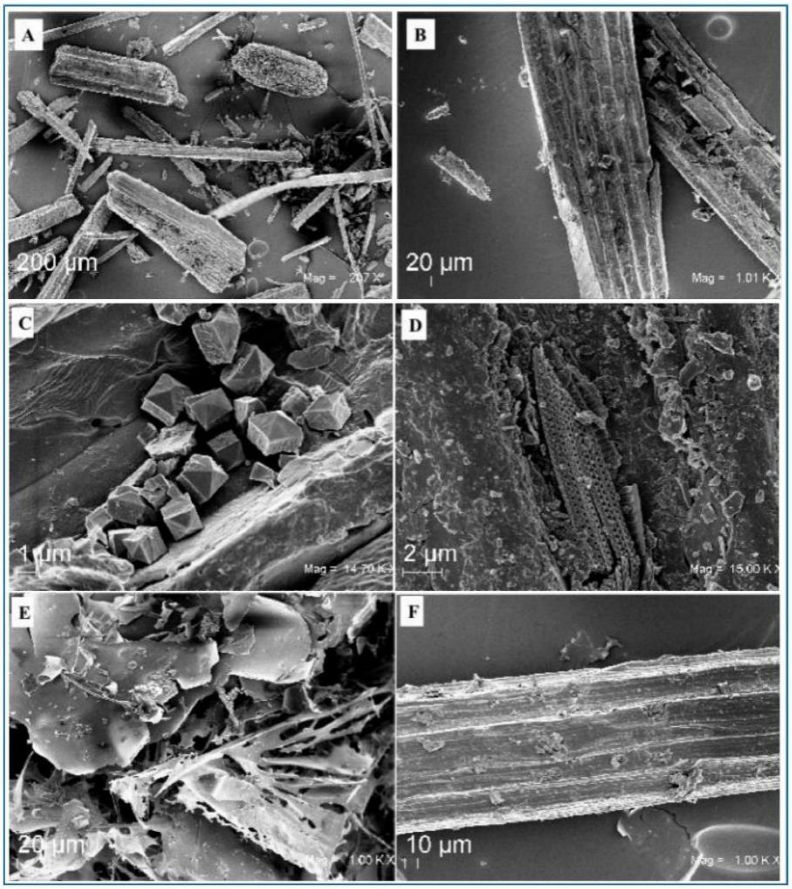

Figure 3. SEM pictures of the fibers of POEGs collected in Poetto Beach (Cagliari, Sardinia, Italy; 39°12′00″ N, 9°09′33″ E) (**A**) at low magnification (207X, scale bar 200 mm) and (**B**) at high magnification (1000X, scale bar 20 mm); (**C**) pictures of the crystals and (**D**) of the diatoms found on these POEG fibers (magnifications 14,7 KX and 15 KX, scale bar 1 and 2 mm), and (**E**) of the lignin and (**F**) of the holocellulose fractions extracted from them (magnification 10KX, scale bar 1 and 2 µm). [The preparation procedure of the samples for SEM analyses was similar to the one reported before (Restaino et al., 2022 [8]): Samples were suspended in 4% formalin in PBS for 18 h, dehydrated in increasing ethanol concentrations (from 30% to 100% for 5–15 min), dried in a critical point dryer, and sputtered with platinum-palladium (sputter coater Denton Vacuum Desk V). Fe-SEM Supra 40 Zeiss (5 kV, detector InLens) and Smart SEM Zeiss software were used for observation].

2. *Poseidonia oceanica* Egagropili as Lignocellulosic Biomass to Valorize

Every year, huge quantities of POEG fragments accumulate on Mediterranean coasts, resulting in a problem and a negative visual impact, creating the necessity for municipalities to remove this waste to keep beaches cleaned and ready for tourists and the summer season [6]. As disposal of this waste is performed every year and does not have negligible costs, it would be useful to find a way to valorize POEGs as readily available, low-cost, and renewable lignocellulose biomass and as a good source of cheap materials and fibers to produce added-value products from the perspective of an eco-friendly society [1,10,14]. The whole POEGs, themselves, have interesting properties that can be used for energy production [15], dye removal from the environment, building materials in the construction sector, as well as in the development of new packaging systems. They are also an optimal source of lignin and cellulose fractions that might be widely used in the paper-making industry, as well as a source of carboxymethyl cellulose in the production of fiber-reinforced composite materials and biopolymeric films. Lastly, they might be used as carbohydrate substrates to grow microorganisms in biotechnological processes. The lignin fraction, made of numerous 4-hydroxybenzoic acid groups, might instead be used for the synthesis of chemicals, such as parabens, and pharmaceutical molecules, such as paracetamol. All new applications of POEGs and their derived fractions are reported in the following paragraphs from the literature published in the last few years in the fields of biotechnology, environmental decontamination and bioremediation processes, bioplastic and biocomposite preparations, and construction materials (Figure 4 and Table 1).

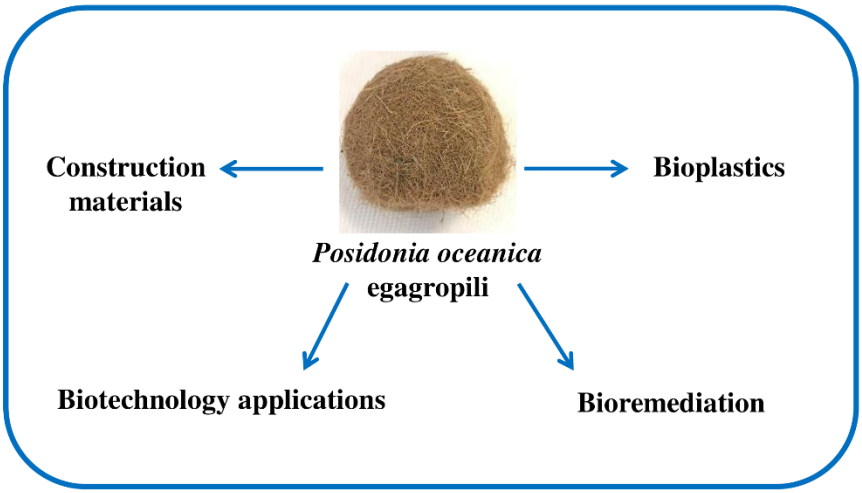

Figure 4. Fields of applications of POEGs.

Table 1. Fields and types of applications of POEGs or their components according to the references reported in this review.

Field of Application	POEGs or Their Components	Application	Reference
Biotechnology	POEG powder	Melanin production by *Streptomyces roseochromogenes*	[8]
	Cellulose component	Cellulase production by *Streptomyces roseochromogenes*	[16]
	POEG fibers	Cellulase and xylanase production by *Microbacterium metallidurans* TL13	[17]
	POEG fibers	Nanofibrillated cellulose production	[18]
	POEGs	Supplementation of the medium composition of brassica microgreens	[19]
	POEG fibers	Medium to boost lentice germination	[20]
Enviromental decontamination	Activated POEG powder	Blackish water decontamination from methylene blue and Pb^{2+}	[21]
	POEG fibers	Water decontamination from Pb^{2+}, Cu^{2+}, Ni^{2+}, Zn^{2+} and Cd^{2+}	[22]
	Activated POEG powder	Water decontamination from Cr^{6+}	[23]
	POEGs and POEG powder	Sea decontamination from hydrocarbon spill pollution	[24]
	POEG powder	Water decontamination from antibiotics like oxytetracycline	[25]
	POEGs	Sea decontamination from plastics	[26]
Bioplastic and biocomposite preparation	Lignin-carbohydrate complex and nanocrystalline cellulose	Reinforcing agents for biodegradable films obtained from hemp	[2,12]
	Lignin-containing cellulose micro/nanofibrils	Packaging materials	[27]
	POEG fibers	Reinforcing agents in matrices of high-density polyethylene and maleated polyethylene	[28,29]
	POEG fibers	Reinforcing agents in matrices of unsaturated polyester resin matrices	[30]
	POEG fibers	Reinforcing agents in polyhydroxybutyrate-co-hydroxyvalerate matrix	[31]
	POEG fibers	Reinforcing agents in polyhydroxybutyrate-co-hydroxyvalerate based bio-containers	[32]
Construction materials	POEGs	Insulating materials in building	[33]
	POEG fibers	Additive in plasters	[34]
	POEG fibers	Additive in cement composites	[35,36]

2.1. *Poseidonia oceanica Egagropili in Biotechnological Applications*

The whole POEGs and/or their lignin and cellulose fractions have been employed in numerous biotechnological applications (Table 1). For example, they have been recently used as substrates for microorganism growth. Recently, POEGs collected in Poetto (Figure 2) were added, after being washed and milled, as a raw source, in a glucose, yeast, and malt extract containing medium to boost the natural synthesis of melanin by *Streptomyces*

roseochromogenes [8]. The researchers found that the addition of 2.5 g/L of POEG powder in shake flasks enhanced the biomass formation of 1.5–1.9 folds in a 120-hour run at 26 °C and 250 rpm and increased the melanin production of 7.4 times, up to about 3.9 g/L, compared to the control. In 2-liter batch experiments, the melanin production reached values of 9.2 g/L in only 96 h, with a further increase in both production and productivity of about 2.4 folds [8]. Melanin is a secondary metabolite that starts to be synthesized by streptomycetes in their late exponential and stationary phases of growth. The first two reactions in the melanin synthetic pathway are catalyzed by the action of a tyrosinase that converts the precursor L-tyrosine to L-3,4-dihydroxyphenylalanine (DOPA) in the presence of molecular oxygen. The scientists discovered that the addition of the POEG powder to the medium enhanced the tyrosinase activity of 1.5–1.7 folds compared to the control during the microorganism growth and drove to a higher and faster melanin production. Furthermore, studies have demonstrated that both the lignin and cellulose components of the POEGs are necessary to boost melanin production, but in different ways. The holocellulose chains were used by the bacteria as a substrate for their growth, whereas the isolated lignin carbohydrate complex was necessary to induce melanin synthesis, but only if the two components were supplied together higher biomass values and melanin concentrations were obtained [8]. In another paper, instead, only the cellulose component, isolated from the POEGs collected in Poetto again, was used to enhance the production of cellulases in the same strain, *S. roseochromogenes* [16]. This fraction, supplemented to the growth medium at a concentration of 2.5 g/L, was able to increase the enzyme production in shake flasks of 4.3 fold compared to the control, aup to 268 U/L in 72 h with a productivity of 3.7 U/L/h and up to 347 U/L in 45 h in 2-liter batch experiments with a productivity of 7.7 U/L/h. The supplementation of cellulose induced the expression of a pool of three cellulases with molecular weights of about 115, 63, and 47 kDa. This pool had optimal activity at 60 °C and pH 5.0, and showed their ability to hydrolyze at the same time substrates such as carboxymethyl cellulose (CMCase activity) and filter paper (FPase activity), and it also showed a β-glucosidase action [16]. As POEGs contain salts in their fibers, they might also constitute an example of marine-origin lignocellulose biomass, a waste that needs to be studied to improve our knowledge of the bioconversion of sea raw materials into fermen-table sugars to produce second-generation biofuels [17]. In a recent paper, the POEGs collected on the beach of Takelsa, Tunisia (36°47′24″ N, 10°37′48″ E) (Figure 2) were used as substrates to check the capacity of cellulose/hemicellulose degradation enzymes expressed by the plant growth-promoting actinobacterium, *Microbacterium metallidurans* TL13. Genomic studies on this strain have shown that it has genes decoding for carbohydrate active enzymes (CAZymes), such as CMCases, β-glucosidases, and xylanases. The POEG fibers were first pretreated by an autoclave at 120 °C for 20 min and then used in enzymatic assays with *Microbacterium metallidurans* TL13; enzyme preparations (20 FPase/g of dry substrate) by incubation at 180 rpm and 37 °C at 180 rpm were conducted for 72 h. The microbial enzymes were extremely halostable and osmoadaptive, and they were able to efficiently degrade POEGs by converting it into fermentable sugars with a yield of about 33% of the theoretical maximum yield, thus showing a promising, green biocatalytic tool for seagrass-based biorefinery [17]. In the literature, not only it was reported the enzyme-assisted hydrolysis of POEGs—but also thermomechanical—and chemical-based methods. A combination of both these methods was used by Kadraoui and co-workers [18], who set up a new pre-treatment process for POEGs with the aim of producing nanofibrillated cellulose to be employed in efficient bioconversion processes. Fibers of sea balls collected on the beach of Monastir, Tunisia (35°46′40″ N, 10°49′34″ E) (Figure 2) were first delignified by using 20% sodium hydroxide and 0.1% anthraquinone and then bleached with sodium chlorite. The obtained pulp was dried, milled, and then subjected to a TEMPO (2,2,6,6-tetramethylpiperidine-1-oxide radical)-mediated oxidation (TEMPO/NaBr/NaClO 0.1/1/6.22 at 25 °C) to convert primary hydroxyl groups to carbo-xylate functions. Then their pulp was exposed to steam explosions at 170 °C, at 8 bar for 30 s to obtain microfibrillated cellulose [18]. The POEGs were also used in innovative and ecofriendly fortification approaches, such as improving

edible plant growth. In the literature, a recent study reported that POEGs collected on the beach of Mola di Bari in Italy (41°3′36″ N, 17°5′24″ E) (Figure 2) were used as supplements for the medium composition of two different brassica microgreens (Mizuna and Rapini) [19]. The POEG fibers were mixed with a commercial medium at rates of 25, 50, and 75% to constitute a natural organic matrix to improve the nutritional quality of the two brassica plants. This supplementation was effective in improving the iodine (I) and boron (B) contents of the microgreens up to 50 and 75%, and thus their nutritional profiles [19]. POEG balls collected on Oliva and Denia beaches in Valencia, Spain (39°28′11″ N, 0°22′38″ W) (Figure 2) were instead used as a medium to improve the germination rate and average germination time of lentils compared to those seeded on cotton [20]. The germination rate was reduced of around 17% on washed and milled short fibers (2–5 mm) and of about 42% on bleached, original long fibers (6–15 mm), while the average germination time was reduced up to 2.8 days.

2.2. *Poseidonia oceanica Egagropili in Environmental Decontamination Processes*

PO is a natural biomonitor of pollution in the sea as it catches heavy metal ions such as arsenic (As), cadmium (Cd), lead (Pb), and zinc (Zn) present in the water to store them in its organs at concentrations of up to several mg/kg [21]. Additionally, the dried fibrous balls of POEGs have promising features, such as being green adsorbents for cationic pollutants since they are already found in nature as cation-imprinted lignocellulose networks that contain a high presence of salts [21] (Table 1). The high biosorption properties of POEGs could constitute a new potential way for their valorization and reusing in cleaning systems of blackish water decontamination processes from dyes, phenol compounds, and heavy metals [10,21]. According to some authors, the POEGs' ability to uptake metals might be due to the porosity of their cell walls, which allow the entrance of small ions, and due to their lignocellulose composition [22]. In the literature, many studies have focused on POEGs' absorption abilities and their possible applications in diverse deconta-mination processes. In these investigations, some key parameters of the process have been taken into account, such as the pH of the contaminant solution, the temperature at which the process is performed, the contact time between the solution and the POEGs, the initial concentration of the contaminant, the amount and size of the POEGs, and the enthalpy and entropy of the process. In a recent paper, some POEGs collected in Marsa Matrouh, Egypt (31°21′15″ N, 27°14′14″ E) (Figure 2) were "activated" by soaking them after pulve-rization in 1 M acetic acid overnight and then used as an eco-adsorbent for the removal (in 30 min of shaken run) of methylene blue and lead ions (Pb^{2+}) present in aqueous solutions in concentration ranges from 0.6 to about 2.6 g/L [21]. The initial acetic acid activation method resulted in greatly reducing the presence of some ions, such as barium (B), cadmium (Cd), chromium (Cr), copper (Cu), magnesium (Mg), and zinc (Zn), in the fibers that are naturally present in the collected samples without altering the lignocellulose composition. On the basis of these analyses of the adsorption isotherms and thermodynamic studies, the authors proposed that the POEG adsorption mechanism of methylene blue, present in water as monomers, dimers, or trimers, might be due to combined electrostatic and physical multi-layer adsorption processes, whereas the lead was chemically adsorbed. The activated fibers were then applied to decontamination of waste blac-kish waters to remove the methylene blue from Manzala Lake, Egypt, with an efficiency of 91.5–99.9% [21]. The use of POEGs as new biosorbents for heavy metals (M) with an oxidation state of II was investigated in another paper using samples collected in Tipaza, Algeria (36°37′4″ N, 2°23′28″ E) (Figure 2). The balls were washed, dried at 40 °C for 48 h, and ground to obtain a size fraction lower than 160 µm. Then, they were employed in batch experiments in water solutions with metal ions of Pb^{2+}, Cu^{2+}, Ni^{2+}, Zn^{2+}, and Cd^{2+} [22]. Physical parameters that influenced biosorption were investigated, such as the pH, the temperature, the metal concentrations, and the contact time with the POEG fibers. According to these authors, the cylindrical shape of the POEG fibers plays an important role in the adsorption and precipitation of the metal ions on the external surface. Maximum absorption was reached in 80 min at a

pH range of 6.0–8.0. Basic pH values made the process quicker, as the metal ions more easily interacted with the negatively charged surface made by the carboxyl, hydroxyl, and amine groups of the lignocellulose structure. Higher absorption was also achieved at 40 °C, which is a temperature value that helped the coordination process of the metal ions with the homogeneous surface binding sites of the fibers. The process of chelation resulted in spontaneous behavior, although positive enthalpy data suggested that the phenomenon was endothermic [22]. Pb^{2+}, Cu^{2+}, Ni^{2+}, Zn^{2+}, and Cd^{2+} were adsorbed up to maximum concentrations of about 48, 44, 41, 38, and 30 mg/g of POEGs, respectively, and the removal capacity was in a range from 70% to 98% [22]. In another paper, POEGs collected on the Monolithi beach of Preveza, in Greece (38°57′3″ N, 20°45′6.1″ E) (Figure 2) were employed for the removal of Cr^{6+} from wastewater in batch experiments after chemical activation [23]. The activated POEGs, obtained this time by treatment with KOH aqueous solution, showed a high surface area of up to 1563 m^2/g, a cumulative pore volume of 0.74 cm^3/g, and a maximum adsorption capacity of 120 mg/g for the fibers. The POEG adsorption reaction was endothermic, mainly due to electrostatic attractions of Cr^{6+} ions with the positively charged pores of the activated surface or by adsorption and complexion with oxygen-containing groups. In another recent paper, POEG samples collected on the beach of Chaffar, in Tunisia (34°33′50″ N, 10°33′50″ E) (Figure 2), were tested as possible pollution biosorbents to remove hydrocarbon spills from seas [24]. The authors tested them as intact raw materials or as milled fibers for their capacity to absorb pure oil, pure water and a mixed oil/water system in batch experiments. Moreover, in this paper, factors such as the oil concentration, the time of sorption, and the amount of sorbent were investigated to optimize this process. Raw and milled fibers were able to absorb 5.5 g/g and 14 g/g of pure oil and about 15 g/g and 16 g/g of water, respectively, whereas in the mixed system, a maximum oil and water sorption capacity of 4.7 g/g, 12.8 g/g, 7.4 g/g, and 8.3 g/g was found. The highest oil removal efficiency was obtained by using milled fibers with sizes in the range of 0.5–1.0 mm (length), which produced a maximum adsorption in 15 min. The isotherm curve analyses confirmed that, in this case, the oil absorption seemed more like a monolayer coverage process of homogeneous sites than a multilayer coverage process of a heterogeneous-like surface [24]. POEGs had significantly higher abilities for oil absorption capacities than other waste vegetable biomasses used as natural sorbents, such as bagasse, wheat, and barley straws, but lower abilities than those of cotton fibers or silk-floss fibers. POEGs collected on the Chebba beach, in Tunisia (35°14′24″ N, 11°07′12″ E) (Figure 2) were employed instead for the removal of antibiotics, such as oxytetracycline, that are present as micro-contaminants in water environments [25]. The POEGs were first washed with water to remove sand and salt residues, and then they were washed with ethanol. They were then dried and milled into particles of three different homogeneous sizes (100, 75, and 50 μm) before being used. The 50 μm size particle resulted in more efficient adsorption of the antibiotic for up to a maximum of 86%, starting with 80 mg/L as the initial concentration of the drug (when the process was performed at 25 °C with 20 min of contact). The pH value at which the experiments were performed was a key factor in the process because oxytetracycline has three pKa values (3.6, 7.5, and 9.4). The maximum adsorption was reached at pH 6.0, probably when hydrogen bond interactions were formed between the hydroxyl and phenolic groups of the lignocellulose surface of the fibers and the antibiotic. The adsorption process of the antibiotic was a spontaneous, exothermic, and entropically favorable process [25]. Whole POEGs are also a common fiber trap that involuntarily work in the sea to catch plastic wastes in the water [26]. Some researchers have estimated that they annually collect nearly 900 million plastic pieces and that around 1500 pieces of plastic are transported for every kilogram of POEGs. For example, it was found that 17% of 1 kg of POEG samples collected on the beaches of Mallorca Island, Spain (39°42′37″ N; 2°59′42″ E) (Figure 2) contained plastics of different sizes: 45.5% of the plastic pieces were microplastics (pieces smaller than 5 mm), 45.5% were mesoplastics (5–25 mm), and about 9.1% were macroplastics (higher than 25 mm). They ranged in size from 1.0 to about 59.0 mm, with an average length of 9.5 mm. Spectrometry

analyses determined that they were mainly made of polymers, such as polyamide (10.8%), polyethylene (21.6%), polyethylene terephthalate (35.1%), polypropylene (13.5%), but also polystyrene, polyurethane, and polyvinyl chloride. These plastic debris were found to be in various forms, such as filaments and fibers (64.9%), fragments (21.6%), films (8.1%), and foams (5.4%). Their total weight was up to 13 mg for each POEG, a weight that constitutes around 0.15% of the POEG's weight [26]. Considering all these data, POEGs might provide a valuable potential trapping service because they are able to sieve up to 867 million of plastic debris each year, which might be particularly important in the future for finding applications to preserve the ecosystem in the Mediterranean Sea, where a very high level of microplastic contamination persists both at the surface waters and seafloor.

2.3. Poseidonia oceanica Egagropili in Bioplastic and Biocomposite Preparations

POEG fibers have been widely used to strengthen the matrix of plastics, both of bio-based and oil-based origins (Table 1). Mirpoor et al. [2] have exploited both the lignin-carbohydrate (LCC) and the nanocrystalline cellulose (NC) fractions, after extraction from egagropili collected in Poetto (Figure 2), as reinforcing agents for hydroplastic materials. The two fractions were able to improve the physicochemical properties of biodegradable films obtained from hemp (*Cannabis sativa*) oil seedcake protein concentrates. In fact, such materials exhibited a high tensile strength and Young's modulus; the Young's modulus increased from around 20 to 45 and to 80 MPa, while the elongation at break was reduced from 300% to 250% and to 120% in the presence of LCC and NC, respectively. They possessed barrier properties towards water vapor, O_2, and CO_2. In addition, both fractions decreased film hydrophilicity, infact, moisture content, solubility, and swelling ratio were lower for the films prepared in the presence of additives. In 2021, the same authors [12] investigated deeply the LCC fraction obtained from the same POEG samples from a chemical point of view using FT-IR and NMR analyses (see also Section 1.2). The LCC fraction was water soluble as it contained monosaccharides and exhibited a brownish-to-black color due to certain functional groups, such as phenylpropane-based polymers. Furthermore, it exhibited a remarkable and stable antioxidant activity that was easily released over 6 months when it was used as an additive in hemp protein-based films. On the other hand, in another paper, lignin-containing cellulose micro/nanofibrils (LCM/NF) were also obtained by combining the steam explosion process or twin-screw extrusion (as energy-efficient pretreatments) with a conventional grinding step [27]. The chemical composition of the fibers, collected in Monastir (Figure 2), before and after pulping, was analyzed. The obtained LCM/NF suspensions were characterized by several techniques, such as morphological and mechanical analysis. It has been shown that if the sulfonation method was coupled with steam explosion or twin-screw extrusion, then it was possible to obtain LCM/NF gels with relatively low viscosity and nano papers with a Young's modulus of around 5 GPa. Sulfonation was revealed to be an effective pretreatment to lower the energy during grinding, and therefore it can be considered a valid technique to be applied in the field of packaging [27]. POEG fibers, collected in Campello Beach in Alicante, Spain (38°21′00.01″ N, 0°29′00″ W) (Figure 2), were exploited in the reinforcement phase and in oil-based polymeric matrices, such as the high-density polyethylene (HDPE) [28] samples), and more recently even in polyesters [28,29]. In the first work, the authors investigated the influence of POEG fibers and deinking paper sludge (DPS) on the thermo-mechanical properties of high-density polyethylene binary and hybrid composites [29]. POEG fibers (samples collected in Monastir, Tunisia) (Figure 2) were simply obtained by drying the washed balls at 80 °C in a hot air oven for 7 days and then reducing them to a powder by milling them with a grinder. They were subsequently sieved to an approx. 1 mm size. It was found that the properties of binary and hybrid composites depended on the chemical composition of the fillers, and the material's mechanical properties depended on the filler content as well (POEG and DPS). A better interfacial adhesion between fillers and matrix was achieved in the presence of maleated polyethylene (MAPE). HDPE/POEG/MAPE composites achieved the highest tensile modulus and strength with 40% of the POEG fibers [29]. The effect of the

POEG fibers on the mechanical properties and water absorption behavior of unsaturated polyester resin matrices obtained by the compression molding process was also evaluated in the following paper [30] (samples collected in Mahdia, Tunisia, 35°30′24″ N, 11°2′48″ E, Figure 2). The obtained results showed that the stiffness, strength, and hardness of the unsaturated polyester resin/POEG fiber composite increased with increasing concentration of fibers, demonstrating that the latter acted as matrix reinforcing agents. Different amounts (10, 20, and 30 %wt) of fibers from POEG collected on the beach at Rosignano Solvay, Livorno, Italy (43°19′1.7″ N, 10°27′52.7″ E; Figure 2) were obtained as described above and incorporated into a thermoplastic matrix made of poly(hydroxybutyrate-co-hydroxyvalerate) (PHBV). Moreover, acetyl tributyl citrate was used as a plasticizer to produce melt-processable and biodegradable composites for specialized applications in marine environments [31]. The produced materials were characterized in terms of processability, thermal/mechanical/morphological properties, and biodegradability under simulated and real marine environmental conditions. The obtained composites showed good thermal stability and mechanical properties, especially in terms of stress at break and impact resistance. The biodegradation test results in the simulated marine environment showed that the presence of POEG fibers in the composites accelerated the biodegradation of the polymeric matrix. Under real marine conditions, the samples with POEGs showed higher weight losses and mechanical feature reduction compared to those prepared without fibers. Due to the obtained results, the authors speculated that these biocomposites could be exploited as starting materials for low-cost and biodegradable items that are usable in the sea and/or sand dunes, increasing the market opportunities for biopolymers, such as PHBV, and at the same time, finding an eco-sustainable valorization for POEG residues accumulated in large quantities on Mediterranean shores [31]. More recently [32], the PHBV mixture with egagropili fibers was further employed to prepare novel bio-containers with the aim of restoring seagrass meadows and coastal dunes. The authors have discovered that the presence of such bio-containers on the coast has favored the establishment and spread of plants because they promoted shoot production, minimized transplant shock, and enhanced the capacity of plants to resist physical disturbances, such as those due to storm events. This novel approach is very useful for substituting polluting, non-biodegradable materials in recipient habitats [32].

2.4. *Poseidonia oceanica Egagropili in Construction Materials and as Decoration*

POEGs have been widely studied in recent years as environmentally friendly materials to be employed in buildings having fire, sound, and water-resistant properties (Table 1). For example, POEGs have been used in the construction sector as insulating material to reduce the risk of energy source shortages and better manage energy consumption in buildings [33]. In this context, the use of insulating materials is a key factor, as they might provide better thermal comfort, sound insulation, and fire protection [37]. It is worth noting that so far, many of the insulation materials used in the building sector were petroleum derivatives, and they must be replaced with materials derived from renewable na-tural resources from the perspective of a sustainable bioeconomy [34]. Benjeddou et al. [35] studied the effect of adding POEGs to cement composites and found that the mecha-nical strength, sound, and thermal diffusivity were all improved. The POEG fibers were able to reduce sound transmission by increasing the fiber volume and, consequently, the air voids in the cement paste. Another study carried out by Jedidi and Abroug [34] reported that the addition of POEG fibers (collected in Monastir, Tunisia; Figure 2), up to 10%, to the plasters significantly improved their mechanical properties. Thermal conductivity also decreased from 0.35 W/m/K in the absence of fibers to 0.11 W/m/K in the presence of 20% of them. The physical-mechanical properties and the resistance to water and fire of the cement made with POEG fibers and the cement based on pine wood have been studied by Mayer et al. [36] (POEG samples collected in Durrës, Albania, 41°19′27″ N, 19°27′21″ E). The results obtained showed that the POEG fiber-based cement had higher mechanical strength and toughness compared to the pine wood-based cement due to its

higher compatibility. In addition, the POEG cement showed a more homogeneous structure with better properties in terms of both water resistance and flame retardance. It has also to be mentioned that the POEGs are nowadays commercialized on the market under the names "*Posidonia* spheroids, Neptune grass, sea weed balls, or Mediterranean tape weeds" as marine-origin artistic materials to be used as decoration of houses and gardens or for boat garland, for handcraft works as insulating materials for apartment walls or roofs, and sold on-line in sets of 5 to 20 pieces at a price ranging from 6 to 25 euros for each set (see for example, https://www.etsy.com/, accessed on 12 April 2023). As decorative objects, they have also been used for artistic purposes by contemporary artists, as in the case of the masterpiece of Bruna Esposito (Figure 5).

Figure 5. Bruna Esposito (Rome, 1960. The artist lives and works in Rome). **Venti di rivolta o rivolta dei venti** 2009. Fans, galvanized iron pipes, an electrical system, sea straw balls, and a breeze. (Reproduced with permission from the artist and by courtesy of Studio Stefania Miscetti-associazione culturale Mantellate).

3. Conclusions

In recent years, POEGs have caught more and more attention as interesting marine-origin raw materials. Due to their structural and physical properties, they have demonstrated that they could be employed in a variety of applications and fields. The whole POEG fiber network constitutes an interesting nutrient that can be supplemented to a medium for both plant and microorganism growth, while their cellulose components have already been used in biotechnological processes to obtain added valuable molecules, such as enzymes and biofuels. Due to their physical and mechanical properties, these fibers could easily constitute the base of newly developed bioplastics and biocomposites, as well as insulating materials for buildings. Moreover, their isolated lignin fractions might be easily used as reinforcement in newly designed biomaterials. The ability of their fibers to adsorb metals and water contaminants also makes POEGs the ideal ecological tools for environmental decontamination.

4. Future Directions

POEGs have many useful structural, mechanical, and physical properties that make them useful in different applications and fields. Further increasing the possible and potential uses of POEGs might also help in the future to sustain the economic growth of all the countries that overlook the Mediterranean basin. As a matter of fact, as the PO is an endemic sea grass of the Mediterranean Sea, it could constitute an easy, low-cost, and natural source of POEGs that could be used as raw materials in different industrial processes and sectors, thus increasing the economy of the Mediterranean basin countries. In this perspective, on the basis of the data reported in the literature and mentioned here in this review, we imagined and designed a generic scheme of a hypothetical bio-refinery as a model for a start-up company that would eventually valorize the POEGs, in a perspective of more sustainable industrial processes and of a circular bio-economy (Figure 6).

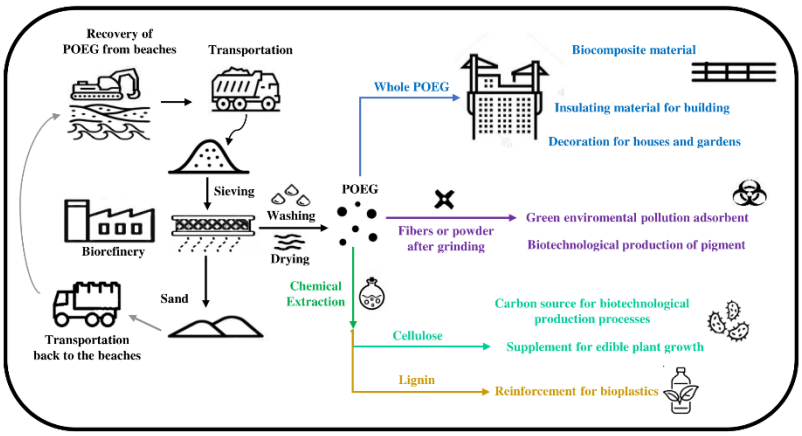

Figure 6. Steps of POEG recovery, transportation, and pre-treatment in a biorefinery (black arrows) before being used in several applications and fields, such as whole POEG(blue arrow); as fibers or powder after grinding (violet arrow); or after chemical extraction (green arrow) of its cellulose (light green arrow) and lignin fractions (yellow arrow). The recovered sand is transported back to the beaches (grey arrow).

Funding: This review received no external funding.

Institutional Review Board Statement: Not applicable.

Informed Consent Statement: Not applicable.

Data Availability Statement: Not applicable.

Conflicts of Interest: The authors declare no conflict of interest.

References

1. Trache, D.; Tarchoun, A.F.; De Vita, D.; Kennedy, J.F. *Posidonia oceanica* (L.) Delile: A Mediterranean seagrass with potential applications but regularly and erroneously referred to as an algal species. *Int. J. Biol. Macromol.* **2022**, *230*, 122624. [CrossRef] [PubMed]
2. Mirpoor, S.F.; Giosafatto, C.V.L.; Di Pierro, P.; Di Girolamo, R.; Regalado-González, C.; Porta, R. Valorisation of *Posidonia oceanica* sea balls (egagropili) as a potential source of reinforcement agents in protein-based biocomposites. *Polymers* **2020**, *12*, 2788. [CrossRef] [PubMed]
3. Lefebvre, L.; Compère, P.; Léonard, A.; Plougonven, E.; Vandewalle, N.; Gobert, S. Mediterranean aegagropiles from *Posidonia oceanica* (L.) Delile (1813): A first complete description from macroscopic to microscopic structure. *Mar. Biol.* **2021**, *168*, 37. [CrossRef]
4. Verhille, G.; Moulinet, S.; Vandenberghe, N.; Adda-Bedia, M.; Le Gal, P. Structure and mechanics of aegagropilae fiber network. *Proc. Natl. Acad. Sci. USA* **2017**, *114*, 4607–4612. [CrossRef]
5. Kumar, A. Egagropili Sand Dunes (Holocene) along the southeastern Gulf of Sirte (Mediterranean Sea) coast of Brega, Libya. *Geophytology* **2022**, *52*, 29–38.
6. Khiari, R.; Belgacem, M.N. Potential for using multiscale *Posidonia oceanica* waste: Current status and prospect in material science. In *Lignocellulosic Fibre and Biomass-Based Composite Materials: Processing, Properties and Applications*; Woodhead Publishing Series in Composites Science and Engineering; Elsevier: Amsterdam, The Netherlands, 2017; pp. 447–471.
7. Pascucci, V.; De Falco, G.; Del Vais, C.; Sanna, I.; Melis, R.T.; Andreucci, S. Climate changes and human impact on the Mistras coastal barrier system (W Sardinia, Italy). *Mar. Geol.* **2018**, *395*, 271–284. [CrossRef]
8. Restaino, O.F.; Scognamiglio, M.; Mirpoor, S.F.; Cammarota, M.; Ventriglia, R.; Giosafatto, C.V.L.; Fiorentino, A.; Porta, R.; Schiraldi, C. Enhanced *Streptomyces roseochromogenes* melanin production by using the marine renewable source *Posidonia oceanica* egagropili. *Appl. Microbiol. Biotechnol.* **2022**, *106*, 7265–7283. [CrossRef]
9. Benito-González, I.; López-Rubio, A.; Martínez-Abad, A.; Ballester, A.-R.; Falcó, I.; González-Candelas, L.; Sánchez, G.; Lozano-Sánchez, J.; Borrás-Linares, I.; Segura-Carretero, A.; et al. In-depth characterization of bioactive extracts from *Posidonia oceanica* waste biomass. *Mar Drugs* **2019**, *17*, 409. [CrossRef]
10. Pfeifer, L. "Neptune balls" polysaccharides: Disentangling the wiry seagrass detritus. *Polymers* **2021**, *13*, 4285. [CrossRef]
11. Rencoret, J.; Marques, G.; Serrano, O.; Kaal, J.; Martínez, A.T.; del Río, J.C.; Gutierrez, A. Deciphering the unique structure and acylation pattern of *Posidonia oceanica* lignin. *ACS Sustain. Chem. Eng.* **2020**, *8*, 12521–12533. [CrossRef]
12. Mirpoor, S.F.; Restaino, O.F.; Schiraldi, C.; Giosafatto, C.V.L.; Ruffo, F.; Porta, R. Lignin/carbohydrate complex isolated from *Posidonia oceanica* sea balls (Egagropili): Characterization and antioxidant reinforcement of protein-based films. *Int. J. Mol. Sci.* **2021**, *22*, 9147. [CrossRef] [PubMed]
13. Kaal, J.; Serrano, O.; del Río, J.C.; Rencoret, J. Radically different lignin composition in *Posidonia* species may link to differences in organic carbon sequestration capacity. *Org. Geochem.* **2018**, *124*, 247–256. [CrossRef]
14. Rudovica, V.; Rotter, A.; Gaudêncio, S.P.; Novoveská, L.; Akgül, F.; Akslen-Hoel, L.K.; Alexandrino, D.A.M.; Anne, O.; Arbidans, L.; Atanassova, M.; et al. Valorization of marine waste: Use of industrial by-products and beach wrack towards the production of high added-value products. *Front. Mar. Sci.* **2021**, *8*, 723333. [CrossRef]
15. Petrounias, P.; Giannakopoulou, P.P.; Rogkala, A.; Antoniou, N.; Koutsovitis, P.; Zygouri, E.; Krassakis, P.; Islam, I.; Koukouzas, N. *Posidonia oceanica* balls (Egagropili) from Kefalonia Island evaluated as alternative biomass source for green energy. *J. Mar. Sci. Eng.* **2023**, *11*, 749. [CrossRef]
16. Restaino, O.F.; Cuomo, S.; D'Ambrosio, S.; Vassallo, V.; Mirpoor, S.F.; Giosafatto, C.V.L.; Porta, R.; Schiraldi, C. Cellulose from *Posidonia oceanica* sea balls (egagropili) as substrate to enhance *Streptomyces roseochromogenes* cellulase biosynthesis. *Fermentation* **2023**, *9*, 98. [CrossRef]
17. Souii, A.; Gorrab, A.; Ouertani, R.; Ouertani, A.; Hammami, K.; Saidi, N.; Souissi, Y.; Chouchane, H.; Masmoudi, A.S.; Sghaier, H.; et al. Sustainable bioethanol production from enzymatically hydrolyzed second-generation *Posidonia oceanica* waste using stable *Microbacterium metallidurans* carbohydrate-active enzymes as biocatalysts. *Biomass Convers. Biorefinery* **2022**, *308*, 1–20. [CrossRef]
18. Kadraoui, M.; Khairi, R.; Brosse, N.; Bergaoui, L.; Mauret, E. Combination of steam explosion and TEMPO-mediated oxidation as pre-treatments to produce nanofibril of cellulose from *Poseidonia oceanica* bleached fibres. *BioResources* **2022**, 17, 2933–2958. [CrossRef]
19. D' Imperio, M.; Montesano, F.F.; Montemurro, N.; Parente, A. *Posidonia* natural residues as growing substrate component: An ecofriendly method to improve nutritional profile of brassica microgreens. *Front. Plant Sci.* **2021**, *12*, 580596. [CrossRef]

20. Bonet-Aracil, M.; Gisbert-Payá, J.; Bou-Belda, E.; Montava, I.; Díaz-García, P. Fibers of the seagrass *Posidonia oceanica* as substrate for germination of lentil seeds. *SN Appl. Sci.* **2019**, *1*, 1414.
21. Elmorsi, R.R.; El-Wakeel, S.T.; Shehab El-Dein, W.A.; Lotfy, H.R.; Rashwan, W.E.; Nagah, M.; Shaaban, S.A.; Sayed Ahmed, S.A.; El-Sherif, I.Y.; Abou-El-Sherbini, K.S. Adsorption of methylene blue and Pb^{2+} by using acid-activated *Posidonia oceanica* waste. *Sci. Rep.* **2019**, *9*, 3356. [CrossRef]
22. Boulaiche, W.; Belhamdi, B.; Hamdi, B.; Trari, M. Kinetic and equilibrium studies of biosorption of M(II) (M = Cu, Pb, Ni, Zn and Cd) onto seaweed *Posidonia oceanica* fibers. *Appl. Water Sci.* **2019**, *9*, 173. [CrossRef]
23. Asimakopoulos, G.; Baikousi, M.; Salmas, C.; Bourlinos, A.B.; Zboril, R.; Karakassides, M.A. Advanced Cr (VI) sorption properties of activated carbon produced via pyrolysis of the *Posidonia oceanica* seagrass. *J. Hazard. Mater.* **2021**, *405*, 124274. [CrossRef] [PubMed]
24. Jmaa, S.B.; Kallel, A. Assessment of performance of *Posidonia oceanica* (L.) as biosorbent for crude oil-spill cleanup in seawater. *Biomed Res. Int.* **2019**, *2019*, 6029654.
25. Ferchichi, K.; Amdouni, N.; Chevalier, Y.; Hbaieb, S. Low-cost *Posidonia oceanica* bio-adsorbent for efficient removal of antibiotic oxytetracycline from water. *Environ. Sci. Pollut. Res.* **2022**, *29*, 83112–83125. [CrossRef]
26. Sanchez-Vidal, A.; Canals, M.; de Haan, W.P.; Romero, J.; Veny1, M. Seagrasses provide a novel ecosystem service by trapping marine plastics. *Sci. Rep.* **2021**, *11*, 254. [CrossRef] [PubMed]
27. Khadraoui, M.; Nader, S.; Khiari, R.; Brosse, N.; Bergaoui, L.; Mauret, E. Effectiveness of sulfonation to produce lignin-containing cellulose micro/nanofibrils (LCM/NF) by grinding. *Cellulose* **2023**, *30*, 815–832. [CrossRef]
28. Puglia, D.; Petrucci, R.; Fortunati, E.; Luzi, F.; Kenny, J.M.; Torre, L. Revalorisation of *Posidonia oceanica* as reinforcement in polyethylene/maleic anhydride grafted polyethylene composites. *J. Renew. Mater.* **2014**, *2*, 66–76. [CrossRef]
29. Haddar, M.; Elloumi, A.; Koubaa, A.; Bradai, C.; Migneault, S.; Elhalouani, F. Synergetic effect of *Posidonia oceanica* fibres and deinking paper sludge on the thermo-mechanical properties of high-density polyethylene composites. *Ind. Crops Prod.* **2018**, *121*, 26–35. [CrossRef]
30. Haddar, M.; Youssef, B.S.; Koubaa, S. Mechanical and water absorption behavior of thermoset matrices reinforced with natural fiber. *Polym. Compos.* **2022**, *43*, 3481–3495. [CrossRef]
31. Seggiani, M.; Cinelli, P.; Mallegni, N.; Balestri, E.; Puccini, M.; Vitolo, S.; Lardicci, C.; Lazzeri, A. New bio-composites based on polyhydroxyalkanoates and *Posidonia oceanica* fibres for applications in a marine environment. *Materials* **2017**, *10*, 326. [CrossRef]
32. Balestri, E.; Vallerini, F.; Seggiani, M.; Cinelli, P.; Menicagli, V.; Vannini, C.; Lardicci, C. Use of bio-containers from seagrass wrack with nursery planting to improve the eco-sustainability of coastal habitat restoration. *J. Environ. Manag.* **2019**, *251*, 109604. [CrossRef] [PubMed]
33. Hamdaoui, O.; Ibos, L.; Mazioud, A.; Safi, M.; Limam, O. Thermophysical characterization of *Posidonia Oceanica* marine fibers intended to be used as an insulation material in Mediterranean buildings. *Constr. Build. Mater.* **2018**, *180*, 68–76. [CrossRef]
34. Jedidi, M.; Abroug, A. Valorization of *Posidonia oceanica* balls for the manufacture of an insulating and ecological material. *Jordan J. Civ. Eng.* **2020**, *14*, 417–430.
35. Benjeddou, O.; Jedidi, M.; Khadimallah, M.A.; Ravindran, G.; Sridhar, J. Effect of *Posidonia oceanica* fibers addition on the thermal and acoustic properties of cement paste. *Buildings* **2022**, *12*, 909. [CrossRef]
36. Mayer, A.K.; Kuqo, A.; Koddenberg, T.; Mai, C. Seagrass- and wood-based cement boards: A comparative study in terms of physico-mechanical and structural properties. *Compos. Part A* **2022**, *156*, 106864. [CrossRef]
37. Varun Teja, K.; Meena, T. Performance of ternary blended concrete and binary concrete made with perlite powder at elevated temperatures. *Jordan J. Civ. Eng.* **2020**, *14*, 198–209.

Clove Essential Oil-Chitosan Based System for Bioactive Packaging: Production and Characterization

(Paper under submission)

Sondos Hejazi [a], Marika Avitabile[a], Sefora Esposito[a], Ana Aleksov[a], Valeria Scala[b], Loredana Mariniello [a], Angela Marotta[c], C. Valeria L. Giosafatto[a]*

[a] *Department of Chemical Sciences, University of Naples "Federico II", Complesso Universitario di Monte Sant'Angelo, 80126 Naples, Italy*

[b] *Research Centre for Plant Protection and Certification, Council for Agricultural Research, and the Analysis of Agricultural Economics (CREA), Rome, Italy*

[c] *Department of Chemical, Materials and Production Engineering, University of Naples "Federico II", P.le Tecchio 80, 80125 Naples, Italy*

*Corresponding authorgiosafat@unina.it

Abstract

Emerging from the depths of nature, we present a novel bio-based material using *citrus* pectin enriched with chitosan nanoparticles. An emulsion ionic gelation technique was employed to encapsulate clove essential oil (CEO) within chitosan nanoparticles (CHNPs). The CEO, extracted using traditional distillation, exhibited remarkable antioxidant activity with an IC_{50} of 2.7 ± 0.13 µg/mL, attributed to its high phenolic content, primarily eugenol. Following encapsulation, different CEO concentrations (0.04-0.32 mg) were evaluated, revealing a maximum encapsulation efficiency of 16% for 0.04 mg and a maximum loading capacity of 8% for 0.16 mg. The ionic crosslinking was confirmed using Fourier Transform Infrared Spectroscopy analysis. The CHNPs exhibited a mean particle size of approximately 200 nm with zeta potential values ranging up to +27 mV. CHNPs were then blended with pectin using polyelectrolyte complexation. The obtained films (CEO-CHNPs/PEC) were characterized for their mechanical properties, morphology, and water vapor permeability, demonstrating their potential application in packaging

* Corresponding author at Department of Chemical Sciences, University of Naples "Federico II", 80126 Naples, Italy.

E-mail address: giosafat@unina.it.

ready-to-cook products for potentially enhancing antimicrobial protection and extending food shelf-life.

Keywords: clove essential oil, ion gelation, chitosan nanoparticles, pectin, polyelectrolytes complexation, active packaging.

1. Introduction

The presence of microplastics (MPs) in the environment, with dimensions ranging from 0.1 to 5 mm, has emerged as a pressing global concern, raising significant environmental, ecological, and human health impacts (Bouwmeester et al., 2015). These tiny plastic fragments originate from various sources, including the breakdown of larger plastic debris and direct release from personal care products and textile microfibers (Bouwmeester et al., 2015). Recently MPs were detected in various biological samples, including human tissues, highlighting the potential for these particles to enter the human body and exert adverse health effects (Yang et al., 2023). Three major pathways of human exposure to MPs include ingestion through contaminated food, inhalation, and dermal contact (Cox et al., 2019). A study by Çobanoglu et al. (2021) investigated the genotoxic and cytotoxic potential of polyethylene microplastics (PEMPs) in human blood lymphocytes, suggesting a link between MPs and potential health risks. To address this pressing issue, innovative packaging solutions, such as edible and bioactive packaging incorporating bioactive compounds, like essential oils, hold immense potential to reduce human exposure to MPs and promote sustainable packaging practices. The development of active packaging technologies has emerged as a prominent area of research in food preservation and materials science (Sabbah et al., 2023; Al-Asmar et al., 2020). These innovative packaging systems incorporate active components that interact with food spoilage agents, thereby enhancing food quality, safety, and shelf life compared to traditional packaging materials (Mirpoor et al., 2023; Corrado et al., 2021). Pectin and chitosan naturally derived biopolymers alongside clove essential oil serve as potential candidates for bio-active packaging. Pectin (PEC), a naturally occurring anionic polysaccharide primarily extracted from *citrus* fruits, is composed of α-(1,4)-linked D-galactopyranosyluronic acid units interspersed with occasional (1,2)-linked L-rhamnopyranosyl units (Iijima et al., 2000). It can be further classified into high methoxyl PEC (HMP) and low methoxyl PEC (LMP) based on the degree of methyl esterification, with more than half of the carboxyl groups esterified in HMP and less than half in LMP (Giosafatto et al., 2014). HMP-based films have demonstrated

favorable mechanical properties, barrier properties, and thermal stability comparable to commercial plastics (Giosafatto et al., 2014).

Chitosan (CH), a linear cationic polysaccharide composed of B-(1–4)-linked D-glucosamine and N-acetyl-D-glucosamine units, has found widespread applications across a broad spectrum of industries, including medicine, pharmaceuticals, food, and animal feed (Hosseinne et al., 2016). Its exceptional properties make it an excellent candidate for nanoparticle synthesis, including abundant natural sources, controllable and simple extraction, biocompatibility, biodegradability, and non-toxicity (Hu & Luo, 2016; Younes & Rinaudo, 2015).

Clove essential oil (CEO) boasts a rich blend of active constituents, including eugenol (4-allyl-2-methoxy phenol), a phenylpropanoid, eugenyl acetate, a monoterpene ester, and β-caryophyllene, a sesquiterpene. These compounds endow CEO with potent antimicrobial and antioxidant properties, making it a valuable tool for extending food shelf life and inhibiting spoilage (Hasheminejad et al., 2019; Chaieb et al., 2007; Sebaaly et al., 2015). However, the antimicrobial efficacy of CEO is somewhat constrained by the volatile and slightly water-soluble nature of its major components, particularly eugenol (Woranuch & Yoksan, 2013; Sebaaly et al., 2015).

Encapsulation of CEO presents an effective strategy to shield its active compounds and facilitate the incorporation of this encapsulated oil into edible films (Hosseini et al., 2013). The ion gelation process is one of the straightforward techniques in which the crosslinker of tripolyphosphate (TPP) plays the main role in interacting with CH to form nanoparticles (NPs), particularly via the emulsion-ionic gelation technique, which has shown promising results in enhancing CEO's stability, preserving its antimicrobial and antioxidant properties, and controlling its release profile. Although TPP-CHNPs generally have larger particle sizes (200-1000 nm), they can accommodate a high loading capacity (up to 80%) (Katouzian & Jafari, 2016). Multiple studies have achieved encapsulation efficiencies ranging from 14% to 47% using this technique, with Jamil et al. (2016) reporting the highest efficiency of 44%. These findings demonstrate the potential of nanoencapsulation to improve CEO's performance in food packaging applications.

To further enhance the efficacy of CEO, two synergistic approaches were employed: ion gelation for nanoparticle synthesis and polyelectrolyte complexation (Hejazi et al., 2023) for grafting these nanoparticles into a PEC film. CHNPs were loaded with CEO extracted from clove buds (*Eugenia*

caryophyllid, L.) using ion gelation techniques (Kamel et al., 2007), and then physically blended with a PEC solution to produce the edible active packaging material (Hejazi et al., 2023). Physicochemical characterizations were conducted to evaluate the antioxidant activity, mechanical, morphological, and water vapor permeability properties of both the encapsulated oil and the prepared films. This novel packaging strategy effectively combines the beneficial properties of the biopolymers PEC and CH, with the synergistic effects of antimicrobial and antioxidant active compounds, offering promising solutions for extending food shelf- life and reducing the MP negative impact on our health thereby reducing food waste.

2. Materials and methods

2.1.Materials

Pectin (PEC) (from citrus fruits (galacturonic acid content 93.5%; methoxyl content 9.4%; dry matter 55.3%; pKa=3.0–4.5), chitosan (CH) (75–85% deacetylated chitin, poly-D-glucosamine,50–190kDa), glycerol (GLY), sodium tripolyphosphate (STPP), Tween 80, and 2,2-diphenyl-1-picrylhydrazyl (DPPH) were purchased by Sigma Aldrich, St. Louis, MO, USA); clove pods were from a local market in Naples, Italy), n-hexane was purchased from Carlo Erba Reagents (Val de Reuil, France). All other chemicals and reagents used were of analytical grade unless specified.

2.2.Clove Essential Oil (CEO) Extraction and antioxidant activity evaluation

Clove flower buds were crushed using a Knife Mill (Retsch GmbH, Haan, Retsch-Allee, Germany) to extract clove oil using the Soxhlet apparatus for oil extraction through distillation as described by Mirpoor et al. (2022) with some modifications. Approximately 25 g of clove buds were ground for oil extraction using n-hexane distillation. The resulting powder was placed into a filter paper extraction thimble, which was then inserted into the lower part of the Soxhlet extractor. A flask containing 200 ml of n-hexane was positioned below, and the system was heated to a temperature of 100ºC. The Soxhlet column was connected to a reflux condenser, and the entire setup was heated on a mantle until n-hexane began to boil. During the process, the boiling vapor ascended through the condenser, condensed, and fell back onto the porous thimble containing the powdered seed sample. n-hexane, acting as a solvent, dissolved the oil content of the seed sample, resulting in the formation of a

homogeneous mixture of n-hexane and oil. This mixture was collected in the receiver of the Soxhlet extractor setup over 6 hours. Subsequently, the extracted oil was concentrated using a STRIKE 300 rotary evaporator (Steroglass S.r.l -Perugia (Italy).

$$\%Yield\ of\ essential\ oil = \left[\frac{Essential\ oil\ weight\ (g)}{Sample\ weight\ (g)} \times 100\right] \quad (1)$$

The antioxidant activity of CEO was evaluated using the technique of radical scavenging capacity with 1,1-diphenyl-2-picrylhydrazyl (DPPH) radical according to the method of Lesjak et al. (2018). Ten microliters of each sample, with initial concentrations of CEO from 0.01 to 10 mg/mL were combined with 100 µL of 67.5 µmol/L DPPH solution in methanol. The resulting mixture was then diluted with an additional 190 µL of methanol. In the control group, 10 µL of the sample was replaced with distilled water. For blank probes, 290 µL of methanol was mixed with each sample (10 µL), while the blank probe for the control involved the addition of only 300 µL of methanol. Absorbance measurements were taken at 515 nm after 1 hour using a microplate reader (Benchmark Plus, BIO-RAD Laboratories, Inc, Italy), and all samples and controls were prepared in triplicate. The percentage of inhibition achieved by various sample concentrations in the antioxidant assays was calculated using the formula:

$$\%\, I = \left[\frac{A0-A}{A0} \times 100\right] \quad (2)$$

Where A_0 represents the absorbance of the control reaction, and A is the absorbance of the examined samples, both corrected for the corresponding blank probe values. Inhibition-concentration curves were constructed using OriginLab software, version 8.0 for Windows (Northampton, USA), and IC_{50} values (the concentration of the extract inhibiting DPPH radical formation by 50%) were determined. The results for each assay were expressed as the mean ± standard deviation (SD) based on three measurements (Lesjak et al., 2018).

2.3.Clove essential oil (CEO) encapsulation

The preparation of oil-loaded and unloaded particles followed a two-step process involving droplet formation and solidification, adapting the methodologies of Hasheminejad (2019). Initially, droplet formation was achieved through the oil-in-water emulsion technique in a CH solution. Subsequently, droplet solidification occurred using STPP solution through the ionic gelation approach, resulting in the formation of spontaneous

nanoparticles (CHNPs). To achieve this, concentrations of CH (0.3% (w/v)) in aqueous acetic acid solution (1% (v/v)) were prepared by overnight stirring at 25°C to form aqueous phases. After adjusting the pH to 4.6 with 0.5N NaOH, the solutions were filtered, and Tween 80 (HLB 15.9, 1% (w/v)) was added as a surfactant, followed by stirring at 25°C for 30 minutes to ensure homogeneous mixtures. Various oil concentrations were gradually introduced into aqueous solutions prepared with two concentrations of CH to generate three mass ratios of CH to CEO (1:0.04; 1:0.16; 1:0.32). Simultaneously, agitation was performed at 700 rpm for 10 minutes at 25°C to create oil-in-water emulsions. STPP solution (0.3% (w/v)) was then prepared in distilled water and mixed with the emulsions to achieve a mass ratio of CH to TPP (1:1). The mixtures underwent agitation for 30 minutes to facilitate crosslinking, and the final pH was adjusted to 4.6. The same procedure, excluding the addition of oil, was applied to produce unloaded particles. The spontaneously formed particles were collected by centrifugation (Avanti J-20 XP, Beckman Coulter, Brea, CA, USA)) at 10,000×g for 35 minutes at 4°C, washed multiple times with a 1% (v/v) aqueous Tween 80 solution, and then dispersed in distilled water. Ultrasonication (Bandelin SONOPULS ultrasonic homogenizers, Binder, Tuttlingen, Germany) for 6 minutes with a sequence of 3 seconds sonication and 7 seconds rest was applied. The homogenized dispersions were stored at 4°C until further analysis. A portion of the prepared dispersions was freeze-dried at −40°C for 24 hours using a freeze dryer (Thermo Savant Modulyo Benchtop, USA).

2.4.Encapsulation efficiency (EE), loading capacity (LC) and yield determination

Encapsulation efficiency (EE) and loading capacity (LC) for CEO-loaded CHNPs (CEO-CHNPs) powder were conducted using ultraviolet-visible (UV–vis) spectrophotometry (SmartSpec™ 3000, Bio-Rad Laboratories, Inc - Italy). The CHNPs were prepared with an initial mass ratio of CH to TPP of 1:1. The methodology followed the procedures outlined by Rahaiee et al. (2015) and Feyzioglu and Tornuk (2016) with some modifications. For the determination of CEO encapsulation, 10 mg/ml CEO-CHNPs were mixed with an aqueous hydrochloric acid solution (2M, 5 mL) and boiled at 95°C for 30 min. After cooling, 1 mL of ethanol was added, and the mixture was centrifuged. Blank CHNPs were also prepared using the same method. The amount of loaded CEO was calculated by reading the absorbance of the supernatant, measured at 282 nm, through a standard curve prepared with

different concentrations of CEO in absolute ethanol. The measurements were conducted in triplicate. Encapsulation efficiency (EE), loading capacity (LC) and yields (Rahaiee et al., 2015) were calculated using the following formulas:

$$\% EE = \left\lfloor \frac{Total\ weight\ of\ loaded\ CEO}{Initial\ weight\ of\ CEO} \times 100 \right\rfloor \quad (3)$$

$$\% LC = \left\lfloor \frac{Total\ weight\ of\ loaded\ CEO}{Weight\ of\ freeze\ dried\ NPs} \times 100 \right\rfloor \quad (4)$$

$$\% CHPs\ Yield = \left\lfloor \frac{Weight\ of\ freeze\ dried\ NPs}{Sum\ of\ the\ dry\ weights\ of\ initial\ materials} \times 100 \right\rfloor \quad (5)$$

2.5.Fourier Transform Infrared Spectroscopy Analysis (FTIR)

Spectra were recorded by an FTIR instrument (JASCO FT/IR-4700, JASCO EUROPE S.R.L., Italy), and 64 scans interferogram was collected with a variable path length cell and KBr windows. Samples were combined with dry KBr. The grounded mixture was then pressed into a transparent desk. The spectra were recorded at a straight baseline of 400–4000 cm^{-1}.

2.6.Pectin-based films prepared with clove essential oil-chitosan encapsulated nanoparticles (CEO-CHNPs/PEC)

For preparing the film-forming solution (FFS), pectin was dissolved in water (2% w/v) until it was completely solubilized, and the pH was adjusted to 7.2. Next, 5 mg of freeze-dried CEO-CHNPs were dissolved in acetic acid and physically blended with the pectin solution for 2 hours, following the polyelectrolyte complexation approach described by Hejazi et al. (2023). Finally, 50 mL of the FFS were cast onto a surface under controlled conditions (50% relative humidity and 25°C) and allowed to dry for 48 hours. This resulted in the formation of a homogeneous and handelable pectin film containing CEO-CHNPs.

2.7.Film Characterization

2.7.1 Size and Zeta Potential of Film Forming Solution (FFS)

Size and Zeta Potential of CHNPs and FFSs were analyzed using the Zetasizer Nano-ZSP (Malvern®, Worcestershire, UK). The Zetasizer Nano combines different techniques of light scattering to obtain a complete characterization of a colloidal system. Three independent measurements were carried out on each sample, diluted to have a final concentration of 1 mg/mL.

2.7.2. Mechanical properties

The mechanical properties of the films, namely tensile strength (TS), elongation at break (EB), and Young's modulus (YM), were examined using an Instron universal testing instrument, model no. 5543A (Instron Engineering Corp., Norwood, MA, USA), following the ASTM method D882-18 (1997). Five strips (8 cm × 1 cm) from each conditioned film were cut and positioned between two grips with an initial distance of 4 cm, and the testing was conducted at a crosshead speed of 5 mm/min.

2.7.3. Water vapor permeability (WVP)

WVP of the film was assessed using a MultiPerm apparatus (ExtraSolution s.r.l, Pisa, Italy) by Standard Methods (ASTM F1249-13, 2013). Each sample was introduced into the instrument, creating a distinct septum between two semi-chambers. The WVP permeability was measured at 50% RH, 25 C, and 1.6 kPa. Before testing, the films underwent a 24-hour conditioning period at 50% relative humidity (RH) and were enclosed in aluminum masks to decrease the film test area to 2 cm^2.

2.7.4. Thermal analysis

Thermal characteristics of freeze-dried CHNPs and pectin-based films were determined by thermogravimetric analysis (TGA) and differential scanning calorimetry (DSC). TGA were conducted with a TA Q50 (TA Instrument, New Castle, DE, USA) in oxidative atmosphere (air, 600ml/min), heating the samples at 10°C/min up to 600°C. DSC were performed with a TA Q2000 (TA Instrument, New Castle, DE, USA) equipped with a refrigerator cooling system (RCS), heating the samples from -50 to 150 °C at a 10°C/min heating rate.

2.8. Statistical Analysis

The results are expressed as mean ± standard deviations from three replicates. Statistical analyses were conducted using Microsoft Excel software (Microsoft Office 2017). The data underwent t-test analysis, and significance was attributed to values with $p < 0.05$.

3. Results and discussion

3.1. Clove essential oil (CEO) yield

CEO, prized for its aromatic properties and wide range of applications, is typically extracted using Soxhlet extraction, a technique that involves immersing the clove material in a solvent and repeatedly cycling it through a heated chamber. In this study, we employed Soxhlet extraction with n-hexane for six hours, followed by rotary evaporation to remove the solvent. The final yield of CEO was determined to be 18% ± 1. Research by Guan (2007) utilizing supercritical fluid extraction yielded slightly higher results, with a 19.5% yield. However, the choice of extraction method significantly impacts the composition of the extracted oil. Supercritical fluid extraction offers slightly higher yields but may have a greater impact on the oil's composition. Soxhlet extraction, with its milder conditions, promotes the extraction of volatile compounds, including eugenol, the primary component of CEO. It has been reported that the optimization process for oil extraction could be greatly influenced by the particle size of the clove material (Khajeh et al., 2004). As the particle size decreases, the surface area increases, leading to enhanced oil release from the broken-down cell walls. This, in turn, increases the extraction yield. However, excessively fine particles can co-extract compounds with higher molecular weights, potentially compromising the oil's purity and quality. Therefore, a balance must be sought between maximizing extraction yield and preserving the desired composition of the CEO (Reverchon et al.,1997).

3.2. Antioxidant activity of clove essential oil (CEO)

The concentration required to neutralize 50% of free radicals is termed IC_{50}, with a lower value indicating stronger antioxidant potential. The IC_{50} values were computed through a graph plotting scavenging capability against concentration (**Figure 1**) (Lesjak et al., 2018). It assesses the inhibition percentages of CEO at concentrations from 0.002 mg/mL up to 2.5 mg/mL revealing, in **Figure 1**, a potent scavenging ability against DPPH radicals, with an IC_{50} value of 2.7 ± 0.13 μg/mL. The robust antioxidant efficacy of CEO may be attributed to its high phenolic content, notably eugenol, which serves as a protective agent against damage induced by reactive oxygen species (Kiki et al., 2023). This aligns with findings from Selles et al. (2020), who reported an IC_{50} value of $4.82 \pm 0.06 \times 10^{-2}$ μg/mL for the antioxidant activity of the same EO by means of the DPPH assay.

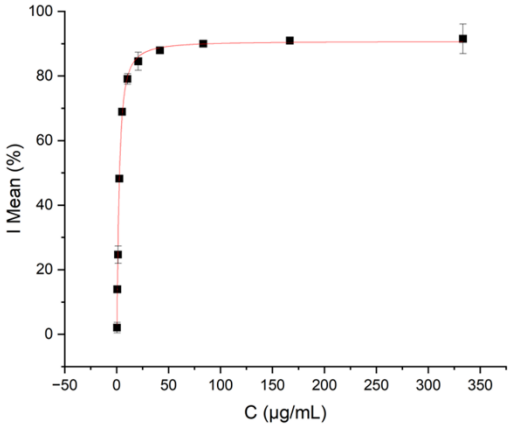

Figure 1. Dependence of inhibition (I mean %) on working concentration (C, µg/mL) of the clove essential oil (CEO) as investigated by DPPH Free-radical-scavenging activity of CEO.

3.3. Encapsulation efficiency (EE), loading capacity (LC), and yield

Table 1 presents the yield percentage of the encapsulated particles. As the concentration of CEO increased, the loading of CEO into the CHNPs decreased. This trend is consistent with findings from a previous study by Hasheminejad et al. (2019), who also encapsulated CEO using CHNPs. EE and LC of different formulations of CEO with CH are shown also in Table 1. The quantity of loaded CEO was assessed through UV–vis spectrophotometry, measuring absorbance at 282 nm. According to the obtained results, the EE% of CEO ranged from 3% to 16% (Table 1). Notably, employing 0.04 mg of CEO yielded the highest EE at 16%, with a slight decrease as CEO concentration increased, reaching 13% for 0.16 CEO and dropping to the lowest at 3% for 0.32 CEO; meanwhile, the lowest CEO amount resulted in an 8% EE. Generally, an increase in initial CEO content correlated with a decrease in EE. However, the maximum EE (16%) was achieved with a CH to OEO weight ratio of 1:0.04. The LC% of CEO, determined through UV–vis spectrophotometry experiments, ranged from 8% to 3% with varying initial CEO content (0.04 to 0.32 g/g CH) (Table 1). This decrease in encapsulation efficiency at higher CEO concentrations may be attributed to the saturation of CEO loaded into CHNPs, as suggested by previous research (Yoksan et al., 2010). The observed decline in EE for samples prepared with higher initial weight ratios of CH to CEO might be attributed to the saturation of CEO loading within the CHNPs. This observation aligns with findings from previous studies (Ajun et al., 2009; Yoksan et al., 2010).

3.4. Particle size and surface charge measurements of encapsulated particles

The impact of CEO addition on both size and surface charge, utilizing the ion gelation technique, was examined through DLS, and is detailed in Table 1. Employing this method and introducing STTP led to a significant reduction in the average particle size, although it did not reach the typical nanoparticle range of 1-100 nm (Rodríguez et al., 2016). Table 1 illustrates that untreated CH had an initial size of 1271, while the addition of STPP reduced it to 353. This size reduction may be attributed to enhanced polymer chain packing, facilitated by the abundant amino groups in CH that interact with the STPP (Russo et al., 2014). Furthermore, the influence of increasing CEO concentration on the average size and surface charge of CEO-loaded particles was investigated. In our study, the addition of varying amounts of oil resulted in decreasing average size, measuring 261, 287, and 212 nm for 0.04 CEO, 0.16 CEO, and 0.32 CEO, respectively. Regarding surface charge, it was +67 for CH, decreasing significantly to +24 for the 1:0.0 CH: CEO ratio, and experiencing a slight increase with the highest CEO amounts, reaching +27 for the 1:0.32 CH: CEO ratio. Higher stability with a higher surface charge might be attributed to the completion of ion crosslinking due to increased protonation of amino groups (Table 1) (Woranuch & Yoksan, 2013, Hasheminejad et al., 2019).

Table 1

Encapsulation efficiency (EE%) and loading capacity (LC%) of CEO in chitosan (CH) nanoparticles (CHNPs) determined by UV–vis spectrophotometry, and Z-average diameter and Zeta potential of 0.5 mg/mL CHNPs loaded with CEO using DLS.

CH: STPP: CEO mass ratio (w/w)	%EE	%LC	Yield (%)	Z-average diameter (nm)	Zeta potential (mV)
1:0.0:0.0	0	0	-	1271±170	67±1.5
1:0.4:0.0	0	0	11.6±2	353±15 [a]	24±3 [a]
1:0.4:0.04	16±0.83	3±0.3	17.6±1 [b]	261±31 [a,b]	23±2 [a]
1:0.4:0.16	13±2.0	8±0.5	18.5±3 [b]	287±34 [a,b]	26±3 [a]
1:0.4:0.32	3.0±0.4 [c]	4±0.1 [c]	14.2±1 [b]	212±40 [a,b]	27±4 [a]

The values that are significantly different compared to chitosan indicated by "a" ($p < 0.05$); the values indicated by "b" are significantly different ($p < 0.05$) from chitosan unloaded with CEO; the values indicated by "c" are significantly different ($p < 0.05$) from chitosan loaded with 0.04 CEO.

3.5. Fourier transform infrared (FTIR) characterization.

The FTIR analysis was employed to characterize the chemical structures of CH powder, pure CEO, CHNPs, and CEO-loaded CHNPs, as illustrated in **Figure 2**. The spectrum of CH exhibited distinctive peaks, including those at 3439 cm^{-1} (O–H stretching), 2883 cm^{-1} (C–H stretching), 1659-1553 cm^{-1} (amide I stretching vibration), 1259 cm^{-1} (C-N stretching and bending vibrations), 1378 cm^{-1} (C–N stretching), 1157 cm^{-1} (β–(1–4) glycosidic linkage), and 1074 cm^{-1} (C–O–C stretching of glucose ring) (**Figure 2A**) (Yoksan et al., 2010; Woranuch & Yoksan, 2013). The characteristics peak at 3439, 1659, 1550, 1324, 1594, 1422, and 1378 cm^{-1} corresponding to the stretching vibration of N-H and O-H groups engaged in intramolecular and intermolecular hydrogen bonds, C=O stretching of amide I, N-H bending of amide II, C-N stretching of amide III, N-H bending of the primary amine, CH_2 bending, and CH_3 symmetrical deformations, respectively (Hejazi et al., 2023). In the context of CHNPs, a comparative analysis of the CH spectrum (**Figure 2B**) reveals notable changes. Most peaks in the CHNPs spectrum are sharper, and a shift to the right is observed, indicative of interactions between the functional groups of CH and STPP. The emergence of a new peak at 2926 cm^{-1} in the FTIR spectrum of CH with STPP, in contrast to neat CH, suggests the presence of aliphatic C-H stretching vibrations. This new peak is likely indicative of alterations in the aliphatic C-H bonding resulting from the interaction between CH and STPP. Another new peak at 1740 cm^{-1} suggests that STPP may induce crosslinking reactions between CH molecules, potentially leading to the formation of new chemical bonds and the appearance of a carbonyl stretching peak. The interaction with STPP might also influence the degree of acetylation in CH, potentially resulting in the appearance of carbonyl groups. Moreover, specific changes in the FTIR spectrum include the shifting of the N–H_2 bending peak of amide II from 1553 to 1540 cm^{-1}. Additionally, new peaks at 1096 and 1250 cm^{-1} are observed, attributed to the stretching vibrations of PO_3 groups and P=O, respectively. These findings suggest complex formation through electrostatic interaction between the ammonium groups of CH and the phosphoric groups of STPP (**Figure 2B**) (Yoksan et al., 2010). The spectrum of pure CEO revealed numerous peaks corresponding to various volatile compounds, with notable peaks at 3525 cm^{-1} (O–H stretching), 2927–2850 cm^{-1} (C–H stretching), and 1603 and 1431 cm^{-1} (C=C stretching of the aromatic ring) (**Figure 2F**) (Woranuch & Yoksan, 2013; Feyzioglu & Tornuk, 2016; Sotelo-Boyás et al., 2017). Eugenol, a major component of CEO, exhibited characteristic peaks at 1511 cm^{-1} and 1614 cm^{-1}, corresponding to the C=C stretching of the aromatic moiety. Additional

peaks observed at 1265, 1236, 915, 818, and 795 cm^{-1} were attributed to specific vibrational modes of eugenol and eugenol acetate (**Figure 2F**). In the spectrum of CHNPs-CEO, where different amounts of CEO (0.04, 0.16, and 0.32 g) were encapsulated, peaks at 1731 cm^{-1} (related to CH spectrum) and several peaks at 1539, 1265, 953, and 850 cm^{-1} (related to CEO spectrum) were monitored (**Figure 2C-E**). The increased intensity of peaks at 2926–2849 cm^{-1} (C–H stretching) and 1454 cm^{-1} (C=C stretching vibration of the aromatic ring) suggested potential interaction between CEO and CH matrix (**Figure 2C-E**) (Keawchaoon & Yoksan, 2011; Hosseini et al., 2013; Feyzioglu & Tornuk, 2016; Sotelo-Boyás et al., 2017). Notably, the spectra of CEO-loaded CHNPs (**Figure 2C-E**) exhibited a new and intense peak at 1652 cm^{-1}, indicating the successful encapsulation of CEO within CHNPs. The shifting of this peak to the right with increasing CEO amount further supported the successful encapsulation and suggested changes in the chemical environment (**Figure 2C-E**).

3.6. CEO-loaded CHNPs thermal properties

The thermograms from the DSC investigations are shown in Figure Xa, where a large exothermic peak can be recognized for every sample. This is related to the loss of water during the dehydration of chitosan (Alkhader et al. 2017, de Moura et al. 2008). When pristine chitosan is crosslinked to generate CHNPs, its dehydration temperature (T_D) rises from 77 °C to 91 °C. Furthermore, the total heat released during the dehydration process increases significantly, indicating a greater interaction between water and chitosan in the form of nanoparticles. The addition of CEO to the chitosan nanoparticles leads to a decrease in the T_D (about 83-85 °C), in agreement with the CEO LC: higher is the CEO loading, lower is T_D and the related reaction enthalpy. These results are in good agreement with the TGA analysis (Figure Xb), where it can be noticed that the CH sample experienced a lower weight loss up to 100° C (i.e., loss of hydration water), compared to the CHNPs at the various loadings. The thermal stability of CHNPs is decreased if compared to that of CH, as reflected by the decrease in degradation temperature from 300°C for CH to 242°C for the CHNPs. However, the nanoparticles show a higher thermal resistance at high temperatures (above 400°C), as also reflected by the presence of a residue at 600°C.

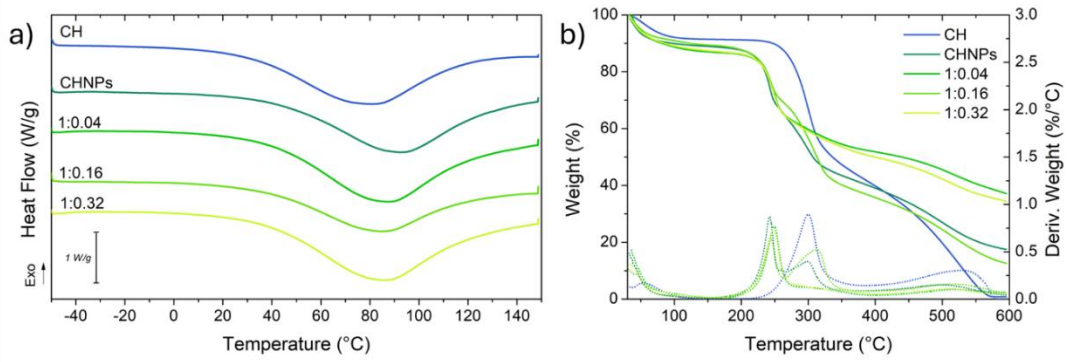

446

Figure X. (a) DSC and (b) TGA thermograms of chitosan (CH) powder, chitosan nanoparticles (CHNPs) and CEO-loaded CHNPs at different CHNPs/CEO ratios: 1:0.04, 1:0.16, 1:0.32. 447 448

449

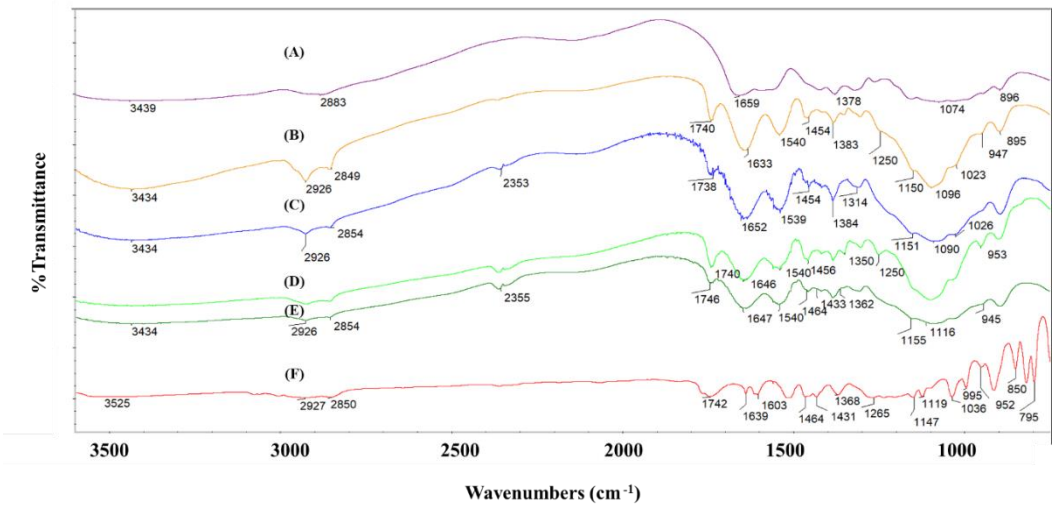

450

Figure 2. FTIR spectra of (A) chitosan (CH) powder; (B) chitosan nanoparticles (CHNPs), (F) Clove Essential Oil (CEO), and CEO-loaded CHNPs (C-E). The CHNPs/CEO ratios examined include (C) 1:0.04; (D)1:0.16; (E) 1:0.32. 451 452 453

3.7. Characterization of film forming solutions (FFSs) and of the derived films 454 455

3.7.1. Particle size and surface charge measurements 456

Table 2 presents the average particle size and Zeta potential of the functionalized films (FFSs) prepared with varying CEO concentrations. The 457 458

average particle size of the FFSs increased with increasing CEO concentration, reaching 1431 ± 38 nm for the 0.32 CEO-CHNPs/PEC film. This expansion in particle size is attributed to the hydrophobic nature of CEO, which promotes aggregation of the CHNPs. The Zeta potential, a measure of electrostatic stability, decreased with increasing CEO concentration, indicating a reduction in electrostatic repulsion among the CHNPs. The negative zeta potential of -58 ± 1 for the PEC film is primarily due to the carboxyl groups of PEC (Esposito et al., 2016). The pH of the solution was maintained at approximately 7, ensuring the stability of the polysaccharide matrix. These findings suggest that the incorporation of CEO into CHNPs leads to increased aggregation and reduced electrostatic repulsion due to its hydrophobic nature.

Table 2

Z-average diameter (nm) and zeta potential (mv) of pectin films containing 30% glycerol (GLY), loaded with 5 mg of different ratios of chitosan nanoparticles (CHNPs) with/without CEO. The CHNPs/CEO ratios examined include 1:0.0, 1:0.04, 1:0.16, and 1:0.32.

FFS	Z-average diameter (nm)	PdI	Zeta potential (mV)
PEC	867±4	0.3	-58±1
0.0 CEO-CHNPs/PEC	766 ±21 [a]	0.3	-57±2
0.04 CEO-CHNPs/PEC	929±17 [a,b]	0.4	-53±3
0.16 CEO-CHNPs/PEC	879 ±26 [b]	0.5	-55±1 [a]
0.32 CEO-CHNPs/PEC	1431±38 [a,b]	0.4	-50±3 [a,b]

The values that are significantly different compared to pectin FFS indicated by "a" ($p < 0.05$); the values indicated by "b" are significantly different ($p < 0.05$) from pectin unloaded with CEO.

3.7.2. Film Mechanical characterization

The mechanical properties of PEC films were assessed with and without the incorporation of CHNPs (5 mg) and CEO. The addition of CHNPs into PEC films significantly enhanced their TS and YM, with TS values increasing from 2.00 ± 0.05 MPa to 6.00 ± 0.002 MPa and YM values increasing from 219.00 ± 60 MPa to 699.00 ± 50 MPa, respectively ($p<0.05$). These substantial increases in film strength and stiffness might be attributed to the interactions between CHNPs and PEC chains, which effectively crosslink and strengthen the polymer network which is likely attributable to the strengthened intermolecular interactions between biopolymer chains induced by nanoparticles. Comparable results were reported by Younis et al. (2019), who demonstrated that the addition of CH to PEC films resulted in a significantly enhanced TS of 6.49 MPa. Lorevice et al. (2016) demonstrated a similar trend, employing higher concentrations of PEC and CH while observing similar

enhancements in film stiffness upon incorporating CHNPs. The authors attributed this improved stiffness to the complementary interactions between CH's amine groups and PEC carboxylic groups. When films are subjected to stress, they absorb energy through various mechanisms. Part of this energy is absorbed by stretching the bonds between polymer chains, enabling alignment without breakage. The addition of CHNPs to PEC matrices necessitates the alignment of more polymer chains, requiring more energy (Lorevice et al., 2016). Additionally, CHNPs are likely to disperse between adjacent chains, strengthening intermolecular interactions, reducing chain mobility, and consequently producing more resistant films. This mechanism could potentially explain the observed stiffness enhancement in this study (**Figure 3**). The presence of CEO appeared to enhance the stiffness of the films, which is evident from the observation that the TS of the CEO-loaded films increased from 6.3 MPa for the unloaded film to 7.5 MPa for the film containing 0.32 mg CEO/5 mg CHNPs (**Figure 3**). Conversely, the elongation at break (EB) decreased with increasing CEO content, indicating a reduction in film flexibility. The EB values ranged from 11% for the unloaded film to 4% for the film containing 0.32 mg CEO/5 mg CHNPs, suggesting that CEO-loaded films offer improved resistance. These findings align with previous studies, such as those of Santos et al. (2023), who investigated the effect of garlic oil-based CH nanocomposites on PEC films. The enhancement in mechanical properties can be attributed to the synergistic interactions between CEO, PEC, and CHNPs. CEO's aromatic compounds are known to interact with the hydroxyl groups on PEC molecules, forming hydrogen bonds that strengthen the polymer network. Additionally, the CEO's hydrophobic nature can induce interactions with the CHNPs, further crosslinking the film matrix and enhancing its mechanical integrity. The incorporation of CEO into CHNPs/PEC films not only improves their mechanical properties but also imparts antimicrobial and antioxidant properties which make CEO-CHNPs/PEC films a promising alternative to conventional synthetic packaging materials.

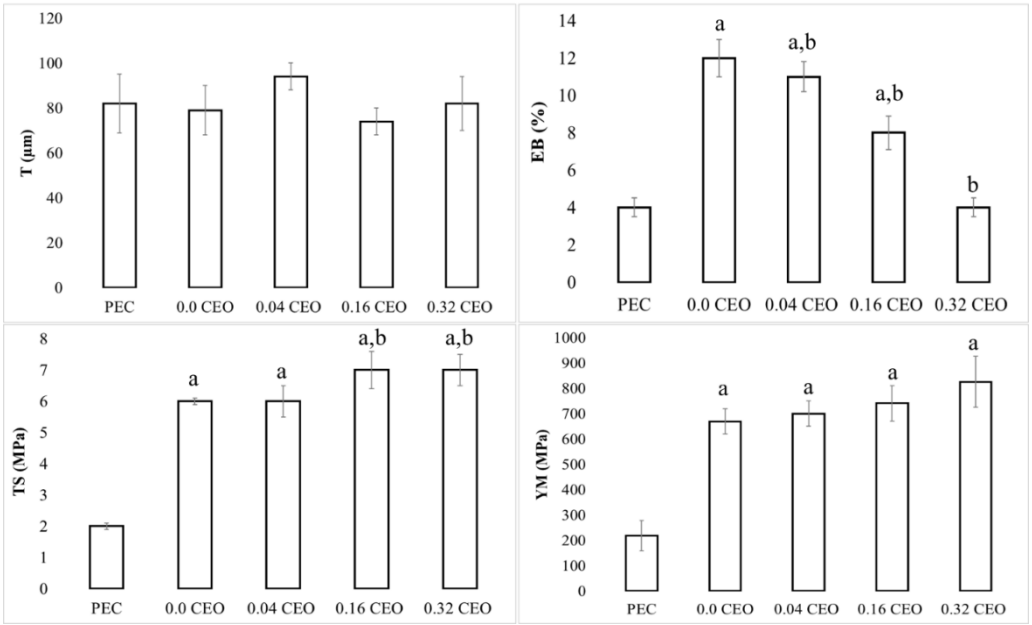

Figure 3. Mechanical characterization of pectin films containing 30% glycerol (GLY), loaded with 5 mg of different ratios of chitosan nanoparticles (CHNPS) with/without CEO. The CH/CEO ratios examined include 1:0.0, 1:0.04, 1:0.16, and 1:0.32. The values that are significantly different compared to pectin unloaded with chitosan nanoparticles indicated by "a" ($p < 0.05$); the values indicated by "b" are significantly different ($p < 0.05$) from the films with chitosan nanoparticles- unloaded with CEO.

3.7.3. Morphological analysis

SEM images revealed distinct differences among unreinforced PEC films, PEC films loaded with CHNPs, and PEC films loaded with CHNPs containing the highest amount of CEO (0.32 CEO). The effect was particularly evident upon the incorporation of CHNPs and CEO, as evidenced by the formation of compact, homogeneous, and smooth microstructures (**Figure 4**). These observed structural changes are attributed to the synergistic interactions between PEC, CHNPs, and CEO, leading to improved film formation properties. The SEM morphology analysis demonstrated a clear distinction between PEC alone, CHNPs/PEC, and CEO-CHNPs/PEC films (**Figure 4**). In all cases, homogeneous and smooth microstructures were observed, indicating the compatibility of these materials for film formation. However, the addition of CHNPs resulted in a more compact and homogeneous structure, and the incorporation of CEO further enhanced this effect, eliminating any visible pores or cracks. These findings align with the study by Lei et al. (2019), who explored the incorporation of tea polyphenol into PEC films, observing similar

structural changes. The observed aggregation of CEO-CHNPs, stacked in compact layers, suggests that CEO was effectively distributed throughout the film matrix, forming strong interactions with the other components. This aggregation can be attributed to the hydrophobic nature of CEO, which can induce interactions with the CHNPs, further crosslinking the film structure and enhancing its mechanical integrity. The synergistic interactions between PEC, CHNPs, and CEO not only improve film formation properties but also impart enhanced mechanical strength and water vapor barrier properties as reported below.

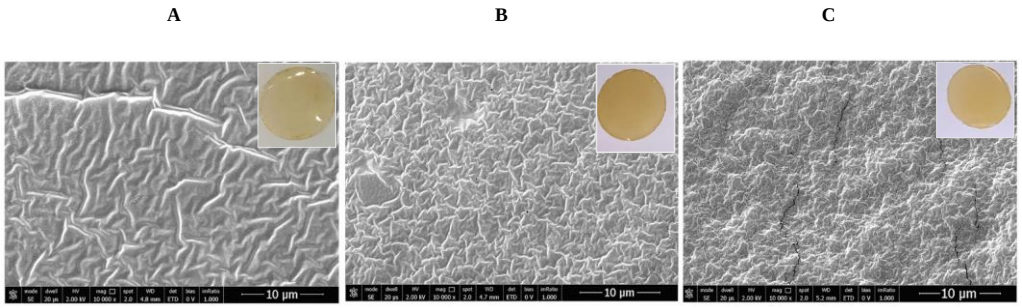

Figure 4. Scanning electron microscopy analysis (SEM) of (A) pectin films prepared with 30% glycerol (GLY);(B) pectin films containing 5 mg of chitosan nanoparticles (CHNPs); (C) pectin films with 5 mg of CEO-CHNPS at a ratio of CH: CEO equal to 1:0.32 at magnification 10000 x.

3.7.4. Water vapor permeability (WVP)

Table 3 summarizes the effects of incorporating CEO at varying concentrations on the WVP of PEC-based films. The WVP of films containing CEO was initially higher compared to the control film (PEC alone, 3.9 ± 0.2 $g \cdot mm \cdot m^2 \cdot 24h^{-1} \cdot kPa^{-1}$). However, the WVP gradually decreased as the CEO concentration increased indicating that CEO and CHNP-modified films significantly improved barrier properties compared to films without CEO. The CHNPs/PEC film exhibited a WVP value of 5.7 ± 0.2 $g \cdot mm \cdot m^2 \cdot 24h^{-1} \cdot kPa^{-1}$, and the lowest permeability was already reached with particles having mass ratio of CH to CEO of 0.16. These values suggest the effectiveness of CEO, a mixture of hydrophobic compounds, such as allicin, in reducing WVP and permeance through the film. This outcome may be attributed to the synergistic effects of the film matrix and CEO hydrophobicity. The homogeneous dispersion of CEO within the polymer chains creates hydrophobic sites that can effectively repel water molecules and reduce the interactions between hydrophilic groups, thereby enhancing the film barrier property (Bravin et al.,

2004; Espitia, et al., 2014; Cazón, et al., 2017; Aitboulahsen, et al., 2020). Additionally, high-methoxylated PEC contains fewer carboxyl groups, further decreasing the hydrophilic sites available for water to interact with and promote permeation (Espitia, et al., 2014). In conclusion, the incorporation of CEO-CHNPs into PEC- films significantly improved their barrier feature toward water. The synergistic interactions between CEO-CHNPs and PEC resulted in a more hydrophobic film matrix, effectively reducing water absorption, and enhancing the film's ability to protect packaged food from moisture loss. These findings demonstrate the potential of PEC-based films (CEO-CHNPs/PEC) as a sustainable and effective alternative to conventional synthetic packaging materials. In fact, due to the well-known antimicrobial activity of CEO (mainly antifungal) (Hasheminejad et al., 2019) together with the efficient water barrier properties of the resulted materials, these films may have the potential to extend the shelf-life of different foods, such as ready-to-cook spices able to reduce the risk of mycotoxin contamination.

Table 3

Water vapor permeability (WVP) of pectin films containing 30% glycerol (GLY), loaded with 5 mg of different ratios of chitosan particles with/without CEO. The CHNPs/CEO ratios examined include 1:0.0, 1:0.04, 1:0.16, and 1:0.32.

Film type	Water vapor permeation [g·mm·m^2·24h^{-1}· kPa^{-1}]
PEC	3.9±0.2
0.0 CEO-CHNPs/PEC	5.7±0.2 [a]
0.04 CEO-CHNPs/PEC	5.1±0.1 [a]
0.16 CEO-CHNPs/PEC	4.4±0.2 [a,b]
0.32 CEO-CHNPs/PEC	4.4±0.4 [a,b]

The values that are significantly different compared to pectin unloaded with chitosan particles indicated by “a” ($p < 0.05$); the values indicated by “b” are significantly different ($p < 0.05$) from the films with chitosan particles- unloaded with CEO.

3.7.5. Thermal properties

The results of DSC and TGA analysis on pectin-based films are reported in Figure Y. As with CHNPs, pectin exhibits an exothermic peak associated with dehydration at 73 °C. The addition of CHNPs at various CEO loadings to the pectin film does not affects the amount of water absorbed, as shown by the TGA thermogram, but decrease the entity of water-polymer interactions (Martelli et al., 2013), as deducible by the decrease of T_D to ~65 °C. Furthermore, the degradation temperature (~200 °C) is only slightly affected

by the addition of CEO-CHNPs, as well as the residue at 600 °C, which is increased from 20% for PEC to 25% for the CEO-CHNPs/PEC.

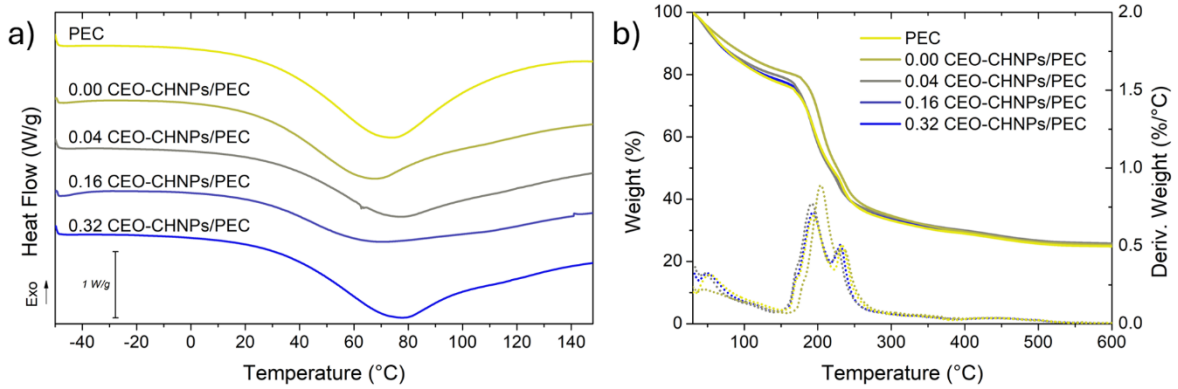

Figure Y. (a) DSC and (b) TGA thermograms of pectin films (PEC), and pectin films loaded with different CEO-loaded CHNPs.

4. Conclusions

In this study, CEO was successfully encapsulated within CH for nanoparticle preparation (CHNPs) using an ion gelation technique for creating a bio-based formulation with enhanced stability. CEO was first extracted from clove pods yielding a substantial 18% oil extract and demonstrated a remarkable ability to scavenge free radicals, with an impressive 50% inhibition concentration of 2.7 ± 0.13 µg/mL. By encapsulating the CEO within CH, we created a protective shield for the CEO from degradation and ensured sustained release, especially for one of the main active volatile compound eugenol. The encapsulation efficiency reached a maximum of 16% for 0.04 mg of CEO, while the loading capacity achieved 8% for 0.16 mg of CEO. The mean average size of the encapsulated nanoparticles exceeded 100 nm, attributed to enhanced complexation due to increased amino group protonation. Further FTIR analysis confirmed the successful complexation and encapsulation of CEO by CH. We expand our attempt to prepare edible films by physically blending the encapsulated CHNPs within *citrus* PEC. The blended films exhibited enhanced mechanical properties and improved water vapor barrier properties. These synergistic interactions between CEO-CHNPs and PEC resulted in a more hydrophobic film matrix, effectively reducing water absorption, and suggesting enhancing the film's ability to protect packaged

food from moisture loss .Overall, this study demonstrates the feasibility of developing bio-based active edible films with CEO-CHNPs blended with PEC for potentially enhancing the antimicrobial protection of packaged food.

Acknowledgements

The authors thanks Mrs Maria Fenderico and Dr Antonella Giarra for their technical support in film preparation and microscopy analysis, respectively.

Conflicts of interest

There are no conflicts to declare.

References

Aitboulahsen, M., El Galiou, O., Laglaoui, A., Bakkali, M., & Hassani Zerrouk, M. (2020). Effect of plasticizer type and essential oils on mechanical, physicochemical, and antimicrobial characteristics of gelatin, starch, and pectin-based films. *Journal of Food Processing and Preservation*, *44*(6), e14480.

Ajun, W., Yan, S., Li, G., & Huili, L. (2009). Preparation of aspirin and probucol in combination loaded chitosan nanoparticles and in vitro release study. *Carbohydrate Polymers*, *75*(4), 566-574.

Al-Asmar, A.; Giosafatto, C.V.L.; Sabbah, M.; Sanchez, A.; Villalonga Santana, R.; Mariniello, L.(2020). Effect of mesoporous silica nanoparticles on the physicochemical properties of pectin packaging material for strawberry wrapping. *Nanomaterials 10*, 52.

Alkhader, E., Billa, N., & Roberts, C. J. (2017). Mucoadhesive chitosan-pectinate nanoparticles for the delivery of curcumin to the colon. *AAPS PharmSciTech, 18, 1009-1018.*

ASTM F1249-13. (2013). Standard test method for water vapor transmission rate through plastic film and sheeting using a modulated infrared sensor.

Bouwmeester, H., Hollman, P. C., & Peters, R. J. (2015). Potential health impact of environmentally released micro-and nanoplastics in the human food production chain: experiences from nanotoxicology. *Environmental Science & Technology*, *49(15)*, 8932-8947

Bravin, B., Peressini, D., & Sensidoni, A. (2004). Influence of emulsifier type and content on functional properties of polysaccharide lipid-based edible films. *Journal of Agricultural and Food chemistry, 52*(21), 6448-6455.

Cazón, P., Velazquez, G., Ramírez, J. A., & Vázquez, M. (2017). Polysaccharide-based films and coatings for food packaging: A review. *Food Hydrocolloids, 68*, 136-148.

Chaieb, K., Hajlaoui, H., Zmantar, T., Kahla-Nakbi, A. B., Rouabhia, M., Mahdouani, K., & Bakhrouf, A. (2007). The chemical composition and biological activity of clove essential oil, Eugenia caryophyllata (Syzigium aromaticum L. Myrtaceae): a short review. *Phytotherapy Research, 21*(6), 501-506.

Çobanoğlu, H., Belivermiş, M., Sıkdokur, E., Kılıç, Ö., & Çayır, A. (2021). Genotoxic and cytotoxic effects of polyethylene microplastics on human peripheral blood lymphocytes. *Chemosphere, 272*, 129805.

Corrado, I., Abdalrazeq, M., Pezzella, C., Di Girolamo, R., Porta, R., Sannia, G., & Giosafatto, C. V. L. (2021). Design and characterization of poly (3-hydroxybutyrate-co-hydroxyhexanoate) nanoparticles and their grafting in whey protein-based nanocomposites. *Food Hydrocolloids, 110*, 106167.

Cox, K. D., Covernton, G. A., Davies, H. L., Dower, J. F., Juanes, F., & Dudas, S. E. (2019). Human consumption of microplastics. *Environmental Science & Technology, 53*(12), 7068-7074

de Moura, M. R., Aouada, F. A., & Mattoso, L. H. (2008). Preparation of chitosan nanoparticles using methacrylic acid. *Journal of colloid and interface science*, *3a 21*(2), 477-483.

Dos Santos, V. S., Lorevice, M. V., Baccarin, G. S., da Costa, F. M., da Silva Fernandes, R., Aouada, F. A., & de Moura, M. R. (2023). Combining Chitosan Nanoparticles and Garlic Essential Oil as Additive Fillers to Produce Pectin-Based Nanocomposite Edible Films. *Polymers, 15*(10), 2244.

Espitia, P. J. P., Du, W. X., de Jesús Avena-Bustillos, R., Soares, N. D. F. F., & McHugh, T. H. (2014). Edible films from pectin: Physical-mechanical and antimicrobial properties-A review. *Food Hydrocolloids, 35*, 287-296.

Feyzioglu, G. C., & Tornuk, F. (2016). Development of chitosan nanoparticles loaded with summer savory (Satureja hortensis L.) essential oil for antimicrobial and antioxidant delivery applications. *LWT*, *70*, 104-110.

Giosafatto, C. V. L., Di Pierro, P., Gunning, P., Mackie, A., Porta, R., & Mariniello, L. (2014). Characterization of Citrus pectin edible films containing transglutaminase-modified phaseolin. *Carbohydrate Polymers, 106*, 200-208.

Guan, W., Li, S., Yan, R., Tang, S., & Quan, C. (2007). Comparison of essential oils of clove buds extracted with supercritical carbon dioxide and other three traditional extraction methods. *Food Chemistry, 101*(4), 1558-1564.

Hasheminejad, N., Khodaiyan, F., & Safari, M. (2019). Improving the antifungal activity of clove essential oil encapsulated by chitosan nanoparticles. *Food Chemistry, 275*, 113-122.

Hejazi, S., Restaino, O. F., Sabbah, M., Zannini, D., Di Girolamo, R., Marotta, A., ... & Porta, R. (2023). Physicochemical Characterization of Chitosan/Poly-γ-Glutamic Acid Glass-like Materials. *International Journal of Molecular Sciences, 24*(15), 12495.

Hosseini, S. F., Zandi, M., Rezaei, M., & Farahmandghavi, F. (2013). Two-step method for encapsulation of oregano essential oil in chitosan nanoparticles: Preparation, characterization and in vitro release study. *Carbohydrate Polymers*, *95*(1), 50-56.

Hu, Q., & Luo, Y. (2016). Polyphenol-chitosan conjugates: Synthesis, characterization, and applications. *Carbohydrate Polymers, 151*, 624-639.

Iijima, M., Nakamura, K., Hatakeyama, T., & Hatakeyama, H. (2000). Phase transition of pectin with sorbed water. *Carbohydrate Polymers, 41*(1), 101-106.

Jamil, B., Abbasi, R., Abbasi, S., Imran, M., Khan, S. U., Ihsan, A., et al. (2016). Encapsulation of cardamom essential oil in chitosan nano-composites: In-vitro efficacy

on antibiotic-resistant bacterial pathogens and cytotoxicity studies. *Frontiers in Microbiology, 7*, 1580.

Katouzian, I., & Jafari, S. M. (2016). Nano-encapsulation as a promising approach for targeted delivery and controlled release of vitamins. *Trends in Food Science & Technology, 53*, 34-48.

Khajeh, M., Yamini, Y., Sefidkon, F., & Bahramifar, N. (2004). Comparison of essential oil composition of Carum copticum obtained by supercritical carbon dioxide extraction and hydrodistillation methods. *Food Chemistry*, *86*(4), 587-591.

Kiki, M. J. (2023). *In Vitro* Antiviral Potential, Antioxidant, and Chemical Composition of Clove (Syzygium aromaticum) Essential Oil. *Molecules*, *28*(6), 2421.

Lei, Y., Wu, H., Jiao, C., Jiang, Y., Liu, R., Xiao, D., ... & Li, S. (2019). Investigation of the structural and physical properties, antioxidant and antimicrobial activity of pectin-konjac glucomannan composite edible films incorporated with tea polyphenol. *Food Hydrocolloids, 94*, 128-135.

Lesjak, M., Beara, I., Simin, N., Pintać, D., Majkić, T., Bekvalac, K., ... & Mimica-Dukić, N. (2018). Antioxidant and anti-inflammatory activities of quercetin and its derivatives. *Journal of Functional Foods*, *40*, 68-75.

Lorevice, M. V., Otoni, C. G., de Moura, M. R., & Mattoso, L. H. C. (2016). Chitosan nanoparticles on the improvement of thermal, barrier, and mechanical properties of high-and low-methyl pectin films. *Food Hydrocolloids, 52*, 732-740.

Marilena Esposito, Prospero Di Pierro, Carlos Regalado-Gonzales, Loredana Mariniello, C. Valeria L. Giosafatto, Raffaele Porta. (2016).Polyamines as new cationic plasticizers for pectin-based edible films, *Carbohydrate Polymers, 153*, 222-228.

Martelli, M. R., Barros, T. T., de Moura, M. R., Mattoso, L. H., & Assis, O. B. (2013). Effect of chitosan nanoparticles and pectin content on mechanical properties and water vapor permeability of banana puree films. *Journal of food science, 78*(1), N98-N104.

Mirpoor, S. F., Zannini, D., Santagata, G., & Giosafatto, C. V. L. (2024). Cardoon seed oil cake proteins as substrate for microbial transglutaminase: Their application as matrix for bio-based packaging to extend the shelf-life of peanuts. *Food Hydrocolloids, 147*, 109339.

Mirpoor, S.F., Giosafatto, C.V.L., Mariniello, L., D'Agostino, A., D'Agostino, M., Cammarota, M., Schiraldi, C., Porta, R., (2022). Argan (Argania spinosa L.) Seed Oil Cake as a Potential Source of Protein-Based Film Matrix for Pharmaco-Cosmetic Applications. *International Journal of Molecular Sciences, 23*, 8478.

Rahaiee, S., Shojaosadati, S. A., Hashemi, M., Moini, S., & Razavi, S. H. (2015). Improvement of crocin stability by biodegradeble nanoparticles of chitosan-alginate. *International Journal of Biological Macromolecules*, *79*, 423-432.

Reverchon, E. (1997). Supercritical fluid extraction and fractionation of essential oils and related products. *The Journal of Supercritical Fluids*, *10*(1), 1-37.

Rodríguez, J., Martín, M. J., Ruiz, M. A., & Clares, B. (2016). Current encapsulation strategies for bioactive oils: From alimentary to pharmaceutical perspectives. *Food Research International*, *83*, 41-59.

Russo, E., Gaglianone, N., Baldassari, S., Parodi, B., Cafaggi, S., Zibana, C., ... & Caviglioli, G. (2014). Preparation, characterization and in vitro antiviral activity evaluation of foscarnet-chitosan nanoparticles. *Colloids and Surfaces B: Biointerfaces*, *118*, 117-125.

Sabbah, M., Al-Asmar, A., Younis, D., Al-Rimawi, F., Famiglietti, M., & Mariniello, L. (2023). Production and Characterization of Active Pectin Films with Olive or Guava Leaf Extract Used as Soluble Sachets for Chicken Stock Powder. *Coatings, 13*(7), 1253.

Sebaaly, C., Jraij, A., Fessi, H., Charcosset, C., & Greige-Gerges, H. (2015). Preparation and characterization of clove essential oil-loaded liposomes. *Food Chemistry, 178*, 52-62.

Selles, S. M. A., Kouidri, M., Belhamiti, B. T., & Ait Amrane, A. (2020). Chemical composition, in-vitro antibacterial and antioxidant activities of Syzygium aromaticum essential oil. *Journal of Food Measurement and Characterization*, *14*(4), 2352-2358.

Woranuch, S., & Yoksan, R. (2013). Eugenol-loaded chitosan nanoparticles: I. Thermal stability improvement of eugenol through encapsulation. *Carbohydrate Polymers, 96*(2), 578-585.

Yang, Y., Xie, E., Du, Z., Peng, Z., Han, Z., Li, L., ... & Yang, X. (2023). Detection of various microplastics in patients undergoing cardiac surgery. *Environmental Science & Technology, 57*(30), 10911-10918.

Yoksan, R., Jirawutthiwongchai, J., & Arpo, K. (2010). Encapsulation of ascorbyl palmitate in chitosan nanoparticles by oil-in-water emulsion and ionic gelation processes. *Colloids and Surfaces B: Biointerfaces*, *76*(1), 292-297.

Younes, I., & Rinaudo, M. (2015). Chitin and chitosan preparation from marine sources. Structure, properties and applications. Marine drugs, 13(3), 1133-1174.

Younis, H. G., & Zhao, G. (2019). Physicochemical properties of the edible films from the blends of high methoxyl apple pectin and chitosan. *International Journal of Biological Macromolecules, 131*, 1057-1066.